Universitat Autònoma de Barcelona

Design and application of nanomaterial-based lateral flow devices

Daniel Quesada González

Universitat Autònoma
de Barcelona

Design and application of nanomaterial-based lateral flow devices

Daniel Quesada González

PhD Thesis

PhD in Chemistry

Director

ICREA Prof. Dr. Arben Merkoçi

Chemistry Department, Science Faculty

2018

The present work entitled “Design and application of nanomaterial-based lateral flow devices”, presented by Daniel Quesada González to obtain the degree of doctor by University Autònoma de Barcelona, was performed at the Nanobioelectronics and Biosensors Group at the Institut Català de Nanociència i Nanotecnologia (ICN2), under the supervision of Prof. Dr. Arben Merkoçi, ICREA Professor and Group Leader.

This work was performed under the framework of the PhD Programme in Chemistry of Universitat Autònoma de Barcelona, under the tutorship of Prof. Dr. Gonzalo Guirado López.

The author

Daniel Quesada González

Approval:

The director

Prof. Dr. Arben Merkoçi

Bellaterra, September 2018

“But still try for who knows what is possible!”

Dr. Michael Faraday, father of Nanoscience

This PhD thesis is focused on the development of lateral flow devices based on the use of nanomaterials with the objective to enhance the detection performance in terms of sensitivity in addition to other analytical parameters.

The state-of-the art studies carried out resulted in three review publications:

Quesada-González, D. & Merkoçi, A. "Nanoparticle-based lateral flow biosensors". *Biosens. Bioelectron.* **73,** 47–63 (2015).

Quesada-González, D. & Merkoçi, A. "Mobile phone–based biosensing: an emerging 'diagnostic and communication' technology". *Biosens. Bioelectron.* **92,** 549–562 (2016).

Quesada-González, D. & Merkoçi, A. "Nanomaterial-Based Devices for Point-of-Care Diagnostic Applications". *Chem. Soc. Rev.* **47**, 4697–4709 (2018).

Also the experimental work performed conducted to four full length articles not yet published:

Quesada-González, D.; Jairo, G. A.; Blake, R.C., Blake, D.A. & Merkoçi, A. "Uranium (VI) detection in groundwater using a gold nanoparticle/paper-based lateral flow device". *In preparation* (2018) – work related to Chapter 3.

Quesada-González, D.; Stefani, C.; González, I.; de la Escosura-Muñiz, I.; Domingo, N.; Mutjé, P. & Merkoçi, A. "Signal enhancement on gold nanoparticle-based lateral flow tests using cellulose nanofibers". *In preparation* (2018) – work related to Chapter 4.

Quesada-González, D.; Baiocco, A.; Martos, A. A.; de la Escosura-Muñiz, A.; Palleschi, G. & Merkoçi, A. "Iridium oxide (IV) nanoparticle-based electrocatalytic detection of PBDE". *In preparation* (2018) – work related to Chapter 5.

Quesada-González, D.; Sena-Torralba, A.; Wicaksono, W. P.; de la Escosura-Muñiz, A.; Ivandini, T. A. & Merkoçi A. "Iridium oxide (IV) nanoparticle-based lateral flow immunoassay". *In preparation* (2018) – work related to Chapter 5.

In this section I would like to thank all the people that has accompanied me during this PhD, those who guided me, those with whom I collaborated and those who were always there. Because a PhD is not an individual work, because it is possible thanks to all of them.

First of all, Prof. Dr. Arben Merkoçi, director of this thesis and group leader in Nanobioelectronics and Biosensors Group. Thank you for accepting me in your group, for guiding me during all these years and for everything you taught me about being a good researcher. When I first arrived to the group, six years ago, I really felt like a child, lost and scared, an undergraduate student afraid of failing, for the first time in a real lab surrounded by true scientists, doubting of everything I knew, doubting of myself. But little by little, I lost my fears, I saw that the group was more than that, like a big family, and Arben, you believed in me, you allowed me to do a master and then the PhD. I grew up, I learnt, I changed and now I'm writing a doctoral work. Thank you for everything.

I would like to acknowledge some people in the UAB. My tutor, Dr. Gonzalo Guirado Lopez, for his support during this work and his kind patience answering all my e-mails. Also to the coordinator of the PhD programme in Chemistry, Dr. Mariona Sodupe, and the responsible of administrative management in Chemistry Department, Elena Jiménez, because I also sent you thousands of e-mails and chased you with many questions during these years. And finally, a huge thank you to Dr. Josefina Pons, because she recommended me to Arben and because without her I would not have entered in the group.

Dr. Alfredo de la Escosura, thank you for all these years supporting me, counselling me and for everything I learnt from you. There were many times when I didn't know how to continue but with your counselling and optimism I found new routes, I understood how to learn from the errors and that going back doesn't mean not moving forward. If now I'm able to progress, to find the way and guiding the new students, it is because I learnt if from you. Thank you!

Dr. Lourdes Rivas, the first person I meet in the group. We spent many hours working together and I learnt a lot things from you, hard to mention all of them but I must at least highlight three: how to build a lateral flow strip, how to synthetize gold nanoparticles and how to produce iridium oxide nanoparticles; three important pillars in this thesis and I learnt them from you! First time I tried to assembly a lateral flow strip I felt like "uf, I don't want to repeat this never again" and look, now I'm writing a thesis focused on that. Probably I've cut more than a million paper strips with the guillotine, and that's not an exaggeration. Thank you for your patience these days, for the time you spent teaching me in the lab and for your friendship.

Now, I'd like to send my thankfulness to the other side of the ocean, to New Orleans. Dr. Diane A. Blake and her collaborators, Dr. Grace A. Jairo and Dr. Robert C. Blake II, who participated in the development of lateral flow strips for the detection of uranium, thank you for this great opportunity and for all the support given. Now closer, in the University of Girona, I'd like to thank LEPAMAP group, Dr. Pere Mutjé and Israel González, for their collaboration in the inclusion of carbon nanofibers in lateral flow. Also thanks to Dr. Neus Domingo and Christina Stefani, from AFM group in ICN2, who also participated in that project. Thanks to Dr. Giuseppe Palleschi, from Tor Vergata, and Tribidasari A. Ivandini, from Jakarta, for their collaboration in the iridium oxide nanoparticles projects. Thanks to Dr. Giulio Rosati for his kindness and friendship, hoping to collaborate in a near future. And finally, a special mention to Dr. Dag Bremnes, who sadly passed away last year; your memory will not be forgotten; thank you for everything you taught me about imaging and data treatment.

Thanks to the Electron Microscopy Unit in ICN2, Belén Ballesteros, Marcos Rosado, Elzbieta Pach and Francisco Javier Belarre, for all their support and patience during these years. Also thanks to Javiez Saiz, from ICN2 Instrumental Core Research Facilities, and to Juan Luis Marte, ICP-MS technician.

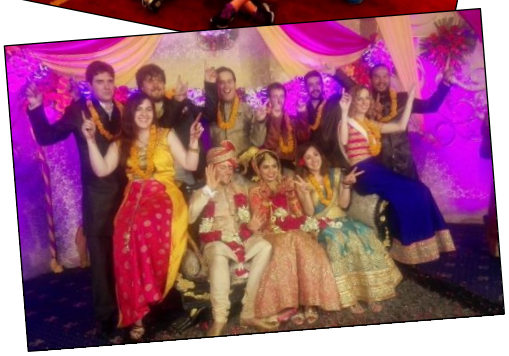

I'm thankfull for all the people I've meet in Nanobioelectronics and Biosensors group. I want to start with the people I met when I was an undergraduate student (forgive me if I forget someone): Deniz, Hassan, Anna F., Lenka, Serdar, Jihane, Yuki, Adaris, Maria, Claudio, Ali, Gisele, Sevinç, Mariana, Wissem, Moneim, Amal, Charlene, Flavio, Marisol, Carmen, Miquel, Alex Ch., Helena, Sandrine, Briza, Edén and Luis. Thank you all for the moments we spent together. Now, the people who came to the group while my master thesis: Andrzej, Jędrzej, Houda, Loubna, Thiago, Giulia, Alessandra, Gravagnoulo, Dun-Wein, Natalia, Hamed, Tina, Peng, Jarinya, Livia, Fabio, Erhan, Daniel H., Oana, Veronika, Victor, David, Marta, Misha, Patricia and Wiyogo. Thanks to all of you! And special thanks to Alessandra and Wiyogo with whom I spent many hours working together in our projects. And, in case the list didn't seem long enough, here comes the people I've meet during the PhD: Robert, Héctor, Hoda, Abdellatif, Ichrak, MªÁngeles, Recep, Esma, Luiza, Jahir, Ruslán, Irene, Antoni, Dalia, Monica, Margherita, Marialuisa, Aida, Juan, Christian, Pablo, Emma, Nopchulee, Dee, Águeda, Gelo, Julio, Petr, Gina, Denise, Alba, Javi, Adrià, Andrea, Sonia, Maddalena, Marc Bo., Marc Ba., Müller, Bernardo, Celia, Carla, Karla, Aleksandra, Xinyi, Lei, Qiuyue, Lorenzo, Bhawna, Mohga, Niloufar, Golay, Caterina, Anna T., José Fran, Enric, Amadeo, Carme, Marta, Jiri, Somayeh, Emily, Mohammad, Sabba, Jülide and the Graphenica Team, Carlos and Laura. Thank you all!! Andrea, you were my first student and I'm glad we met again when you came

back for your TFG; keep your motivation and you'll be a great scientist. Héctor, I'll never forget the days I spent with you and your strong passion, keep it and you'll go far (if you lose your fear to fly, it will be literally far). Gelo, if you read this, remember our promise, we should finish together the PhD this year! Bhawna, Lorenzo, Carme and Mohga, your thesis are the next so I wish you all the best and good luck, "our generation" is ending so thank you for sharing these years with me! José Fran, I keep really good memories from when we worked together doing lateral flow strips with real blood, I learnt a lot of "bio" things from you and spent many good moments together, thank you!! Amadeo, I also enjoyed working with you, your motivation pushed the experiments I thought that never would work and succeed, keep that motivation always with and thank you for all the funny moments. Enric, now you'll carry the flame of the new PhD generation, I know it may be hard sometimes, but you have the capacity of being constant and never give up, you are an inspiring person and I know you'll keep the flames sparkling. Irene, you were one of the craziest and funniest office mates I ever had, thank you for all these moments and memories! Marc, the lab would be in chaos without you!!! You are an important piece in the group and I'm thankful for all the help you gave me. Jahir and Luiza, thank you for sharing your hints, wisdom and friendship with me, I really learnt a lot from your advices about the scientist world. Ruslán, my office mate!! It means a lot for me having you in the same office, I learnt a lot from your experience, your ideas, your way of thinking, your tips and we had funny moments too. Without your support and companionship I would have lost sanity and common sense during last year.

There are still two people from the group that I have not mentioned yet because I want to give them a very special acknowledgement. Anna Puig, a really essential pillar in our

group. In brief, everything works in the group because of Anna. Thank you for all these years and for the tremendous patience you had with me (e.g. “Anna, I want to buy this…”, “Anna I don’t know how to fill this…”, “Anna I’ve lost that paper…”, “Anna I forgot to ask that other paper…”, etc.) Anna, thank you very much for everything!! The other person is Alex Zamora, we met twelve years ago and we did together the career, the lab practices, many courses, the master and the PhD. We have gone through lots of adventures and we have thousands of anecdotes to tell. Alex, thank you for your friendship and for being there all these years, with you the hard moments became small!

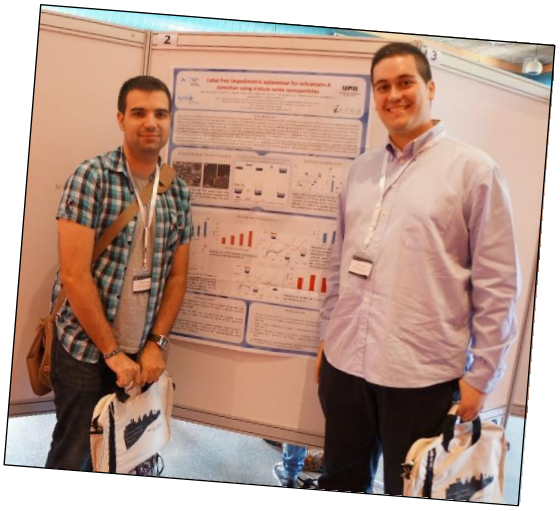

I’m not finished yet with ICN2. Besides the people from my group and the people which I’ve collaborated, I’ve meet a lot of people who I would also acknowledge: Yegraf, Anna, Alba, Roque, Bogdan, Aron, Jordi, Javier, Tania, Laura, Igor, Cristina, Núria, Patricia, Denise, Laura, Anabel, Loïs, Rocío, Antonio, Carlos, Daniel, Li, Yang, Jan, Gerard, Jorge, Sweeta, Javi, Sam, Jesús, Rafa, Xavi, Ainhoa, Nadia and… sorry because probably I’m forgetting many names!! Thank you all!!! Some special thanks to Anabel Rodríguez, because your happy spirit spreads around all ICN2; José Pérez, for your efforts teaching us to be safe; IT department, for keeping my computer working while writing thesis; Pau París, Xavier Ros and the maintenance team, Ismael and Dani, for always being quickly there; the Marketing & Communication department, Àlex Argemí, Ana de la Osa, Rachel Spencer and Dámaso Torres, for all the work you do and for giving me the chance to participate in many constructive activities; again, Dámaso for the designs of the figures for the manuscript; and finally the people from reception,

Laura, Marta, Luis and Alberto, because you are the first persons who I say good morning every day.

Now, to all my friends from Chemistry. I know you opened this thesis and went direclty to this section. “Oh, where we are?” “Oh, almost at the end?” Yes, I know I could have mentioned you before, maybe when I mentioned Alex, but you know that I like to make you suffer a bit. Núria, Ana, Marta, Javi, Dani, Mª Àngels, Alberto, Susana, Berta, Edu, Eva, Sara, César, Arnau and Gina, my dear friends, thank you for all these years of friendship. Núria, thank you for always being there, for your advices and your empathy. Ana, thank you for being as you are, for your happiness, your craziness and your non-sense. Marta, I know that you are not understanding what is written, that you will ask someone else to translate it, and whoever is translating it please, tease her for a while and then tell her that I acknowledge all the funny moments we have spent together. Dani, you are the almost rational mind in this group full of extremely crazy people, without you I don’t know where we will be… Mª Àngels, you are the party spirit in the group, your joyfulness motivates us all; next is your turn for PhD, you can!!

I can’t forget to acknowledge my family. To my parents, who have always been there, all these years, who never gave up on me, a child that one day decided that wanted to be a scientist and they always supported me in that dream. Thank you. Also, special message to my little cousin Bruno who has decided also to get in this world of science. I wish you all the best and no matter how difficult the path may look, never give up.

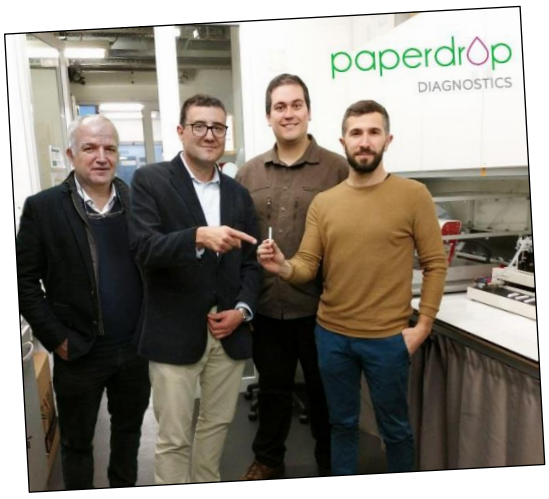

Almost at the end of my acknowledgements, I would like to thank the Paperdrop Diagnostics team, Dr. Marc Gallegos and Dr. Ángel Alonso. Not at the end of the acknowledgements for being less important, rather as a symbolism. My PhD is ending and a now, with Paperdrop, a new stage starts. Thank you for all your support, for believing in me

and for this great opportunity. Also, I would thank to all the “spin-off accelerators” and programmes in which I’ve been able to participate: EMPENTA, Ship2B and Barcelona Activa. Special thanks to Nadia Pons, from ICN2, for the support and counselling given.

Also I would like to thank George R. R. Martin and Patrick Rothfuss, my two favourite sci-fi writers. Before joining ICN2 I was waiting for their new books, “The Winds of Winter” and “The Doors of Stone”. I’ve done a master, I’ve written a thesis and I’m going to finish my PhD and yet the books have not been released. I can only say thank you. Every time I was writing a review, a manuscript or this thesis and I felt slow-writing, I thought of you and I felt better “meh, I’m not so slow”. Thank you.

Finally, to conclude this section, I would like to thank the reader, especially if you read until that point, if you took the time to read all the acknowledgements I wrote so that the names of those people that matter to me are present in this work. Whoever you are, part of my thesis jury or a student seeking knowledge in my “memories”, my most sincere gratitude. I hope you’ll enjoy reading!

ACKNOWLEDGEMENTS FOR FINANCIAL AND LOGISTIC SUPPORT

AEC	3-amino-9-ethylcarbazole
AFM	atomic force microscopy
AgNPs	silver nanoparticles
“AND”	logic gate “and”
AR	augmented reality
AuNPs	gold nanoparticles
BDE-47	3,3',4,4'-tetrabromodiphenyl ether
BSA	bovine serum albumin
BB	borate buffer
CL	control line
CNF	cellulose nano-fibers
CNPs	carbon nanoparticles
CNTs	carbon nanotubes
DCP	2,9-dicarboxyl-1,10-phenanthroline
DCT	diagnostic and communication technology
DNA	deoxyribonucleic acid
EDTA	ethylenediaminetetraacetic acid
ELISA	enzyme-linked immunosorbent assay
EPA	U.S. Environmental Protection Agency
et al.	*et alia* (and others)
Fig.	figure
GMR	giant magnetoresistive sensor
GO	graphene oxide
HBS	HEPES-buffered saline
HEPES	4-(2-hydroxyethyl)-1-piperazineethanesulfonic acid
HIgG	human immunoglobuline
HIV	human immunodeficiency virus
HRP	horseradish peroxidase
ICP-MS	inductively coupled plasma mass spectrometry

IgG	immunoglobulin
“INH”	logic gate “two-input inhibit”
IrO_2 NPs	iridium oxide (IV) nanoparticles
ITO	indium tin oxide
K_d	equilibrium dissociation constant
LBs	latex beads
LED	light-emitting diode
LFBs	lateral flow biosensor/s
LFs	lateral flow strip/s
LOD	limit of detection
MARs	magnetic assay readers
MBs	magnetic beads
MNPs	magnetic nanoparticles
NFC	near-field communication
NMR	nuclear magnetic resonance
“OR”	logic gate “or”
OVA	ovalbumin
PB	phosphate buffer non-saline
PBS	phosphate buffer saline
PC	photonic crystals
PET	polyethylene terephalate
PoC	point-of-care
PBDE	Polybrominated diphenyl ether
QDs	quantum dots
QR	quick response (code)
r	correlation coefficient
RGB	red, green and blue
SDS	sodium dodecyl sulfate
SEM	scanning electron microscopy
SERS	surface-enhanced Raman scattering
SPCE	screen printed carbon electrode

SWCNTs	single-walled carbon nanotubes
TEM	transmission electron microscopy
TL	test line
TMB	3,3’,5,5’-tetramethylbenzidine
UCPs	up-converting phosphor reporters
UV	ultraviolet
U(VI)	uranium (VI), UO_2^{2+} ion
WHO	World Health Organization
WOR	water oxidation reaction
0D	0-dimensional
1D	1-dimensional
12F6	antibody clone nº12F6
2D	2-dimensional
3D	3-dimensional

TABLE OF CONTENTS

THESIS OVERVIEW

Fig. 0.1. Lateral flow device. From left to right: 3D-printed cassette, lateral flow strip in a 3D-printed cassette and a single lateral flow strip.

Lateral flow biosensors (Fig. 0.1) are paper-based devices of high relevance in point-of-care diagnostics and environmental monitoring. In the recent years, many publications in regard to this topic have been published. Some authors exhibit **new applications** for lateral flow strips, detecting new analytes or molecules. Other authors focus on **new signal enhancement strategies**, applying label modifications or novel designs. And there is a third group seeking for **new signal recognition methods**, more sensitive than naked-eye response or just more simple for the final user. It is the goal of this research to reach these three objectives, give a **new application** to lateral flow strips, find a **new signal enhancement strategy** and propose a **new signal recognition method**. To fulfil these objectives the properties of nanomaterials will be explored and taken in consideration.

This thesis is divided in five chapters followed by a general conclusions section. A brief explanation of each chapter is given below:

Chapter 1. Introduction. An overview of the state-of-the-art regarding the use of nanomaterials in different point-of-care tools, among which are lateral flow biosensors, is given. First, classification of different nanomaterials according their shape or “dimensions” and the most relevant reported works is described. This is followed by discussion of various examples of nanomaterial-based lateral flow assays. Finally, some examples about the integration of lateral flow devices in real world applications are discussed. This first chapter is based in the published review works (Fig. 0.2).

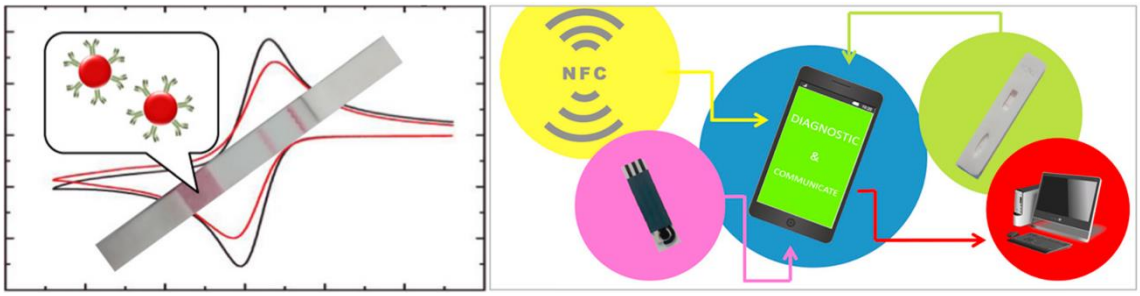

Fig. 0.2. Graphical abstracts of the published works:
Quesada-González, D. & Merkoçi, A. "Nanoparticle-based lateral flow biosensors". *Biosens. Bioelectron.* **73**, 47–63 (2015).
Quesada-González, D. & Merkoçi, A. "Mobile phone–based biosensing: an emerging 'diagnostic and communication' technology". *Biosens. Bioelectron*. **92**, 549–562 (2016).

Chapter 2. Objectives of the thesis. This chapter briefly describes the objectives that motivated and conducted this work.

Chapter 3. U(VI) detection using a gold nanoparticle/paper-based lateral flow device. In this chapter is shown a **new application** for lateral flow strips. For the first time, it is reported the detection of uranium in groundwater, tested on real samples, using lateral flow strips. This is the first equipment-free and selective uranium detection method since the current ones are laboratory-based (e.g. ICP-MS) or, if they are portable, they are not selective (e.g. radioactivity detectors).

Fig. 0.3. Iridium oxide (IV) nanoparticles-based lateral flow strips, first time reported in this thesis work.

Chapter 4. Signal enhancement in lateral flow tests by using cellulose nanofibers. Cellulose nanofibers are introduced onto nitrocellulose membrane (the material from which is made the detection zone on lateral flow strips) to increase the probability of stopping gold nanoparticles only in the case of positive samples. Thus, in this chapter it is reported a **new signal enhancement strategy** for lateral flow biosensors.

Chapter 5. Iridium oxide (IV) nanoparticle-based lateral flow immunoassay. This chapter includes two works related to each other. First, the electrocatalytical properties of iridium oxide (IV) nanoparticles are tested following a competitive strategy to detect 3,3',4,4'-tetrabromodiphenyl ether, a marine water contaminant of interest nowadays due its toxicity and stability. Secondly, the nanoparticles are integrated on lateral flow strips for the optical detection of a model protein (Fig. 0.3). Although this objective was not reached during this thesis, the combination of both works could lead to **new signal recognition method** based on the electrochemical detection of iridium oxide (IV) nanoparticles on lateral flow strips.

General conclusions. Summary of objectives achieved, conclusion remarks, future perspectives and work to be done are given in this section.

CHAPTER 1

Introduction

The advancements made on medicine in the last years have been impressive. However, diseases not detected on time or not properly monitored are still the main causes of death in today's society. Ischemic heart diseases, respiratory infections, diabetes or bacterial infections as tuberculosis or diarrheal diseases are some of the examples that cause more deaths around the world but, if detected on time, could be prevented.

We have the potential technologies and the tools to detect all of them, therefore, why so many people are still dying due to these diseases? Probably the main reasons are two. First the lack of equipment, especially in development countries where the costs are not affordable for all the population or even for the medical centers. Second, the time frame between the moment when the symptoms are appreciable by the patient and the time when diagnostic is accomplished by the specialist. How could these problems be solved? May we have a doctor anywhere for a single patient, ready at any time, accurate and fast, or is this a

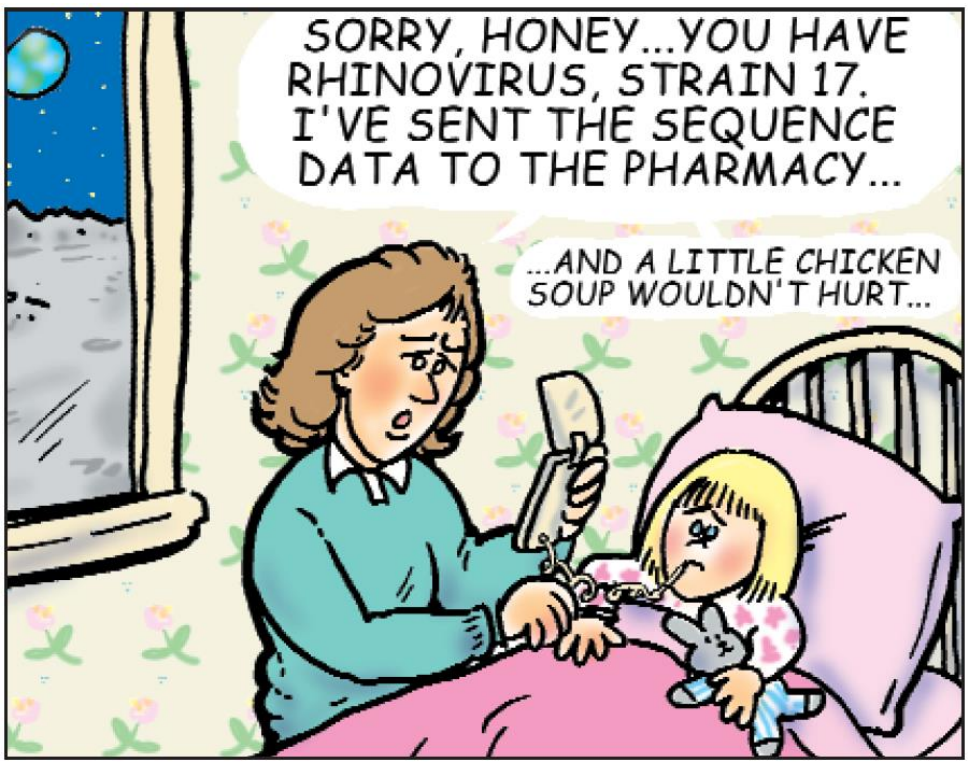

Fig. 1.1. Caricature illustrating the simplicity expected from a PoC. Reprinted with permission from ref. 1, Copyright 2002 American Association for the Advancement of Science (AAAS).

utopia? Now, instead of having a real doctor imagine having a little device, portable and easy-to-use, able to monitor several parameters and variables, like a portable laboratory[1]. With all the data collected this tiny device could decide in few minutes either by itself or by an immediate communication with a specialist/medical doctor, which action is required by the patient being everything done at home or even in the field, without requiring any kind of medical knowledge by the user. This "futuristic" idea is exemplified in Fig.1.1: a mother is using a portable device to diagnose what virus has her daughter, send the data to the pharmacy and conclude that some chicken soup may make the child feel better (no need for any medication at all).

Nowadays some portable devices able to monitor and diagnose the condition of the user are already available. A well-known example is the glucose meter that, with few microliters of blood, is able to determine the glucose concentration in the sample and notify the diabetes patient if there is any action required as the injection of insulin or the intake of food.

It is noteworthy the capabilities of mobile phones to carry out these type of tasks[2] given the huge amount of population that has, at least, one mobile phone and the tools that these devices include as cameras, light sensors, power sources, movement detectors and wireless connection among others (and more to appear in the future). Some parts of a mobile phone as the camera[3], the light sensor[4] or even the NFC (near-field communication) antenna[5] can be used to monitor different variables in nanomaterials-based platforms with interest for future diagnostics. In fact, the power of current mobile phones, also called smartphones, is far beyond that of the computer that controlled Apollo 11, first rocket landing on the Moon[6]. That computer had a processing unit of 1 MHz and an internal memory of roughly 4 kB. In comparison, the processing speed of an iPhone X is about 2.5 GHz and its storage capacity is 256 Gb. This means that, today, anyone can carry in their pockets 64 million times more information, and access it 2,500 times faster, than could the Apollo 11 crew.

1.1. Point-of-Care tests

Devices able to perform fast analysis and accurate diagnostics near the patient care are known as "bedside" or "point-of-care" (PoC) tests[7]. The ideal PoC test should be user-friendly and as simple as possible so that any user, even without any type of medical or

laboratory knowledge, will be able to use it and understand its response (as shown in the example of Fig. 1.1). Also, low-cost is an important and desirable quality of PoC to ensure that the device is easy to be acquired by everyone and anywhere. Because of this, one of the most popular materials employed as substrate for PoC devices is paper[8–12], which is cheap, abundant, recyclable and biosustainable. Other qualities that PoC test should have are robustness (the capacity to withstand changes on environmental conditions), selectivity (the ability to respond to a unique analyte or parameter, not to be affected by interferences) and sensitivity (the quality to discriminate between similar values).

There exist different methodologies to produce the signal on PoC devices (or in any other type of sensor and biosensor) and in most of the cases the chosen methodology will depend on the transducer employed. Optical and electrochemical-based PoC devices are probably the most popular, as they are the examples of pregnancy test and glucose meter respectively. With the emerging of nanotechnology both kind of devices are taking advantages of nanomaterials integrating these in different parts of existing sensing platforms or offering quite innovative detection systems.

1.2. Nanomaterials for Point-of-Care

Regarding the transducer, synthetic nanomaterials (with a diameter between 1 and 100 nm) offer a wide range of possibilities due to their size, shape and properties as can be biocompatibility, fluorescence, electrical and thermal conductivity, magnetism, etc. Nanomaterials can be classified according to their shape as: “0D” (spherical nanomaterials), “1D” (e.g. nanotubes, nanowires), “2D” (e.g. graphene or other well-known 2D materials), 3D (e.g. nanoprisms, nanoflowers etc.)[13]. In the following sections POC based on different kinds of nanomaterials and their advantages and drawbacks during applications in diagnostics will be reviewed.

1.2.1. Spherical nanomaterials (0D)

The most widely used nanomaterials are spherical ones, owing to their simple preparation and manipulation. When a spherical nanoparticle is attached to a biomarker, a molecule that reacts only under specific pathological conditions, the resulting functionalized nanosphere can serve as a biological label and, for instance, to signal the presence of a given analyte or pathogen. The detection mechanisms for such nanoparticles can be quite diverse[14]:

measuring the light absorption of the nanoparticles when attached to the analyte (after a cleaning step), measuring the shift of peak wavelength due to the agglomeration of the nanoparticles, enhancement by secondary enzymatic reactions onto nanoparticles surface, by a quenching effect (an intensity decrease of a fluorescent signal), surface plasmon resonance (optical changes and radiative enhancements on a nanomaterial due to disturbance of the dielectric constant induced by the adsorption of a molecule), electrical or electrochemical changes (when the nanomaterial is conductive or can catalyse a reaction that is electrochemically detectable), electrical impedance spectroscopy (changes on the electrical resistance of a medium), etc.

Among all the 0D nanomaterials, gold nanoparticles (AuNPs) have been highly reported and discussed[15]. This nanomaterial stands out due to its high bioaffinity, strong colour (whose wavelength varies with small changes on its diameter or its surface) and even catalytic properties, thus it is commonly used for both optical and electrochemical PoC devices.

1.2.1.1. 0D optical-based PoC devices

Lateral flow biosensors (LFBs)[10] are optical-based PoC devices fabricated on paper substrates. Among the best-known examples are common the pregnancy tests. LFBs evolved from thin-layer immunoaffinity chromatography[16], a method based on the formation of a "sandwich" comprising a primary biomarker (often an antibody) attached onto the paper substrate (cellulose or, to favor the attachment of the biomarkers, nitrocellulose), an analyte (proteins, cells, bacteria, molecules or even heavy metals) and a secondary biomarker, which is conjugated to the tag nanoparticle. The formation of this sandwich triggers the appearance of colour in the "test zone" (where the first biomarker has been deposited) for the positive sample and, if the sandwich is not assembled (lack of analyte in the sample), the test zone remains colourless (a negative sample). Latex beads were commonly used on LFBs and still are used, for most commercial pregnancy tests. However, the inclusion of AuNPs on LFBs[17], among other nanomaterials, improved the sensitivity of the method because of the strong colour of the nanomaterial which is due to the surface plasmon resonance effect, present in metallic nanoparticles but not on latex beads. Furthermore, the shrinking of the label size down to the nanoscale eases the flow and boosts the label/analyte ratio. These improvements enabled semi-quantitative assays, relating the color intensity with the analyte

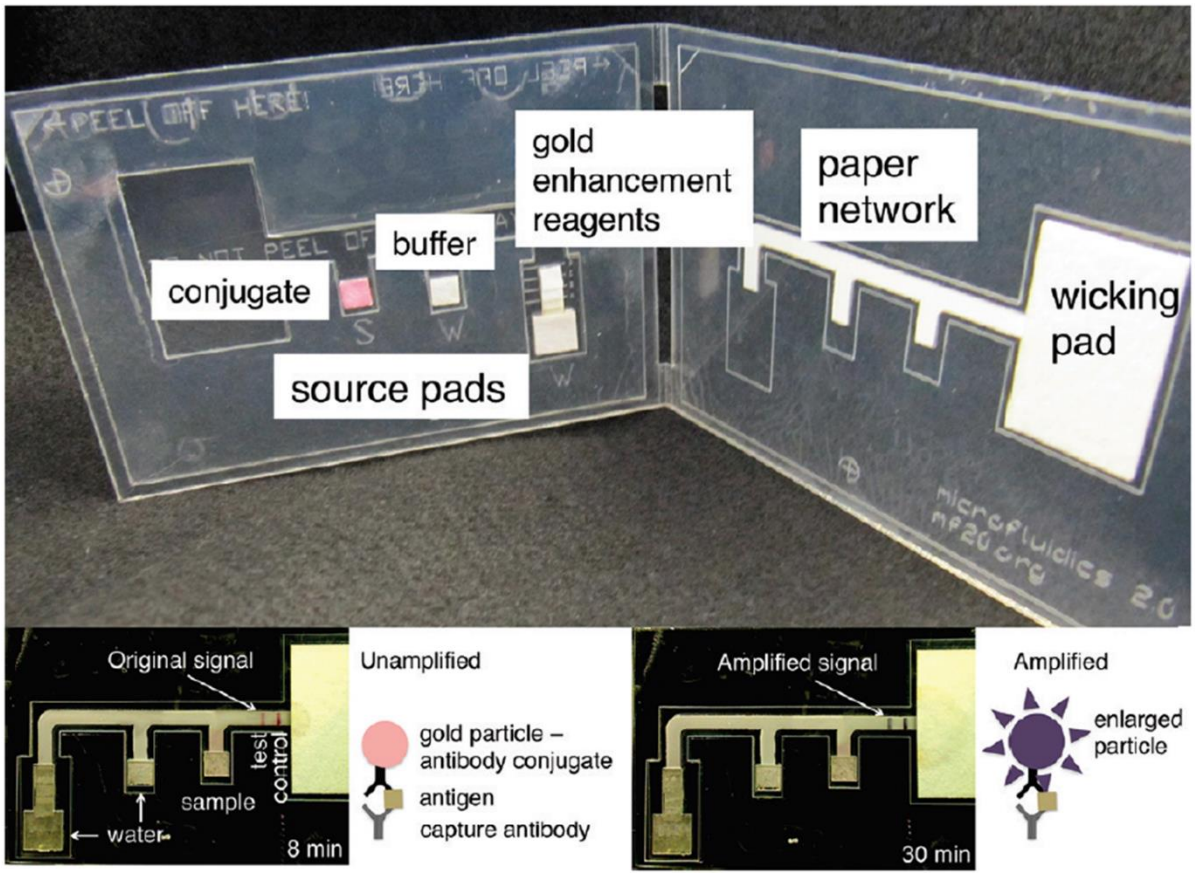

Fig. 1.2. PoC colorimetric device in which the signal of a LFBs system is increased by means of a paper network consisting on paper pads storing colour enhancement reagent. Adapted with permission from ref. 22, copyright 2012 American Chemical Society.

concentration, similarly as with a pH paper. By using a colorimetric reader or even a mobile phone[2] the quantification level can be improved.

Besides AuNPs, other nanomaterials as silver nanoparticles (AgNPs) have been used in LFBs; the wavelength variations provoked by size and shape modifications are bigger with AgNPs than with AuNPs, leading to color tonalities quite different between nanoparticles with less than 10 nm of difference in size. Thus, AgNPs permit the performance of multiplexed tests[18] (i.e. for the simultaneous detection of different analytes on the same device), in which a different colour is obtained in each test zone. Also fluorescent nanoparticles, like quantum dots[19] (QDs) or up-converting phosphor reporters[20,21] (UCPs; although these are expensive, since they are made using rare elements such as europium or yttrium), are making their way on LFBs. Fluorescent nanoparticles lead to greater sensitivity and specificity than do non-fluorescent nanomaterials, since in fluorescence methods only the signal coming from the

nanomaterial is read. However, the response cannot be observed by the naked eye: they always require equipment to excite and read the resulting fluorescence signal.

There exist various signal enhancement strategies for nanoparticles on paper substrate[9–11], however they often require the user to apply several additional steps, making the PoC system less user-friendly increasing the human error factor. A way to simplify these steps was reported by Fu *et al.*[22]. They present a two-dimensional paper network combining LFBs with other paper pads used for storing enhancement reagents (as shown in Fig. 1.2). In this PoC system, the user must add the sample to the conjugate pad, on which the analyte is captured by AuNPs, and water to the other pads and then close the system. At first, it works like a conventional LFB strip, AuNPs stop in the detection zone, but once the enhancement reagents reach the detection zone the colour of the AuNPs changes to dark purple as their size increases. Against the white background, dark purple grants a higher contrast compared to the original red. The limit of detection (LOD) achieved with this enhancement strategy was

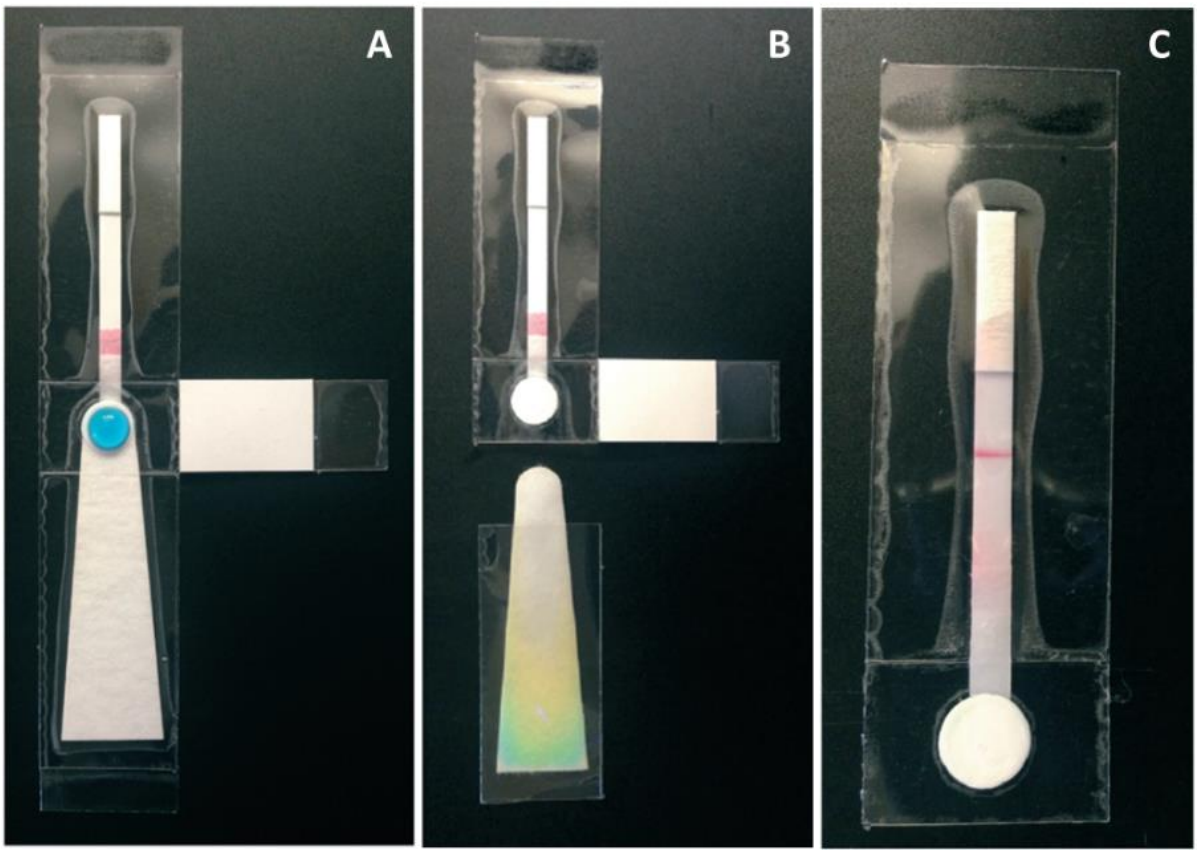

Fig. 1.3. LFBs system to extract, amplify and detect nucleic acids: (A) sample is added on sample port, (B) absorbent pad is removed after washing steps, (C) after the addition of amplification reagents, purified analytes flow across the LFBs. Adapted with permission from ref. 23, copyright 2016 Royal Society of Chemistry.

four times lower than with standard LFBs. Rodriguez *et al.*[23] also propose an interesting LFBs able to isolate, amplify and detect nucleic acids, all-in-one, equipment-free and much faster than conventional methods. Their system comprises a LFs equipped with some additional removable parts (Fig. 1.3): a pad for washing the sample but retaining the purified DNA (Fig. 1.3A); a tab to prevent evaporation of isothermal amplification reagents (Fig. 1.3B); and some hydrophobic tape barriers to prevent DNA and other solvents from flowing prematurely to the LFs (Fig. 1.3C). Besides strips format, other possibilities to store nanomaterials on paper are reported, but with the same signalling mechanism as on previous mentioned immunoassays. One example is the prototype proposed by Pauli *et al.*[24], a lab-on-a-syringe used to collect urine and pump it to paper pads stored in serially connected cartridges. The first cartridge contains AuNPs for the capture of the analyte, a cancer biomarker, and the second one the detection pad. The detection pad consists on nitrocellulose paper with detection antibodies inside a wax ring to focus the flow to pass through the antibodies. As on AuNPs-based LFBs, the inner part of the ring will turn more reddish as higher the amount of analyte is. Contrary to LFBs, the lab-on-a-syringe requires the user to control the flow, being it less user-friendly than a paper strip, however it permits modifying the incubation times for AuNPs with analyte, which can lead to improved sensitivities. Also, a filter can be coupled to the syringe in order to reduce matrix effects.

It is also remarkable the application of nanopaper, also known as bacteria cellulose paper as it is produced by bacteria. As reported by Morales-Narváez *et al.*[25], 0D nanoparticles can be stored and even produced on this colorless substrate resulting in a plasmonic or fluorescent paper with great potential as an alternative to enzyme-linked immunosorbent assay (ELISA) plates. This work demonstrates that PoC devices fabricated with nanopaper can take other forms besides ELISA plates as they are cuvettes or simple spots on a piece of paper. Plasmonic resonance, fluorescence and quenching effects are some of the measurements that can be done these systems by using nanomaterials as AgNPs, AuNPs or QDs. Similarly to nanopaper, hydrogel can be used to store nanomaterials for their use in PoC applications as Yetisen *et al.*[26] did with AgNPs and a phenylboronic acid-functionalized hydrogel. Their system can filter urine samples retaining glucose. Then, a laser can measure within five minutes the diffraction provoked by the interaction of AgNPs and glucose. Surprisingly the system is reusable, unlike paper-based systems.

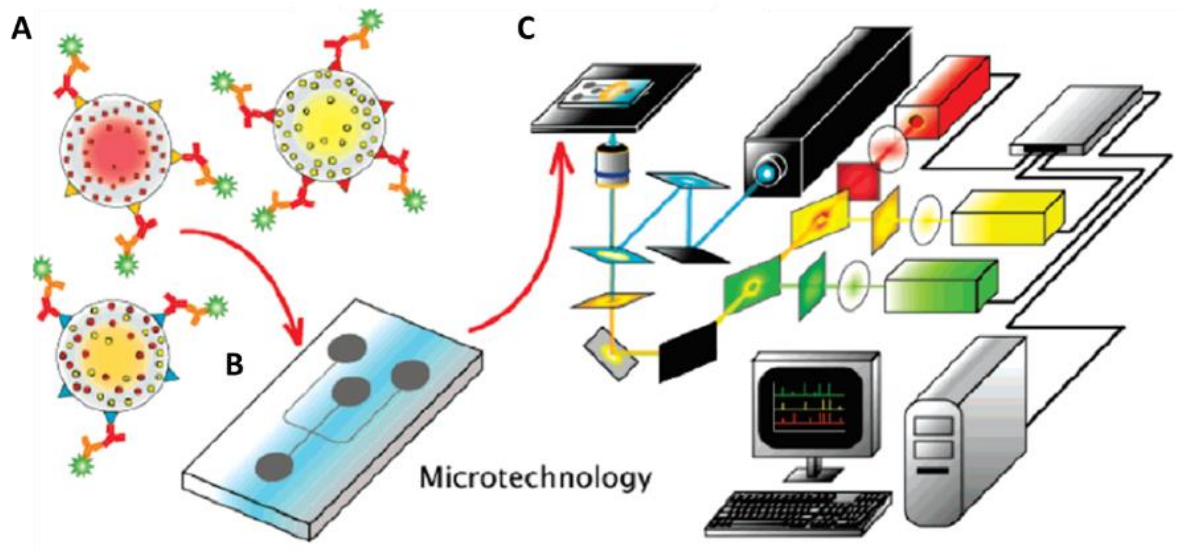

Fig. 1.4. Multiplexed barcode system including QDs: (A) QDs of different colours encapsulated into microbeads with specific biomarkers for different targets, (B) microfluidics system and (C) detection platform. Adapted with permission from ref. 27, copyright 2007 American Chemical Society.

As previously mentioned, QDs are small 0D nanomaterials with fluorescent properties. Klostranec *et al.*[27] took advantage of the intense signal of QDs to construct a multiplex system able to detect different blood infectious diseases related targets by using a "barcode" system (Fig. 1.4). Different colored QDs were encapsulated into microbeads (Fig. 1.4A), each bead being conjugated with antibodies specific to a different target, and the particles then were mixed inside a microfluidic system (Fig. 1.4B) with the sample. The incubation inside the microfluidics was controlled electrokinetically. Data collection was performed with a software and a detection platform (Fig. 1.4C) which as claimed by authors could be miniaturized for PoC diagnosis in the future was developed. Their platform can identify independently the wavelength of each QDs type, normalize it and, like a barcode reading, estimate the amount of each target.

Another interesting work involving QDs was reported by Álvarez-Diduk *et al.*[3]. As shown in Fig. 1.5 they took advantage of the fluorescence quenching effect occurred on graphene QDs in presence of some polyphenolic compounds (Fig. 1.5A). They fabricated a 3D-printed dark chamber (Fig. 1.5B) including an UV LED (ultraviolet light-emitting diode) powered by a mobile phone to excite the QDs (Fig. 1.5D). Using wax-printed traced spots onto a paper strip, QDs were physisorpted inside the spots obtaining an ELISA plate-like system (Fig. 1.5C). When the polyphenolic compounds are dropped onto the spots, fluorescence is

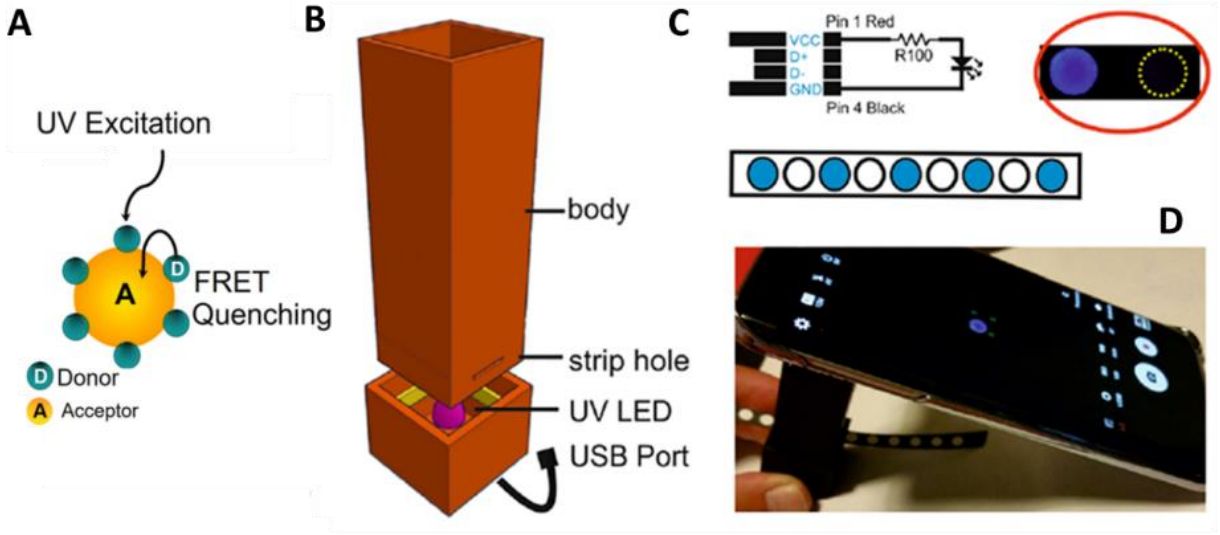

Fig. 1.5. Mobile phone integrated PoC system: (A) graphene QDs are quenched in presence of acceptor compounds, (B) 3D-printed device with UV LED, (C) LED mechanism and paper substrate containing dried graphene QDs, (D) mobile phone measuring the quenching of QDs. Adapted with permission from ref. 3, copyright 2017 Nature Publishing Group.

quenched and captured by the mobile phone camera (Fig. 1.5D). The images can be analyzed directly on the mobile phone, with an app, or later with computer software.

1.2.1.2. 0D electrochemical-based PoC devices

Electrochemical measurements allow to identify electrical phenomena related to a chemical change. The function of nanomaterials in this kind of measurements is not limited to analyte labelling only. Nowadays nanoparticles are commonly used in commercial inks for fabrication of electrodes. 0D nanomaterials as AuNPs or AgNPs and 1D nanomaterials as carbon nanotubes (CNTs) are the most common ones. As an example, in the work of da Silva *et al.*[28] they used commercial AgNPs to fabricate a miniaturized and portable Ag/AgCl reference electrode, of known and stable potential. They printed the electrode on two different flexible substrates, paper and polyethylene terephthalate (PET), using a high resolution piezoelectric inkjet materials printer (Fig. 1.6A). Once printed, AgNPs ink was cured at 120ºC and treated with bleach (sodium hypochlorite, NaClO) to produce the Ag/AgCl mixture to serve as pseudo reference electrode.

Silver reduction reaction is catalysed by the presence of AuNPs which in turn given their high affinity to biological molecules are extensively reported as transducers in electrochemical assays[29]. Another reaction which is often applied in electrochemistry and

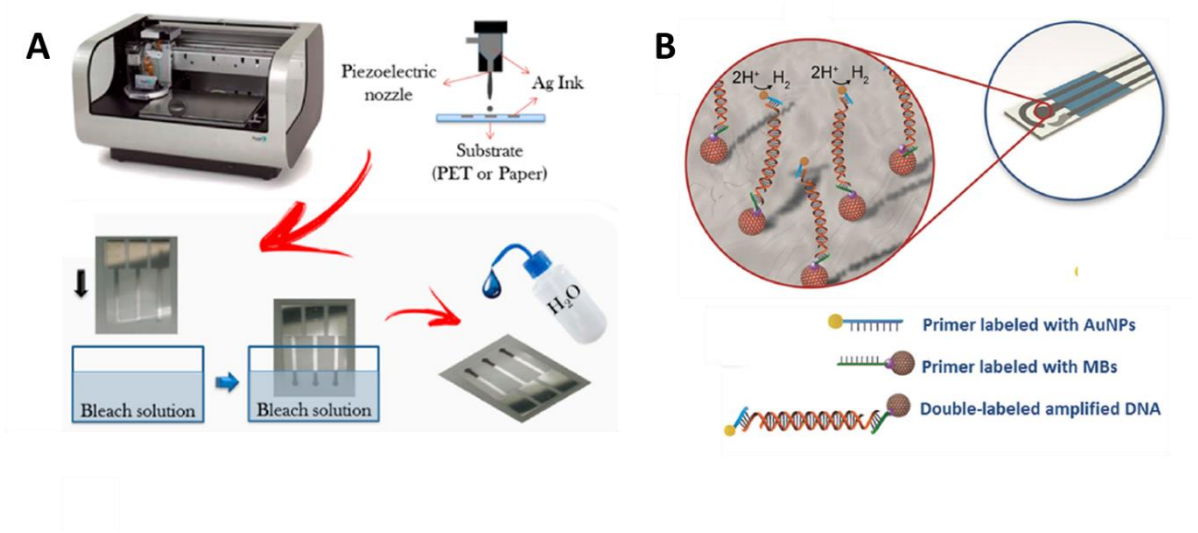

Fig. 1.6. (A) Ag/AgCl reference electrodes fabricated from AgNPs using inkjet technology and bleach treatment. Adapted with permission from ref. 28, copyright 2014 American Chemical Society. (B) Combination of AuNPs and MBs for the detection of DNA on a SPCE. Adapted with permission from ref 30, copyright 2015 John Wiley and Sons.

catalysed by AuNPs is the hydrogen evolution reaction, the formation of H_2 gas by the reduction of H^+ ions. This reaction was measured by de la Escosura-Muñiz *et al.*[30] who, combining DNA amplification strategies, magnetic beads (MBs) and AuNPs, developed a system on screen printed carbon electrodes (SPCE) that discriminates dog DNA from Leishmania parasite DNA, hosted inside the cells. MBs and AuNPs are linked to the amplified DNA and, using a magnet, the conjugate is placed onto the working electrode of the SPCE so the signal can be measured efficiently (Fig. 1.6B). Iridium oxide nanoparticles (IrO_2 NPs) are other 0D nanomaterials used due to their catalytic properties towards water oxidation reaction[31,32], the production of oxygen from water, and their application in impedimetric sensors[33,34]. Impedance is a technique used to measure frequency changes on the dielectric medium close to the nanoparticles. So, by binding biomarkers on IrO_2NPs it is possible to detect variations on the conductivity of the medium depending on capturing of a biomarker to a target analyte.

Regarding AuNPs-based LFBs, in analogy to optical detection, some researchers are trying to integrate electrochemical sensing strategies into the paper strips to achieve lower detection limits and higher sensitivity in comparison to colorimetric lecture[35]. However, to do that it is necessary to cut the detection zone of the strips and dissolve it with acid, so the detection is performed with external electrodes on the dissolved nanoparticles. The addition

of this extra step enhances the quantification on LFBs but the methodology still needs to be improved either by including the step into an automated PoC device or by finding an alternative to dissolve a part of the strip. A more user-friendly paper-based PoC tool was designed by Wu *et al.*[36] which permits the electrochemical analysis of eight samples sequentially (Fig. 1.7A). This device comprises eight electrodes pre-treated with antibodies specific to the target analyte. The samples are added to the electrodes and then, SiO_2 nanoparticles are dispensed on the electrodes (note that SiO_2 nanoparticles are inexpensive and easy to load with various compounds such as dyes, proteins or enzymes). In this case, the SiO_2 nanoparticles are loaded with antibodies specific to the analyte, to perform a sandwich assay, and with horseradish peroxidase, the enzyme that triggers the electrochemical reaction. The electrodes are washed and then a reactive solution is added to the core of the device, from where it then flows to the electrodes, thereby activating the electrochemical reaction. Another interesting paper PoC device was made by Cunningham *et al.*[37], an origami-styled system that, as proof-of-concept, was used for detection of AgNPs by oxidizing them using a gold-made working electrode. The device consists of four folded paper layers (Fig. 1.7B): first layer containing electrodes, inlet and outlet; second and third layers containing a paper circuit delimited by wax and a blue dye that works as indicator of the stoppage of the flow; and the forth layer which contains a "sink" to redirect all the flow there.

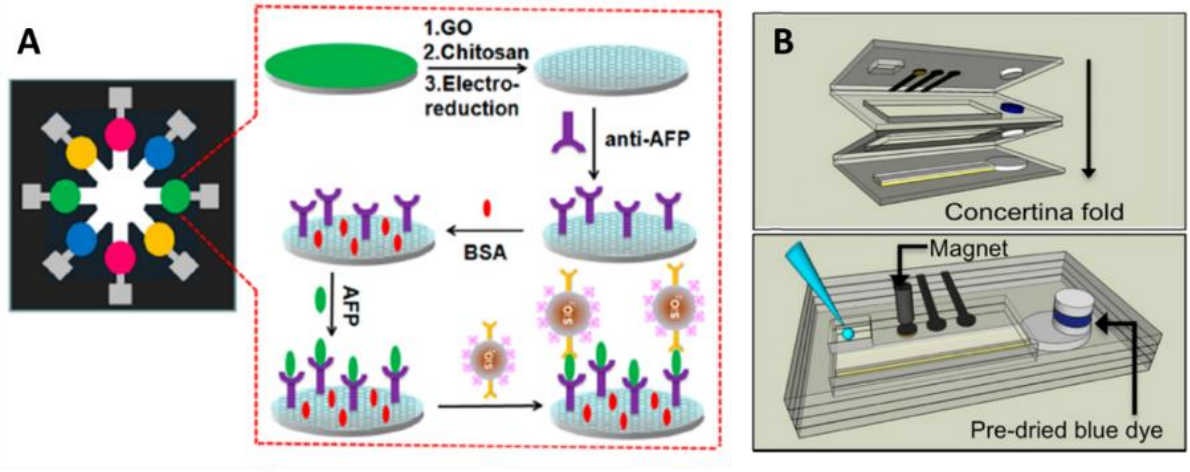

Fig. 1.7. (A) Paper PoC device for the electrochemical measurement of eight samples. Adapted with permission from ref. 36, copyright 2013 American Chemical Society. (B) Paper origami PoC for the electrochemical detection of AgNPs. Unfolded (up) and folded (down). Adapted with permission from ref. 37, copyright 2016 American Chemical Society.

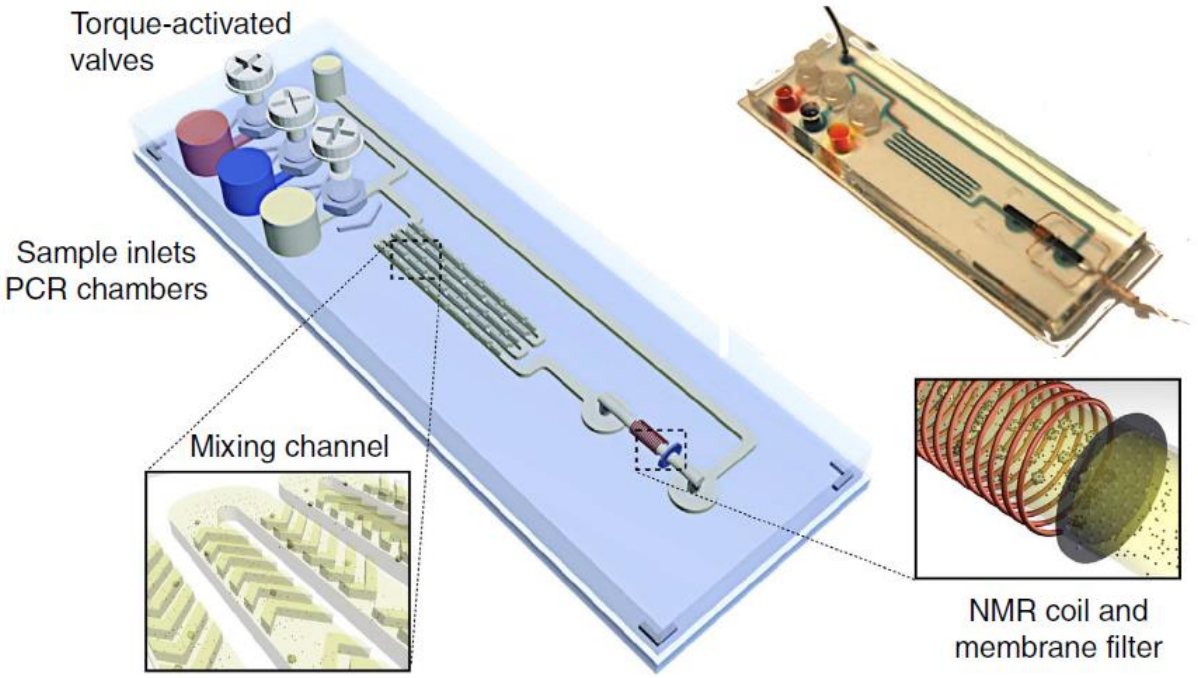

Fig. 1.8. NMR-based microfluidic PoC device. Reprinted with permission from ref. 38, copyright 2013 Nature Publishing Group.

1.2.1.3. 0D magnetic PoC devices

MBs and magnetic nanoparticles (MNPs) are often used as support in PoC devices, usually in washing and pre-concentration/amplification steps or in the precipitation of the analyte and other nanoparticles for example onto an electrode[30]. Some researchers are also taking advantage of the magnetic properties of MNPs and use these as transducers[38,39] by means of nuclear magnetic resonance (NMR). This technique is highly sensitive due to the low back-ground signal since non-magnetic substances should not interfere. In addition, NMR is able to detect all the tags present in the detection zone, while in optical and electrochemical sensors it is not always possible (in optical sensors, generally only the tags on the substrate surface are visible; in electrochemical sensors, it is often required that the tags are in contact with the electrode to be able to generate a signal). In addition, the detection time is faster than electrochemical assays. However, NMR systems are still expensive and may not be affordable to all the possible users.

Liong *et al.*[38] propose a microfluidics PoC device (Fig. 1.8) to detect amplified nucleic acids from a bacterium related to tuberculosis. The device is able to perform DNA amplification, MNPs-DNA incubation, washing and NMR detection. The device has three inlets

for DNA, MNPs and a washing buffer; some mixing channels for the incubation steps and a NMR coil that counts the amount of MNPs, proportional to the initial value of DNA concentration. As main drawback in this device, although the NMR detection is fast, the amplification and the incubation steps can elongate the duration of the assay more than two hours. Anyhow, it is faster than other tuberculosis detection methods based on cell culture and microscopy. Chung *et al.*[39] developed another NMR-based microfluidics PoC device which they use for the detection of a biomarker in urine. Despite the matrix is complex, the noise signal is low due, as previously mentioned, to non-magnetic that substances do not interfere on the readout. Their device is compared to a reported colorimetric dipstick method obtaining a LOD 8 times lower.

1.2.2. One-dimensional nanomaterials (1D)

1D nanomaterials are those materials which growth is oriented in one dimension, on a linear way. The thickness could be as small as just one nanometer, as single-walled carbon nanotubes (SWCNTs), but the length could be a million times larger, hundreds of micrometers. The shape of these nanomaterials has an important effect on their application: the length and the diameter define the absorption wavelengths. Moreover, length and thickness also grant mechanical strength, useful in the creation of larger nanostructured materials. Nonetheless, the growth of 1D nanomaterials is not simple and often requires meticulous synthetic routes that in turn would determine their homogeneity

Nanowires are the simplest 1D nanomaterial, that can be created from other 0D nanomaterials or directly, being cooper, nickel, silver, gold, platinum and silicone the most used elements. In the work of Mostafalu and Sonkusale[40], they introduced nanowires (made from platinum, nickel and cooper) into paper substrate to create electrodes for electrocardiogram monitoring by means of tissue-electrode impedance which work in dry conditions. This approach that doesn't require the addition of electrolytic gel between the electrodes and the skin is advantageous since gels use to get dry quickly and are degraded with movement. The high surface area of nanowires provides good quality of response in the electrodes, from 100 to 1 KΩ in impedimetric measurements. Besides medical application, Mostafalu and Sonkusale demonstrated that the same paper electrodes worked properly as well as cathode in an acidic battery.

In the recent years CNTs and SWCNTs have been widely used on electrochemical applications[41–43] since these nanomaterials are highly conductive, both electrical and thermal. CNTs are easy to functionalize as well, not only with biological compounds, but also with other nanomaterials (especially with metallic oxide nanoparticles) provoking an enhancement of their electrical properties, among others[41]. CNTs are also included in several commercial inks for the fabrication of screen printed electrodes (as well as AgNPs are commonly used for the fabrication of reference electrodes, CNTs are used for the fabrication of counter and working electrodes[42]). In comparison to metallic nanowires, CNTs contribute to the fabrication of larger nanostructured materials with new properties as high flexibility, elasticity and very high lightness, since they are hollow inside. Also, CNTs are more robust than nanowires against temperature variations due to the fact that the thermal expansion coefficient of carbon bonds is much lower than in metals. However, it is important to consider that many reactions which could be applied on their surface will not be reversible, making the lifetime of CNTs shorter than other materials applied in sensing. Then, as an example of use of these materials, it should be mentioned the work of Nemiroski *et al.*[43] where they integrated electrodes made

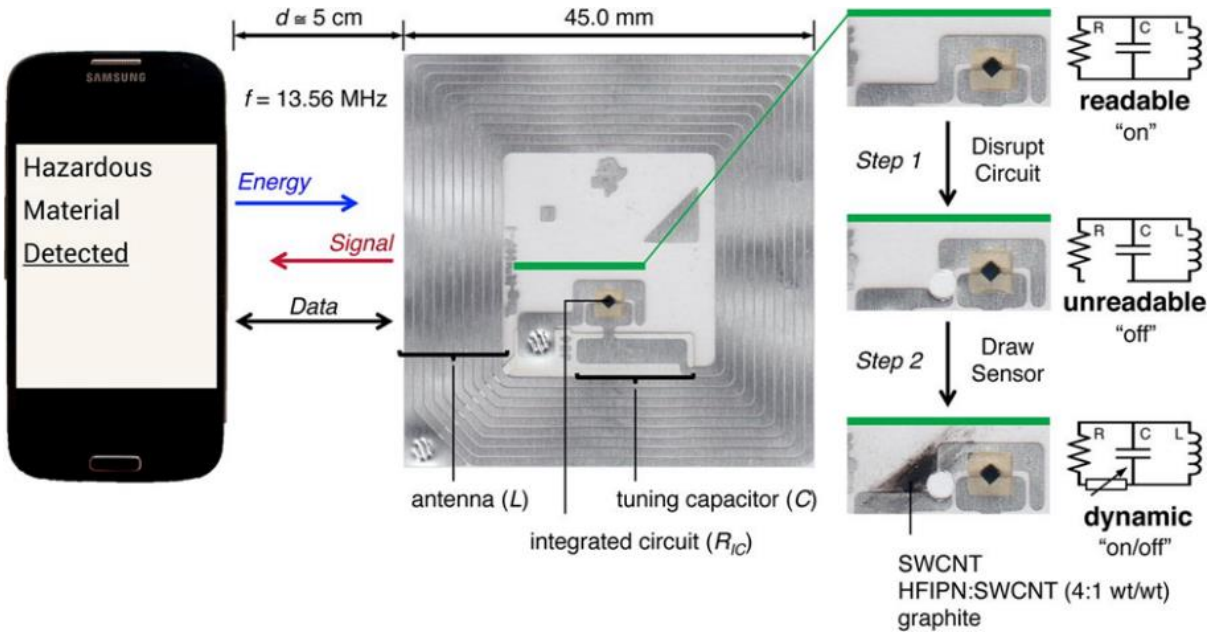

Figure 1.9. NFC tag circuit modified with SWCNTs to work as on/off logic gate in the presence of different analytes. Adapted with permission from ref. 5, copyright 2014 National Academy of Sciences.

with CNTs into a mobile phone system by means of the audio jack of the device (the audio jack has the advantage that can send and receive information at the same time).

In a very smart way and for the first time, Azzarelli *et al.*[5] used SWCNT to apply NFC technology for sensing. NFC technology is able to detect an antenna without requiring it to have an electrical power supply. This technology nowadays is present in most of the smartphone models, hotel doors lock systems, metro stations, toys and even in mail stamps, so NFC tags are becoming every day cheaper and easier to fabricate and modify. So, they tuned an NFC tag by replacing part of the circuit with SWCNTs which, by means of a chemiresistive reaction, alter the conductivity in the circuit depending of the presence of different compounds in the air and, consequently, make it act as an on/off logic gate inside the NFC tag (Fig. 1.9). This technique was applied for the detection of compounds in the air, but for future PoC applications it could be used to detect analytes on the breath or probably even in body fluids as blood or sweat.

One more surprising inclusion of CNTs was done by Darabi *et al.* into chewing gum[44]. They washed a chewing gum with water and ethanol and mixed it with a solution containing CNTs; the mixture was stretched and folded several times in one direction to favor the orientation of CNTs. The sensor worked properly for the detection of humidity in the medium (dryness of the mouth can be caused by certain medications or illnesses, by damage to the

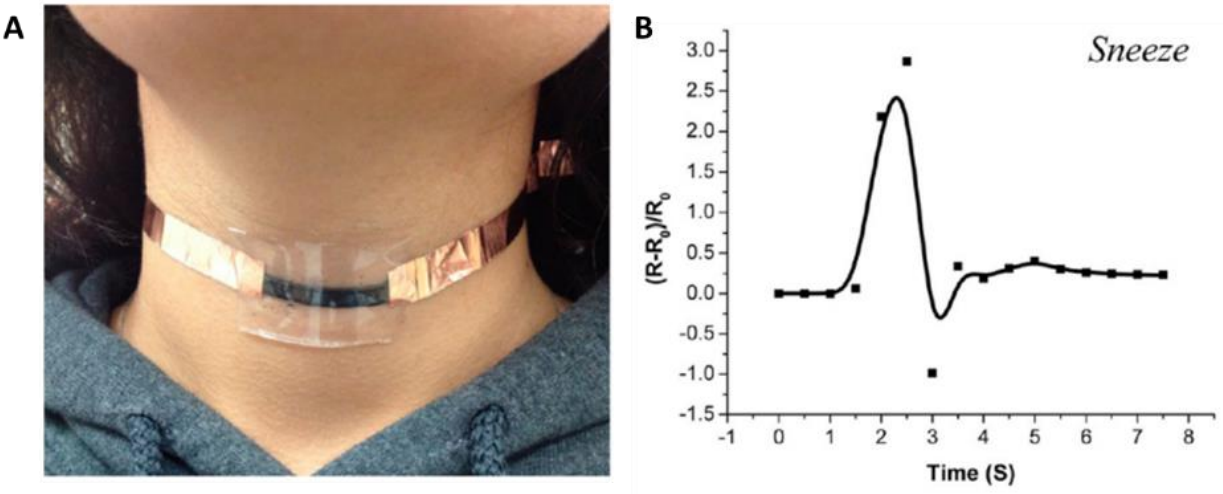

Fig. 1.10. (A) Chewing gum containing CNTs adapted for motion monitoring and (B) the response obtained when sneezing. Reprinted with permission from ref. 44, copyright 2015 American Chemical Society.

salivary glands or by hormonal changes) by measuring electrical resistance on the gum. Also as motion sensor as shown in Fig. 1.10A, able to detect not only body (neck in the figure) movements (Fig. 1.10B), also the breaths of the user. This device could be really interesting for PoC diagnostics (biting problems, dry mouth, pulsations or even could take advantage of chemical reactions to detect different targets). However, there are two important drawbacks that preclude the introduction of the device into the mouth: the response is measured using electrical circuits and CNTs are currently classified as cytotoxic nanomaterials.

1.2.3. Single-layer nanomaterials (2D)

The compounds which enter in 2D-nanomaterials classification are those who expand themselves in two directions, composed by a monolayer of atoms or by an ultrathin layer of a few. Albeit there exist several inorganic 2D nanomaterials, graphene has been by far the most used 2D material in the last years. Although graphene is considered a material composed by one single layer of atoms it is quite hard to find it with this nature, being usually found in groups of graphene layers. Depending on the number of layers the electrical, optical and mechanical properties of graphene may differ. Other important parameters that affect to the graphene behavior are its oxidation level, the number of structural defects, the purity degree, etc.[45] Values that can be controlled by the synthetic route.

Graphene can be combined with QDs working as quencher (silencing the fluorescent signal of QDs when both are approached). This property was harnessed for the fabrication of LFBs by Morales-Narváez *et al.*[19]. On their system they dispensed two lines of QDs on paper substrate, as test and control, being the first line capable of capturing some bacteria (by means of antibodies attached on QDs). After adding the sample on the LFBs it is added a solution of graphene oxide (GO), an oxidized form of graphene containing epoxy bridges, carboxyl and hydroxyl groups. GO will turn off the fluorescence of QDs in the control line and, if there are no bacteria in the sample, the test line. However, in presence of bacteria captured on the test line it will produce a gap between GO and QDs letting the fluorescence to emit. In comparison to traditional LFBs this method prevents the formation of false positives during the assay since a negative sample will always turn off both lines (in case that something external provokes the test line not to be quenched, control line will be also affected, obtaining an invalid strip but not a false positive). However, the assay time (more than 1 h) is longer

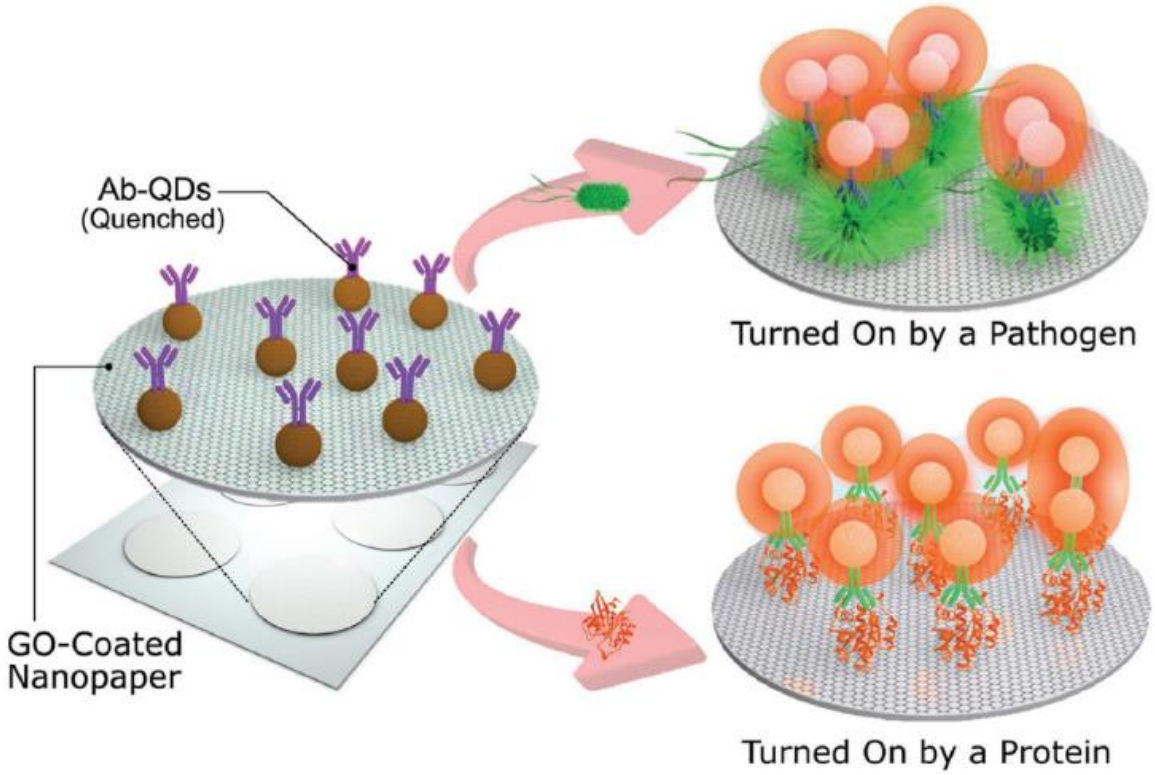

Fig. 1.11. Nanopaper coated with GO. QDs can be stored inside remaining quenched but when the analyte (e.g. bacteria or proteins) is additioned then the fluorescence is released. Adapted with permission from ref 46, copyright 2017 John Wiley and Sons.

---

than for standard LFBs (usually of 5-10 min) due to the extra step of GO addition and drying, including the waiting time for the bacteria to flow across the strip.

Cheeveewattanagul *et al.*[46] coated nanopaper with GO and introduced on this composite a suspension of antibodies attached to QDs. Again, the quenching effect keeps the fluorescence of QDs silenced. It is when adding an analyte (e.g. bacteria or proteins; for which the antibodies are selective) that a gap between the QDs and GO is produced, negating the quenching effect and releasing the fluorescence (Fig. 1.11). This technique is quite advantageous since does not require washing steps, is portable and fast, a promising alternative to ELISA tests.

Owing to its electrical properties, graphene can be used for the fabrication of working electrodes[47,48]. Antibodies can be conjugated onto graphene surfaces by coating pure graphene with polymers or by exploiting the chemistry of carboxylic or hydroxyl groups in GO. Moreover, since graphene is planar, the antibodies can all be oriented perpendicularly to the

graphene layer to increase the probability of capturing the analyte[47]. Going further, graphene electrodes are enough sensitive to allow label-free sensing, small changes (i.e. electrochemical[47,48] or impedimetric[45,49] alterations) on the electrode surface are easy to detect. On the other hand, as drawback, it demands a highly meticulous control on the reproducibility of graphene synthesis, especially in regard to the number of layers and structural defects.

Baptista-Pires *et al.*[49] designed a new solvent-free method for printing GO on different substrates using wax-printed patterns, printed on nitrocellulose membranes, and vacuum filtration. GO remains on the non-wax-printed areas and by pressure is transferred to the target substrate. To demonstrate the possibilities of this technique a touch sensor based on the resistance changes provoked by finger contact on the GO printed circuit was printed. This GO touch sensor is shown in Fig. 1.12, connected to a LED and a power source (Fig. 1.12A): the sensor works as a simple switch, turning on/off the LED (Fig. 1.12B and 1.12C respectively). This technology could be used to replace current touchscreens, which use controversial elements like indium and rare-Earth metals[2], and in wearable PoC applications that require flexible devices (e.g. skin tattoo sensors[40]) or those based on contact-sensing (e.g. pressure or motion sensors[44]).

Additionally to the mentioned characteristics, graphene also is an electrochromic material, it can be tuned to change its colour in a reversible way depending on the current

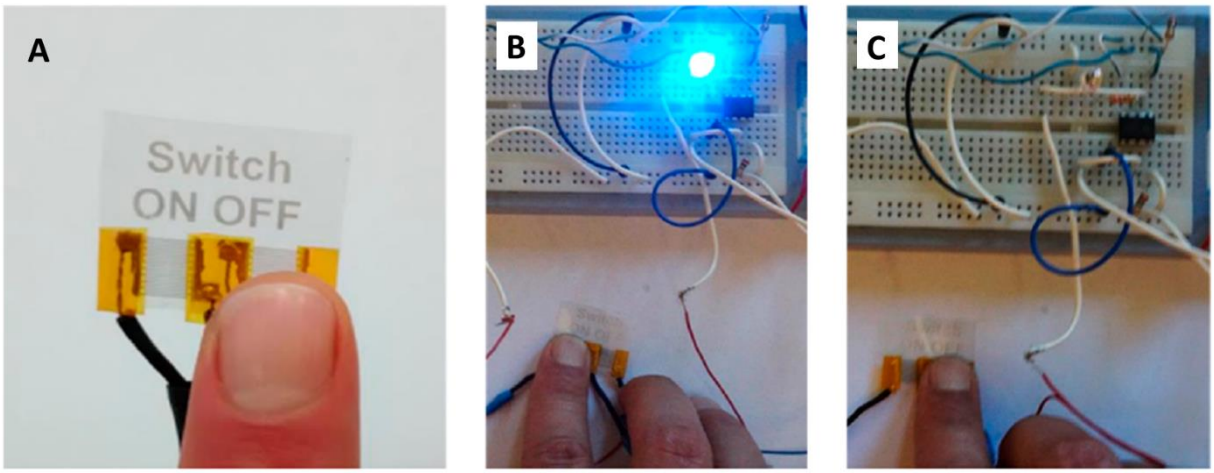

Fig. 1.12. GO tactile device: (A) GO switch works by skin contact turning a LED from (B) ON to (C) OFF status. Adapted with permission from ref. 49, copyright 2016 American Chemical Society.

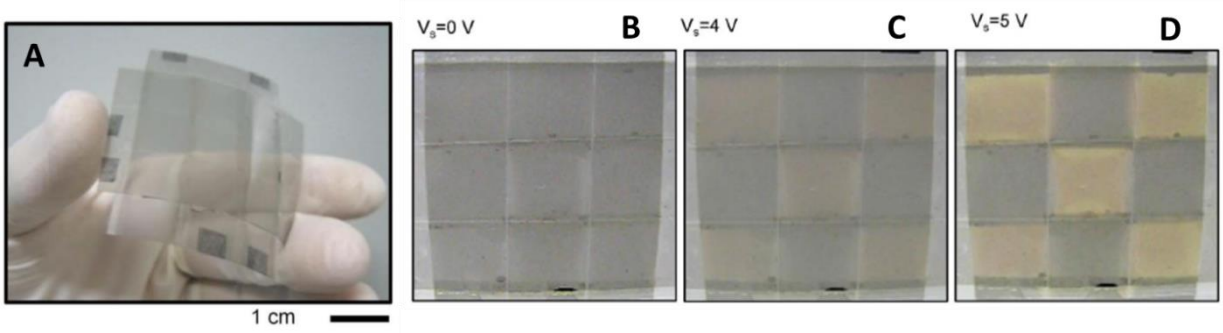

Fig. 1.13. Electrochromic device composed by (A) flexible graphene electrodes whose transmittance is increased when applying current: (B) 0 V and (C, D) chess pattern visible at higher voltage. Adapted with permission from ref. 50, copyright 2014 Nature Publishing Group.

supplied. Polat *et al.*[50] developed different electrochromic flexible devices using this property. In one of their devices they attached two plastic substrates coated by one side with graphene electrodes and a liquid electrolyte in between. When applying some voltage across the electrodes, graphene turns translucent due the voltage is enough to penetrate the graphene layers creating structural defects that fade its characteristic black colour. Their final device is shown in Fig. 1.13 made by various graphene electrodes. The device is flexible (Fig. 1.13A) and graphene can resist a curvature of 1 cm radius without being damaged. By applying different voltage on some of the electrodes they create a chess pattern as transmittance is increased on the layers in which the current is increased: 0V (Fig. 1.13B), 4V (Fig. 1.13C), 5V (Fig. 1.13D). Thanks to this technology, electrochemical signalling can be converted into optical responses *in situ*, thus enabling wearable PoC devices that are more user-friendly.

1.2.4. Other nanomaterials (3D)

There exist an extensive variety of 3D materials both in shape as in size, which leads to different possibilities in the final sensing application. Non-spherical nanoparticles exhibit properties quite similar to 0D nanomaterials, however the change of shape often drifts into absorbance changes (i.e. the colour of a solution of gold nanospheres may be different from a solution of nanocubes or nanotriangles, even when the chemical composition and size are the same). Taking advantage of this fact, plasmonic-based PoC sensors can be fabricated as the one reported by Fu *et al.*[4]. Their device is portable and can be coupled into a mobile phone, using its light sensor, included on most of modern mobile phones to improve photography quality or control the screen brightness. The device consists on a plate, where

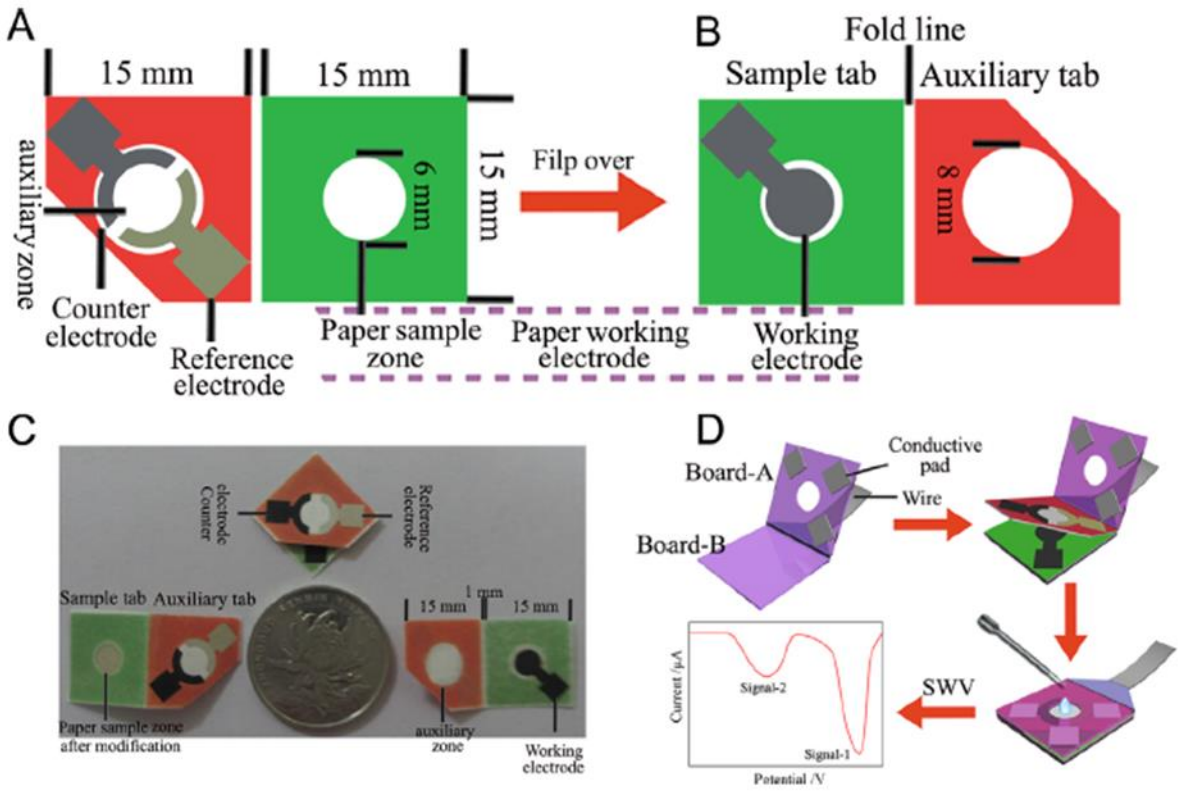

Fig. 1.14. Multiplex electrochemical origami paper device: (A) front part, silver reference electrode and carbon counter electrode; (B) back part, carbon working electrode; (C) size comparison of the device and (D) its application for electrochemical measurements. Adapted with permission from ref. 51, copyright 2014 Elsevier.

sample is added, and a LED that illuminates the sample in the plate and reaches the light sensor. To demonstrate the capabilities of their device they use it to measure the plasmonic changes occurred on triangular silver nanoprisms in absence of a cancer biomarker, indirect detection method, by provoking a shape transformation on the nanoparticles with hydrogen peroxide. Li *et al.*[51] used another 3D silver nanomaterial too, nanoporous silver which can be used as signal enhancer, label and metallic ions carrier. Their system consists in a multiplex electrochemical origami paper device (Fig. 1.14) that uses nanoporous silver loaded with different metallic ions as label for tumor sensing. Silver electrode is used as reference (Fig. 1.14A) and screen printed carbon electrodes as counter and working electrodes (Fig. 1.14B). The paper device can be folded (fig. 1.14 C) and integrated into an electrical circuit (fig. 1.14 D).

Some non-spherical nanoparticles exhibit electrochromic properties, as WO_3 nanoparticles, used by Marques *et al.*[52] on paper substrate. The nanoparticles change from

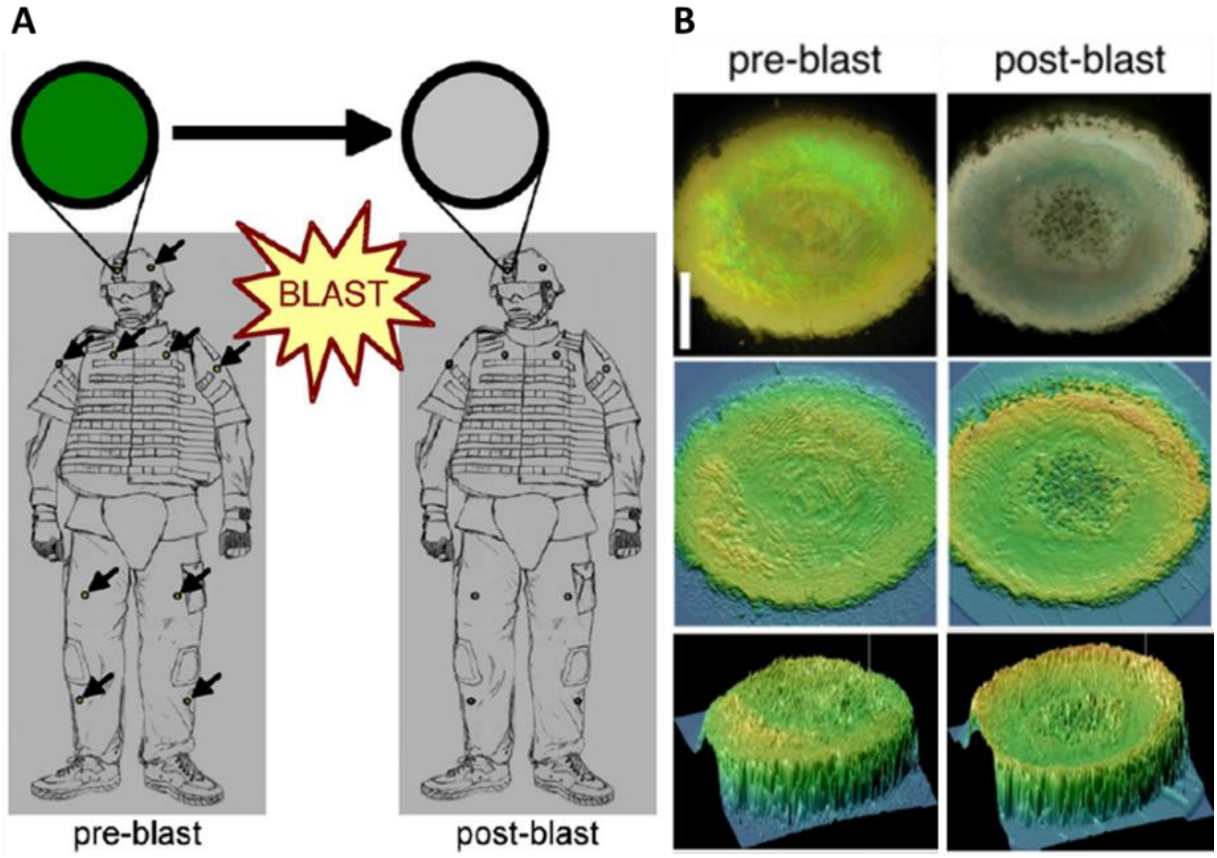

Fig. 1.15. (A) PC-based wearable that changes colour in response to the shock wave of a blast. (B) The PC before and after the blast (up: light microscopy; middle: top view generated with Image Pro Plus; down: 3D rotated view). Reprinted with permission from ref. 56, copyright 2011 Elsevier.

yellow to blue colour in presence of electrochemically active bacteria. Thus, this is a simple sensor able to work as ELISA assays but without requiring long-time steps or the use of delicate reagents (i.e. biological reagents have short expiration dates, while nanomaterials can last long periods of time even stored at room temperature). Photonic crystals (PC) are other example of electrochromic materials often composed by other nanoparticles that are assembled following a crystalline pattern. These nanomaterials have demonstrated good adaptability in different types of sensors due to their resistance to being bent[53], being used in microfluidic systems, both in polymeric channels[54] or in paper[55], permitting label-free sensing (colour change occurs when the analyte attaches or passes near the PC). Cullen *et al.*[56] converted PC into simple PoC wearable stickers that can be settled on clothes and warn its user, in war zones, about possible aftermath related to expansive wave of a blast (Fig. 1.15.). PC are broken when brought under high pressure as consequence of an explosion thus

Table 1.1. Summary of the nanomaterial types: examples, corresponding PoC detection principles, advantages and disadvantages. Reprinted with permission from published work ref. 7. Copyright 2018, Royal Society of Chemistry.

Nanomaterial type	Examples of nanomaterials	PoC detection principle	Advantages	Disadvantages
0D	• AuNPs • AgNPs • QDs • UPCs • Magnetic nanoparticles	• Optical • Fluorescent • Electrochemical • Magnetic	• Simple synthetic procedures • Small size • Easy to bioconjugate • Adaptable into other nanomaterials	• No special structural properties • Some 0D nanomaterials can easily agglomerate
1D	• Nanowires • CNTs	• Electrochemical • Motion	• Highly conductive • Orientable • Structurally resistant	• Complex synthesis • Difficult to control their shape
2D	• Graphene	• Electrochemical • Fluorescence • Tactile	• Easy to modify • Flexible • Fluorescence quencher	• Difficult to separate a single graphene sheet • Structural defects are common
3D	• Non-spherical nanoparticles • PCs	• Optical • Electrochemical	• Can combine the properties of other nanomaterials • Tunable optical properties	• Like 0D nanomaterials, 3D nanomaterials can easily agglomerate • Usually, not as small as 0D nanomaterials

changing the colour, a notification to the user that the blast could have induced non-visible injuries as internal traumatisms or brain damage.

1.2.5. Nanomaterials for Point-of-Care conspectus

Table 1.1 summarizes the different nanomaterial types, with the most common examples of each classification, the possible detection methods that the final PoC could employ and some of the strengths and weaknesses for each case. Depending on the properties of nanomaterials and the way how these are integrated within PoC devices various detection technologies are used being optical and electrochemical ones the most reported.

1.3. Lateral flow biosensors

Since the appearance of the first biosensor[57], the technology has evolved, but it is still not crowned with the expected devices that would work as easily as a glucose biosensor or a pregnancy test, present in any pharmacy all over the world. Low cost and efficient devices for the detection of other analytes such as DNA, proteins or even whole cells in real scenarios are still in the way. As previously mentioned, paper is a simple, cheap, abundant and an easy-to-manufacture material that fulfils cost/efficient requirements in biosensing technology[58]. It is noteworthy that it is in developing countries where this type of biosensors are more requested due to the lack of resources to use conventional laboratory tools which are more expensive and require trained operators, huge amount of equipment and installations.

Paper, this mere material made from cellulose (the most abundant polymer on Earth), offers many others advantages in the development of biosensors. Various biochemical reactions with interest for biosensing applications can easily be carried out within this matrix. In addition, simple microfluidics including platform architectures tuning can be applied thanks to the controlled porosity and capillary forces of the nitrocellulose network in addition to simple modification or integration processes. Moreover paper-based platforms are compatible with either naked eye detection or simple optical or electrical readers.

As seen on section 1.2.1.1., LFBs are an important example of how paper can be applied for the development of PoC devices. LFBs fit all the requirements expected from a biosensor: low limit of detection, high sensitivity, good selectivity, low quantity of sample volume required, no washing steps are necessary, robustness, low cost, quick assay

performance in just one step and a user-friendly format. Nevertheless LFBs also have some weaknesses, such as the fact that the response obtained on naked-eye is just qualitative, not quantitative, although with the help of certain reading devices it can be converted into semiquantitative. Another drawback is that the sample must be always in liquid state, with enough viscosity to flow across the porous of the nitrocellulose. These pores, in some cases, could be obstructed by different matrix compounds and provoke unspecific adsorptions in the membrane; it is in those cases when a sample pre-treatment or pre-dilution will be required. Because of the limitation of the detection area, the surface where receptors (e.g. antibodies, enzymes, proteins, etc.) are placed, at higher concentrations of analyte, can be oversaturated, giving false blank response; it is another factor to consider making the predilution of the sample before the analysis.

LFBs can be used to detect a large range of biomarkers that may include not only proteins but also nucleic acids and even whole cells, among other biocompounds. Furthermore, LFBs are not limited only to biomolecules detection; several publications have appeared in the last years about the detection of pollutants such as metallic ions, pesticides, etc. The range of LFBs applications is including detection of hazardous substances[17], heavy metals in drinking waters [59–63], allergens and pathogens in food[64–69], pesticides[70–72], drugs screening[73], etc.

There exist different commercial LFBs[74–76], being pregnancy and fertility tests the most known examples beside tests for human immunodeficiency virus (HIV)[77–79], drugs of abuse[80], Malaria[81,82], etc. Behind LFBs there is a well-known technology[9–11,83–86] with several publications reporting different modifications of the standard designs/structure, either in terms of the materials used as transducers for the signal generation, in the methodology employed to translate the signal or in improving the device with different enhancement strategies.

With the recent development and explorations of nanomaterials in the field of sensors and biosensors LFB has been taking advantages for their use as alternative materials to improve their performance requested in real sample applications. Application of nanomaterials in DNA, protein, cell and various inorganic/organic compounds in various biosensing technologies is now being extended to LFB field bringing interesting results to this technology[14,87–89].

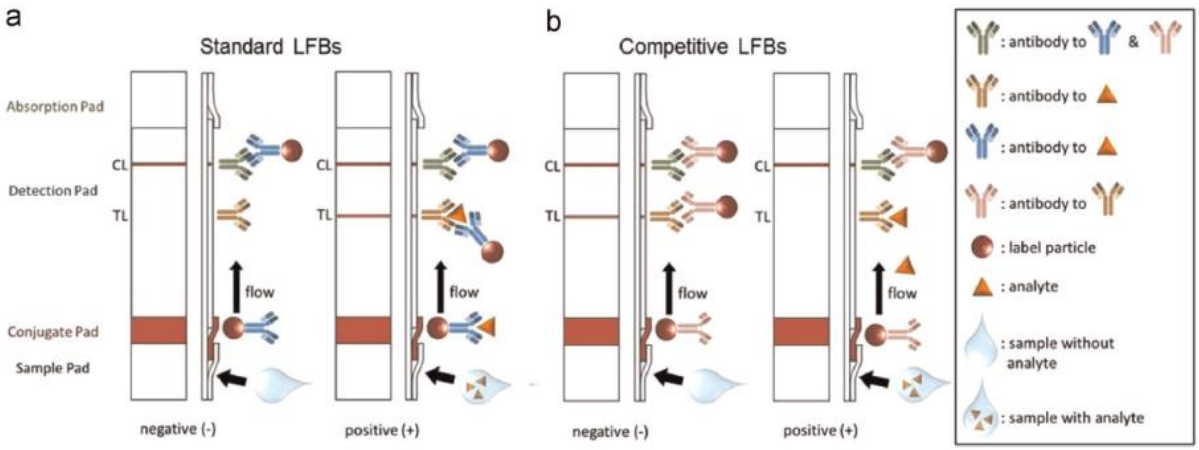

Fig. 1.16. Schematic representation of the different parts of a LFs and movement of analytes and label particles across by means of (a) standard and (b) competitive designs. Adapted with permission from published work ref. 10. Copyright 2015, Elsevier.

1.3.1. How do lateral flow strips work?

LFBs are manufactured in strip form, a convenient format for the user, normally with a width between 4-6 mm and a length no more than 6-7 cm. A standard lateral flow strip (LFs) consists of four main sections made of different materials, as shown in Fig. 1.16: sample pad, made of cellulose, where the sample is dropped; conjugate pad, made of glass fiber, impregnated with the bioconjugates solution (the label particle and a receptor for the analyte); detection pad, a nitrocellulose sheet[85,90] where test line (TL) and control line (CL) are printed; and absorption pad, also made of cellulose. Other additional parts can be integrated on LFS as blood filters, substituting the sample pad, to retain big particles like blood red cells and avoiding their hemolysis. Another example of material which can be integrated on LFs is CNTs paper, with high conductive properties to connect LFs to electronic devices[91].

The performance of an assay with a LFs is quite simple: the sample is added on the sample pad and then the liquid will start flowing to the conjugate pad where the analyte, if present on the sample, will be linked to the transducers (the label particles), previously conjugated with a bioreceptor specific to the analyte. The conjugate, rehydrated by the liquid, will flow by capillarity forces across the detection pad to the absorbent pad, passing through the TL, where it will be captured only if the conjugate has the analyte attached (positive response), and to the CL, being always captured, evidencing that the assay works. This design corresponds to a standard model of LFs (Fig. 1.16a), but there exists also the competitive

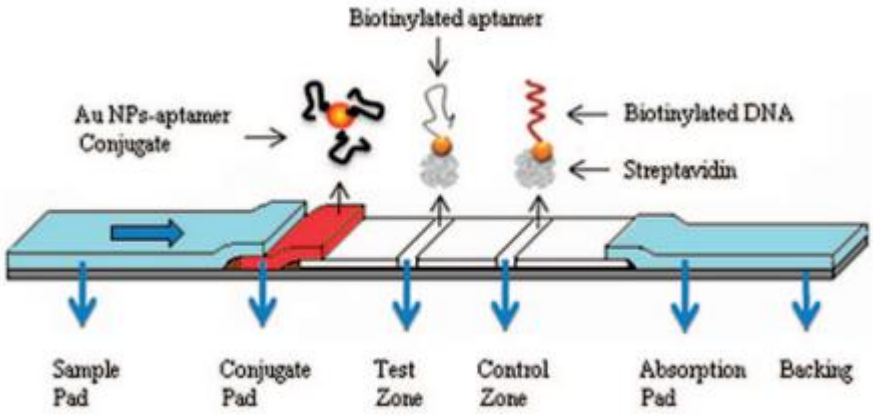

Fig. 1.17. LFs with aptamers conjugated AuNPs. Reprinted with permission from ref. 98. Copyright 2009 American Chemical Society.

model (Fig. 1.16b) in which the analyte and the transducers compete for being captured on TL, obtaining a response inversely proportional to the concentration of analyte.

1.3.2. Optical detection on LFBs

Although a large variety of strategies to read the LFs signal has been reported the optical methods remain the most explored because of their simplicity (even naked eye detection) and effectiveness (high sensitivity). As extension of the examples mentioned in section 1.2.1.1., we will revise the most relevant technological and analytical aspects related to the application of LFs labels such as AuNPs, QDs, CNTs, carbon nanoparticles (CNPs) and liposomes, between others.

1.3.2.1. Gold nanoparticles (AuNPs)

One of the first examples of the use of AuNPs as labels on LFs was reported by Shyu *et al.*[17] for the detection of ricin. On this LFs, without conjugate pad neither sample pad, anti-ricin antibody conjugated AuNPs were deposited over nitrocellulose membrane near the bottom of the strip.

Few years later, the number of reports about LFBs increased and the design evolved including a pad, made of glass fiber, for the AuNPs suspension[92]. Also, besides antibodies, other biocompounds like aptamers[93,94] and DNA probes[79,95–97] were conjugated with AuNPs. Xu *et al.*[98] designed a LFs with AuNP-aptamer conjugate as label (Fig. 1.17) for the detection of thrombin. The system demonstrates that the use of the thrombin aptamer exhibits a high

sensitivity, comparable or even superior to the systems which use antibodies. The experiment shows that the color intensity of AuNPs can be detected up to a concentration of analyte of 0.6 pM in diluted plasma samples being this value lower than in antibody-based assays[17,92,99], without detecting any unspecific adsorption; that evidences the good selectivity of aptamers combined with AuNPs.

It was also demonstrated that AuNPs can be used not only for biocompounds detection[99]; toxins[69,100] and metallic cations[59–63,101] also can be detected using several strategies. In the case of the work of Fang *et al.*[101], Cu^{2+} ions can be detected taking advantage of the cleavage that cooper causes, in presence of ascorbate, on Cu^{2+}-specific-DNAzymes (linked to AuNPs) which, if broken, will be captured on TL. This strategy grants a good selectivity against other metallic ions, but the limit of detection does not reach the levels achieved in the detection of antigens. An alternative high sensitive strategy to detect metallic ions consists on the use of antibodies specific to a metal-ligand complex but not to the free metal. The metal-ligand complex competes for being hooked on the test line with the same complex but already linked to AuNPs, thereby obtaining a competitive format of LFs. This strategy is seen on López-Marzo *et al.*'s work[62] to detect Cd^{2+} ions using ethylenediaminetetraacetic acid (EDTA) as ligand. The system, nevertheless, is shown to have some problems of unspecificity to some metals; however it can be solved reducing the concentration of the ligand but also adding extra conjugation pad that ensures Cd^{2+} complexation with EDTA and interference masking through ovalbumin (OVA)[63] (to be discussed later in the text).

In some cases, multidetection of analytes could be required, so it would be necessary to use various nanoparticles easy to be concentrated so as to achieve an intense color. Hereby, AuNPs are a good choice to develop multidetection LFs[102–104]. These LFs could replace ELISA assays, which are time-consuming and expensive, as was demonstrated by the work of Song *et al.*[103], developed to detect different mycotoxins at the same time (Fig. 1.18). Their work, additionally, demonstrates that LFs, besides of the qualitative response, permit the quantitative interpretation of the signal by means of a colorimetric reader. The quantitative response can be represented as relative optical density (the ratio in percentage between the signal of a positive sample and the blank). This data can be used to construct a calibration curve of the measuring system.

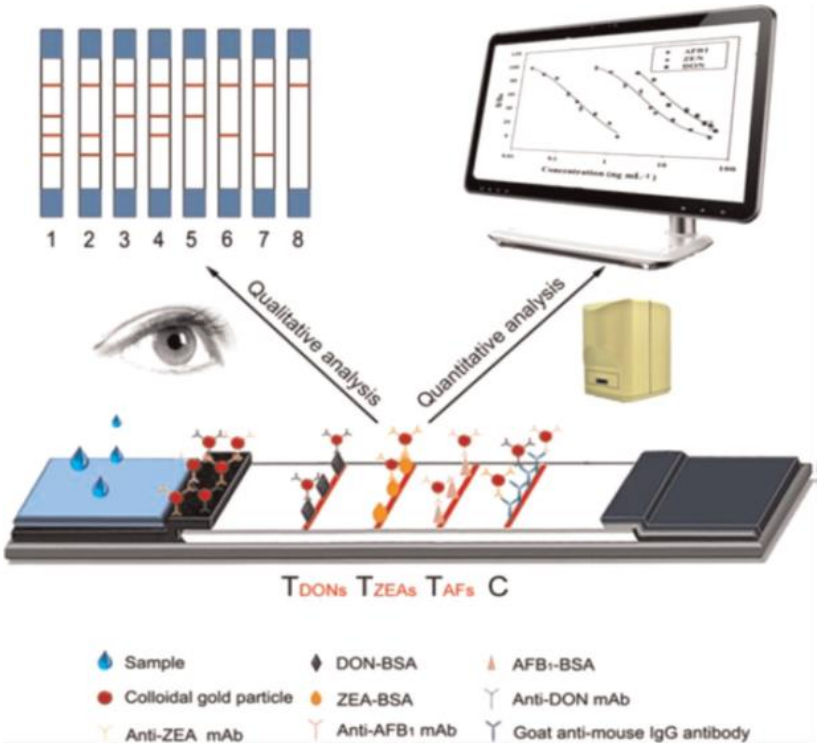

Figure 1.18. LFs for the multidetection of different mycotoxins. Qualitative (left) and quantitative (right) response. Reprinted with permission from ref. 103, copyright 2014 American Chemical Society.

The work of Chen *et al.*[105] and Huang *et al.*[106] reveals another interesting application of AuNPs on LFs, the development of logic gates systems. AuNPs can afford more than one biocompound conjugated on their surface, therefore easily a LFs could detect the presence of various analytes on the same line ("OR" logic gate: the LFs will mark positive signalling in the presence of any of the analytes). Also the signal can indicate only the presence of both analytes at the same time[105] ("AND" logic gate: the signal on TL will only appear if both analytes are present). Huang *et al.*'s system[106] can also detect the presence of a single analyte in a system where the analytes are inhibited by each other ("INH" logic gate: the LFs will mark positive signalling in the presence of only one of the analytes, but not if both are present in the sample at the same time).

Although LFBs with AuNPs have demonstrated to have good sensitivity and low limits of detection, there are cases when it is necessary to achieve better performance. Different enhancement strategies with potential to significantly improve LFSs devices have been reported. These strategies can be based on chemical methods, like the modifications of the label's surface (the AuNPs) to afford secondary reactions or attachments, or in altering the

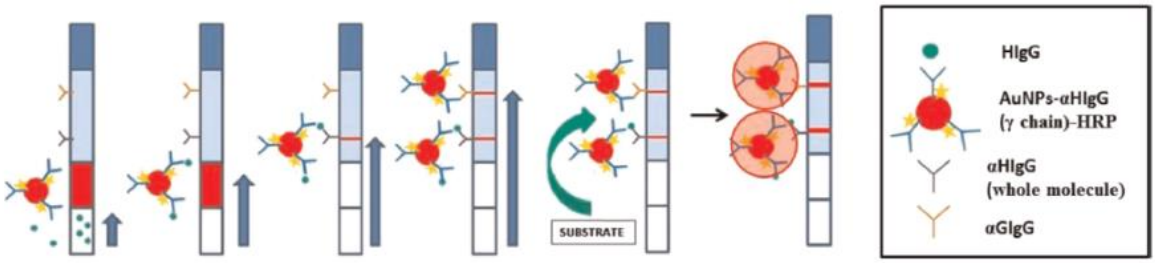

Fig. 1.19. Signal enhancement of LFs signal by means of enzymatic reactions. Adapted with permission from ref. 107, copyright 2013 Elsevier.

physical properties of the device (flow movement, speed, etc.) by modifying the design/architecture.

One of the strategies used to amplify the signal on TL and CL is to surround AuNPs with other compounds which enhance the color by means of enzymatic reactions (Fig. 1.19) as the reaction occurring between HRP (horseradish peroxidase) and some chromogenic substrates[95,107], such as AEC (3-amino-9-ethylcarbazole) or TMB (3,3',5,5'-tetramethylbenzidine). AEC mixed with H_2O_2, use to provide color enhancement (and consequently, higher sensitivity) on HRP catalysed reactions. Nevertheless it is when using TMB that the quantification limit is further decreased due to the fact that this substrate grants higher contrast between the lines and the background than the AEC. The reported detection limit of these enhancement strategies can reach the 200 pg/mL[107].

Although enzymatic reactions exhibit low limit of detection and good sensitivity, the short stability of the reagents and the long conjugate development and testing times are drawbacks to consider. The amplification method proposed by Rastogi *et al.*[108]by means of gold deposition over the strip after the assay solves the problem of reagents stability and seems to increase the signal effectively at low concentrations, but at higher concentrations, when detection lines are already saturated, the signal enhancement is slight. Fridley *et al.*[109] studied the release of dry reagents stored in porous media (rehydrated afterwards) and demonstrated that this strategy could be used to enhance up to four times the intensity of AuNPs (previously deposited on the strip). This strategy, if developed on a real assay (with AuNPs and analyte flowing) could lessen the testing time in comparison with the methods in which amplification is performed after the assay. However, it is important to be taken into

account the properties of the reagents to be stored on the membrane, their stability once dried and their potential as signal enhancers after rehydration.

Another interesting work was reported by Li *et al.*[110]. Taking advantage of the quenching effect of gold ions on QDs, they dissolved the AuNPs captured on TL using HCl–Br_2 mixed solution and, in a 96-well microplate, they measured the fluorescence of QDs. The method provides a good sensitivity, a wide working range and a fairly low limit of detection (90 pg/mL). Despite these advantages, the procedure is long and difficult to execute on field since it requires treating of the strips, fluorescence equipment to read the 96-well microplate and trained personnel. Instead of solving the AuNPs, Shi *et al.*[111] developed a system which allowed fluorescence quenching measurements without the need of dissolving the nanoparticles; they dispensed fluorescent polymer dots of 50 nm on the TL and CL and observed how the fluorescence decreased with the increase of concentration of AuNPs, which competed against the analyte. The detection limit of their method reached the 160 pg/mL. As an alternative to fluorescence detection, silver deposition onto AuNPs could be used to enhance the colorimetric response, turning into black the color of TL and CL[69]. This strategy not necessary requires the use of colorimetric reader, if only qualitative assay is needed, but the detection limits achieved are not as low as when using QDs and fluorescence.

Xu *et al*.[112] developed LFs in which, as labels, AuNPs were loaded over silica nanorods surface (Fig. 1.20A), raising quite a lot the sensitivity of the method due to the increase of AuNPs density over detection lines (Fig. 1.20B). The detection limit is also improved, when

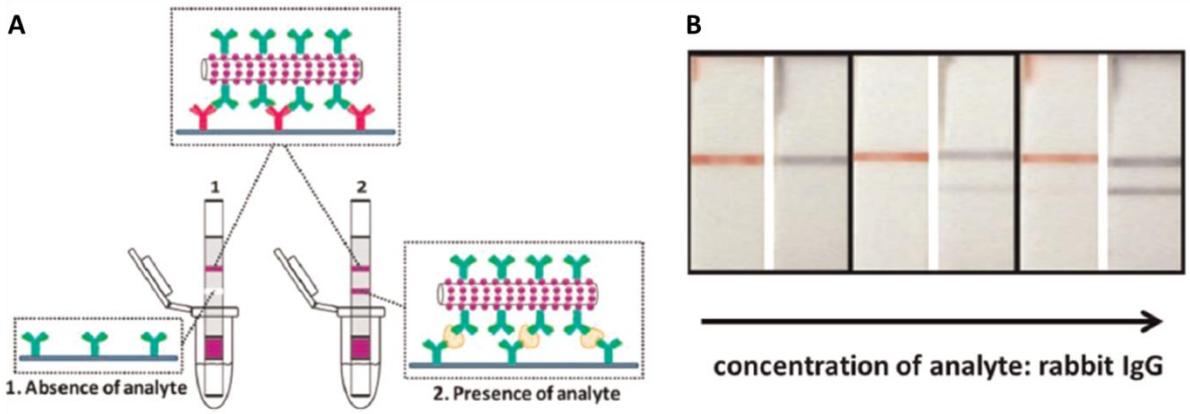

Fig. 1.20. AuNPs carried on silica nanorods: (A) design and performance of the LFB assay and (B) results comparison with standard AuNPs labels (left strips) and silica nanorods decorated with AuNPs (right strips). Adapted with permission from ref. 112. Copyright 2014 American Chemical Society.

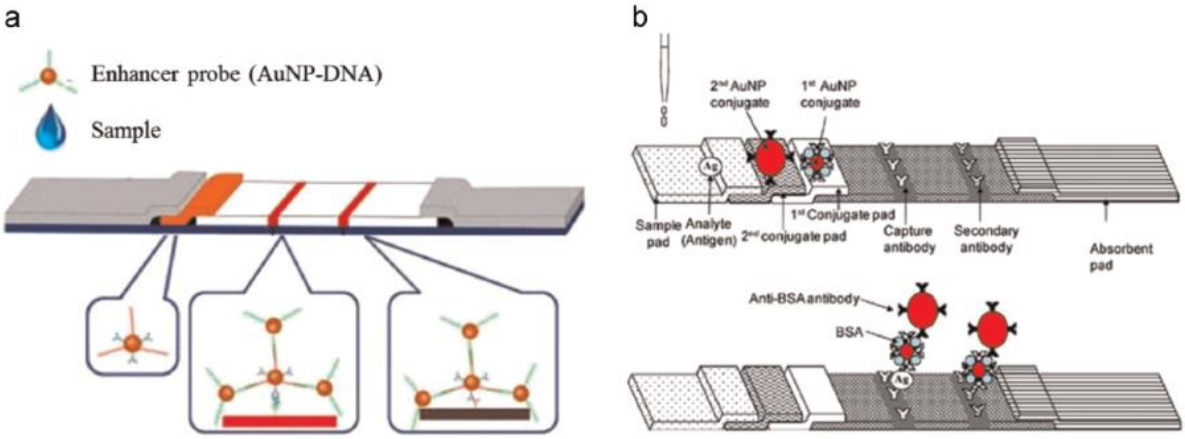

Figure 1.21. Strategies to increase the density of AuNPs on TL and CL: (a) LFs with AuNPs-probes cocktail on the conjugate pad. Adapted with permission from ref. 114. Copyright 2013 American Chemical Society. (b) LFs with double conjugate pad. Reprinted with permission from ref. 115. Copyright 2010 Elsevier.

compared to the previous mentioned strategies, being 10 pg/mL the estimated value. Another observable improvement of this method is that the amount of antibodies dispensed on TL and conjugated onto AuNPs could be reduced. Nevertheless, one should keep in mind that the silica nanorods preparation and their decoration with AuNPs could be a time-consuming step, besides that the size of the rods (tens of micrometers) slows the flow across the membrane thus increasing the testing time. The size of the labels also precludes the use of small pore membranes, which use to exhibit higher sensitivity than the membranes with bigger pores.

To increase the density of AuNPs on the detection lines, another strategy is to interconnect AuNPs by means of DNA probes[113,114] conjugated onto their surface. The binding between AuNPs can be performed previously to the assay, adding the AuNPs-probes cocktail to the conjugate pad[113], or during the assay, adding the enhancer nanoparticles mixed with the sample[114] (Fig. 1.21A). As in the case of AuNPs decorated silica rods and the deposition of dry reagents on the membrane method, these designs are user-friendly, being able to be performed in one only step, without the need for post-treatments on the strip.

Another strategy to increase the density of AuNPs on the TL is to modify the architecture of the LFs. An example of this modification can be easily achieved by adding an extra conjugate pad, as shown in the work of Choi *et al.* [115]. On this design, two different sized AuNPs conjugated with different types of antibodies on two pads are used. The smallest

AuNPs are conjugated with the antibodies which are selective to the antigen and will flow faster than the biggest AuNPs, which are conjugated with anti-BSA antibodies and will bind to the previous AuNPs, covered with BSA as blocking agent, obtaining an enhanced signal due to this new sandwich format (Fig. 1.21B). The detection limit of this LFs is 1ng/mL, so the enhancement is not as good as in the previously discussed methods. Nevertheless this method is advantageous due to the fact that the assay is performed as a real one-step procedure, without pre-treatments on the sample neither post-treatments on the strip. Should also be noted that the preparation of both conjugates is simple and the biocompounds which are used are not very expensive.

In cases where pre-treatment of the sample is required an extra pad can also be used to pre-treat the sample, simplifying the test procedure. In the work of López-Marzo *et al.*[63], an improvement of a previous design[62] by adding an extra pad with EDTA, which binds the metallic ions to allow their detection, and OVA, to help masking the interferences has been carried out (Fig. 1.22). More pads could be added, to enrich the flowing liquids with buffers

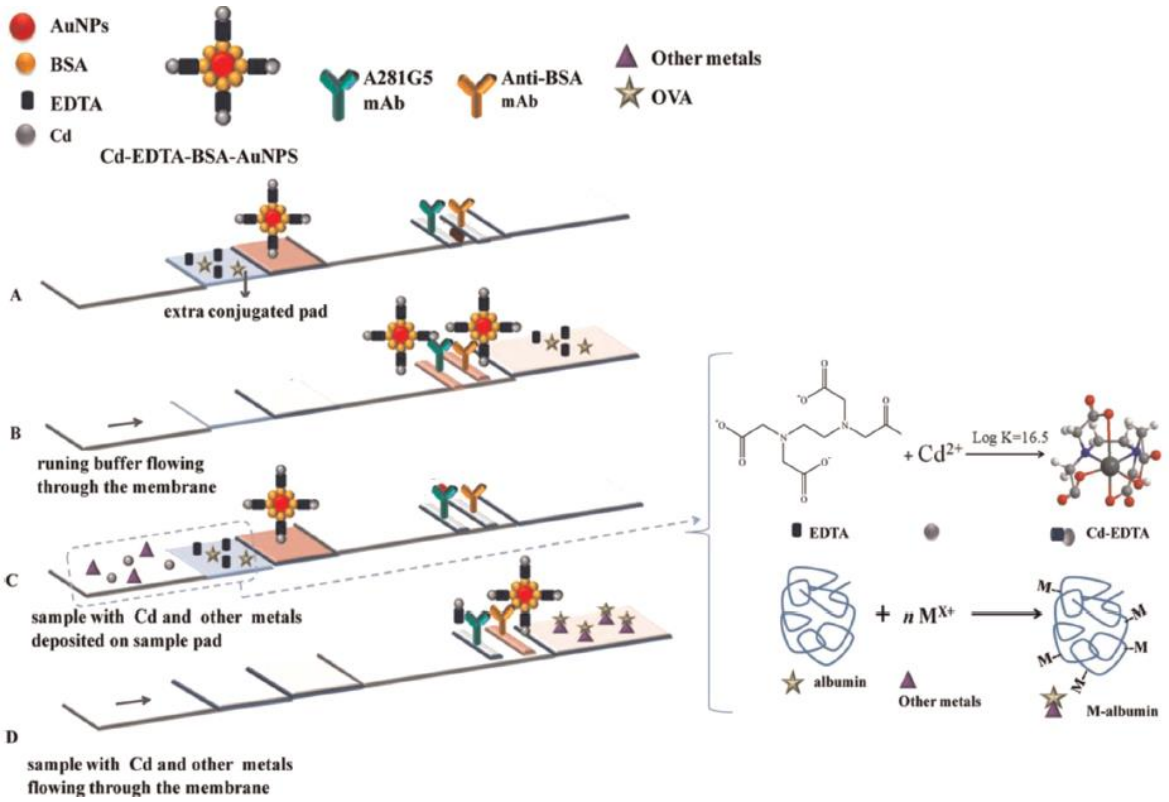

Figure 1.22. LFs with additional conjugate pad for sample pre-treatment. Reprinted with permission from ref. 63. Copyright 2013 American Chemical Society.

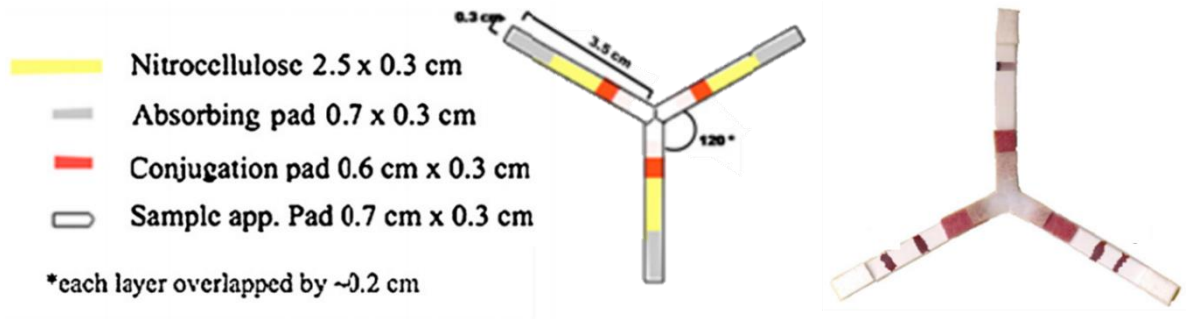

Figure 1.23. Multidetection device composed by three LFs specific to different analytes. Scheme of the design (left) and the final LFB (right). Adapted with permission from ref. 119, copyright 2011 Elsevier.

---

or to improve the signal with enhancer solutions once the assay is finished, but it could require several steps, having to wait for the timely moment of each one, hindering the reproducibility of the device. That problem can be solved using the two-dimensional paper network format of Fu *et al.*[116]. Buffer, sample and signal enhancer are added at the beginning of the assay, then the device is closed and, when the pads contact, the flowing across the paper network starts. In this manner the reproducibility of the liquid mixing is better controlled. This design was later simplified in another work of Fu *et al*.[22], already discussed (Fig. 1.2).

Multidetection of analytes is another interesting area in which architecture tuning can be helpful. Fu *et al.*[117] and Fenton *et al.*[118] experimented with the division of the flow on paper format, proving that multiplex design on lateral flow could work without the need of pumps or other auxiliary devices. Li *et al.*[119] adapted LFs to the multiplex format in which three strips shared one sample pad (Fig.1.23).

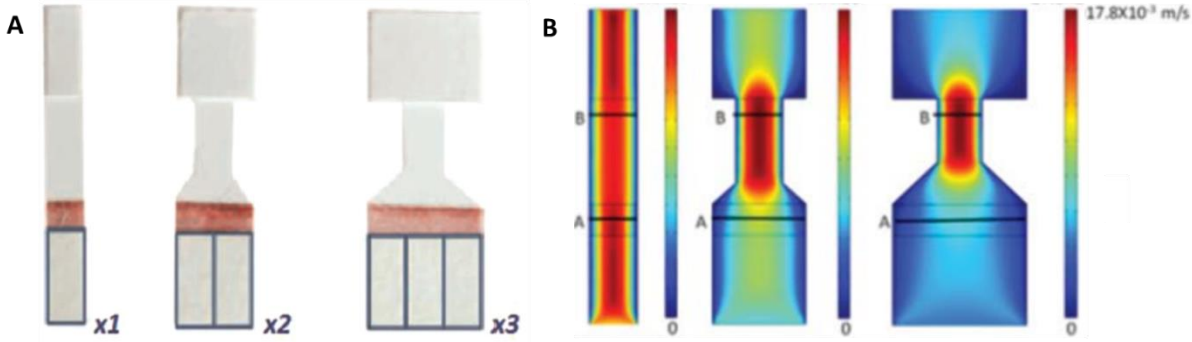

Fig. 1.24. Paper architecture modification to enhance the signalling. (A) LFs shape and (B) the flow speed across the paper. Reprinted with permission from ref. 120. Copyright 2013 Royal Society of Chemistry.

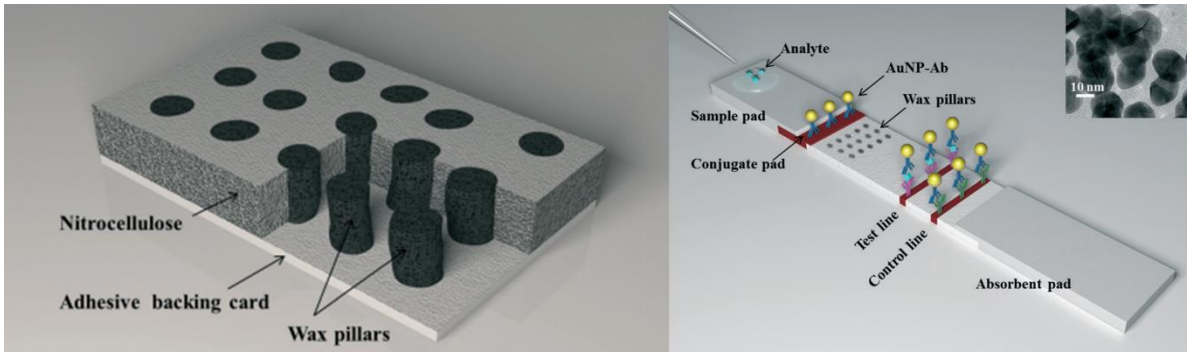

Fig. 1.25. Design with wax pillars printed on LFs membrane to modify the flow across the pores. Reprinted with permission from ref. 123. Copyright 2014 Royal Society of Chemistry.

Increasing the quantity of gold nanoparticles in the TL can boost the sensitivity of the system. Parolo *et al.*[120] reached this purpose by simply modifying the architecture of paper. The authors tried different designs (Fig. 1.24A) in which the flow was accelerated inside the detection pad due to a funnel effect, which at the same time was concentrating the amount of AuNPs and analytes inside. The optimal results were obtained when the width of sample pad and conjugate pad was 3 times the width of the detection pad, lower assay speed (Fig. 1.24B), enhancing the sensitivity and reducing about eight times the limit of detection in comparison to a standard LFs.

Another way to modify the flow is to disturb it, instead of provoking its acceleration the time that the transducers have to conjugate with analytes can be increased, ensuring that all AuNPs are conjugated and, consequently, captured on TL and CL. In the work of Hong *et al.*[121] the antibodies were dispensed as patterns of parallel and zigzag dots on the detection pad, being the zigzag pattern the one which gave the highest intensities, presumably because flow slower on this design. It has been demonstrated that wax is a useful tool due its hydrophobicity to control flow on paper devices and create channels on it[122]. In the work of Rivas *et al.*[123], wax is used to create pillars inside the membrane (Fig. 1.25) slowing the movement of the fluids and amending their mixing. Furthermore, the pressure exercised when printing the wax patterns reduces the membrane's pore size, also contributing to the brake of the flow. Again, as happened in Hong *et al.*'s work[121], the zigzag design exhibits the highest response. On Rivas *et al.*'s work[123] the detection limit is improved three times regarding a non-modified strip, less than on Parolo *et al.*'s method[120]; however wax pillars compose a more inexpensive design, since it does not require higher quantities of AuNPs and antibodies, in addition that wax is a cheap material.

1.3.2.2. Fluorescent nanoparticles

It is well known that fluorescence methods use to exhibit higher sensitivity that those based on absorption colorimetry. The behaviour of fluorescent nanomaterials with interest to be used in LFs has been extensively explored and some reported examples discussed below.

In the already discussed work of Li *et al.*[110] was demonstrated that the use of quantum dots (QDs) exhibits a good sensitivity and a really low limit of detection; but on their work, quantum dots were used to indirectly detect the amount of AuNPs on TL by quenching effect. In other works QDs are used directly as labels on LFs, with both antibodies[68,110,124] and aptamers[125,126]. The assays are as fast as with AuNPs, regardless the time that fluorimetric analysis could take, and the limits of detection achieved with QDs as tags are in the order of

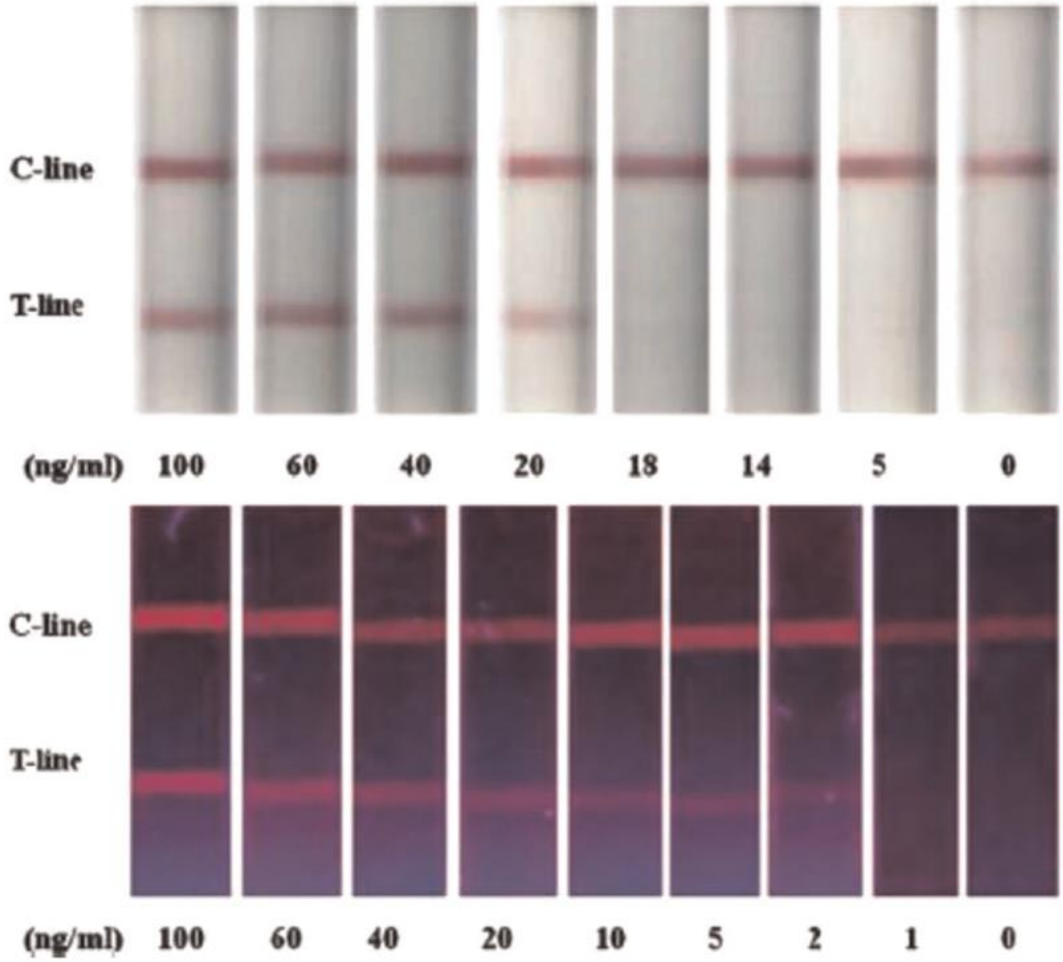

Fig. 1.26. Comparison of assay made with AuNPs (up) and silica nanoparticles loaded with QD (down). Reprinted with permission from ref. 127, copyright 2012 Royal Society of Chemistry.

few nanograms per milliliter. The differences between AuNPs and QDs based LFs are heighten when QDs are carried[127] or encapsulated[128] in other materials. In the work of Bai *et al.*[127], QDs were loaded over silica nanoparticles, which are between 10-20 times larger than QD, and these nanocomposites were used as labels obtaining a good sensitivity and a detection limit ten times lower than with AuNPs LFs (Fig. 1.26). These achievements were overwhelmed by Ren *et al*.'s work[128], who managed to encapsulate QDs on polymeric beads improving the limit of detection to only 0.42 pg/mL and fixing problems of flow and unspecific adsorptions of free QDs on nitrocellulose. In some cases, the conjugation of QDs with biocompounds can be a complex work due to their small size; also the number of antibodies per QDs is lower than in larger particles, so the probability of binding the label to the antigen is also a bit lower; therefore, these works[127,128], besides enhancing the signal, they are noteworthy easing the development and behaviour of the LFs.

Besides QDs, other fluorescent materials are being used on LFs, as UCPs, which are considered ceramic materials of large size, few hundreds of nanometers, composed by the combination of rare earth elements, being europium one of the most used. UCPs transform low energies (infra-red) into high energies (visible light, depending on their crystalline structure). Corstjens *et al.*[20,129–131] worked with this materials to detect nucleic acids and antigens in complex matrixes with improved results in comparison to the ELISA tests. Paterson *et al.*[132] also worked with this type of materials on LFs, obtaining similar results as Corstjens *et al.*[20,129–131]. UCPs seem more stable in front of photobleaching effect (decrease of fluorescence) than QDs, making UCPs more suitable for direct assays and QDs for quenching related modes.

As seen with QDs, to carry the fluorescent tags on larger particles it helps enhancing the signal and avoids unspecific adsorptions onto the membrane. Europium, present on most of UCPs, emits fluorescence when reduced from Eu^{3+} to Eu^{2+}, so several researchers have exploited that property and combined europium with microparticles[133] and silica beads[134–136] to use them as transducers on LFs. Although the results are satisfying, QDs and UPTs exhibit better limits of detection and working ranges. Huang *et al.*[137] covered silica microparticles with $Ru(phen)_3^{2+}$ complex, which also exhibits fluorescent properties, obtaining a good limit of detection, 20 pg/mL. Liposomes can be used to encapsulate fluorescent dyes[138,139], getting higher sensitivity when using larger particles, with limits of detection close to 20 pg/mL.

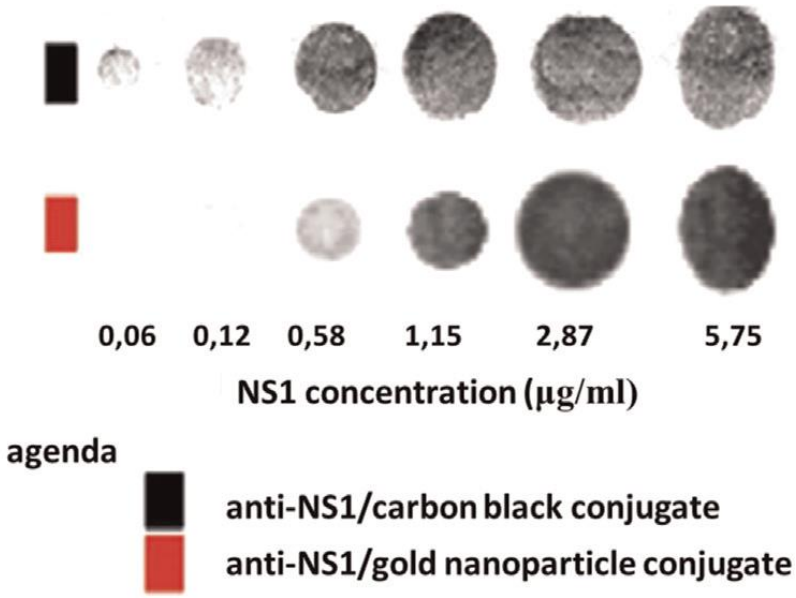

Fig. 1.27. Comparison of contrast obtained when using carbon nanoparticles (CNPs) and AuNPs. Reprinted with permission from ref. 143, copyright 2012 Elsevier.

Commercial fluorescent microspheres which can be used on LFs also are available[140–142]. Interestingly, Xie *et al.*[140] evaluated the optimal quantity of antibodies required to be conjugated with their microspheres and compared it with AuNPs, resulting that when using microspheres this quantity can be reduced four times; moreover, even using less quantity of antibodies in the labels, the sensitivity, the working range and the limit of detection are improved in comparison to AuNPs assays.

1.3.2.3. Other nanomaterials

Linares *et al.*[143] applied CNPs on LFs exhibiting a limit of detection ten times lower than LFs in which AuNPs or LBs (latex beads) are used. CNPs, also known as "carbon black", are strongly dark colored nanoparticles that exhibit a higher contrast against the background than AuNPs (Fig. 1.27), a factor which helps to obtain good parameters of sensitivity, working range and limit of detection. CNPs, as AuNPs, can be used for the detection of antigens[144–146], DNA chains[147,148] and molecules[149–151], also in multidetection format[148].

Another allotropic form of carbon used on LFs are CNTs[152,153]. As mentioned, CNTs are large 2D materials, whereby using these materials on a LFs will turn them in slow tests (around 20 min to see the response). On the other hand, Qiu *et al.*'s work[153] demonstrated that the

limit of detection is improved in comparison to related AuNPs systems. Furthermore, CNTs are stable in time and against aggregation, which increases the life time of the conjugates.

One of the first nanomaterials used to develop LFBs was colloidal selenium[154], with rust color. On this firstling design, the detection of analyte was semiquantitative by means of various TL on the membrane, instead of comparing the intensity of a single TL. The detection limit of this LFs was only of few milligrams per milliliter, so rapidly selenium colloids were substituted by gold colloids which exhibit stronger color. However, several years later, Wang *et al.*[155] used again selenium nanoparticles, claiming the cost effectiveness of this material in comparison to AuNPs, to develop modern LFBs. They could not obtain a low limit of detection, but their system with selenium nanoparticles proved to be quite specific to melamine in different matrixes.

MNPs can be used as labels as well due to their strong brown color (also because of their magnetic properties, as will be discussed up ahead). Nevertheless, this strong color covers practically all the visible spectra obstructing its identification by means of colorimetric devices. The advantage of MNPs is that their optical properties do not change as much as

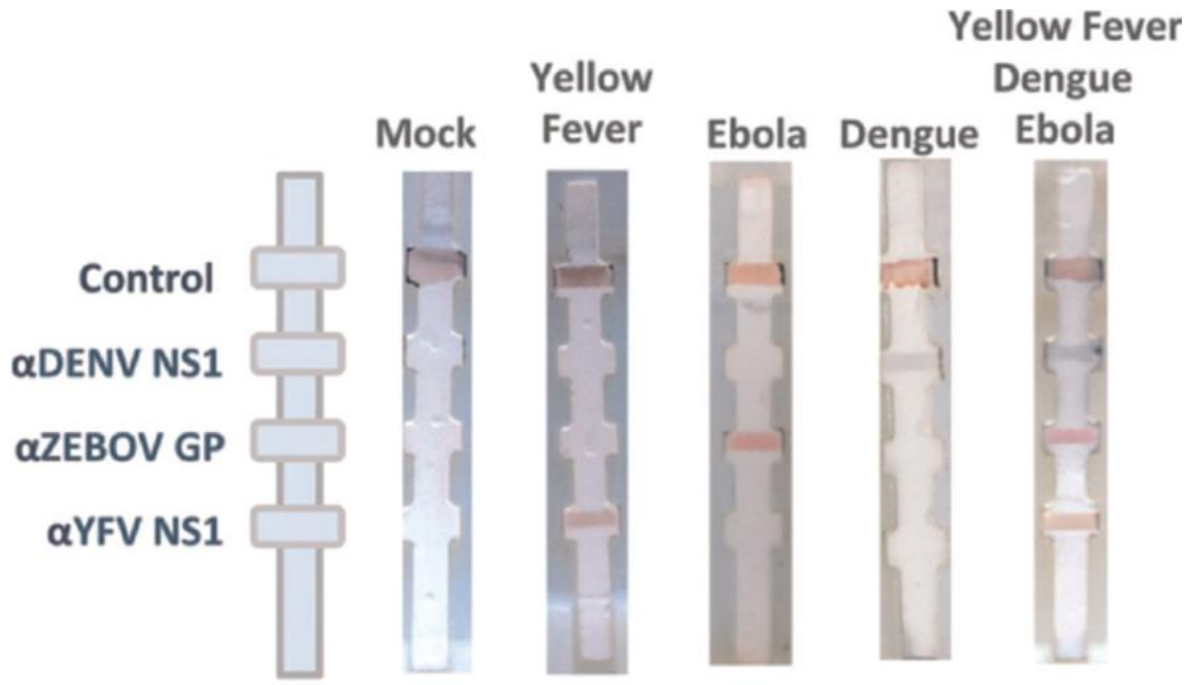

Fig. 1.28. Multiplex LFs developed with silver nanoparticles. Reprinted with permission from ref. 18, Copyright 2015 Royal Society of Chemistry.

AuNPs when aggregated. So Liu *et al.*[156] took advantage of this property and created LFs where MNPs were aggregated using poly-L-lysine on TL. The aggregated MNPs maintained a similar sensitivity to the non-aggregated MNPs, but the limit of detection was improved, reaching 1.7 ng/mL.

Silver can be used to enhance the intensity of AuNPs[69], but silver by itself is also an interesting nanomaterial. Silver nanoparticles present different colours depending on their size and shape so, exploiting this property, Yen *et al.*[18] developed multiplexed LFs in which not only each antigen had their own line, but each of the lines had a different colour, avoiding confusions to the final user (Fig. 1.28).

In the work done by Park *et al.*,[157] platinum nanoparticles are used as transducers due to their properties catalysing luminol oxidation provoking chemiluminiscence. In comparison with HRP, platinum nanoparticles are more stable-in-time and robust against environmental conditions. They compared the lighting response of platinum versus the conventional AuNPs LFs obtaining a higher working range and a limit of detection one thousand times lower.

LBs or polystyrene nanoparticles are homogeneous-size particles which, after being dyed, can be used to develop LFs. Several companies use LBs on their LFs due to the fact it is a cheap material and has a similar behavior as AuNPs. Greenwald *et al.*[158] compared AuNPs and LBs and observed that LFs prepared with LBs on conjugate pad gave a higher sensitivity and specificity than the ones prepared with AuNPs. Comparing other studies with LBs[159–161], the LFs always show a good response in terms of selectivity and sensitivity, however the limits of detection are not as low as with other materials, which makes the strips suitable for qualitative assays, for clinic tests where it is only necessary to know if an antigen is over a determinate threshold. Instead of latex, cellulose[115] can also be used as dyed label on LFs, which is an even cheaper material.

As discussed above on Edwards *et al*.[138] and Khreich *et al*.[139] experiments, liposomes can be used to encapsulate dyes (whether fluorescent or not). There are some reports about the use of liposomes on LFBs[65,67,162–166] with good levels of sensitivity due to the high quantities of dye that can be loaded inside the liposomes. Nevertheless, the synthesis of liposomes is often a long procedure, with difficult size-control, so the reproducibility of the test could be affected if the protocol is not well controlled.

1.3.3. Electrochemical detection on LFBs

Despite of the fact that LFB response can be quantitative, sometimes it can be hard to discriminate between the strips, especially by naked eye. The combination of LFBs with electrochemical detection is expected to provide a more sensitive response, higher reproducibility, wider working range and lower limits of detection than optical measurements. Nowadays electrodes can be easily miniaturized by different methods as screen printing, ink-jet printing or photolithography, allowing their easy incorporation into a LFs design. In the work of Inoue *et al.*[73] the authors used photolithography to fabricate three gold electrodes, working, counter and reference (Fig. 1.29), over a glass slide and then coupled a small piece of nitrocellulose on a well into the device. They demonstrated that electrochemical reactions, cyclic voltammograms and amperometric measurements, could be performed on nitrocellulose substrate so, then, they cut a small piece from a LFs, corresponding to the TL, and carried out the measurements. The amperometric responses, based on the reduction of ferrocenemethanol catalysed by HRP (which was previously linked to a known quantity of testosterone, used also as analyte), decreased when the concentration of the analyte was increased in the sample (competitive LFB model), obtaining wider working range than by chemiluminiscence measurements and good values of sensitivity and limit of detection. The main drawback of Inoue *et al.*'s method[73] is that the electrochemical assay is

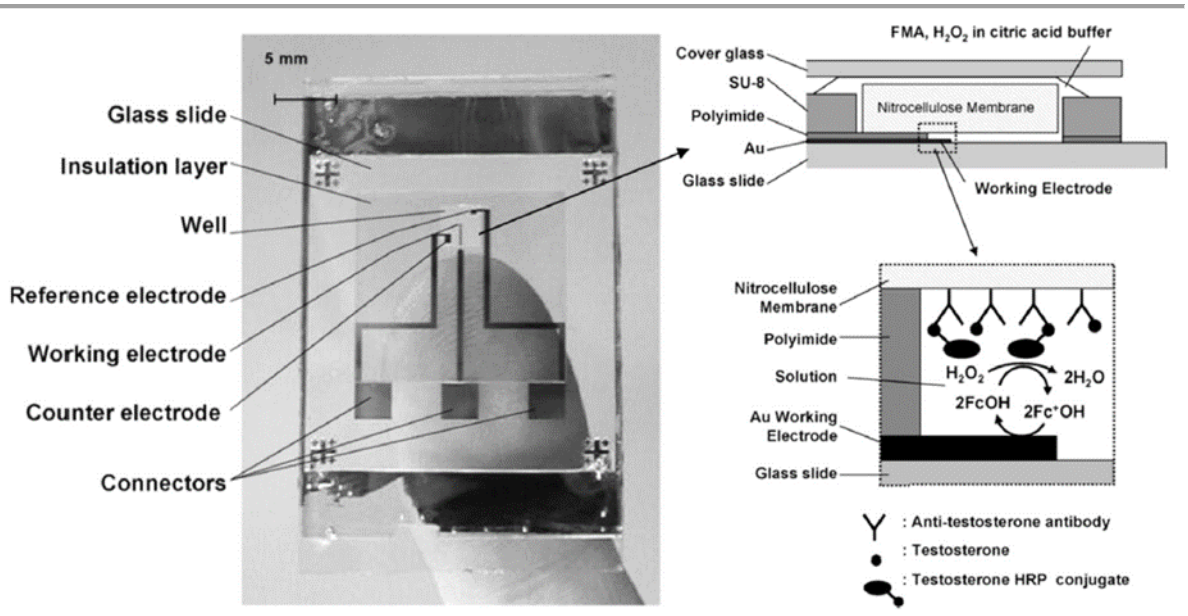

Fig. 1.29. Photograph of a standard electrode chip and the scheme of its well when LFs is coupled inside. Adapted with permission from ref. 73, copyright 2007 Elsevier.

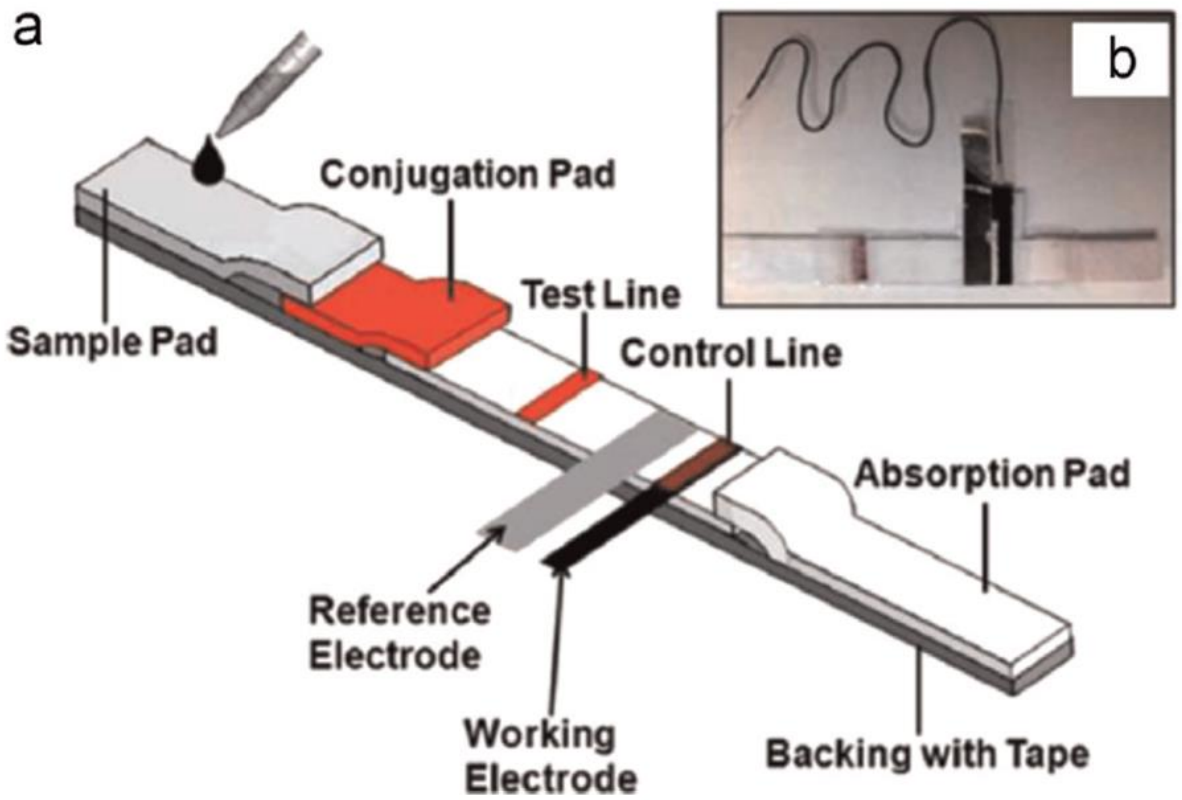

Fig. 1.30. (a) Schematic representation of a LFs with electrical chip coupled and (b) its corresponding photography. Reprinted with permission from ref. 91, Copyright 2014 Royal Society of Chemistry.

performed separately. As the reduction is carried out as an additional step, the electrodes are not truly integrated into the LFs and it has to be cut. Some later designs[167,168] tried to fuse the electrode and the strip inside a cassette, including a cutter to section/cut the TL once the immunoassay was completed.

Liu *et al.*[169], Lin *et al.*[170], Zhu *et al*.[91]; Akanda *et al*.[171] integrated the electrodes in the LFs on different ways. On the cases of Liu *et al.*[169] and Lin *et al.*[170], QDs containing cadmium were used; after the test was performed and QDs were captured on TL, chlorhydric acid was used to release cadmium ions from QDs, which were detected by the electrodes, located under the TL, when a detection solution (Hg/Bi) was added on it. The obtained limit of detection was really low, 30 and 20 pg/mL respectively in each report. Liu *et al.*[169] observed that when the immunoassay time was extended, the detection limit was decreased to 10 pg/mL. In the work of Zhu *et al*.[91], the colorimetric and electrochemical measurements were performed at the same time, without the addition of detection solution, thanks to the integration of commercial CNTs paper in the LFs as working electrode, placed on the CL, and printed silver/silver chloride ink as reference and counter electrode (Fig. 1.30a), being the

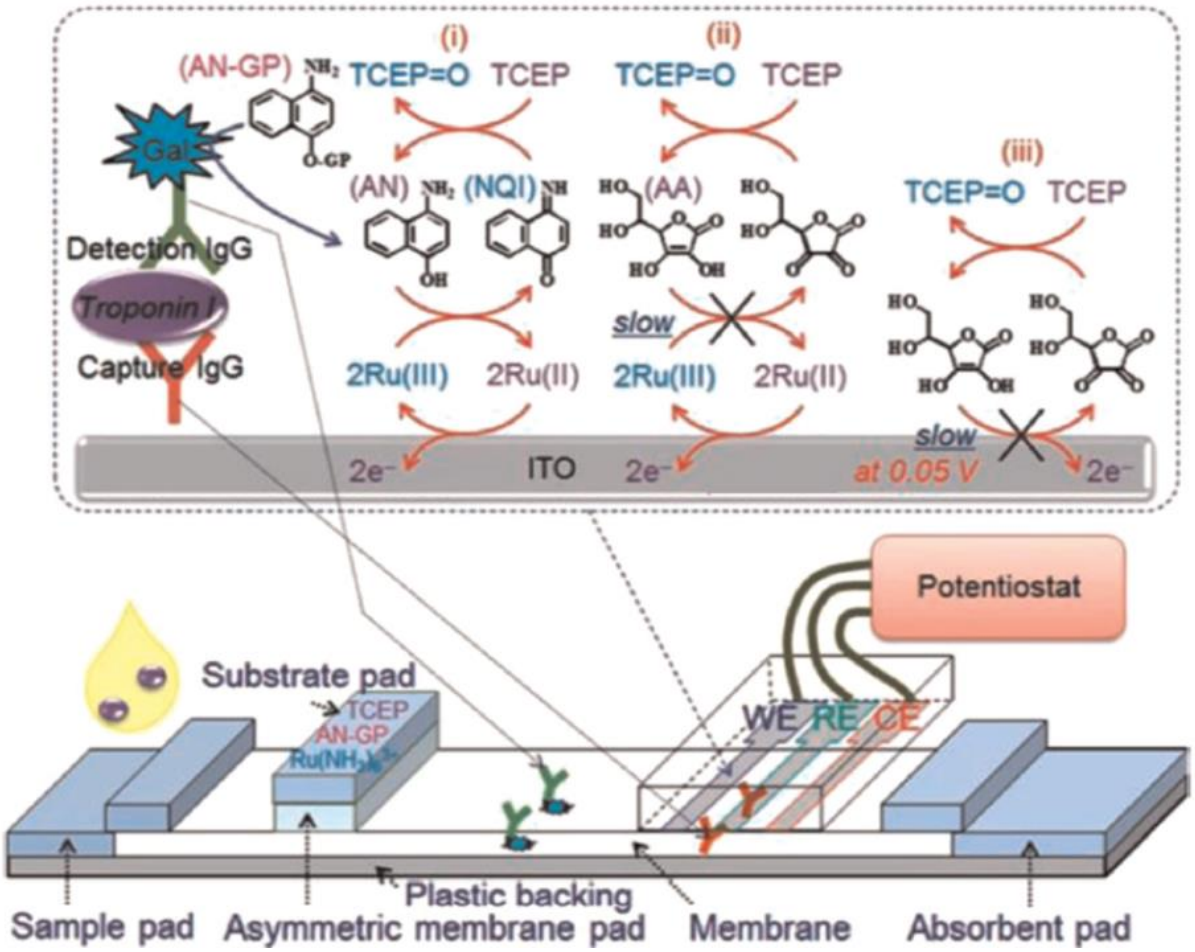

Fig. 1.31. Electrochemical immunoassay occurring on a LFs with an additional substrate pad. Reprinted with permission from ref. 171. Copyright 2014 Royal Society of Chemistry.

electrodes laminated to ensure the contact between them and the nitrocellulose membrane (Fig. 1.30b). Following a competitive LFBs model and using AuNPs as labels, the colorimetric response was measured comparing the TL on photographs of the LFs and, at the same time, the chronoamperometric response was measured from the remaining AuNPs on the CL.

It must be highlighted the work of Akanda *et al*.[171], where they report a really low limit of detection, of only 0.1 pg/mL. Their LFs includes an extra pad with different substrates to perform a redox reaction on the electrodes which allows detecting the analyte without being affected by electroactive interfering species present on the sample (Fig. 1.31). Thanks to this pad the need for sample pre-treating for both eliminating of interferences and to perform the electrochemical reaction is taken away, simplifying the test for the end user. On this design the electrodes, previously printed through photolithography on indium tin oxide substrate

(ITO), were placed directly over the membrane, onto the detection antibodies. Hence, the detection on the LFs is only electrochemical and the strip does not provide optical checking.

1.3.4. Other detection methods

MNPs, as previously discussed, can be used as labels on lateral flow[156] due to the fact they are strongly colored and can be easily conjugated with biomarkers. Usually, MNPs are used to preconcentrate the analyte in a sample through an washing step[100,172], or are conjugated with colored particles (e.g. AuNPs) to assemble them, helping in the purification of the conjugate by means of magnetic separation and to increase the intensity of the color in TL[173]. Nevertheless, MNPs can be used to a more interesting purpose; the magnetic field that the nanoparticles generate can be measured through a proper magnetic reader and transformed into a useful analytical signal. The advantage of this technique is that all the nanoparticles in the detection line should produce signal, contrary to optical and electrochemical methods where only nanoparticles on the surface or in contact with the electrodes, respectively, contribute significantly on the signalling.

There exist several methods to produce and measure a signal using MNPs, being commercial magnetic assay readers (MARs) the most popular. MARs generate a magnetic field which excites the MNPs that simultaneously will produce their own magnetic field, detectable using the sensing coils of the apparatus. This effect can qualitatively measure groups of MNPs. Many authors[174–179] reported the use of MAR on their works, obtaining wide working ranges, high selectivity, robust assays, good sensitivity and lower limits of detection than standard AuNPs LFs. However, the intensity of the signal was related to the size of the MNPs, being the larger ones which produced higher responses being this a drawback inasmuch as it slows significantly the assay time. Another manner to increase the signal, producing a higher magnetic field, is to increase the concentration of magnetite inside MNPs. It must not be forgotten that MNPs are strongly colored, so colorimetric response could also be measured from these LFs.

Even though nitrocellulose membranes contain pores with widths of some micrometers, the largest MNPs, combined with big analytes as spores, bacteria or cells, could clog the pores obstructing the flow of the conjugates across the membrane producing retention lines (“road closure effect”). Curiously, Wang *et al.*[179] took advantage of this

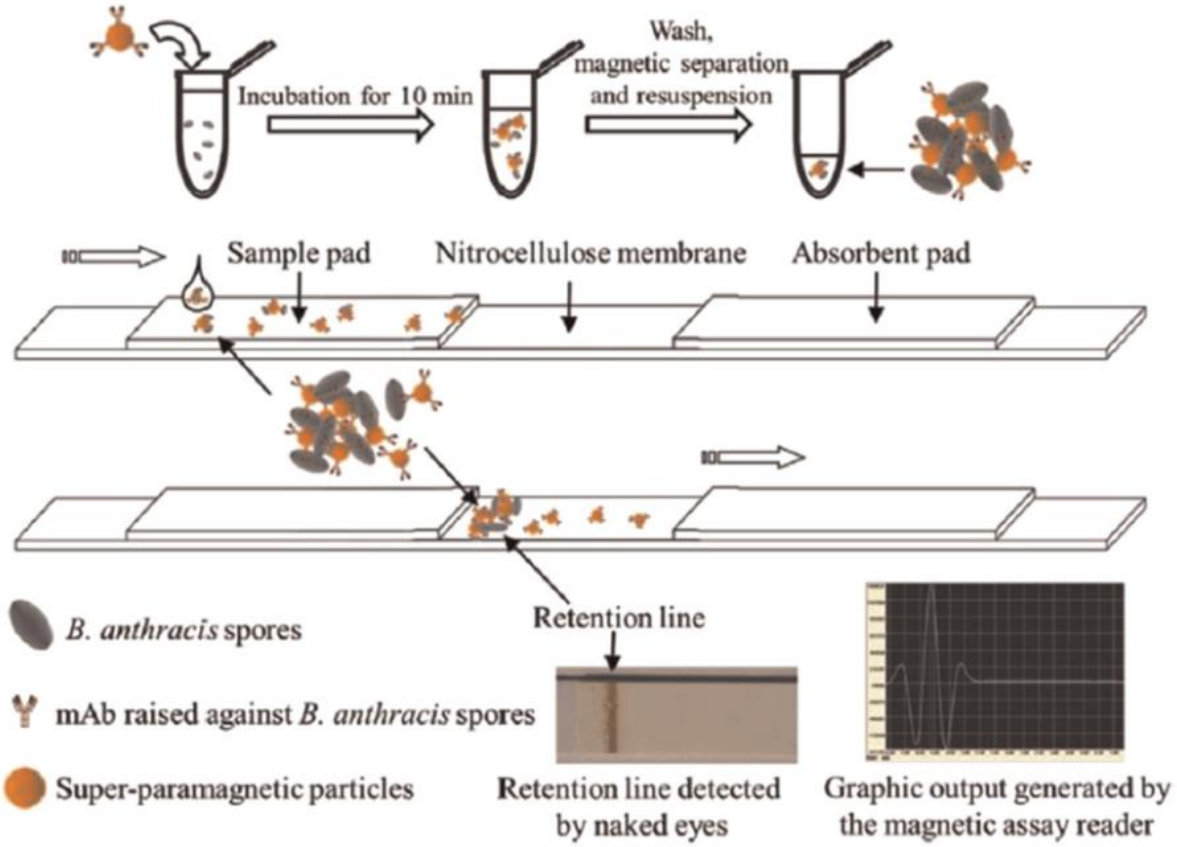

Fig. 1.32. LFs developed with MNPs as labels but without antibodies on the detection pad; "road closure effect". Reprinted with permission from ref. 179, Copyright 2015 Elsevier.

inconvenience to develop a novel LFs free of dispensed antibodies on the detection pad. Merely, in the presence of analyte, the MNPs-analyte conjugate formed the retention line at the beginning of the nitrocellulose membrane and it was measured with the MAR (Fig. 1.32). A clear advantage of this design is the cheapness of the LFs, due to the fact that antibodies printed on it use to represent near the half of its costs; also the assay is faster than in the other magnetic LFs; nonetheless the absence of CL is a huge drawback because it impedes the detection of false positives.

In addition to MAR, other technologies like the use of giant magnetoresistive sensors (GMR) are emerging[180–182]. GMR signalling is produced when the electrical resistance of the sensor is reduced by the effect of an external magnetic field derived from the MNPs. The technique can show a quite low limit of detection (12 pg/mL, Taton *et al.*[180]) but seems that its robustness and sensitivity still have to be improved.

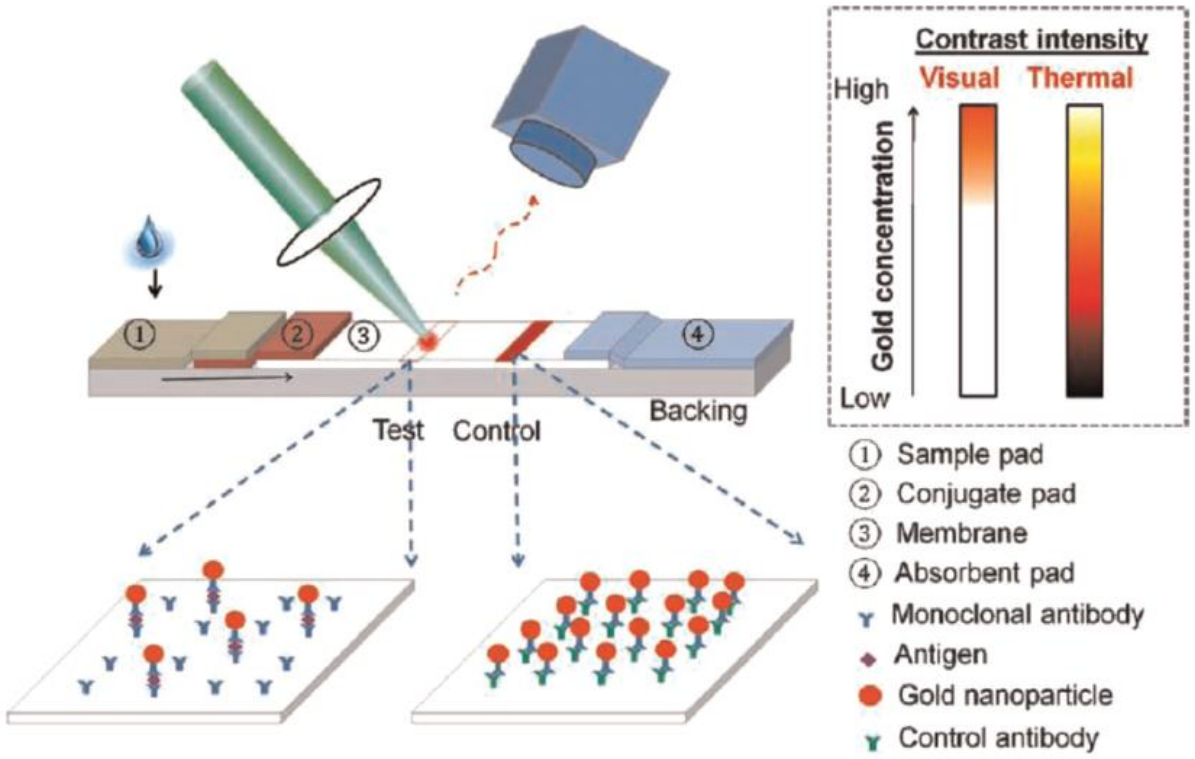

Fig. 1.33. Thermal contrast sensor applied on LFs. Reprinted with permission from ref. 183, copyright 2012 Wiley-VCH.

Thermal contrast is a technique that measures the radiation that the materials, over to absolute zero temperature, produce at infrared range. In LFs, thermal contrast can detect small variations of concentration which are not detectable with visible light, providing lower limits of detection than in the optical methods, including fluorescence in comparison to which, furthermore, avoids photobleaching effect; for this reason thermal contrast is considered a really robust and reproducible technique. Qin *et al.*[183] reported the use of thermal contrast sensor (Fig. 1.33) on AuNPs LFs and compared the registered data against visual detection, reaching a 32-fold improvement on the sensitivity. Besides spherical nanoparticles, other shapes were tested (nanorods and nanoshells), by becoming shell AuNPs the one which exhibited higher response on thermal contrast.

A technique which can be combined with LFBs to enhance its response is isotachophoresis, an electrophoretic technique used to displace and preconcentrate several kinds of compounds, from large biocompounds to small inorganic ions, forcing their displacement with other ions. Moghadam *et al.*[184,185] used this technique on LFs to concentrate the conjugate and to transport it to the TL (Fig. 1.34). The time of the assay is

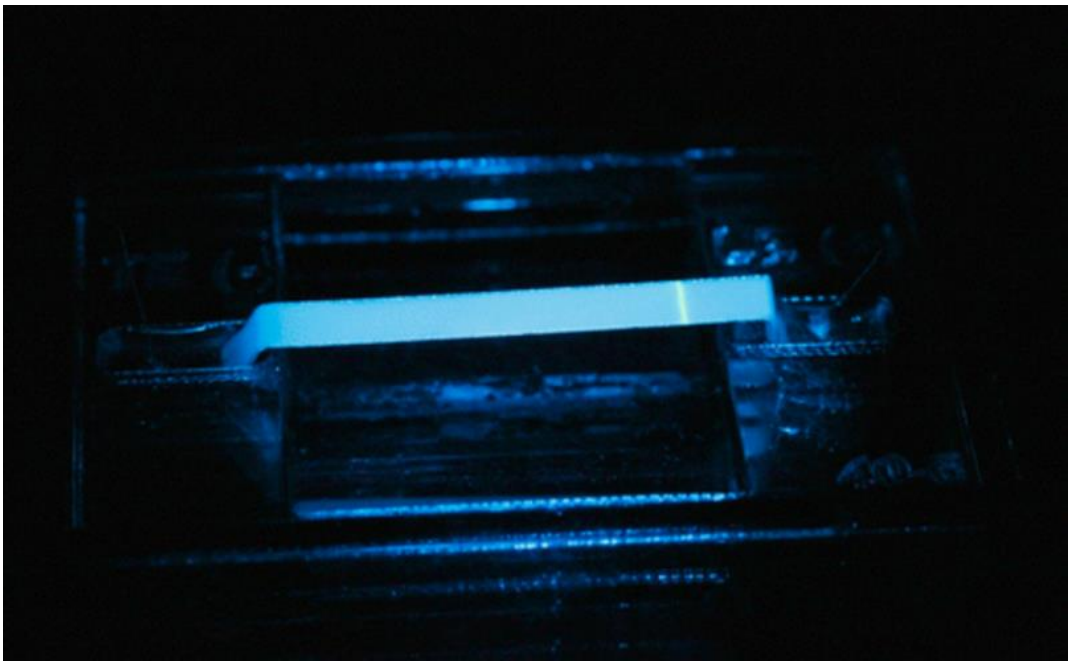

Fig. 1.34. Electrophoretic device for the pre-concentration of biological compounds applied on fluorescent microparticle-based LFBs. Adapted with permission from ref. 184. Copyright 2014 American Chemical Society.

reduced and interfering substances are left behind, as well as the limit of detection is decreased, however must be taken into account that this method requires calibration, membrane pretreatment and current application (in which is strongly dependent the sensitivity of the device).

Another detection method which can be applied on LFs is surface-enhanced Raman scattering (SERS), a technique that enhances the Raman scattering of molecules (Raman reporters: chromophores or fluorescent dyes with high photostability and that exhibit resonance at Raman frequencies) previously attached in the label nanoparticles, increasing significantly the sensitivity of the assay. Li *et al.*[186] reported the use of LFs on SERS, using AuNPs covered with 4-mercaptobenzoic acid (a Raman reporter). Their experiments demonstrated the great precision of the technology, the high selectivity against the reporters and a really low limit of detection, 0.32 pg/mL.

1.3.5. Lateral flow biosensors conspectus

Table 1.2 summarizes different detection methods which can be applied on LFBs and some of the labels reported on these methods.

1.3.6. Integration and connection of LFBs to real world applications

The use of LFBs is not restricted only to laboratory or hospital environments. LFBs are designed to be portable devices which can be used overall at home or in the field. Their use is expected to be increased in the future so, consequently, it is important to adapt LFBs to the end user. At that point, it is necessary to focus not only in the LFs design, but also to the reader that should be user-friendly and low-cost. A mobile phone contains all the components required for a common analytical reader: the screen, which can act as display and controller; an input to capture a signal, which could work via the camera[187–191]; ambient light sensors[4] and headphone jacks[192]; memory to store the data; and several wired and wireless (Wi-Fi, Bluetooth, NFC, etc.) connectivity modes. Therefore, considering the billions of mobile-phone

Table 1.2. Comparison of most remarkable methods and materials used in LFBs. Reprinted with permission from published work ref. 10. Copyright 2015 Elsevier.

Detection method	Labels	Advantages	Disadvantages
Optical (colorimetry)		• Naked-eye detection • Fast qualitative response	• Normally, only qualitative or semiquantitative response
	AuNPs	• Easy to synthetize and modify • Highly biocompatible and versatile • Intense colored • Relatively inexpensive	• Without the application of enhancement techniques, poor sensitivity and limits of detection in comparison to other methods.
	Carbon based materials	• Strong contrast against background • Different shapes and behaviors • Inexpensive and stable-in-time	• Unspecific adsorptions • Some forms have big-size: slow response assay
	Nano-/micro-particles loaded/ modified with dyes	• Inexpensive and high variety of commercial products • Good sensitivity and limits of detection	Difficult to synthesize and modifyRequire to load high quantities of dye to have a good signaling
Optical (fluorescence)		• High sensitivity • Low limits of detection	• Naked- eye detection normally is not possible • Requires equipment with both excitation light and fluorescence measurement • Materials normally exhibit photobleaching effect, lose intensity in time
	QDs	• Small-sized: fast assay • Strong intensity	• Difficult to synthetize and conjugate
	Other fluorescent materials (ex. UPTs)	• Could require less energy to be excited than QDs	• Rare elements can be expensive • Big-sized: slow assay
Electrochemical	Electroactive nanoparticles	• Highly sensitive • Low limits of detection • Devices easily miniaturized and cheap	• Requires equipment to produce and translate the signal • Reproducibility problems related to electrodes
Magnetic	Nano-/micro-particles loaded/ modified with magnetite	• Relatively inexpensive	• Require magnetic detectors
		• Colorimetric response is also possible (multi signals)	• Sensitivity related to the size of the particles: slow assays
Thermal contrast	AuNPs	• High improvement of sensitivity and reproducibility • Any material can emit signal	• Expensive equipment
SERS	Raman reporter materials	• High improvement of sensitivity and detection limits	• Expensive equipment • Requires pretreatment of the nanomaterials

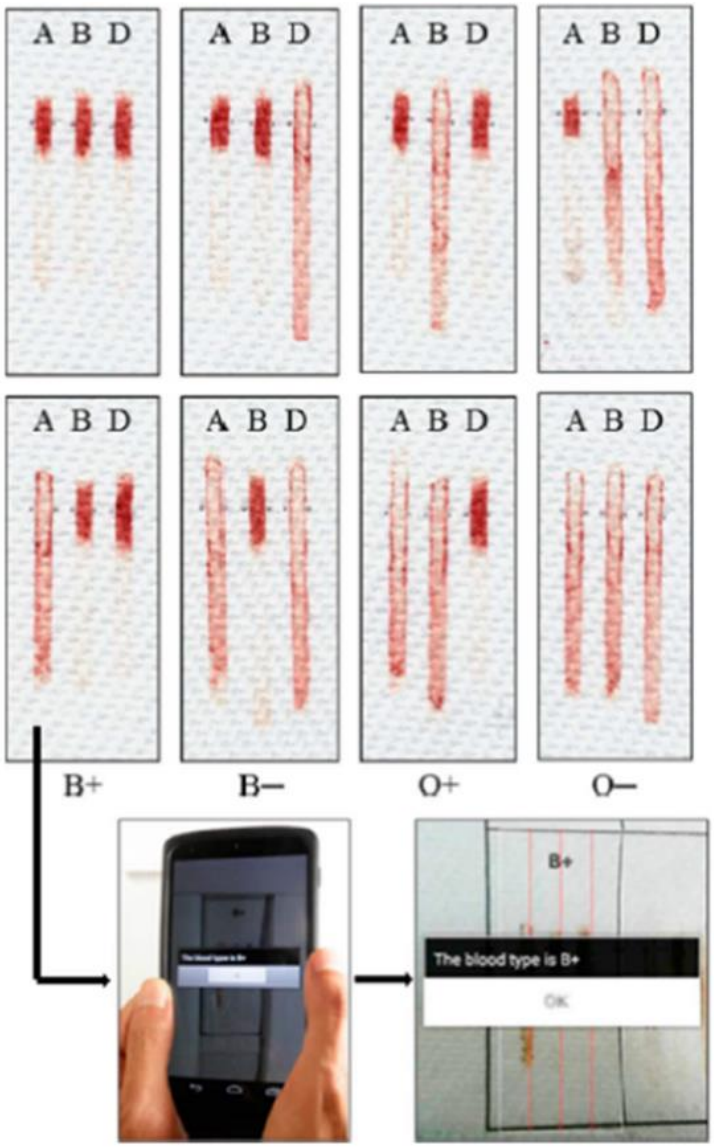

Fig. 1.35. Use of a mobile phone to interpret a paper-based biosensor for the determination of blood type. Adapted with permission from ref. 195. Copyright 2014 American Chemical Society.

users in the world, these phones are an invaluable resource for biosensing. This premise leads us to the emerging "diagnostic and communication" technology (DCT).

Mobile phone cameras can recognize small differences in color tone, as can be confirmed even in simple home experiments. This capability is based on the Lambert-Beer law, which relates the concentration of an analyte to the intensity of its color in solution[187,193,194]. A mobile phone app that can assign quantifiable values to these tonality differences could be used to maximize the potential of mobile phones coupled to optical-based biosensors as DCTs.

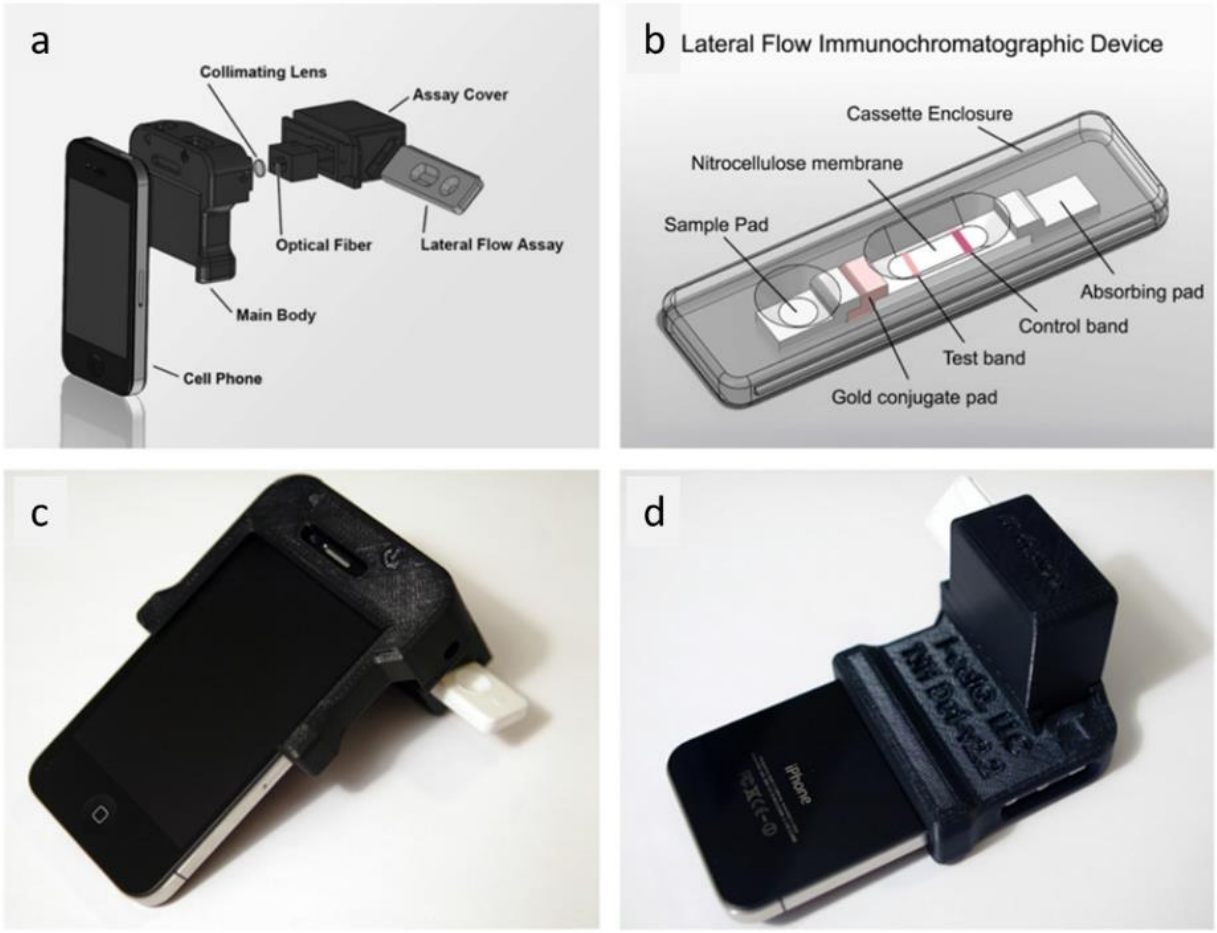

Fig. 1.36. (a) Schematic representation of LF adapter for mobile phones, (b) LF cassette composition and (c) and (d) images of the real adapter. Adapted with permission from ref. 198. Copyright 2013 Elsevier.

The simplest apps for performing colorimetric detection are based on the detection of the primary colors: red, green and blue (RGB). The standard RGB scale assigns a whole-number value from 0 to 255 for each of these three colors in a given tone, such that [0, 0, 0] corresponds to absolute black and [255, 255, 255], to true white. A good HD camera should be able to distinguish until 16777216 colors. Yetisen *et al.*,[26] developed a smartphone application algorithm for commercial colorimetric tests based on RGB detection. However, accurate use of colorimetric measurements requires careful control over parameters such as ambient light, temperature, and the distance between the camera and the sample.

Guan *et al*.[195] performed pioneering work by developing a paper-based assay for blood-typing, whereby they printed hydrophobic bar-channels, made of alkyl ketene dimer, onto Kleenex® paper. In their assay, drops of a blood sample are added to three different channels: one channel to determine the presence of antigen A; another one, for antigen B;

and a third channel, to ascertain the Rh factor. Then, buffer is added to help the blood flow through the channels. Finally, the results are transferred to a mobile phone, which informs the user of the blood type (Fig. 1.35).

LFBs and similarly-structured paper strips are easy to integrate into mobile phones, owing to their simple architecture and to the fact that they can usually just be dipped into the sample and subsequently read by a mobile phone camera. Examples of this approach have been highly reported[191,196–200]. Fig. 1.36 (You *et al.*[198]) illustrates how LFs are introduced onto an adapter (previously fabricated by stereolithographic 3D-printing) for reading via light-scattering. Mainly, these adapters exploit the mobile phone flash, as a light source and the camera, with collimating lenses, as the detector[198–200]. Alternatively, in other designs[196,197] a LED is used as the light source. Using LEDs facilitates monitoring of the incipient light (e.g. wavelength, exposure time, light angle and intensity), but requires the use of an external battery. An example of test-strip reading and signal extraction is provided in Fig. 1.37 (from Mudanyali *et al.*[196]). The test-strip image is adapted to gray-scale, and then the signalling areas are compared against the background, so that the software can decide whether the

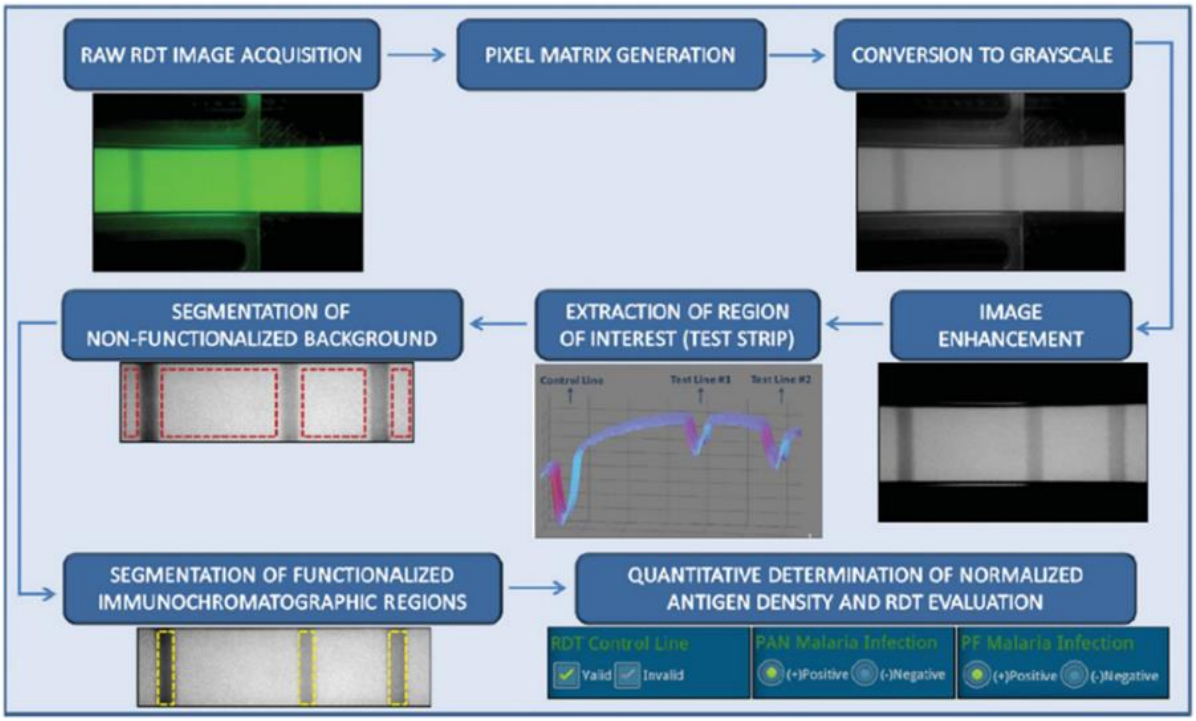

Fig. 1.37. Different steps during the image processing of a LF strip with mobile phone software. Adapted with permission from ref. 196. Copyright 2012 Royal Society of Chemistry

signal corresponds to a negative or a positive sample. Importantly, the data recorded by their app can be used to create a spatiotemporal map, based on a Google Maps interface, for tracking the possible spread of a disease.

There are emerging companies dedicated to developing software for reading and processing the data from LFs using mobile phones, through personalized software in each case. For example, Novarum[201] has created mobile phone apps that read a quick response (QR) code integrated onto LFs cassettes. The system knows how to scan and interpret the response by simply comparing pixel colors. The phone does not require any adapter. Continuing with optical sensors, there are also companies that are developing mobile phone camera lenses that offer enhanced zoom or image quality, or even enable true microscopy. For example, Blips Lenses[202] is a crowd-funded project that offers cheap lenses compatible with any mobile phone. They work by simply being attaching onto the camera.

Indisputably, mobile phones have become the ideal tools for development of DCT devices. However, in the near future, will they remain the best option? Other devices could

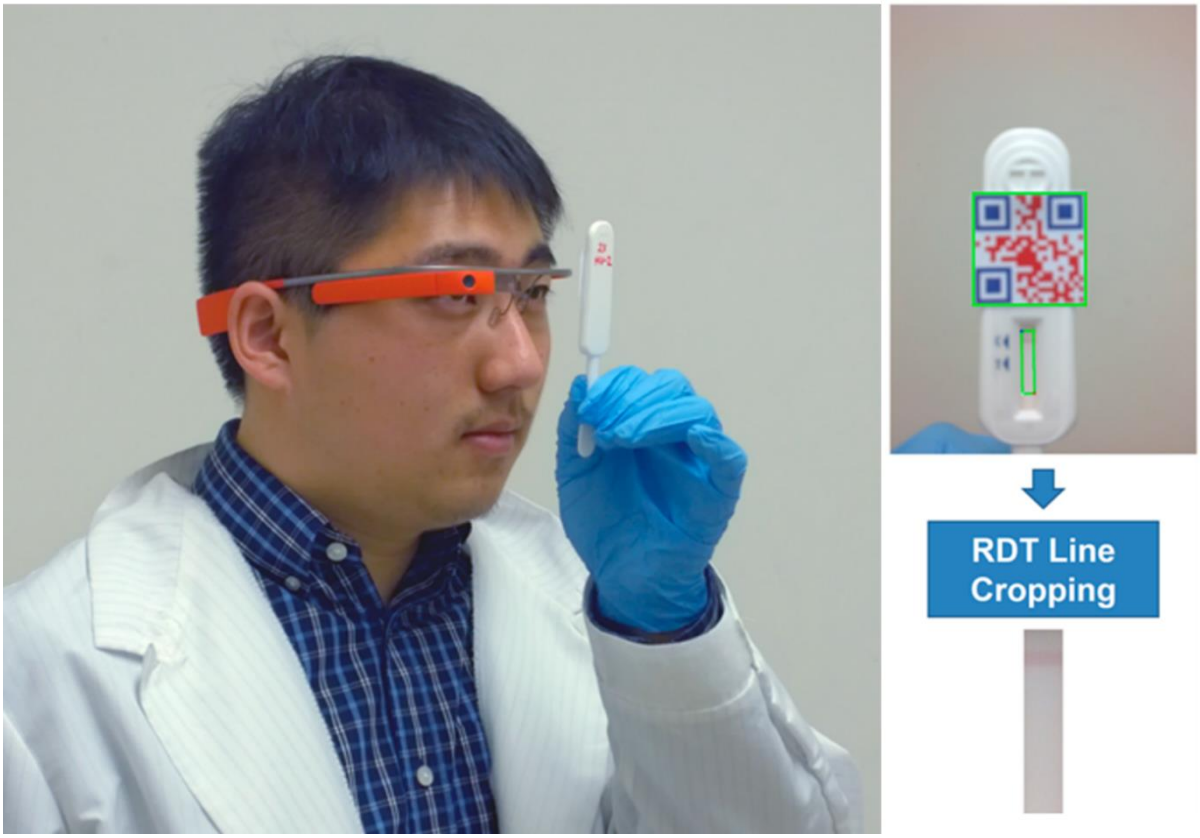

Fig. 1.38. Using Google Glass to translate the response of a LFs. By detecting the QR code the type of LFs is identified. Adapted with permission from ref. 204, copyright 2014 American Chemical Society.

appear that supersede mobile phones. A recent example that ultimately did not arrive to market is Google Glass[203], an eyeglasses-like device that was supposed to integrate augmented reality (AR) in our life by displaying images (messages, maps, video chats, text, etc.) directly in front of our eyes. In terms of the potential of Google Glass, Feng et al., 2014[204] showed that LFs could be read by simply looking at a QR code stamped on the cassette (Fig. 1.38), and then having Google Glass check the data base to determine the analyte that is being measured and its concentration relative to the intensity of the lines.

1.4. Conclusions

LFs have demonstrated to be affordable and portable tools to detect a huge variety of compounds (e.g. proteins, metallic ions, organic molecules, DNA, cells, etc.) in a really short period of time, usually shorter than 30 min, that may include pre- and post- treatments if necessary. LFs are compatible with different detection methods and nanomaterials in which strongly depend the costs, the robustness, the sensitivity and the detection limits of these devices. The variety of properties of nanoparticles allows secondary reactions to be performed onto their surface or their assembly and other modifications enhancing the intensity of the analytical signals. However, the signal of a LFs can also be easily enhanced just by modifying its architecture allowing tuning of the microfluidics beside other changes.

LFs are expected to deepen more in fast diagnostics and PoC, enabling its use at home to identify diseases or allergens, or simply to monitor biological parameters that affect our security and health. Because of this, electronic devices of common use, like smart-phones or augmented reality apparatus (like Google Glass) or future DCTs, will probably be able to work as LFs readers, providing comprehensible test instructions and results to the user.

More in detail conclusions from the state-of-the-art study of point of care devices in general and also particularly to LFs and their application can be read at the published reviews[2,7,10], attached in the annexes section.

1.5. References

1. Burns, M. A. Everyone's a (Future) Chemist. *Science* **296,** 1818 – 1819 (2002).

2. Quesada-González, D. & Merkoçi, A. Mobile phone–based biosensing: an emerging 'diagnostic and communication' technology. *Biosens. Bioelectron.* **92,** 549–562 (2016).

3. Álvarez-diduk, R., Orozco, J. & Merkoçi, A. Paper strip-embedded graphene quantum dots : a screening device with a smartphone readout. *Sci. Rep.* **7**, 976 (2017).

4. Fu, Q. *et al.* A portable smart phone-based plasmonic nanosensor readout platform that measures transmitted light intensities of nanosubstrates using an ambient light sensor. *Lab Chip* **16,** 1927–1933 (2016).

5. Azzarelli, J. M., Mirica, K. a, Ravnsbæk, J. B. & Swager, T. M. Wireless gas detection with a smartphone via rf communication. *Proc. Natl. Acad. Sci. U. S. A.* **2014,** 1–5 (2014).

6. NASA. Computers in Spaceflight: The NASA Experience. Available at: https://history.nasa.gov/computers/Part1.html. (Accessed: 8th August 2018)

7. Quesada-González, D. & Merkoçi, A. Nanomaterial-based devices for point-of-care diagnostic applications. *Chem. Soc. Rev.* 47, 4697–4709 (2018).

8. Yetisen, A. K., Akram, M. S. & Lowe, C. R. Paper-based microfluidic point-of-care diagnostic devices. *Lab Chip* **13,** 2210–2251 (2013).

9. Parolo, C. & Merkoci, A. Paper-based nanobiosensors for diagnostics. *Chem. Soc. Rev.* **42,** 450–457 (2013).

10. Quesada-González, D. & Merkoçi, A. Nanoparticle-based lateral flow biosensors. *Biosens. Bioelectron.* **73,** 47–63 (2015).

11. López-marzo, A. M. & Merkoçi, A. Paper-based sensors and assays: a success of the engineering design and the convergence of knowledge areas. *Lab Chip* **16,** 3150–3176 (2016).

12. Sher, M., Zhuang, R., Demirci, U. & Asghar, W. Paper-based analytical devices for clinical diagnosis: recent advances in the fabrication techniques and sensing mechanisms. *Expert Rev. Mol. Diagn.* **17,** 351–366 (2017).

13. Tiwari, J. N., Tiwari, R. N. & Kim, K. S. Zero-dimensional, one-dimensional, two-dimensional and three-dimensional nanostructured materials for advanced electrochemical energy devices. *Prog. Mater. Sci.* **57,** 724–803 (2012).

14. Perfézou, M., Turner, A. & Merkoçi, A. Cancer detection using nanoparticle-based sensors. *Chem. Soc. Rev.* **41,** 2606–2622 (2012).

15. Wuithschick, M., Birnbahum, A., Witte, S., Sztucki, M., Vainio, U., Pinna, N., Rademann, K., Emmerling, F., Kraehnert, R. & Polte, J. Turkevich in New Robes: Key Questions Answered for the Most Common Gold Nanoparticle Synthesis. *ACS Nano* **9,** 7052–7071 (2015).

16. Birnbaum, S., Udénxa, C., Magnusson, C. G. M. & Nilsson, S. Latex-based thin-layer immunoaffinity chromatography for quantitation of protein analytes. *Anal. Biochem.* **206,** 168–171 (1992).

17. Shyu, R. H., Shyu, H. F., Liu, H. W. & Tang, S. S. Colloidal gold-based immunochromatographic assay for detection of ricin. *Toxicon* **40,** 255–258 (2001).

18. Yen, C. W., de Puig, H., Tam, J. O., Gómez-Márquez, J., Bosch, I., Hamad-Schifferli, K. and Gehrke, L. Multicolored silver nanoparticles for multiplexed disease diagnostics: distinguishing dengue, yellow fever, and Ebola viruses. *Lab Chip* **15,** 1638–1641 (2015).

19. Morales-Narváez, E., Naghdi, T., Zor, E. & Merkoçi, A. Photoluminescent Lateral-Flow Immunoassay Revealed by Graphene Oxide: Highly Sensitive Paper-Based Pathogen Detection. *Anal Chem* **87,** 8573–8577 (2015).

20. Corstjens, P. L. A. M., Zuiderwijk, M., Nilsson, M., Feindt, H., Sam Niedbala, R. & Tanke, H.J. Lateral-flow and up-converting phosphor reporters to detect single-stranded nucleic acids in a sandwich-hybridization assay. *Anal. Biochem.* **312,** 191–200 (2003).

21. Corstjens, P. L. A. M. *et al.* Tools for diagnosis, monitoring and screening of Schistosoma infections utilizing lateral-flow based assays and upconverting phosphor labels. *Parasitology* **141,** 1841–1855 (2014).

22. Fu, E., De Dood, C.J., Kornelis, D., Fat, E.M., Wilson R.A., Kariuki T.M., Nyakundi, R.K., Loverde P.T., Abrams W.R., Tanke H.J., Van Lieshout, L., Deelder, A.M. & Van Dam, G.J. Two-dimensional paper network format that enables simple multistep assays for use in low-resource settings in the context of malaria antigen detection. *Anal. Chem.* **84,** 4574–4579 (2012).

23. Rodriguez, N. M., Wong, W. S., Liu, L., Dewar, R. & Klapperich, C. M. A fully integrated paperfluidic molecular diagnostic chip for the extraction, amplification, and detection

of nucleic acids from clinical samples. *Lab Chip* **16,** 753–763 (2016).

24. Nunes Pauli, G. E., de la Escosura-Muñiz, A., Parolo, C., Helmuth Bechtold, I. & Merkoçi, A. Lab-in-a-syringe using gold nanoparticles for rapid immunosensing of protein biomarkers. *Lab Chip* **15,** 399–405 (2014).

25. Morales-Narváez, E., Golmohammadi, H., Naghdi, T., Yousefi, H., Kostiv, U., Horák, D., Pourreza, N. & Merkoçi, A., Nanopaper as an Optical Sensing Platform. *ACS Nano* **9,** 7296–7305 (2015).

26. Yetisen, A. K., Montelongo, Y., da Cruz Vasconcellos, F., Martinez-Hurtado, J. L., Neupane, S., Butt, H., Qasim, M. M., Blyth, J., Burling, K., Bryan Carmody, J., Evans, M., Wilkinson, T. D., Kubota, L. T., Monteiro, M. J. & Lowe, C. R., Reusable, robust, and accurate laser-generated photonic nanosensor. *Nano Lett.* **14,** 3587–3593 (2014).

27. Klostranec, J. M., Xiang, Q., Farcas, G. A., Lee, J. A., Rhee, A., Lafferty, E. I., Perrault, S. D., Kain, K. C. & Chan, W. C. W. Convergence of quantum dot barcodes with microfluidics and signal processing for multiplexed high-throughput infectious disease diagnostics. *Nano Lett.* **7,** 2812–2818 (2007).

28. Da Silva, E. T. S. G., Miserere, S., Kubota, L. T. & Merkoçi, A. Simple on-plastic/paper inkjet-printed solid-state Ag/AgCl pseudoreference electrode. *Anal. Chem.* **86,** 10531–10534 (2014).

29. Park, S. J., Taton, T. A. & Mirkin, C. A. Array-Based Electrical Detection of DNA with Nanoparticle Probes. *Science* **295,** 1503–1506 (2002).

30. De La Escosura-Muñiz, A., Baptista-Pires, L., Serrano, L., Altet, L., Francino, O., Sánchez, A. & Merkoçi, A. Magnetic Bead/Gold Nanoparticle Double-Labeled Primers for Electrochemical Detection of Isothermal Amplified Leishmania DNA. *Small* **12,** 205–213 (2016).

31. Harriman, A. & Thomas, J. M. Catalytic and structural properties of iridium-iridium dioxide colloids. *New J. Chem.* **11,** (1987).

32. Rivas, L., de la Escosura-Muñiz, A., Pons, J. & Merkoçi, A. Alzheimer Disease Biomarker Detection Through Electrocatalytic Water Oxidation Induced by Iridium Oxide

Nanoparticles. *Electroanalysis* **26,** 1287–1294 (2014).

33. Rivas, L., Mayorga-Martinez, C. C., Quesada-González, D., Zamora-Gálvez, A., de la Escosura-Muñiz, A. & Merkoçi, A. Label-free impedimetric aptasensor for ochratoxin-A detection using iridium oxide nanoparticles. *Anal. Chem.* **87,** 5167–5172 (2015).

34. Mayorga-Martinez, C. C., Chamorro-García, A., Serrano, L., Rivas, L., Quesada-González, D., Altet, L., Francino, O., Sánchez, A. & Merkoçi, A. An iridium oxide nanoparticle and polythionine thin film based platform for sensitive Leishmania DNA detection. *J. Mater. Chem. B* **3,** 5166–5171 (2015).

35. Mao, X., Baloda, M., Gurung, A. S., Lin, Y. & Liu, G. Multiplex electrochemical immunoassay using gold nanoparticle probes and immunochromatographic strips. *Electrochem. commun.* **10,** 1636–1640 (2008).

36. Wu, Y., Xue, P., Kang, Y. & Hui, K. M. Paper-based microfluidic electrochemical immunodevice integrated with nanobioprobes onto graphene film for ultrasensitive multiplexed detection of cancer biomarkers. *Anal. Chem.* **85,** 8661–8668 (2013).

37. Cunningham, J. C., Kogan, M. R., Tsai, Y. J., Luo, L., Richards, I. & Crooks, R. M. Paper-Based Sensor for Electrochemical Detection of Silver Nanoparticle Labels by Galvanic Exchange. *ACS Sensors* **1,** 40–47 (2016).

38. Liong, M., Hoang, A.N., Chung, J., Gural, N., Ford, C.B., Min, C., Shah, R. R., Ahmad, R., Fernandez-Suarez, M., Fortune, S. M., Toner, M., Lee, H. & Weissleder R. Magnetic barcode assay for genetic detection of pathogens. *Nat. Commun.* **4,** 1752–1759 (2013).

39. Chung, H. J. *et al.* Nanoparticle detection of urinary markers for point-of-care diagnosis of kidney injury. *PLoS One* **10,** 1–11 (2015).

40. Mostafalu, P. & Sonkusale, S. A high-density nanowire electrode on paper for biomedical applications. *RSC Adv.* **5,** 8680–8687 (2015).

41. Ali, M. A., Solanki, P. R., Srivastava, S., Singh, S., Agrawal, V. V., John, R. & Malhotra, B. D. Protein Functionalized Carbon Nanotubes-based Smart Lab-on-a-Chip. *ACS Appl. Mater. Interfaces* **7,** 5837–5846 (2015).

42. Teixeira, S., Conlan, R. S., Guy, O. J. & Sales, M. G. F. Novel single-wall carbon nanotube

screen-printed electrode as an immunosensor for human chorionic gonadotropin. *Electrochim. Acta* **136,** 323–329 (2014).

43. Nemiroski, A., Christodouleas, D. C., Hennek, J. W., Kumar, A. A., Maxwell, E. J., Fernández-Abedul, M. T. and Whitesides, G. M. Universal mobile electrochemical detector designed for use in resource-limited applications. *Proc. Natl. Acad. Sci. U. S. A.* **111,** 11984–9 (2014).

44. Darabi, M. A., Khosrozadeh, A., Wang, Q. & Xing, M. Gum Sensor: A Stretchable, Wearable, and Foldable Sensor Based on Carbon Nanotube/Chewing Gum Membrane. *ACS Appl. Mater. Interfaces* **7,** 26195–26205 (2015).

45. Morales-Narváez, E., Baptista-Pires, L., Zamora-Gálvez, A. & Merkoçi, A. Graphene-Based Biosensors: Going Simple. *Adv. Mater.* **29,** (2017).

46. Cheeveewattanagul, N., Morales-Narváez, E., Hassan, A. R. H. A., Bergua, J. F., Surareungchai, W., Somasundrum, M. & Merkoçi, A. Straightforward Immunosensing Platform Based on Graphene Oxide-Decorated Nanopaper: A Highly Sensitive and Fast Biosensing Approach. *Adv. Funct. Mater.* **27,** 1–8 (2017).

47. Teixeira, S., Conlan, R. S., Guy, O. J. & Sales, M. G. F. Label-free human chorionic gonadotropin detection at picogram levels using oriented antibodies bound to graphene screen-printed electrodes. *J. Mater. Chem. B* **2,** 1852–1865 (2014).

48. Tuteja, S. K., Priyanka, Bhalla, V., Deep, A., Paul, A. K., Suri, C.R. Graphene-gated biochip for the detection of cardiac marker Troponin I. *Anal. Chim. Acta* **809,** 148–154 (2014).

49. Baptista-Pires, L., Mayorga-Martínez, C. C., Medina-Sánchez, M., Montón, H. & Merkoçi, A. Water activated graphene oxide transfer using wax printed membranes for fast patterning of a touch sensitive device. *ACS Nano* **10,** 853–860 (2016).

50. Polat, E. O., Balci, O. & Kocabas, C. Graphene based flexible electrochromic devices. *Sci. Rep.* **4,** 6484 (2015).

51. Li, W. *et al.* Multiplex electrochemical origami immunodevice based on cuboid silver-paper electrode and metal ions tagged nanoporous silver-chitosan. *Biosens. Bioelectron.* **56,** 167–173 (2014).

52. Marques, A. C., Santos, L., Costa, M. N., Dantas, J. M., Duarte, P., Gonçalves, A., Martins, R., Salgueiro, C. A. & Fortunato, E. Office paper platform for bioelectrochromic detection of electrochemically active bacteria using tungsten trioxide nanoprobes. *Sci. Rep.* **5,** 1–7 (2015).

53. Xu, X., Subbaraman, H., Chakravarty, S., Hosseini, A., Covey, J., Yu, Y., Kwong, D., Zhang, Y., Lai, W. C., Zou, Y., Lu, N. and Chen, R. T. Flexible single-crystal silicon nanomembrane photonic crystal cavity. *ACS Nano* **8,** 12265–12271 (2014).

54. Choi, C. J. & Cunningham, B. T. A 96-well microplate incorporating a replica molded microfluidic network integrated with photonic crystal biosensors for high throughput kinetic biomolecular interaction analysis. *Lab Chip* **7,** 550–556 (2007).

55. Schudel, B. R., Choi, C. J., Cunningham, B. T. & Kenis, P. J. A. Microfluidic chip for combinatorial mixing and screening of assays. *Lab Chip* **9,** 1676–1680 (2009).

56. Cullen, D. K., Xu, Y., Reneer, D. V., Browne, K. D., Geddes, J. W., Yang, S. & Smith, D.H. Color changing photonic crystals detect blast exposure. *Neuroimage* **54,** S37–S44 (2011).

57. Clark. Continuous Recording of Blood Oxygen Tensions by Polarography. *J. Appiel Physiol.* **6,** 189–193 (1953).

58. Costa, M. N., Veigas, B., Jacob, J. M., Santos, D. S., Gomes, J., Baptista, P. V., Martins, R., Inácio, J. & Fortunato, E. A low cost, safe, disposable, rapid and self-sustainable paper-based platform for diagnostic testing: lab-on-paper. *Nanotechnology* **25,** 094006 (2014).

59. Mazumdar, D., Liu, J., Lu, G., Zhou, J. & Lu, Y. Easy-to-use dipstick tests for detection of lead in paints using non-cross-linked gold nanoparticle-DNAzyme conjugates. *Chem. Commun.* **46,** 1416–8 (2010).

60. Torabi, S. F. & Lu, Y. Small-molecule diagnostics based on functional DNA nanotechnology: a dipstick test for mercury. *Faraday Discuss.* **149,** 125–135 (2011).

61. Kuang, H. *et al.* Rapid and highly sensitive detection of lead ions in drinking water based on a strip immunosensor. *Sensors* **13,** 4214–4224 (2013).

62. López-Marzo, A. M., Pons, J., Blake, D. A. & Merkoçi, A. High sensitive gold-nanoparticle based lateral flow Immunodevice for Cd2+ detection in drinking waters. *Biosens. Bioelectron.* **47,** 190–198 (2013).

63. López Marzo, A. M., Pons, J., Blake, D. A. & Merkoçi, A. All-integrated and highly sensitive paper based device with sample treatment platform for Cd2+ immunodetection in drinking/tap waters. *Anal. Chem.* **85,** 3532–3538 (2013).

64. Wang, X. *et al.* Development of an immunochromatographic lateral-flow test strip for rapid detection of sulfonamides in eggs and chicken muscles. *J. Agric. Food Chem.* **55,** 2072–2078 (2007).

65. Shukla, S., Leem, H. & Kim, M. Development of a liposome-based immunochromatographic strip assay for the detection of Salmonella. *Anal. Bioanal. Chem.* **401,** 2581–2590 (2011).

66. Preechakasedkit, P. *et al.* Development of a one-step immunochromatographic strip test using gold nanoparticles for the rapid detection of Salmonella typhi in human serum. *Biosens. Bioelectron.* **31,** 562–566 (2012).

67. Leem, H., Shukla, S., Song, X., Heu, S. & Kim, M. An Efficient Liposome-Based Immunochromatographic Strip Assay for the Sensitive Detection of SalmonellaTyphimurium in Pure Culture. *J. Food Saf.* **34,** 239–248 (2014).

68. Berlina, A. N., Taranova, N. A., Zherdev, A. V., Vengerov, Y. Y. & Dzantiev, B. B. Quantum dot-based lateral flow immunoassay for detection of chloramphenicol in milk. *Anal. Bioanal. Chem.* **405,** 4997–5000 (2013).

69. Anfossi, L., Di Nardo, F., Giovannoli, C., Passini, C. & Baggiani, C. Increased sensitivity of lateral flow immunoassay for ochratoxin A through silver enhancement. *Anal. Bioanal. Chem.* **405,** 9859–9867 (2013).

70. Zhou, P. *et al.* Nanocolloidal gold-based immunoassay for the detection of the N-methylcarbamate pesticide carbofuran. *J. Agric. Food Chem.* **52,** 4355–4359 (2004).

71. Kim, Y. A. *et al.* Competitive immunochromatographic assay for the detection of the organophosphorus pesticide chlorpyrifos. *Anal. Chim. Acta* **693,** 106–113 (2011).

72. Wang, L. *et al.* A bare-eye-based lateral flow immunoassay based on the use of gold nanoparticles for simultaneous detection of three pesticides. *Microchim. Acta* **181,** 1565–1572 (2014).

73. Inoue, K., Ferrante, P., Hirano, Y., Yasukawa, T., Shiku, H., Matsue, T. A competitive immunochromatographic assay for testosterone based on electrochemical detection. *Talanta* **73,** 886–892 (2007).

74. Cazacu, A. C. *et al.* Comparison of a new lateral-flow chromatographic membrane immunoassay to viral culture for rapid detection and differentiation of influenza A and B viruses in respiratory specimens. *J. Clin. Microbiol.* **42,** 3661–3664 (2004).

75. Held, J., Schmidt, T., Thornton, C. R., Kotter, E. & Bertz, H. Comparison of a novel Aspergillus lateral-flow device and the Platelia® galactomannan assay for the diagnosis of invasive aspergillosis following haematopoietic stem cell transplantation. *Infection* **41,** 1163–1169 (2013).

76. John, A. S., Boyd, J. C., Lowes, A. J. & Price, C. P. The Use of Urinary Dipstick Tests to Exclude Urinary Tract Infection. *Am. J. Clin. Pathol.* **126,** 428–436 (2006).

77. Vidal, J. E. *et al.* Asymptomatic cryptococcal antigen prevalence detected by lateral flow assay in hospitalised HIV-infected patients in São Paulo, Brazil. *Trop. Med. Int. Heal.* **21,** 1539–1544 (2016).

78. Dector, A. *et al.* Towards autonomous lateral flow assays: Paper-based microfluidic fuel cell inside an HIV-test using a blood sample as fuel. *Int. J. Hydrogen Energy* **42,** 27979–27986 (2017).

79. Rohrman, B. A., Leautaud, V., Molyneux, E. & Richards-Kortum, R. R. A Lateral Flow Assay for Quantitative Detection of Amplified HIV-1 RNA. *PLoS One* **7,** (2012).

80. Carrio, A., Sampedro, C., Sanchez-Lopez, J. L., Pimienta, M. & Campoy, P. Automated low-cost smartphone-based lateral flow saliva test reader for drugs-of-abuse detection. *Sensors* **15,** 29569–29593 (2015).

81. Cordray, M. S., Amdahl, M. & Richards-Kortum, R. R. Gold nanoparticle aggregation for quantification of oligonucleotides: Optimization and increased dynamic range. *Anal.*

Biochem. **431,** 99–105 (2012).

82. Kersting, S., Rausch, V., Bier, F. F. & Von Nickisch-Rosenegk, M. Rapid detection of Plasmodium falciparum with isothermal recombinase polymerase amplification and lateral flow analysis. *Malar. J.* **13,** 1–9 (2014).

83. Qian, S. & Bau, H. H. A mathematical model of lateral flow bioreactions applied to sandwich assays. *Anal. Biochem.* **322,** 89–98 (2003).

84. Assadollahi, S., Reininger, C., Palkovits, R., Pointl, P. & Schalkhammer, T. From lateral flow devices to a novel nano-color microfluidic assay. *Sensors* **9,** 6084–6100 (2009).

85. Lee, J. Y. *et al.* Importance of membrane selection in the development of immunochromatographic assays for low-molecular weight compounds. *Anal. Chim. Acta* **757,** 69–74 (2012).

86. Linares, E. M., Kubota, L. T., Michaelis, J. & Thalhammer, S. Enhancement of the detection limit for lateral flow immunoassays: Evaluation and comparison of bioconjugates. *J. Immunol. Methods* **375,** 264–270 (2012).

87. De La Escosura-Muñiz, A., Parolo, C. & Merkoi, A. Immunosensing using nanoparticles. *Mater. Today* **13,** 24–34 (2010).

88. Parolo, C., de la Escosura-Muñiz, A., Polo, E., Grazú, V., de la Fuente, J. M. & Merkoçi, A. Design, preparation, and evaluation of a fixed-orientation antibody/gold-nanoparticle conjugate as an immunosensing label. *ACS Appl. Mater. Interfaces* **5,** 10753–10759 (2013).

89. Aragay, G., Montón, H., Pons, J., Font-Bardía, M. & Merkoçi, A. Rapid and highly sensitive detection of mercury ions using a fluorescence-based paper test strip with an N-alkylaminopyrazole ligand as a receptor. *J. Mater. Chem.* **22,** 5978–5983 (2012).

90. Ahmad, A. L., Low, S. C., Abd Shukor, S. R. & Ismail, A. Morphological and thermal-mechanical stretching properties on polymeric lateral flow nitrocellulose membrane. *Ind. Eng. Chem. Res.* **48,** 3417–3424 (2009).

91. Zhu, X., Shah, P., Stoff, S., Liu, H. & Li, C. A paper electrode integrated lateral flow immunosensor for quantitative analysis of oxidative stress induced DNA damage.

Analyst **139,** 2850–7 (2014).

92. Oh, J. S., Ha, G. W., Cho, Y. S., Kim, M. J., An, D. J., Hwang, K. K., Lim, Y. K., Park, B. K., Kang, B. K., Song, D. S. One-Step Immunochromatography Assay Kit for Detecting Antibodies to Canine Parvovirus One-Step Immunochromatography Assay Kit for Detecting Antibodies to Canine Parvovirus. *Clin. Vaccine Immunol.* **13,** 520–524 (2006).

93. Liu, J., Mazumdar, D. & Lu, Y. A simple and sensitive 'dipstick' test in serum based on lateral flow separation of aptamer-linked nanostructures. *Angew. Chemie - Int. Ed.* **45,** 7955–7959 (2006).

94. Liu, G. *et al.* Aptamer - Nanoparticle Strip Biosensor for Sensitive Detection of Cancer Cells. *Anal. Chem.* **81,** 10013–10018 (2009).

95. Mao, X. *et al.* Disposable nucleic acid biosensors based on gold nanoparticle probes and lateral flow strip. *Anal. Chem.* **81,** 1660–1668 (2009).

96. Lie, P. *et al.* A lateral flow biosensor for detection of nucleic acids with high sensitivity and selectivityw. *Chem. Commun. Chem. Commun* **48,** 236–238 (2012).

97. Claudia Kolm, Robert L. Mach, R. K. and K. B. A rapid DNA lateral flow test for the detection of transgenic maize by isothermal amplification of the 35S promoter. *Anal. Methods* **7,** 129–134 (2015).

98. Xu, H. *et al.* Aptamer-Functionalized Gold Nanoparticles as Probes in a Dry-Reagent Strip Biosensor for Protein Analysis Aptamer-Functionalized Gold Nanoparticles as Probes in a Dry-Reagent Strip Biosensor for Protein. **81,** 669–675 (2009).

99. Karakus, C. Development of a lateral flow immunoassay strip for rapid detection of CagA antigen of Helicobacter pylori. *J. Immunoassay Immunochem.* **36,** 324–33 (2015).

100. Liu, D. *et al.* A modified lateral flow immunoassay for the detection of trace aflatoxin M1 based on immunomagnetic nanobeads with different antibody concentrations. *Food Control* **51,** 218–224 (2015).

101. Fang, Z. *et al.* Lateral flow nucleic acid biosensor for Cu2+ detection in aqueous solution with high sensitivity and selectivity. *Chem. Commun. (Camb).* **46,** 9043–9045 (2010).

102. Elenis, D. S., Ioannou, P. C. & Christopoulos, T. K. A nanoparticle-based sensor for visual

detection of multiple mutations. *Nanotechnology* **22,** 155501 (2011).

103. Song, S. *et al.* Multiplex lateral flow immunoassay for mycotoxin determination. *Anal. Chem.* **86,** 4995–5001 (2014).

104. Kim, K. Y., Shim, W. B., Kim, J. S. & Chung, D. H. Development of a simultaneous lateral flow strip test for the rapid and simple detection of deoxynivalenol and zearalenone. *J. Food Sci.* **79,** M2048–M2055 (2014).

105. Chen, J., Fang, Z., Lie, P. & Zeng, L. Computational lateral flow biosensor for proteins and small molecules: A new class of strip logic gates. *Anal. Chem.* **84,** 6321–6325 (2012).

106. Huang, Y. *et al.* A universal lateral flow biosensor for proteins and DNAs based on the conformational change of hairpin oligonucleotide and its use for logic gate operations. *Biosens. Bioelectron.* **61,** 598–604 (2014).

107. Parolo, C., de la Escosura-Muñiz, A. & Merkoçi, A. Enhanced lateral flow immunoassay using gold nanoparticles loaded with enzymes. *Biosens. Bioelectron.* **40,** 412–416 (2013).

108. Rastogi, S. K. *et al.* DNA detection on lateral flow test strips: enhanced signal sensitivity using LNA-conjugated gold nanoparticles. *Chem. Commun.* **48,** 7714 (2012).

109. Fridley, G. E., Le, H. Q., Fu, E. & Yager, P. Controlled release of dry reagents in porous media for tunable temporal and spatial distribution upon rehydration. *Lab Chip* **12,** 4321–7 (2012).

110. Li, X. *et al.* A fast and sensitive immunoassay of avian influenza virus based on label-free quantum dot probe and lateral flow test strip. *Talanta* **100,** 1–6 (2012).

111. Shi, C. Y. *et al.* A fluorescent polymer dots positive readout fluorescent quenching lateral flow sensor for ractopamine rapid detection. *Anal. Chim. Acta* **854,** 202–208 (2015).

112. Xu, H. *et al.* Gold-nanoparticle-decorated silica nanorods for sensitive visual detection of proteins. *Anal. Chem.* **86,** 7351–7359 (2014).

113. Hu, J. *et al.* Oligonucleotide-linked gold nanoparticle aggregates for enhanced

sensitivity in lateral flow assays. *Lab Chip* **13,** 4352 (2013).

114. Ge, C., Yu, L., Fang, Z. & Zeng, L. An enhanced strip biosensor for rapid and sensitive detection of histone methylation. *Anal. Chem.* **85,** 9343–9349 (2013).

115. Choi, D. H. *et al.* A dual gold nanoparticle conjugate-based lateral flow assay (LFA) method for the analysis of troponin I. *Biosens. Bioelectron.* **25,** 1999–2002 (2010).

116. Fu, E. *et al.* Paper Network Format. *Cellulose* 7941–7946 (2011). doi:10.1021/ac201950g.Enhanced

117. Fu, E., Lutz, B., Kauffman, P. & Yager, P. Controlled reagent transport in disposable 2D paper networks. *Lab Chip* **10,** 918 (2010).

118. Fenton, E. M., Mascarenas, M. R., López, G. P. & Sibbett, S. S. Multiplex lateral-flow test strips fabricated by two-dimensional shaping. *ACS Appl. Mater. Interfaces* **1,** 124–129 (2009).

119. Li, C. Z. *et al.* Paper based point-of-care testing disc for multiplex whole cell bacteria analysis. *Biosens. Bioelectron.* **26,** 4342–4348 (2011).

120. Parolo, C., Medina-Sánchez, M., de la Escosura-Muñiz, A. & Merkoçi, A. Simple paper architecture modifications lead to enhanced sensitivity in nanoparticle based lateral flow immunoassays. *Lab Chip* **13,** 386–390 (2013).

121. Hong, S. Y., Park, Y. M., Jang, Y. H., Min, B. H. & Yoon, H. C. Quantitative lateral-flow immunoassay for the assessment of the cartilage oligomeric matrix protein as a marker of osteoarthritis. *Biochip J.* **6,** 213–220 (2012).

122. Renault, C., Koehne, J., Ricco, A. J. & Crooks, R. M. Three-dimensional wax patterning of paper fluidic devices. *Langmuir* **30,** 7030–7036 (2014).

123. Rivas, L., Medina-Sánchez, M., de la Escosura-Muñiz, A. & Merkoçi, A. Improving sensitivity of gold nanoparticle-based lateral flow assays by using wax-printed pillars as delay barriers of microfluidics. *Lab Chip* **14,** 4406–14 (2014).

124. Yang, H. *et al.* A novel quantum dots-based point of care test for syphilis. *Nanoscale Res. Lett.* **5,** 875–881 (2010).

125. Wang, L. *et al.* Fluorescent strip sensor for rapid determination of toxins. *Chem. Commun.* **47,** 1574–1576 (2011).

126. Bruno, J. Application of DNA Aptamers and Quantum Dots to Lateral Flow Test Strips for Detection of Foodborne Pathogens with Improved Sensitivity versus Colloidal Gold. *Pathogens* **3,** 341–355 (2014).

127. Bai, Y. *et al.* A sensitive lateral flow test strip based on silica nanoparticle/CdTe quantum dot composite reporter probes. *RSC Adv.* **2,** 1778 (2012).

128. Ren, M. *et al.* Immunochromatographic Assay for Ultrasensitive Detection of A fl atoxin B 1 in Maize by Highly Luminescent Quantum Dot Beads. (2014).

129. Corstjens, P. *et al.* Use of up-converting phosphor reporters in lateral-flow assays to detect specific nucleic acid sequences: A rapid, sensitive DNA test to identify human papillomavirus type 16 infection. *Clin. Chem.* **47,** 1885–1893 (2001).

130. Corstjens, P. L. A. M. *et al.* Up-converting phosphor technology-based lateral flow assay for detection of Schistosoma circulating anodic antigen in serum. *J. Clin. Microbiol.* **46,** 171–176 (2008).

131. Corstjens, P. L. A. M. *et al.* A user-friendly, highly sensitive assay to detect the IFN-?? secretion by T cells. *Clin. Biochem.* **41,** 440–444 (2008).

132. Paterson, A. S. *et al.* Persistent luminescence strontium aluminate nanoparticles as reporters in lateral flow assays. *Anal. Chem.* **86,** 9481–9488 (2014).

133. Rundström, G., Jonsson, A., Mårtensson, O., Mendel-Hartvig, I. & Venge, P. Lateral flow immunoassay using europium (III) chelate microparticles and time-resolved fluorescence for eosinophils and neutrophils in whole blood. *Clin. Chem.* **53,** 342–348 (2007).

134. Xia, X., Xu, Y., Zhao, X. & Li, Q. Lateral flow immunoassay using europium chelate-loaded silica nanoparticles as labels. *Clin. Chem.* **55,** 179–182 (2009).

135. Tang, X. *et al.* Sample-pretreatment-free based high sensitive determination of aflatoxin M1 in raw milk using a time-resolved fluorescent competitive immunochromatographic assay. *RSC Adv.* **5,** 558–564 (2015).

136. Zhang, F. *et al.* Lanthanide-labeled immunochromatographic strips for the rapid detection of Pantoea stewartii subsp. Stewartii. *Biosens. Bioelectron.* **51,** 29–35 (2014).

137. Huang, X. *et al.* Fluorescent Ru(phen)32+-doped silica nanoparticles-based ICTS sensor for quantitative detection of enrofloxacin residues in chicken meat. *Anal. Chem.* **85,** 5120–5128 (2013).

138. Edwards, K. A. & Baeumner, A. J. Optimization of DNA-tagged dye-encapsulating liposomes for lateral-flow assays based on sandwich hybridization. *Anal. Bioanal. Chem.* **386,** 1335–1343 (2006).

139. Khreich, N. *et al.* Detection of Staphylococcus enterotoxin B using fluorescent immunoliposomes as label for immunochromatographic testing. *Anal. Biochem.* **377,** 182–188 (2008).

140. Xie, Q. Y. *et al.* Advantages of fluorescent microspheres compared with colloidal gold as a label in immunochromatographic lateral flow assays. *Biosens. Bioelectron.* **54,** 262–265 (2014).

141. Wang, Z. *et al.* Development and Application of a Quantitative Fluorescence-Based Immunochromatographic Assay for Fumonisin B 1 in Maize. *J. Agric. Food Chem.* **62,** 6294–6298 (2014).

142. Zhou, J. *et al.* Development of a microsphere-based fluorescence immunochromatographic assay for monitoring lincomycin in milk, honey, beef, and swine urine. *J. Agric. Food Chem.* **62,** 12061–12066 (2014).

143. Linares, E. M., Kubota, L. T., Michaelis, J. & Thalhammer, S. Enhancement of the detection limit for lateral flow immunoassays: Evaluation and comparison of bioconjugates. *J. Immunol. Methods* **375,** 264–270 (2012).

144. Lönnberg, M. & Carlsson, J. Quantitative detection in the attomole range for immunochromatographic tests by means of a flatbed scanner. *Anal. Biochem.* **293,** 224–31 (2001).

145. Van Dam, G. J. *et al.* Diagnosis of schistosomiasis by reagent strip test for detection of circulating cathodic antigen. *J. Clin. Microbiol.* **42,** 5458–5461 (2004).

146. Rayev, M. & Shmagel, K. Carbon-protein covalent conjugates in non-instrumental immunodiagnostic systems. *J. Immunol. Methods* **336,** 9–15 (2008).

147. Kalogianni, D. P., Boutsika, L. M., Kouremenou, P. G., Christopoulos, T. K. & Ioannou, P. C. Carbon nano-strings as reporters in lateral flow devices for DNA sensing by hybridization. *Anal. Bioanal. Chem.* **400,** 1145–1152 (2011).

148. Noguera, P. *et al.* Carbon nanoparticles in lateral flow methods to detect genes encoding virulence factors of Shiga toxin-producing Escherichia coli. *Anal. Bioanal. Chem.* **399,** 831–838 (2011).

149. Koets, M., Sander, I., Bogdanovic, J., Doekes, G. & van Amerongen, A. A rapid lateral flow immunoassay for the detection of fungal alpha-amylase at the workplace. *J. Environ. Monit.* **8,** 942–6 (2006).

150. Blažková, M., Mičková-Holubová, B., Rauch, P. & Fukal, L. Immunochromatographic colloidal carbon-based assay for detection of methiocarb in surface water. *Biosens. Bioelectron.* **25,** 753–758 (2009).

151. Blažková, M., Rauch, P. & Fukal, L. Strip-based immunoassay for rapid detection of thiabendazole. *Biosens. Bioelectron.* **25,** 2122–2128 (2010).

152. Abera, A. & Choi, J.-W. Quantitative lateral flow immunosensor using carbon nanotubes as label. *Anal. Methods* **2,** 1819–1822 (2010).

153. Qiu, W. *et al.* Carbon nanotube-based lateral flow biosensor for sensitive and rapid detection of DNA sequence. *Biosens. Bioelectron.* **64,** 367–372 (2015).

154. Lou, S. C., Patel, C., Ching, S. & Gordon, J. One-step competitive immunochromatographic assay for semiquantitative determination of lipoprotein(a) in plasma. *Clin. Chem.* **39,** 619–624 (1993).

155. Wang, Z. *et al.* Lateral flow test strip based on colloidal selenium immunoassay for rapid detection of melamine in milk, milk powder, and animal feed. *Int. J. Nanomedicine* **9,** 1699–1707 (2014).

156. C, L. *et al.* Lateral flow immunochromatographic assay for sensitive pesticide detection by using Fe3O4 nanoparticle aggregates as color reagents. *Anal Chem* **83,** 6778–6784

(2011).

157. Park, J. M. *et al.* Chemiluminescence lateral flow immunoassay based on Pt nanoparticle with peroxidase activity. *Anal. Chim. Acta* **853,** 360–367 (2015).

158. Greenwald, R. *et al.* Improved serodetection of Mycobacterium bovis infection in badgers (Meles meles) using multiantigen test formats. *Diagn. Microbiol. Infect. Dis.* **46,** 197–203 (2003).

159. Waters, W. R. *et al.* Early antibody responses to experimental Mycobacterium bovis infection of cattle. *Clin. Vaccine Immunol.* **13,** 648–654 (2006).

160. Campbell, K. *et al.* Development and validation of a lateral flow device for the detection of nicarbazin contamination in poultry feeds. *J. Agric. Food Chem.* **55,** 2497–2503 (2007).

161. Lyashchenko, K. P. *et al.* PrimaTB STAT-PAK assay, a novel, rapid lateral-flow test for tuberculosis in nonhuman primates. *Clin. Vaccine Immunol.* **14,** 1158–1164 (2007).

162. Ho, J. A. A. & Wauchope, R. D. A strip liposome immunoassay for aflatoxin B1. *Anal. Chem.* **74,** 1493–1496 (2002).

163. Baeumner, A. J., Pretz, J. & Fang, S. A Universal Nucleic Acid Sequence Biosensor with Nanomolar Detection Limits. *Anal. Chem.* **76,** 888–894 (2004).

164. Baeumner, A. J., Jones, C., Wong, C. Y. & Price, A. A generic sandwich-type biosensor with nanomolar detection limits. *Anal. Bioanal. Chem.* **378,** 1587–1593 (2004).

165. Wen, H. W., Borejsza-Wysocki, W., Decory, T. R. & Durst, R. A. Development of a competitive liposome-based lateral flow assay for the rapid detection of the allergenic peanut protein Ara h1. *Anal. Bioanal. Chem.* **382,** 1217–1226 (2005).

166. Ho, J. A. A., Zeng, S. C., Tseng, W. H., Lin, Y. J. & Chen, C. H. Liposome-based immunostrip for the rapid detection of Salmonella. *Anal. Bioanal. Chem.* **391,** 479–485 (2008).

167. Wang, L. *et al.* A novel immunochromatographic electrochemical biosensor for highly sensitive and selective detection of trichloropyridinol, a biomarker of exposure to chlorpyrifos. *Biosens. Bioelectron.* **26,** 2835–2840 (2011).

168. Du, D., Wang, J., Wang, L., Lu, D. & Lin, Y. Integrated lateral flow test strip with electrochemical sensor for quantification of phosphorylated cholinesterase: Biomarker of exposure to organophosphorus agents. *Anal. Chem.* **84,** 1380–1385 (2012).

169. Liu, G. *et al.* Disposable electrochemical immunosensor diagnosis device based on nanoparticle probe and immunochromatographic strip. *Anal. Chem.* **79,** 7644–7653 (2007).

170. Lin, Y. Y. *et al.* A nanoparticle label/immunochromatographic electrochemical biosensor for rapid and sensitive detection of prostate-specific antigen. *Biosens. Bioelectron.* **23,** 1659–1665 (2008).

171. Akanda, M. R. *et al.* An interference-free and rapid electrochemical lateral-flow immunoassay for one-step ultrasensitive detection with serum. *Analyst* **139,** 1420–5 (2014).

172. Fisher, M. *et al.* A combined immunomagnetic separation and lateral flow method for a sensitive on-site detection of Bacillus anthracis spores - Assessment in water and dairy products. *Lett. Appl. Microbiol.* **48,** 413–418 (2009).

173. Tang, D. *et al.* Magnetic nanogold microspheres-based lateral-flow immunodipstick for rapid detection of aflatoxin B2 in food. *Biosens. Bioelectron.* **25,** 514–518 (2009).

174. Wang, Y. *et al.* Study of superparamagnetic nanoparticles as labels in the quantitative lateral flow immunoassay. *Mater. Sci. Eng. C* **29,** 714–718 (2009).

175. Zheng, C., Wang, X., Lu, Y. & Liu, Y. Rapid detection of fish major allergen parvalbumin using superparamagnetic nanoparticle-based lateral flow immunoassay. *Food Control* **26,** 446–452 (2012).

176. Wang, D. B. *et al.* Rapid detection of Bacillus anthracis spores using a super-paramagnetic lateral-flow immunological detectionsystem. *Biosens. Bioelectron.* **42,** 661–667 (2013).

177. Shi, L. *et al.* A novel method to detect Listeria monocytogenes via superparamagnetic lateral flow immunoassay. *Anal. Bioanal. Chem.* **407,** 529–535 (2015).

178. Barnett, J. M. *et al.* An inexpensive, fast and sensitive quantitative lateral flow

magneto-immunoassay for total prostate specific antigen. *Biosensors* **4,** 204–220 (2014).

179. Wang, D. B. *et al.* Detection of Bacillus anthracis spores by super-paramagnetic lateral-flow immunoassays based on 'Road Closure'. *Biosens. Bioelectron.* **67,** 608–614 (2015).

180. Taton, K., Johnson, D., Guire, P., Lange, E. & Tondra, M. Lateral flow immunoassay using magnetoresistive sensors. *J. Magn. Magn. Mater.* **321,** 1679–1682 (2009).

181. Ryu, Y., Jin, Z., Kang, M. S. & Kim, H. S. Increase in the detection sensitivity of a lateral flow assay for a cardiac marker by oriented immobilization of antibody. *Biochip J.* **5,** 193–198 (2011).

182. Marquina, C. *et al.* GMR sensors and magnetic nanoparticles for immuno-chromatographic assays. *J. Magn. Magn. Mater.* **324,** 3495–3498 (2012).

183. Qin, Z. *et al.* Significantly improved analytical sensitivity of lateral flow immunoassays by using thermal contrast. *Angew. Chemie - Int. Ed.* **51,** 4358–4361 (2012).

184. Moghadam, B. Y., Connelly, K. T. & Posner, J. D. Isotachophoretic Preconcenetration on Paper-Based Micro fl uidic Devices. *Anal Chem* **86,** 5829–5837 (2014).

185. Moghadam, B. Y., Connelly, K. T. & Posner, J. D. Two orders of magnitude improvement in detection limit of lateral flow assays using isotachophoresis. *Anal. Chem.* **87,** 1009–1017 (2015).

186. Li, M. *et al.* Ultrasensitive and Quantitative Detection of a New beta-Agonist Phenylethanolamine A by a Novel Immunochromatographic Assay Based on Surface-Enhanced Raman Scattering (SERS). *J. Agric. Food Chem.* **62,** 10896–10902 (2014).

187. Otten, L., Richards, S.-J., Fullam, E., Besra, G. S. & Gibson, M. I. Gold nanoparticle-linked analysis of carbohydrate–protein interactions, and polymeric inhibitors, using unlabelled proteins; easy measurements using a 'simple' digital camera. *J. Mater. Chem. B* **1,** 2665 (2013).

188. Chen, A. *et al.* Smartphone-interfaced lab-on-a-chip devices for field-deployable enzyme-linked immunosorbent assay. *Biomicrofluidics* **8,** 1–11 (2014).

189. Coskun, A. F. *et al.* A personalized food allergen testing platform on a cellphone. *Lab*

Chip **13,** 636–40 (2013).

190. Wei, Q. *et al.* Terms of Use Detection and Spatial Mapping of Mercury Contamination in Water Samples Using a Smart-Phone. *ACS Nano* **8,** 1121–1129 (2014).

191. Oncescu, V., Mancuso, M. & Erickson, D. Cholesterol testing on a smartphone. *Lab Chip* **14,** 759–63 (2014).

192. Wang, X. *et al.* Audio jack based miniaturized mobile phone electrochemical sensing platform. *Sensors Actuators, B Chem.* **209,** 677–685 (2015).

193. Kehoe, E. & Penn, R. L. No Title. *J Chem Educ* **90,** 1191–1195 (2013).

194. Kuntzleman, T. S. & Jacobson, E. C. Teaching Beer's Law and absorption spectrophotometry with a smart phone: A substantially simplified protocol. *J. Chem. Educ.* **93,** 1249–1252 (2016).

195. Guan, L. *et al.* Barcode-like paper sensor for smartphone diagnostics: An application of blood typing. *Anal. Chem.* **86,** 11362–11367 (2014).

196. Mudanyali, O. *et al.* Integrated rapid-diagnostic-test reader platform on a cellphone. *Lab Chip* **12,** 2678–86 (2012).

197. Lee, S., Kim, G. & Moon, J. Performance improvement of the one-dot lateral flow immunoassay for aflatoxin B1 by using a smartphone-based reading system. *Sensors (Basel).* **13,** 5109–5116 (2013).

198. You, D. J., Park, T. S. & Yoon, J. Y. Cell-phone-based measurement of TSH using Mie scatter optimized lateral flow assays. *Biosens. Bioelectron.* **40,** 180–185 (2013).

199. Oncescu, V., O'Dell, D. & Erickson, D. Smartphone based health accessory for colorimetric detection of biomarkers in sweat and saliva. *Lab Chip* **13,** 3232–8 (2013).

200. Lee, S., Oncescu, V., Mancuso, M., Mehta, S. & Erickson, D. A smartphone platform for the quantification of vitamin D levels. *Lab Chip* **14,** 1437–42 (2014).

201. Novarum. Available at: https://www.novarumdx.com/. (Accessed: 9th August 2018)

202. Smart Micro Optics (Blips lenses). Available at: https://www.smartmicrooptics.com/blips/. (Accessed: 22nd July 2018)

203. Google Glass - Wikipedia. Available at: https://en.wikipedia.org/wiki/Google_Glass. (Accessed: 9th August 2018)

204. S., F. *et al.* Immunochromatographic diagnostic test analysis using Google Glass. *ACS Nano* **8,** 3069–3079 (2014).

CHAPTER 2

Thesis objectives

The main objective of this PhD thesis was to study and learn about lateral flow technology, not only concerning to its development, also its benefits and drawbacks, the current state-of-the-art and the future possibilities that this technology has. Furthermore, novel ways to apply nanomaterials on lateral flow as well as the application of the developed devices were pursued.

During this research work, different projects and milestones emerged, which are detailed as:

- The development of LFs for the detection of U(VI) ions in groundwater.
    - Design and prepare LFs strips able to reach a LOD under 30 ppb, the minimum amount recommended in consume water by the EPA and the WHO.
    - Strips evaluation and application in real samples.
- Signal enhancement for LFs.
    - Integration of cellulose nanofibers onto nitrocellulose to retain more AuNPs increasing the color intensity on the TL.
- Application of a mobile phone as colorimetric reader for LFs, being a fast and user-friendly tool.
- Detection of PBDE (a flame retardant now classified as contaminant).
    - Explore the advantages of the electrocatalytic properties of IrO_2 NPs in saline medium to detect PBDEs.
    - Integration of IrO_2 NPs on LFs for the future objective to combine optical and electrochemical detection of PBDE, among other analytes.

CHAPTER 3

U(VI) detection using a gold nanoparticle/paper-based lateral flow device

3.1. Introduction

Uranium enters in the environment from mining and ore processing[1,2] and the extensive use of phosphate fertilizers[3,4]. The uranium that exists naturally in granite and other mineral deposits[1] can also contribute to groundwater contamination. Uranium contamination in both ground and surface waters have also significantly increased in the last two decades due to military use of the depleted metal[5,6]. In groundwater, this heavy metal is most commonly found in its hexavalent form, U(VI), also referred to as uranyl ion (UO_2^{2+}). The current maximum contamination level for uranium in drinking water, as stipulated by the U.S. Environmental Protection Agency (EPA)[7] and the World Health Organization (WHO)[1] is 30 µg/L (126 nM). The consumption of high amounts of uranium has been associated with renal problems (accumulation in kidney), genotoxicity and cancer development (e.g. leukaemia due uranium accumulation on bones)[8,9], among others. Current detection methods for uranium, such as ICP-MS (inductively coupled plasma mass spectrometry)[10] or radiation detection systems[11], require several sample extraction and pre-treatment steps, expensive equipment, and highly trained personnel; such analyses are mainly performed in high-tech laboratory settings. Although there exist portable radiation detection equipment, the detection is mostly qualitative and only possible for high amounts of the radioactive isotopes[11]. It has been the long term interest of environmental scientists to seek new methods to rapidly detect and quantify water contaminants at the site of contamination. Lateral flow strips (LFs) are paper-

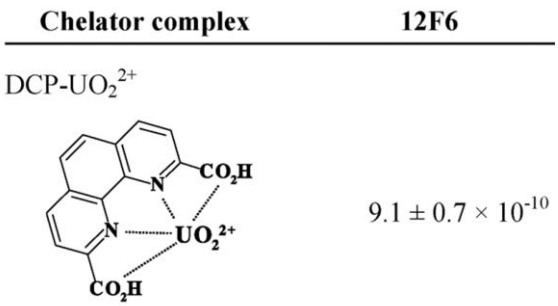

Fig. 3.1. DCP chelator structure binding UO_2^{2+} ion. Equilibrium dissociation constant (K_d/M) value of the complex for the binding with 12F6 antibody. Reprinted with permission from ref. 20, copyright 2004, American Chemical Society

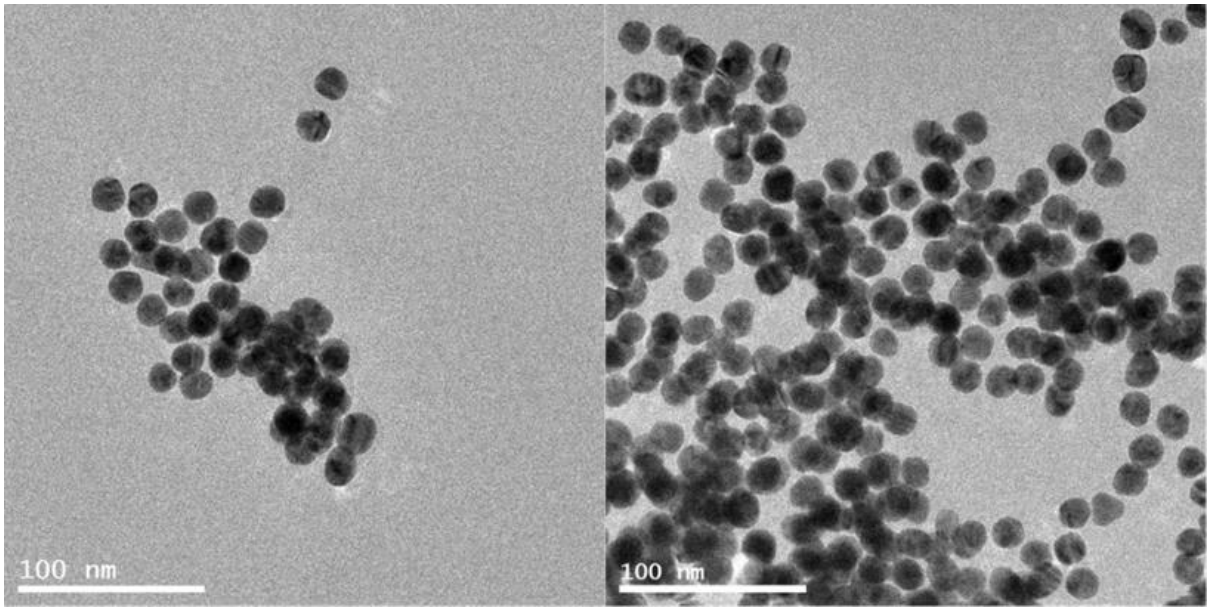

Figure 3.2. AuNPs characterized by transmission electron microscopy (TEM).

based immunosensors that can be used to detect the presence of specific molecules in a given sample. These devices are simple, portable, cheap to produce, and do not require highly skilled labor[12-15].

In this chapter it is reported the development of LFs for quantitative detection of U(VI) in groundwater samples. The use of LFs has previously been reported for the detection of other heavy metals such as lead[16], cadmium[17,18] and mercury[19]. In the present study, an antibody (clone 12F6) that specifically recognizes UO_2^{2+} complexed to the chelator, 2,9-dicarboxyl-1,10-phenanthroline (DCP) was used for the analysis[20] (Fig. 3.1). This chelator binds to UO_2^{2+} with an affinity five orders of magnitude greater than that of conventional metal chelators such as ethylenediaminetetraacetic acid (EDTA)[20].

The integration of nanoparticles[14] on LFs leads to higher sensitivity and lower detection limits in comparison to other materials used as labels, being gold nanoparticles (AuNPs) chosen as labels in this assay due to their strong red color and biocompatibility with antibodies[21-24].

3.2. Materials and methods

3.2.1. Materials

The 12F6 antibody and the BSA-DCP-U(VI) conjugate were prepared and characterized as previously described[20,25,26]. Bovine serum albumin (BSA), goat anti-mouse IgG polyclonal antibody, tetrachloroauric acid ($HAuCl_4$), trisodium citrate, Tween 20, sucrose and the reagents used to prepare HEPES-buffered saline (HBS: NaCl 137 mM, KCl 3 mM and HEPES 10 mM; pH 7.4) were purchased from Sigma Aldrich. The U(VI) stock solution was purchased from Perkin Elmer and the chelator, DCP was purchased from Alpha Aesar. Cellulose membrane (CFSP001700), glass fibber (GFCP00080000), nitrocellulose membrane (HF180), and adhesive laminated card were purchased from Millipore.

3.2.2. Synthesis of gold nanoparticles

AuNPs of approximately 20 nm diameter were synthesized by citrate reduction of $HAuCl_4$ following the Turkevich method[27]. A 0.01 % (w/v) solution of $HAuCl_4$ was prepared by diluting 0.5 ml of a 1 % $HAuCl_4$ to a final volume of 50 mL in Milli-Q water. This solution was heated to boiling point and 1.25 mL of 1 % (w/v) sodium citrate was added under continuous vigorous stirring. The solution was allowed to boil for an additional 10 minutes then allowed to cool down to room temperature. The AuNP solution was adjusted to a pH of 9.0 by addition of 0.01 mM borate buffer. The AuNPs were characterized by TEM (Fig. 3.2).

3.2.3. Preparation of the 12F6-AuNP conjugate

An aliquot (200 µg/mL in HBS, 100µL) of the 12F6 antibody was added to 1.5 mL of AuNP solution and incubated for 20 minutes at room temperature. BSA solution (5% (w/v), 100 µL) was then added and the mixture was allowed to incubate for another 20 minutes followed by centrifugation at 4°C (14000 rpm, 20 minutes). The supernatant was discarded and the pellet was reconstituted in 0.5 mL HBS buffer containing 10 % sucrose.

The ratio antibody:AuNP was calculated to be 7:1, estimated dividing the surface area of a nanoparticle by the area occupied by an antibody. The surface area (A_1) of a spherical nanoparticle was calculated as 1258 nm^2 by the formula $A_1 = 4\pi r_1^2$, being the radius (r_1) of 10 nm. Then, the area occupied by an IgG molecule was estimated considering that the antibody

occupies the area of a circle, being the radius of 7.5 nm according to reference 28. The formula applied was $A_2 = \pi r_2^2$, obtaining an area of 176.71 nm^2.

The sample pad was prepared by dipping the cellulose membrane in HBS buffer containing 5 % BSA and 0.05 % Tween 20. The membrane was dried at 60°C for 2 hours and stored in barrier zip-lock pouches with drying pearls at 4 ºC. The conjugate pad was prepared by dispensing freshly prepared AuNP-antibody conjugate suspension onto the glass fibber. The fibber was dried by quickly transferring to a vacuum chamber for 2.5 hours, and then stored in barrier zip-lock pouches with drying pearls at 4 ºC. The detection pad consists of a nitrocellulose membrane assembled onto an adhesive laminated card backing. Using the Biofluidix Biospot Workstation, approximately 1 µL/mm of the U(VI)-DCP-BSA conjugate (0.25 mg/mL) and goat anti-mouse IgG polyclonal antibody (1.00 mg/mL) solutions were dispensed onto the TL and the CL on the detection pad, respectively. The detection pad was dried at 37°C for 2 hours and stored at room temperature under dry conditions.

The conjugate pad was assembled onto the adhesive backing with a 1 mm overlap over the detection pad. The sample pad was assembled overlapping the conjugate pad at the end of the strip. On the other end, an absorption pad (untreated cellulose membrane) was assembled overlapping the detection pad, at 3 mm away from the CL. The strips were cut to a width of 6 mm using a guillotine and stored at room temperature in dry conditions.

3.2.4. Assay performance

Standard U(VI) solutions (25nM to 800 nM) were prepared by diluting the uranium stock solution (1000 ppm; 4.2 mM) in HBS. An aliquot (100 µL) of each U(VI) sample was mixed with 100 µL of 2 µM DCP solution and after incubation for 10 minutes at room temperature, the samples were applied on the sample pad of the strips. After 5 minutes, TL and CL were observed. After 20 minutes, images of the strips were taken using a mobile phone camera[29-32] (Moto Z, 13 megapixel). Image J software was used to quantify the color intensities of the TLs. The images were converted to 8-bit black-and-white format and the intensities of white pixels were measured on the TL, with an intensity value of 255 considered pure white while an intensity value of 0.0, pure black. Data was normalized into % color where 0 % and 100 % equal to 255 and 0 values respectively.

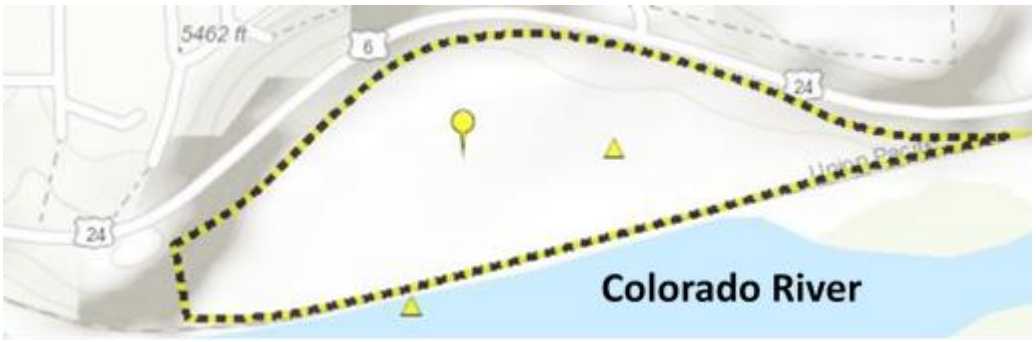

Fig. 3.3. Site of collection of uranium-contaminated groundwater. The United States Department of Energy monitors a number of site of former uranium mine/ore processing plants as part of the Uranium Mill Tailings Remedial Action (UMTRA) project.

3.2.5. Evaluation of strips with contaminated groundwater samples

Uranium-contaminated groundwater samples were obtained from a uranium contaminated site in Rifle, Colorado (Fig. 3.3)[20]. These groundwater samples were filtered through a 0.45-micron non-uranium binding filter to remove any particulate matter before they were received at Tulane University. To prevent the precipitation of uranium, the samples were acidified to a pH of 2.0 by adding 125 µL of 8 M nitric acid per 50 mL of sample. Because the binding of the 12F6 antibody to the U(VI)-DCP complex is inhibited by mM quantities of ionic calcium (Fig. 3.4), standard curves for groundwater samples were therefore adjusted to have the same [Ca^{2+}] as the groundwater sample (Table 3.1). This was achieved by treating a small quantity of the contaminated water sample with uranium absorbing particles that completely remove the U(VI) but not the Ca^{2+} from the groundwater[33]. The Ca^{2+} concentration

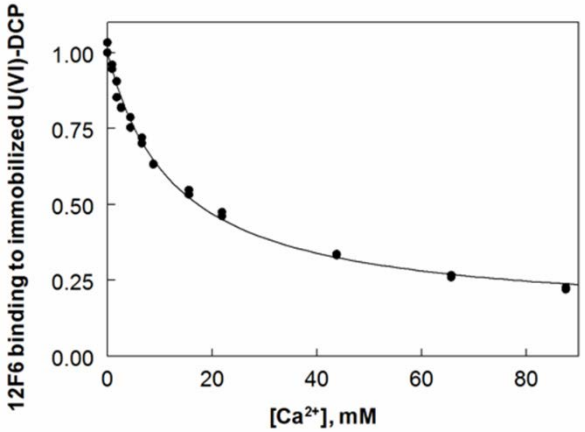

Fig. 3.4. Effect of [Ca^{2+}] on the binding affinity of 12F6 to immobilized U(VI)-DCP-BSA. The effect of calcium on 12F6 binding was studied using a KinExA 3000 instrument.

Table 3.1. Preparation of standards containing pre-treated groundwater samples.

$[UO_2^{2+}]$ (nM):	0	12.5	25	35	50	75	100	200
Vol. of stock (2 µM U(VI), in HBS) (µL)	0	3.13	6.25	8.75	12.5	18.75	25	50
Pre-treated Rifle groundwater (µL)	50	50	50	50	50	50	50	50
HBS (µL)	200	196.87	193.75	191.25	187.5	181.25	175	150
2000 nM DCP in HBS (µL)	250	250	250	250	250	250	250	250
Total Vol. (µL)	500	500	500	500	500	500	500	500

Table 3.2. Preparation of environmental samples with U(VI) concentrations.

Sample dilution factor	10fold	~15fold	20fold
Vol. of Rifle groundwater (Acidified) (µL)	50	35	25
Pretreated Rifle groundwater (Neutralized)	0	15	25
HBS	200	200	200
2000 nM DCP in HBS	250	250	250
Total Vol. (µl)	500	500	500

in the standards and the samples could then be normalized by keeping the final proportion of untreated and treated groundwater at 10 % in all samples and standards (Tables 3.1 and 3.2). The pH of the samples and the standards were checked before they were applied to the strips.

3.3. Results and discussion

3.3.1. Design of the AuNP-based LFs for the detection of U(VI)

This lateral flow assay relies on the 12F6 monoclonal antibody's specific recognition of the U(VI)-DCP complex. Due to the small size of the chelated uranium, it is not possible to form the typical "capture antibody-analyte-recognition antibody" immunosandwich on the test line (TL), as seen with most standard LFs models[14]. Therefore, this immunoassay was designed based on a competitive model[17,18] as illustrated in Fig. 3.5. The 12F6 monoclonal antibody was conjugated to gold nanoparticles and dispensed onto the conjugate pad. The operating principle of this assay is based on the competition between the U(VI)-DCP complex (prepared by mixing the U(VI)-contaminated/spiked sample with DCP) and U(VI)-DCP-BSA immobilized on the TL for the binding site of the AuNP-conjugated 12F6 antibody (on the conjugate pad). In the absence of U(VI) in the sample, the 12F6-AuNP conjugate will bind to the immobilized U(VI)-DCP-BSA on the TL, resulting in an intense red color. However, when

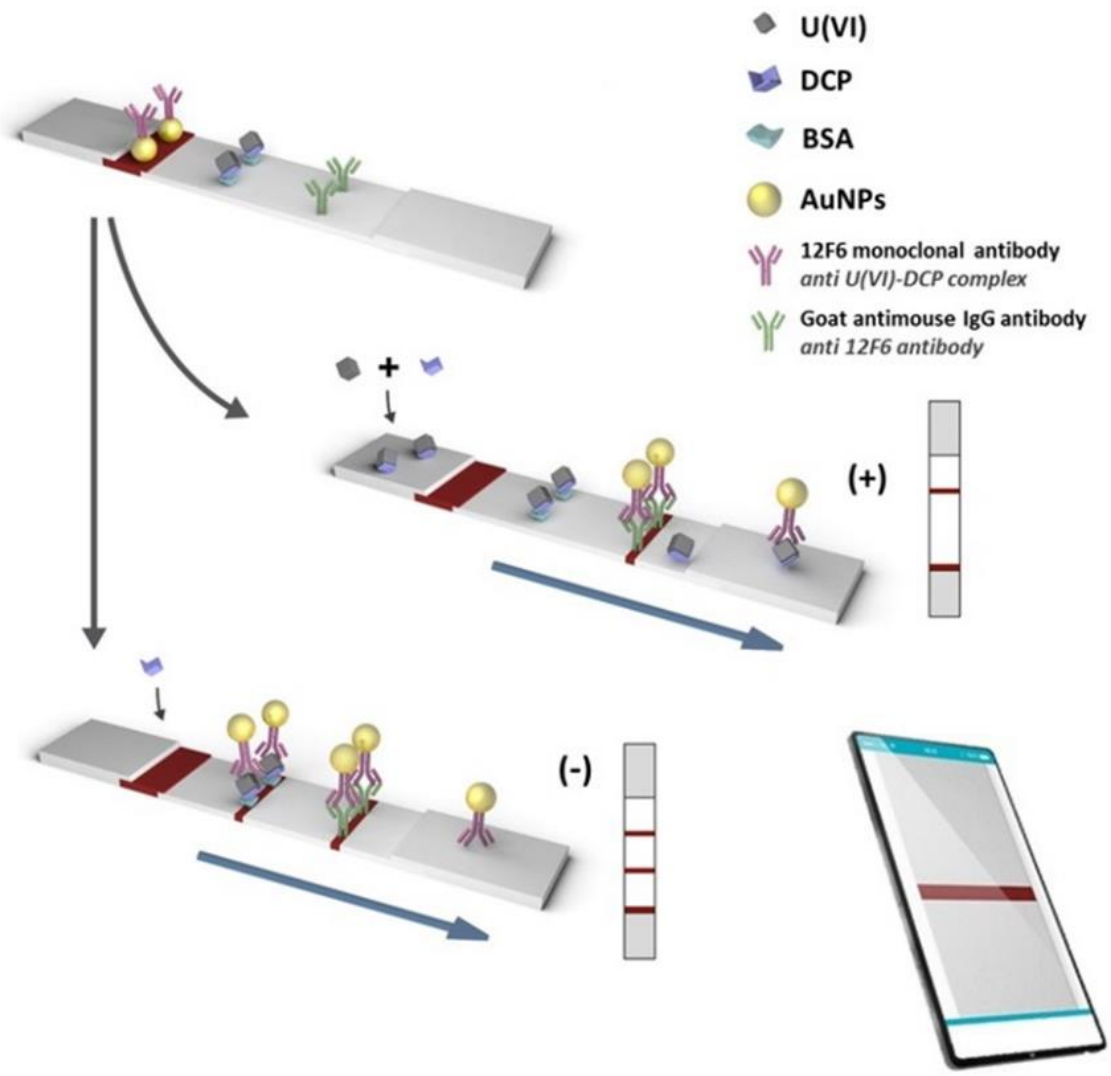

Fig. 3.5. Schematic (not drawn to scale) of the configuration and operating principle of the lateral flow strip for the detection of U(VI). The intensity on the strips can be measured by using a mobile phone camera.

U(VI) is present in the sample, the U(VI)-DCP complex will bind to the AuNP-12F6 conjugate, thus leaving less of 12F6 antibody available to bind to the U(VI)-DCP-BSA on the TL. This results in less red coloration on the TL. In both the positive and negative control assays, the excess AuNP-12F6 complex is captured on the control line (CL) by an immobilized goat anti-mouse antibody, resulting in an intense red line. Thus, in a negative assay (-), both the TL and CL should have an intense red coloration. Increasing concentrations of U(VI) in the sample should result in a decrease in the intensity of the TL. The color intensity of the TL is thus inversely proportional to the concentration of U(VI) in the sample.

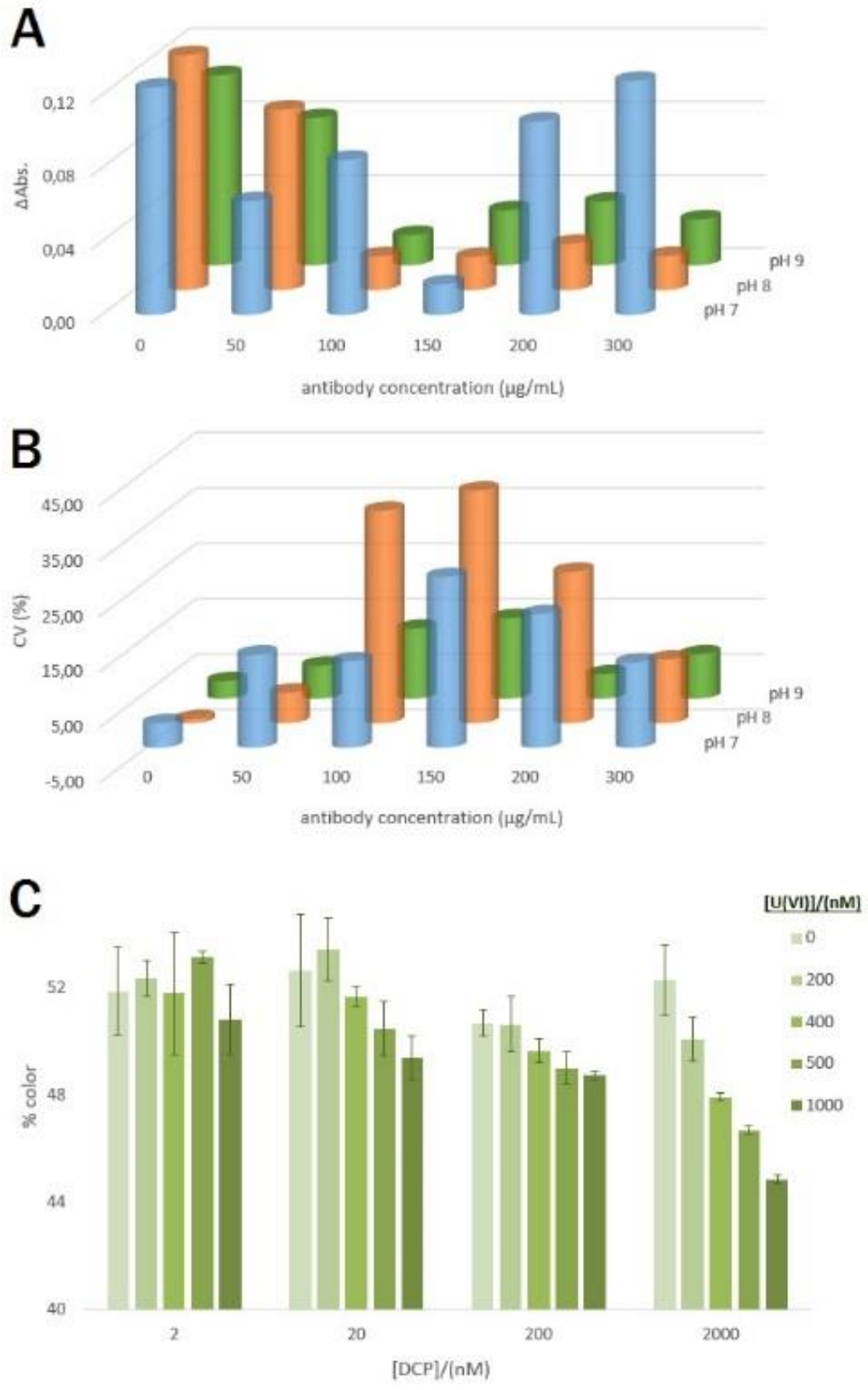

Fig. 3.6. (A) Evaluation of the conjugation of 12F6 antibody at different concentrations on AuNPs at pH 7, 8 and 9 by means of the variation of absorbance (ΔAbs.) caused by the addition of NaCl and (B) the corresponding coefficient of variation (CV, %) of each point. (C) Evaluation of the linearity of the color decrease related to U(VI) concentration for LFs at different concentrations of DCP chelator.

3.3.2. Optimization of assay conditions

It was necessary to optimize various assay conditions in order to ensure proper functionality of the LFs. First, a gold nanoparticle aggregation test[34] was performed to determine the optimal concentration of the 12F6 antibody that could be conjugated onto AuNPs. AuNP suspensions at various pH values (7, 8, and 9) were mixed with varying concentrations (0, 50, 100, 150, 200, and 300 µg/mL) of the 12F6 antibody. The UV-Vis absorbance of these solutions at 520 nm were measured before and after addition of NaCl, using a Spectra Max iD3 spectrophotometer. If the amount of antibody was not enough to cover the surface of the AuNPs, the presence of the NaCl in solution would cause the AuNPs to aggregate and subsequently precipitate out of solution. Fig. 3.6A shows the absorbance values recorded at various pH values with different concentrations of antibody and Fig. 3.6B shows the corresponding % CV values of the absorbance values reported in Fig. 3.6A. Based on the data obtained, a pH 9.0 and antibody concentration of 200 µg/mL were chosen for the

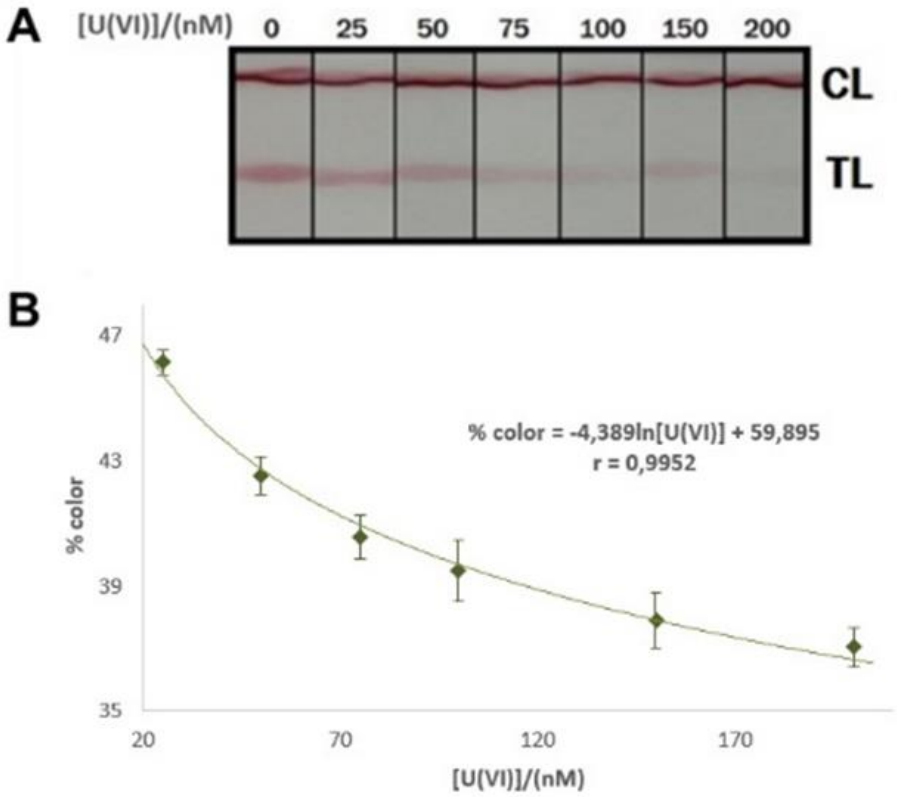

Figure 3.7. (A) LFs response at U(VI) concentrations between 0 and 200 nM in HBS buffer and (B) the corresponding working range equation.

conjugation.

In this assay, sample pre-treatment with the chelator, DCP was required before dispensing onto the LFs. Various concentrations (2, 20, 200 and 2000 nM) of DCP were mixed with different concentrations (0, 200, 400, 500 and 1000 nM) of U(VI), and applied onto the LFs. The DCP and U(VI) solutions were mixed at a 1:1 ratio and allowed to incubate for 10 minutes at room temperature. 200 µL of each mixture were applied onto the LFs. Images of the strips were taken and color intensities of the TL were quantified using ImageJ software. Fig. 3.6C shows the % color observed from these experiments. Based on these data, a DCP concentration of 2000 nM was chosen for the rest of the assays since higher sensitivity and linear behaviour were observed.

Samples containing various concentrations of U(VI) standards were prepared as described in the methods section and evaluated with the LFs to determine the optimal working range of the assay. All samples and standards were prepared in HBS buffer, pH 7.4. Fig. 3.7A is an image of the LFs and Fig. 3.7B shows the mathematical fit of the data obtained from the standards following the equation:

$$\textbf{\% color} = -4{,}389 \ln [\mathrm{U(VI)}] + 59{,}895$$

The r^2 for this fit was 0.9952 and the theoretical LOD (limit of detection) was calculated by replacing "% color" in the equation with the average signal of blank, 49%, plus 3 times its standard deviation, ±1 %, resulting in a value of 6 nM.

3.3.3. Detection and quantification of U(VI) in contaminated groundwater samples

Since this LFs assay relies on the 12F6 antibody's ability to recognize U(VI) in a complex with DCP, it was important to ensure that all the uranium in the environmental sample be dissociated from the various natural complexants[35] in the groundwater before being complexed with DCP. To ensure dissociation of U(VI) from these natural complexants, the filtered groundwater samples were treated with 8 M nitric acid to lower the pH to ~2.0. This pre-treatment strategy was found to be the most successful in a previous study[19], and the acidified samples could be stored for several months at 4°C. A portion of the acidified environmental samples was sent for analysis by ICP-MS. Samples were neutralized before applying onto the strips by mixing with HBS buffer containing DCP.

Table 3.3. Concentration of uranium and calcium in untreated groundwater and in groundwater treated with uranium absorbing particles.

	Untreated	Treated	% Removed
Uranium	687.68 nM	8.36 nM	98.78
Calcium	7.00 mM	6.54 mM	6.60

It has been previously observed that the presence of calcium inhibits the binding activity of the 12F6 antibody (Fig. 3.4). The environmental samples contain ~7 mM calcium. Thus, presence of calcium in the groundwater samples could cause false positives in the results if the amount is not normalized in both the standards and the samples. To address this issue, uranium-contaminated groundwater samples were pre-treated with uranium absorbing particles[33]. These particles rapidly (within 5-10 minutes) and selectively remove uranyl ions in groundwater samples. These particles were used to adsorb the uranium from an aliquot the groundwater sample. Up to 98.7% of the uranium in the contaminated groundwater sample was removed (as quantified by ICP-MS, Table 3.3), and this pre-treated, U(VI)-free groundwater was used to supplement all the new standard solutions (10 % pre-treated Rifle groundwater in each standard). This ensured that both the standards and the environmental samples were in the same background matrix. Samples were prepared by diluting the untreated acidified groundwater into HBS buffer containing DCP. The pre-treated groundwater was then used to adjust each sample to ensure that each prep contained 10 % groundwater.

Three dilutions (10-, 15-, and 20-fold) of the groundwater sample were assessed. The pH of all the standards and samples applied to the lateral flow strips ranged between 7.2 and 7.4. Each standard and sample was assayed in duplicate. A representative image of the LFs used to generate standard curves with standards containing 10 % pre-treated groundwater is shown in Fig. 3.8A. Fig. 3.8B shows the standard curve generated from these LFs. The standard curve fits to the equation:

$$\textbf{\% color = -3,626 ln [U(VI)] + 54,962}$$

The r^2 value for the equation was 0.9697 and the LOD 36.38 nM (the color intensity of blank plus 3 times its standard deviation was of 42 %).

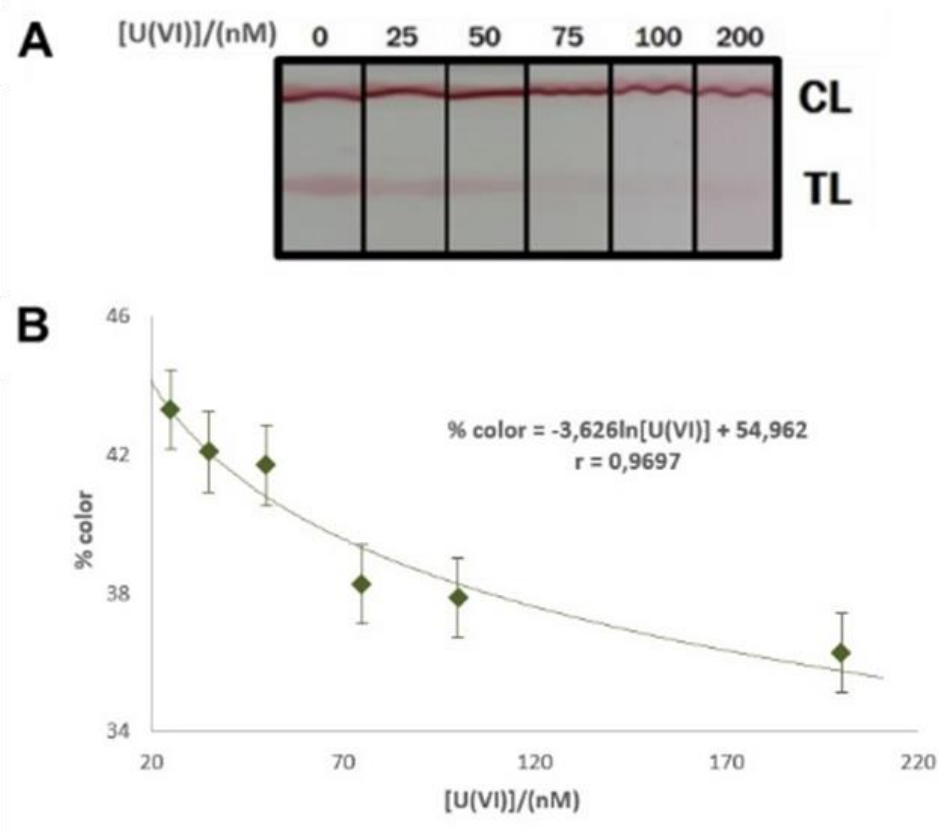

Fig. 3.8. (A) LFs response at various standard U(VI) concentrations in HBS buffer containing 10 % pre-treated groundwater and (B) the corresponding working range equation.

U(VI) concentrations in the diluted groundwater samples were interpolated from the standard curve and the results are shown in Table 3.4. At a 10-fold dilution of the environmental sample, the measured U(VI) concentration was 70.23 nM, similar to the concentration measured by ICP-MS. However, at higher dilution factors, 15-fold and 20-fold, bigger errors were observed. The U(VI) concentrations in the in these samples are closer to the LOD and therefore could not be accurately quantified by this assay.

3.4. Conclusions

A lateral flow assay for the detection and quantification of uranium in groundwater, using the 12F6 monoclonal antibody labelled with AuNPs as signal producer, has been developed for the first time. The 12F6 antibody has a primary specificity for uranyl ions complexed with the chelator, DCP. A competitive immunoassay format was used due to the small size of the analyte. Pictures of these lateral flow strips could be taken 20 minutes after adding sample and the color intensities were analysed using ImageJ software.

Table 3.4. Environmental groundwater sample evaluation. Comparison of LFs and ICP-MS.

Environmental sample dilution factor	% colour	[U(VI)], nM, interpolated from the standard curve	[U(VI)], nM, by ICP-MS
10	39.55	70.23	68.90
15	40.05	61.08	48.23
20	40.17	59.17	34.45

The strips exhibited a LOD of 6 nM when standards and samples were prepared in HBS buffer. When samples and standards were prepared in HBS buffer supplemented with pre-treated environmental samples, a LOD of 36.38 nM was observed. Both limits of detection are well below 126 nM, the maximum contaminant level for uranium in drinking water stipulated by the WHO and the United States EPA.

These lateral flow strips provide a potentially simpler and cheaper alternative to the current uranium detection and quantification methods. The assays can be performed *in situ* and provide results in less than 20 minutes. These strips can be used for both qualitative and quantitative analysis by combining the readout with a mobile phone application system.

3.5. References

1. WHO. Uranium in Drinking-water. *Guidel. Drink. Qual*. 1–29 (2012).

2. Noubactep, C., Meinrath, G., Dietrich, P. & Merkel, B. Mitigating Uranium in Groundwater : Prospects and Limitations. *Environ. Sci. Technol.* **37**, 4304–4308 (2003).

3. Landa, E. R. Naturally occurring radionuclides from industrial sources: characteristics and fate in the environment. *Radioact. Environ.* **10**, 211–237 (2007).

4. Raińska, E., Biziuk, M., Sarbu, C., Szczepaniak, K., Frontasyeva, M. V., Culicov, O., Bode, P. & Astel, A. Assessment of Phosphatic Fertilizer Production Impact on Occupational Staff Based on NAA of Hair, Nails, and Inhald Particles. *J. Environ. Sci. Heal. Part A* **40**, 2137–2152 (2005).

5. Depleted Uranium Effect on Veterans. U.S. Department of Veterans Affairs Available at: https://www.publichealth.va.gov/exposures/depleted_uranium/. (Accessed: 26th April 2018)

6. Bleise, A., Danesi, P. R. & Burkart, W. Properties, use and health effects of depleted uranium (DU): a general overview. *J. Environ. Radioact.* **64**, 93–112 (2003).

7. EPA. Drinking Water Requirements for States and Public Water Systems. Available at: https://www.epa.gov/dwreginfo/radionuclides-rule. (Accessed: 26th April 2018)

8. Committee on Uranium Mining in Virginia. Uranium Mining in Virginia. (2012). doi: 10.17226/13266

9. Bersimbaev, R. I. & Bulgakova, O. The health effects of radon and uranium on the population of Kazakhstan. *Genes Environ.* 1–10 (2015). doi:10.1186/s41021-015-0019-3

10. Rožmarić, M., Ivšić, A. G. & Grahek, Ž. Determination of uranium and thorium in complex samples using chromatographic separation, ICP-MS and spectrophotometric detection. *Talanta* **80**, 352–362 (2009).

11. U.S. Department of Health and Human Services. Toxicological Profile for Uranium. (2013).

12. Parolo, C. & Merkoci, A. Paper-based nanobiosensors for diagnostics. *Chem. Soc. Rev*. **42**, 450–457 (2013).

13. López-marzo, A. M. & Merkoçi, A. Paper-based sensors and assays: a success of the engineering design and the convergence of knowledge areas. *Lab Chip* **16**, 3150–3176 (2016).

14. Quesada-González, D. & Merkoçi, A. Nanoparticle-based lateral flow biosensors. *Biosens. Bioelectron*. **73**, 47–63 (2015).

15. Yetisen, A. K., Akram, M .S. & Lowe, C. R. Paper-based microfluidic point-of-care diagnostic devices. *Lab Chip* **13**, 2210-2251 (2013).

16. Mazumdar, D., Liu, J., Lu, G., Zhou, J. & Lu, Y. Easy-to-use dipstick tests for detection of lead in paints using non-cross-linked gold nanoparticle-DNAzyme conjugates. *Chem. Commun. (Camb).* **46**, 1416–8 (2010).

17. López-Marzo, A. M., Pons, J., Blake, D. A. & Merkoçi, A. High sensitive gold-nanoparticle based lateral flow Immunodevice for Cd2+ detection in drinking waters. *Biosens. Bioelectron.* **47**, 190–198 (2013).

18. López Marzo, A. M., Pons, J., Blake, D. A. & Merkoçi, A. All-integrated and highly sensitive paper based device with sample treatment platform for Cd2+ immunodetection in drinking/tap waters. *Anal. Chem*. **85**, 3532–3538 (2013).

19. Torabi, S.-F. & Lu, Y. Small-molecule diagnostics based on functional DNA nanotechnology: a dipstick test for mercury. *Faraday Discuss.* **149**, 125–135 (2011).

20. Blake II, R. C., Pavlov, A. R., Khosraviani, M., Ensley, H. E., Kiefer, G. E., Yu, H., Li, X. & Blake, D. A. Novel monoclonal antibodies with specificity for chelated uranium(VI): isolation and binding properties. *Bioconjug. Chem.* **15**, 1125–1136 (2004).

21. Parolo, C., De La Escosura-Muñiz, A., Polo, E., Grazú, V., De La Fuente, J. M. & Merkoçi, A. Design, preparation, and evaluation of a fixed-orientation antibody/gold-nanoparticle conjugate as an immunosensing label. *ACS Appl. Mater. Interfaces* **5**, 10753–10759 (2013).

22. Hadi, M., Amani, H., Akbar, A., Pazoki-toroudi, H. & Sedighimoghaddam, B. Various methods of gold nanoparticles (GNPs) conjugation to antibodies. *SBSR* **9**, 17–22 (2016).

23. Chinen, A. B., Guan, C. M., Ferrer, J. R., Barnaby, S. N., Merkel, T. J. & Mirkin C. A. Nanoparticle probes for the detection of cancer biomarkers, cells, and tissues by fluorescence. *Chem. Rev*. **115 (19)**, 10530–10574 (2015).

24. Quesada-González, D. & Merkoçi, A. Nanomaterial-based devices for point-of-care diagnostic applications. *Chem. Soc. Rev*. **47**, 4697-4709 (2018).

25. Melton, S. J., Yu, H., Williams, K. H., Morris, S. A., Long, P. E. & Blake, D. A. Field-based detection and monitoring of uranium in contaminated groundwater using two immunosensors. *Environ. Sci. Technol*. **43**, 6703–6709 (2009).

26. Zhu, X., Ban, B., Yang, X., Shevkoplyas, S. S. & Blake, D. A. Development of an Immunochromatographic Strip for Rapid, Instrument-Free, On-Site Detection of Uranium The New Uranium Mining Boom, 499–504 (2011).

27. Turkevich, J., Stevenson, P. C. & Hillier, J. A study of the nucleation and growth processes in the synthesis of colloidal gold. *Discuss. Faraday Soc.* **11**, 55–75 (1951).

28. Jøssang, T., Feder, J., Rosenqvist & E. Photon correlation spectroscopy of human IgG. *J. Protein. Chem*. **7 (2)**, 125-171 (1988).

29. Quesada-González, D. & Merkoçi, A. Mobile phone–based biosensing: an emerging "diagnostic and communication" technology. *Biosens. Bioelectron*. **92**, 549–562 (2016).

30. Ozcan, A., Mobile phones democratize and cultivate next-generation imaging, diagnostics and measurement tools. *Lab Chip* **14 (17)**, 3187–3194 (2014).

31. Kühnemund, M., Wei, Q., Darai, E., Wang, Y., Hernández-Neuta, I., Yang, Z., Tseng, D., Ahlford, A., Mathot, L., Sjöblom, T., Ozcan, A. & Nilsson, M. Targeted DNA sequencing and in situ mutation analysis using mobile phone microscopy. *Nat. Commun*., **8**, 13913 (2017).

32. Roda, A., Michelini, E., Cevenini, L., Calabria, D., Calabretta, M. M. & Simoni, P. Integrating Biochemiluminescence Detection on Smartphones: Mobile Chemistry Platform for Point-of-Need Analysis *Anal. Chem*., **86 (15)**, 7299–7304 (2014).

33. Sahiner, N., Yu, H., Tan, G., He, J., John V. T. & Blake, D. A. Highly Porous Acrylonitrile-Based Submicron Particles for UO_2^{2+} absorption in an immunosensor assay *ACS Appl. Mater. Interfaces* **4 (1)**, 163–170 (2012).

34. Cordray, M. S., Amdahl, M. & Richards-Kortum, R. R. Gold nanoparticle aggregation for quantification of oligonucleotides: Optimization and increased dynamic range. *Anal. Biochem.* **431**, 99–105 (2012).

35. Brooks, S., Fredrickson, J. K., Carroll, S. L., Kennedy, D. W., Zachara, J. M., Plymale, A. E., Kelly, S. D., Kemner, K. M. & Fendorf S. Inhibition of Bacterial U(VI) Reduction by Calcium. *Environ. Sci. Technol.* **37**, 1850–1858 (2003).

3.6. Contributions

This work has been performed in collaboration with Dr. Diane A. Blake, from the Department of Biochemistry and Molecular Biology of Tulane University (New Orleans, USA) and her collaborators, Dr. Robert C. Blake II and Dr. Grace A. Jairo. They produced the 12F6 antibody and tested the strips with the real groundwater samples.

We thank Mr. Dámaso Navarro Torres for the design of figure 3.5. We also thank Dr. Kenneth Hurst Williams of Lawrence Berkeley National Laboratory for collecting the uranium-contaminated groundwater samples and Dr. Nurettin Sahiner for assisting in the synthesis of the uranium binding particles.

CHAPTER 4

Signal enhancement on lateral flow tests by using cellulose nanofibers

4.1. Introduction

The World Health Organization (WHO) urges the development of affordable, sensitive, selective, user-friendly, rapid and robust, equipment-free and derivable to the end-user devices (ASSURED criteria)[1]. Lateral flow strips (LFs) are paper-based biosensors which can afford that demand[2–4]. Paper substrate is inexpensive, recyclable, tunable and allows the storage of bioreceptors (e.g. antibodies[5]) and nanomaterials[3] in dry state, properties that make LFs suitable for point-of-care (PoC) diagnsotics[6–8]. However, LFs may present in some cases not enough sensitivity levels, thus not allowing or making it difficult to perform quantitative analysis. Because of that reason, many studies and signal enhancement strategies have been proposed during last years, as they are the addition of extra amplification steps[9–12], secondary chemical reactions[13–16], architecture modifications[17,18] or even exploring alternative signal translation methods beyond the optical response[19–22].

The porosity of paper is a key factor regarding the sensitivity of the strips[23]. Small pores will lead to higher sensitivity, as demonstrated by Rivas *et al.*[18], nevertheless the sample may have difficulties to flow, increasing the assay time and the probability of having membrane defects. Herein, we propose to decrease the pore size of the membrane only on

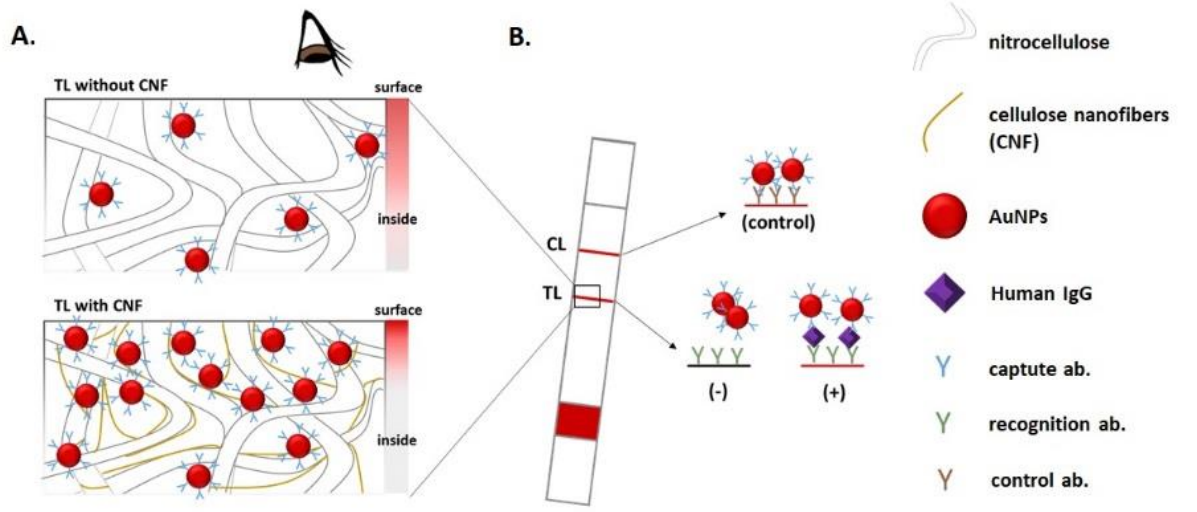

Fig. 4.1. (A) Schematic representation of a positive TL not modified (up) and modified with cellulose nanofibers dispensed (down). (B) Schematic representation of a LFs with all its components.

the test area, where the recognition antibodies are dispensed. To accomplish this milestone, in this work we have used for the first time cellulose nano-fibers (CNF), a nanomaterial often used as reinforcement additive on papermaker pulps[24–31]. This nanomaterial can be produced as a gel, thus it can be easily dispensed and dried inside the paper pores. In addition to the structural modification, CNF are biocompatible with antibodies, thus increasing the areas where they can be attached, so that more of them are retained near the paper surface, where it is best appreciated the color of transducer particles (Fig. 4.1A). In regard to the transducer particles, we have chosen gold nanoparticles (AuNPs) since they are easy to synthetize[32], bioconjugate[33–35] and have a strong red color readily detectable[36]. Our LFs design is represented in Fig. 4.1B.

On the other hand, mobile phones are important support tools in nowadays biosensing[37–47], not only due the capacity to record and store the data, also because of the portability, cloud storage, accessibility and software capabilities that these devices offer. In this work we attach microscopic lenses (Blips Micro Lens[48]) to the mobile phone camera to improve the quality of close-up images taken of the test area in LFs, therefore increasing the number of pixels that can be read.

4.2. Materials and methods

4.2.1. Materials

Tetrachloroauric acid ($HAuCl_4$), bovine serum albumin (BSA), goat anti-human IgG antibody, human IgG, trisodium citrate, sucrose, Tween 20, phosphate buffer saline (PBS) tablets and the reagents to prepare phosphate buffer non-saline (PB; sodium phosphate basic and dibasic) and borate buffer (BB; sodium tetraborate and boric acid) were purchased from Sigma Aldrich. Chicken anti-goat antibody was purchased from Abcam.

Nitrocellulose membrane (HF180), cotton membrane (CFSP001700), glass fiber (GFCP00080000) and supporting adhesive cards were purchased from Millipore.

CNF (10 mM, 0.92 % C) were provided by LEPAMAP group, fabricated following a reported protocol[29] by using commercial bleached pine tree pulp as raw material, provided by Ence: Celulosas y Energía S.A.

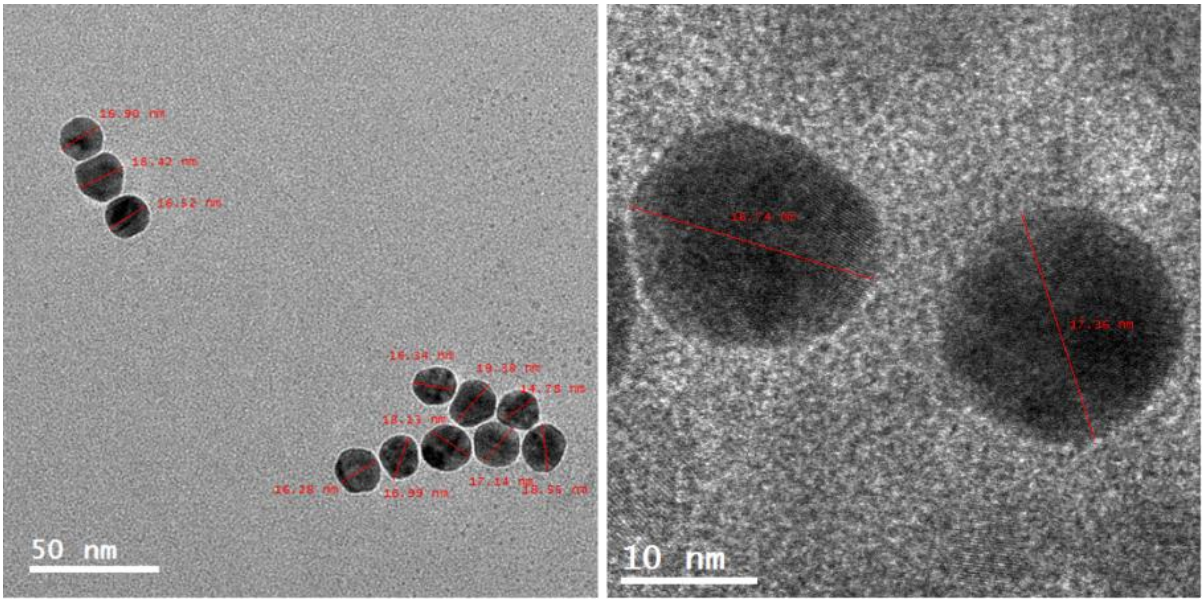

Fig. 4.2. TEM images of AuNPs.

Blips Lens Basic Kit, from Smart Micro Optics[48], was purchased in a Kickstarter campaign.

4.2.2. Synthesis of gold nanoparticles

Following Turkevich method[32], AuNPs of approximately 20 nm diameter were synthesized by citrate reduction of $HAuCl_4$. 50 mL of a 0.01 % (w/v) solution of $HAuCl_4$ were prepared in Milli-Q water. This solution was taken to boiling point and 1.25 mL of 1 % (w/v) sodium citrate solution was added under continuous vigorous stirring. The solution was kept boiling for 10 more minutes and then allowed to cool down to room temperature. The AuNP solution was adjusted to a pH of 9.0 by addition of 0.01 mM BB. AuNPs were characterized by transmission electron micro-scope (TEM, Tecnai F20) as shown in Fig. 4.2.

4.2.3. Gold nanoparticles conjugation

100 µL of goat anti-human IgG antibody (100 µg/mL in PB) were added to 1.5 mL of AuNP solution and incubated for 20 minutes at room temperature. BSA solution (0.1 % (w/v), 100 µL) was then added to the mixture, which was incubated for another 20 minutes and then centrifuged at 4°C (14000 rpm, 20 minutes). The supernatant was discarded and the pellet was reconstituted in 0.5 mL BB (2 mM, pH 7.4) containing 10 % sucrose.

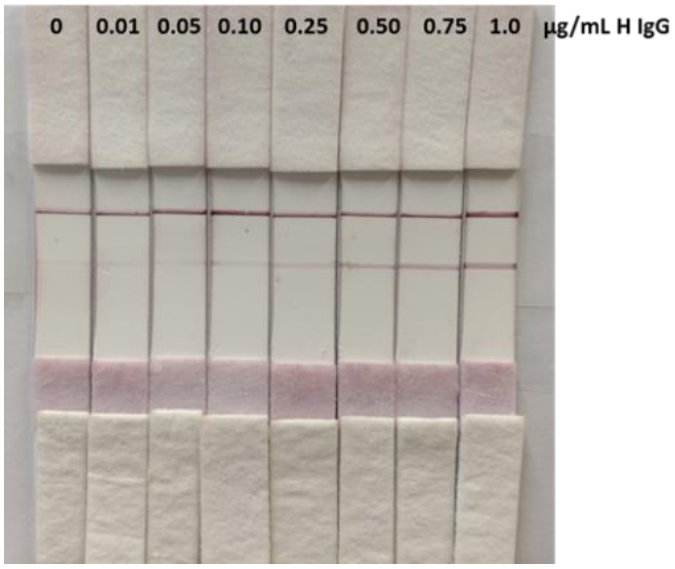

Fig. 4.3. CNF-LFs after the addition of different concentrations of HIgG in PB.

4.2.4. Lateral flow strips preparation

The conjugate pad was prepared by dipping the glass fiber into the AuNP-antibody conjugate suspension. The fiber was dried in a vacuum chamber for 3-4 hours, and then stored in barrier zip-lock pouches with drying pearls at 4 ºC. The sample pad was prepared by dipping the cotton membrane in PBS buffer containing 0.05 % Tween 20 and 5 % BSA. The pad was dried in the oven at 60°C for 2 hours and stored in barrier zip-lock pouches with drying pearls at 4 ºC. The detection pad was made assembling nitrocellulose membrane onto a supporting adhesive card.

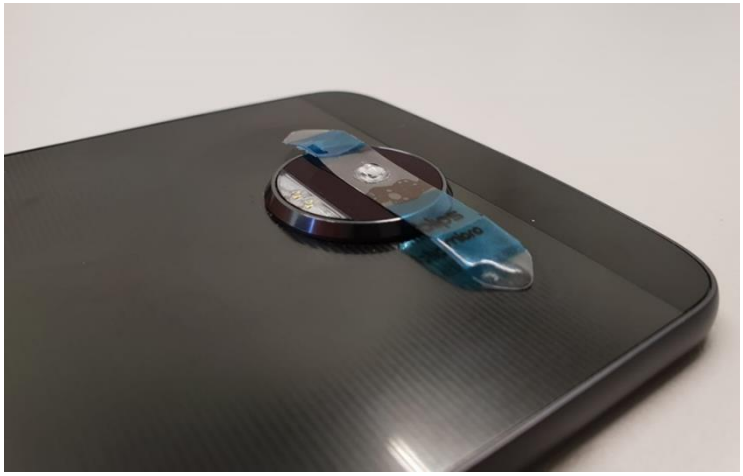

Fig. 4.4. Blips micro lens attached to the mobile phone camera.

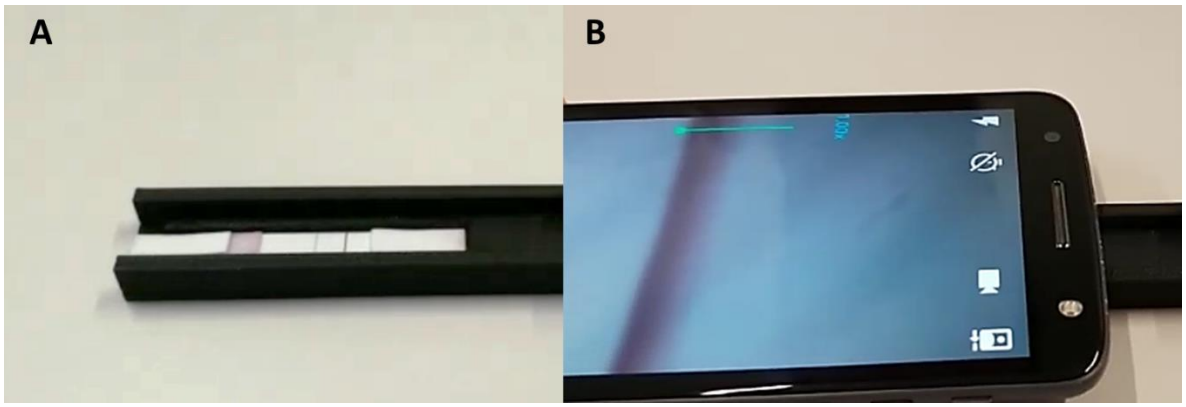

Fig. 4.5. (A) Simple 3D-printed tool to keep the distance between strip and (B) mobile phone always constant (6 mm).

CNF gel (10 mM) was diluted by half with Milli Q water to make it less viscous and was dispensed using a Biofluidix Biospot Workstation over nitrocellulose membrane forming a line. The line was dispensed repeatedly on the same position to increase the concentration of CNF within nitrocellulose pores (from one to six times; i.e. 5 to 30 mM). After drying the membrane overnight at room temperature, goat anti-human IgG antibody (1.0 mg/mL in PB) was dispensed over the previous line. Chicken anti-goat antibody (1.0 mg/mL in PB) was dispensed at 5.5 mm distance from TL as control line (CL). The detection pad was dried at 37°C for 2 hours and stored at room temperature under dry conditions.

The conjugate pad was assembled onto the adhesive card with a 1 mm overlap over the detection pad, on the farthest side from the detection lines. The sample pad was assembled overlapping the conjugate pad at the end of the card. An absorption pad (untreated cellulose membrane) was assembled on the other end of the card, overlapping the detection pad, at 4 mm away from the CL. The strips were cut to a width of 6 mm using a guillotine and stored at room temperature with drying pearls.

4.2.5. Assay performance

Human IgG solutions, from 0.01 to 1.00 µg/mL, were prepared in PB (which was also used as blank sample). 200 µL of each concentration were dropped on the sample pad of the strips (Fig. 4.3). After 5 minutes, TL and CL were observed. Images of the strips were taken at 6 mm of distance using a Moto Z mobile phone camera (13 megapixel) in which Micro Lens, from Blips Lens Basic Kit, were sticked on the objective (Fig. 4.4). A 3D-printed tool (Fig. 4.5A)

was made using BCN-3D Sigma printer (melting polylactic acid filament) in order to keep the distance between the strips and the camera constant (Fig. 4.5B).

Image J software[44,45] was used to quantify the TL intensity of color in the images. The intensity of white pixels (maximum value 255, being 0 the blackest color) was measured in 8-bit black-and-white format reconverted images. Data was normalized into % color where 0 % and 100 % equal to 255 and 0 values respectively.

4.2.6. Characterization of CNF on nitrocellulose

After the assay, two positive LFs were selected and the areas corresponding to the TL were cut for its study. The sample concentration added in both strips was the same, being one strip made with CNF gel and the other without. Both samples were observed on SEM (FEI Magellan 400L XHR).

The same samples were observed by atomic force microscopy (AFM) technique. AFM imaging was performed with a MFP-3D Asylum AFM (Oxford Instruments, Scotts Valley, CA). In all the experiments, PPP-EFM tips (Nanosensors; Schaffhausen, Switzerland) with a stiffness constant k=2 N/m and coated with “Ptlr5” were used. Multi-Frequency AFM is based in the use of multiple excitation modes with different characteristic frequencies. In this case, the fundamental excitation mode was used together with the second Eigen mode.

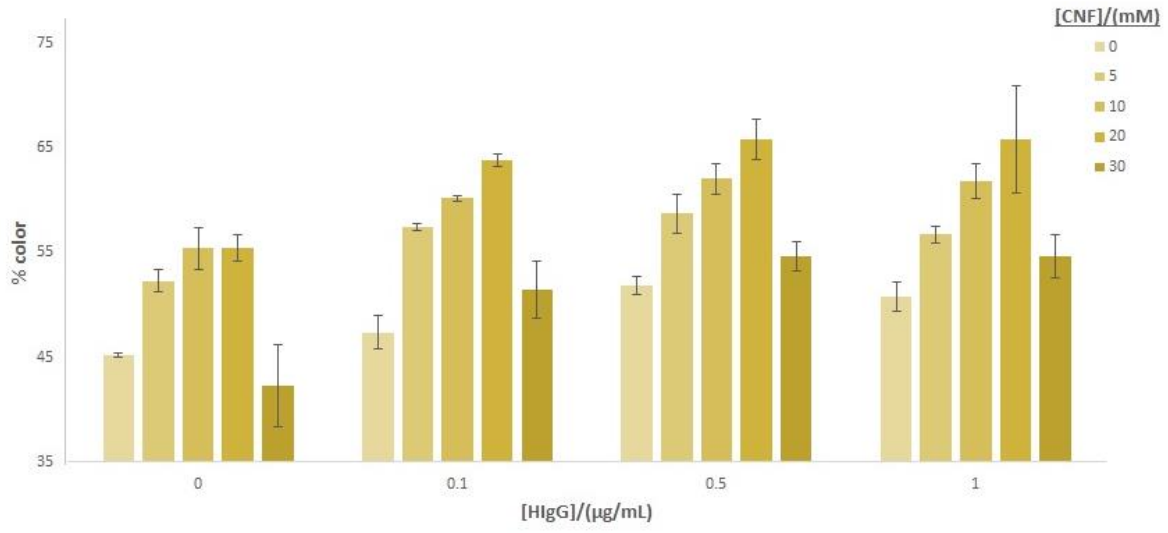

Figure 4.6. Comparison, at different concentrations of H IgG, of the effect of adding different concentrations of CNF in the TL of LFS.

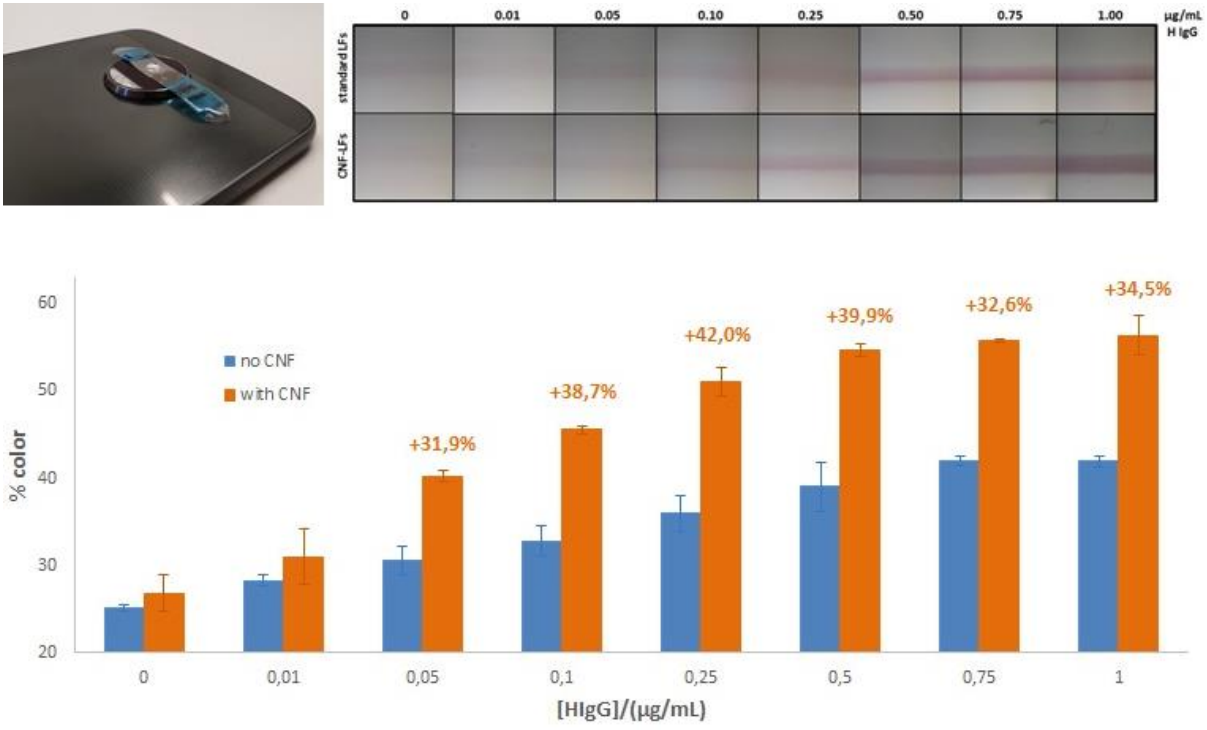

Figure 4.7. Data obtained from LFs assay performed with both standard and CNF-LFs and the images of the strips taken with Blips Micro Lens (inset).

In simple bimodal AFM operation mode, the tip is excited at both frequencies, with amplitudes A2 < A1. A remarkable benefit of MF bimodal imaging is the fact that the forces between the tip and the sample are very small while still allowing a clear non-destructive differentiation of composition, which makes it a very convenient way to investigate samples composed of different materials. The excitation at the fundamental mode was used to measure the topography in amplitude-modulation AFM, while changes in amplitude and phase for the second Eigen mode, not affected by the feedback loop restrictions, are monitored.

4.3. Results and discussion

AuNPs-based LFs were prepared for the detection of human IgG (as described in methods section), a protein often used as model on the optimization of lateral flow assays[14,17,18]. To demonstrate that CNF gel can increase the density of antibodies near the paper surface, thus enhancing the signal (i.e. quantity of AuNPs retained on positive samples), four concentrations of this nanomaterial were dispensed on nitrocellulose. Different concentrations of human IgG were dropped on the distinct LFs, without CNF and with the

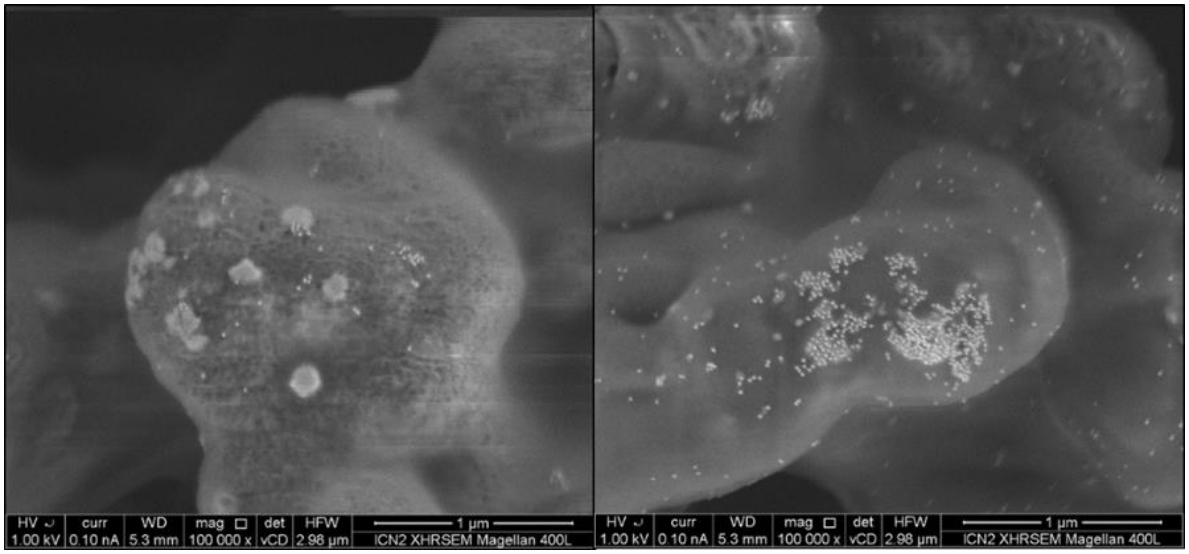

Figure 4.8. SEM images of nitrocellulose corresponding to the TL of two LFs. The amount of AuNPs being retained is lower on a standard LFs (left) that on the one treated with NFC (right).

different four CNF concentrations, and the intensities were recorded by a mobile phone camera with magnification lens attached on the objective.

Results obtained are shown on Fig. 4.6. It can be observed how, as higher the concentration of CNF within nitrocellulose, higher is the color enhancement of test line (TL) until a CNF concentration of 20 mM. At higher concentrations of the gel the intensity stops being enhanced. Seemingly an excess of CNF impedes AuNPs to attach on nitrocellulose pores. Thus, 20 mM concentration of CNF was chosen as optimal for the signal enhancement of LFs and applied on the further experiments.

Standard LFs versus CNF-LFs (containing 20 mM CNF in the test line) were compared. Different concentrations of Human IgG were added on the strips and the intensities were measured as explained at methods section. As shown in Fig. 4.7, over a concentration of 0.05 µg/mL human IgG the signal of the CNF-LFs is increased by an average of 36.6 % in comparison to those strips without CNF gel.

The calibration curve obtained for standard LFs follows the equation:

$$\% \text{ color} = 3.217 \ln [\text{HIgG } (\mu g/mL)] + 41.437$$

On the other hand, the calibration curve obtained for CNF-LFs follows the equation:

$$\% \text{ color} = 5.6881 \ln [\text{HIgG } (\mu g/mL)] + 57.768$$

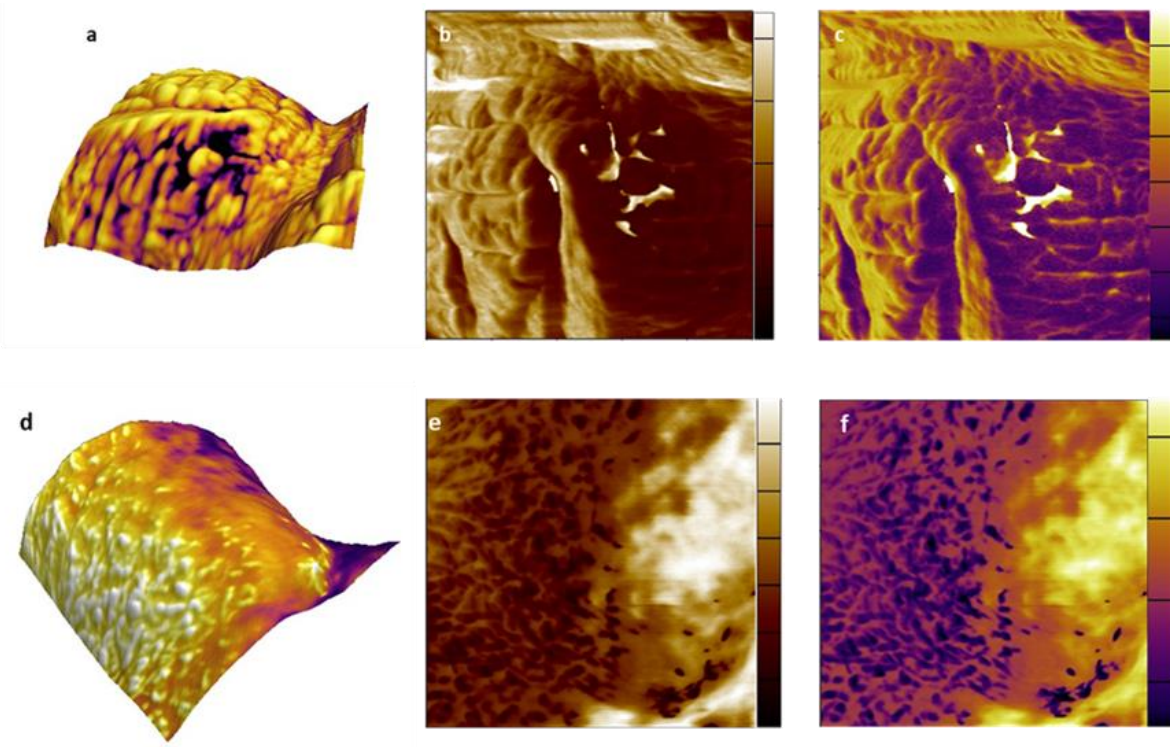

Figure 4.9. AFM imaging of sample without and with NFC. (a) to (c) refers to the sample without NFC and (d) to (f) refers to the sample with NFC. (a) and (d) AFM 3D topography imaging. (b) and (e) second amplitude (A_2) images of bimodal AFM, corresponding to the dynamics of the first excited Eigenmode and (c) and (f) correspond to the second frequency (f_2) accordingly. The dimension of all images is 1 um. From phase and amplitude image is obvious the existence of an extra material (CNF).

The limit of detection (LOD) was of 0.01 µg/mL in both cases, being calculated by using as % color in the equation the corresponding value of blank sample plus 3 times its standard deviation. The method shows a reproducibility (RSD) of 2 % (n=6) for a HIgG concentration of 0.05 µg/mL.

As observed on scanning electron microscope images (SEM), for two strips in which the same amount of H IgG was added, the population of AuNPs on the TL is greater on the CNF-LFs (Fig. 4.8). It demonstrates that more AuNPs are being retained, at least on the surface of the strip, although CNF are not visible in the images due their low density.

The same samples were also observed by AFM. Initially, AFM was used to prove the existence of CNF on nitrocellulose samples, by testing two different samples of nitrocellulose, with and without CNF, as shown in Fig. 4.9. Subsequently, it was demonstrated that for the strip sample with CNF-LFs the amount of AuNPs is significantly bigger than the case of the strip sample without CNF (Fig 4.10).

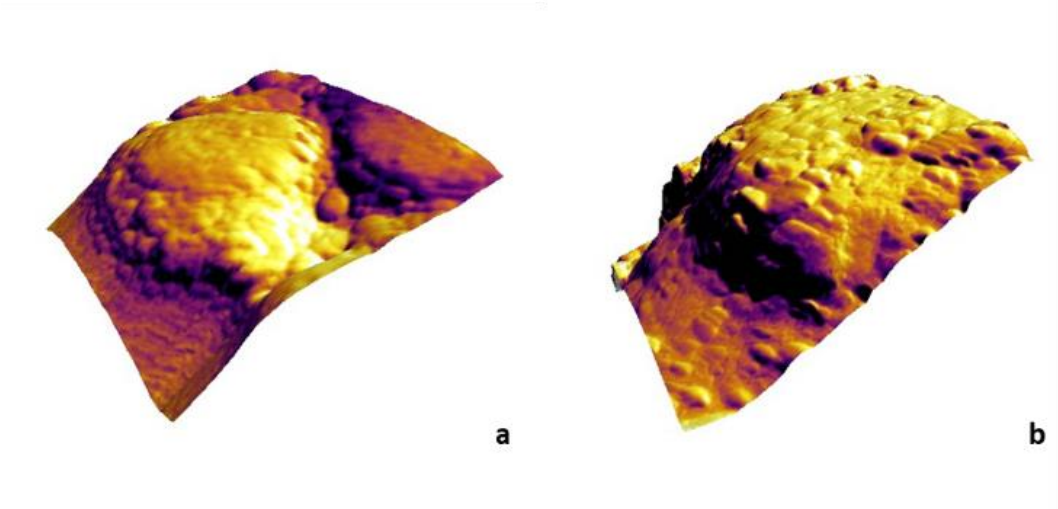

Figure 4.10. AFM 3D topography imaging. (a) corresponds to the strip without CNF and (b) to the stripe with CNF. From topography imaging we were able to detect a significantly higher concentration of AuNPs in the stripe sample with CNF.

4.4. Conclusions

We have devised a new signal enhancement strategy for LFs consisting in the addition of CNF on paper nitrocellulose to decrease the pore size in a determined area, the TL, thus increasing the amount of bioreceptors (capture antibodies) near the surface. Due this modification, on positive samples we observed an increase of 36.6 % of the colorimetric signal, which means that effectively we succeed increasing the amount of AuNPs retained. SEM and AFM images also demonstrate this phenomenon.

Due the blank values and the LOD are similar, this modification does not suppose any unspecific absorption of AuNPs, no false positives detected. Thus, the method facilitates the differentiation between concentrations, supporting a better quantification.

The characterization of the nitrocellulose performed in SEM and AFM demonstrates the presence of the CNF and how it affects to the interaction with AuNPs.

4.5. References

1. LaBarre, P.; Boyle, D.; Hawkins, K.; Weigl, B. Instrument-Free Nucleic Acid Amplification Assays for Global Health Settings. *Int. Soc. Opt. Eng.*, 802902 (2011).

2. Parolo, C.; Merkoci, A. Paper-Based Nanobiosensors for Diagnostics. *Chem. Soc. Rev*. **42**, 450–457 (2013).

3. Quesada-González, D.; Merkoçi, A. Nanoparticle-Based Lateral Flow Biosensors. *Biosens. Bioelectron*. **73**, 47–63 (2015).

4. López-marzo, A. M.; Merkoçi, A. Paper-Based Sensors and Assays: A Success of the Engineering Design and the Convergence of Knowledge Areas. *Lab Chip* **16**, 3150–3176 (2016).

5. Wu, G.; Srivastava, J.; Zaman, M. H. Stability Measurements of Antibodies Stored on Paper. *Anal. Biochem*. **449**, 147–154 (2014).

6. Burns, M. A. Everyone's a (Future) Chemist. *Science* **296**, 1818–1819 (2002).

7. Kratz, A.; Lewandrowski, K. B. Principles & Practice of Point-of-Care Testing*. Arch. Pathol. Lab. Med.* **127**, 511 (2003).

8. Quesada-González, D.; Merkoçi, A. Nanomaterial-Based Devices for Point-of-Care Diagnostic Applications. *Chem. Soc. Rev.* **47**, 4697–4709 (2018).

9. Fu, E.; Lutz, B.; Kauffman, P.; Yager, P. Controlled Reagent Transport in Disposable 2D Paper Networks. *Lab Chip* **10**, 918 (2010).

10. Fu, E.; Ramsey, S. A.; Kauffman, P.; Lutz, B.; Yager, P. Transport in Two-Dimensional Paper Networks. *Microfluid. Nanofluidics* **10**, 29–35 (2011).

11. Fridley, G. E.; Le, H. Q.; Fu, E.; Yager, P. Controlled Release of Dry Reagents in Porous Media for Tunable Temporal and Spatial Distribution upon Rehydration. *Lab Chip* **12**, 4321–4327 (2012).

12. Rodriguez, N. M.; Wong, W. S.; Liu, L.; Dewar, R.; Klapperich, C. M. A Fully Integrated Paperfluidic Molecular Diagnostic Chip for the Extraction, Amplification, and Detection of Nucleic Acids from Clinical Samples. *Lab Chip* **16**, 753–763 (2016).

13. Anfossi, L.; Di Nardo, F.; Giovannoli, C.; Passini, C.; Baggiani, C. Increased Sensitivity of Lateral Flow Immunoassay for Ochratoxin A through Silver Enhancement. *Anal. Bioanal. Chem.* **405**, 9859–9867 (2013).

14. Parolo, C.; de la Escosura-Muñiz, A.; Merkoçi, A. Enhanced Lateral Flow Immunoassay Using Gold Nanoparticles Loaded with Enzymes. *Biosens. Bioelectron*. **40**, 412–416 (2013).

15. Chapman, R.; Lin, Y.; Burnapp, M.; Bentham, A.; Hillier, D.; Zabron, A.; Khan, S.; Tyreman, M.; Stevens, M. M. Multivalent Nanoparticle Networks Enable Point-of-Care Detection of Human Phospholipase-A2 in Serum. *ACS Nano* **9**, 2565–2573 (2015).

16. Loynachan, C. N.; Thomas, M. R.; Gray, E. R.; Richards, D. A.; Kim, J.; Miller, B. S.; Brookes, J. C.; Agarwal, S.; Chudasama, V.; McKendry, R. A. & Stevens, M. M. Platinum Nanocatalyst Amplification: Redefining the Gold Standard for Lateral Flow Immunoassays with Ultrabroad Dynamic Range. *ACS Nano* **12**, 279–288 (2018).

17. Parolo, C.; Medina-Sánchez, M.; de la Escosura-Muñiz, A.; Merkoçi, A. Simple Paper Architecture Modifications Lead to Enhanced Sensitivity in Nanoparticle Based Lateral Flow Immunoassays. *Lab Chip* **13**, 386–390 (2013).

18. Rivas, L.; Medina-Sánchez, M.; de la Escosura-Muñiz, A.; Merkoçi, A. Improving Sensitivity of Gold Nanoparticle-Based Lateral Flow Assays by Using Wax-Printed Pillars as Delay Barriers of Microfluidics. *Lab Chip* **14**, 4406–4414 (2014).

19. Li, M.; Yang, H.; Li, S.; Zhao, K.; Li, J.; Jiang, D.; Sun, L.; Deng, A. Ultrasensitive and Quantitative Detection of a New Beta-Agonist Phenylethanolamine A by a Novel Immunochromatographic Assay Based on Surface-Enhanced Raman Scattering (SERS). *J. Agric. Food Chem.* **62**, 10896–10902 (2014).

20. Zhu, X.; Shah, P.; Stoff, S.; Liu, H.; Li, C. A Paper Electrode Integrated Lateral Flow Immunosensor for Quantitative Analysis of Oxidative Stress Induced DNA Damage. *Analyst* **139**, 2850–2857 (2014).

21. Tang, D.; Sauceda, J. C.; Lin, Z.; Ott, S.; Basova, E.; Goryacheva, I.; Biselli, S.; Lin, J.; Niessner, R.; Knopp, D. Magnetic Nanogold Microspheres-Based Lateral-Flow Immunodipstick for Rapid Detection of Aflatoxin B2 in Food. *Biosens. Bioelectron*. **25**, 514–518 (2009).

22. Marquina, C.; De Teresa, J. M.; Serrate, D.; Marzo, J.; Cardoso, F. A.; Saurel, D.; Cardoso, S.; Freitas, P. P.; Ibarra, M. R. GMR Sensors and Magnetic Nanoparticles for Immuno-Chromatographic Assays. *J. Magn. Magn. Mater.* **324**, 3495–3498 (2012).

23. Wong, R. C.; Tse, H. Y. Lateral Flow Immunoassay. *Springer*, 2009.

24. González, I.; Boufi, S.; Pèlach, M. A.; Alcalà, M.; Vilaseca, F.; Mutjé, P. Nanofibrillated Cellulose as Paper Additive in Eucalyptus Pulps. *BioResources* **7**, 5167–5180 (2012).

25. Alcalá, M.; González, I.; Boufi, S.; Vilaseca, F.; Mutjé, P. All-Cellulose Composites from Unbleached Hardwood Kraft Pulp Reinforced with Nanofibrillated Cellulose. *Cellulose*, **20**, 2909–2921 (2013).

26. González, I.; Vilaseca, F.; Alcalá, M.; Pèlach, M. A.; Boufi, S.; Mutjé, P. Effect of the Combination of Biobeating and NFC on the Physico-Mechanical Properties of Paper. *Cellulose* **20**, 1425–1435 (2013).

27. González, I.; Alcalà, M.; Chinga-Carrasco, G.; Vilaseca, F.; Boufi, S.; Mutjé, P. From Paper to Nanopaper: Evolution of Mechanical and Physical Properties. *Cellulose*, **21**, 2599–2609 (2014).

28. Delgado-Aguilar, M.; González, I.; Tarrés, Q.; Alcalà, M.; Pèlach, M. À.; Mutjé, P. Approaching a Low-Cost Production of Cellulose Nanofibers for Papermaking Applications. *BioResources* **10**, 5330–5344 (2015).

29. Tarrés, Q.; Delgado-Aguilar, M.; Pèlach, M. A.; González, I.; Boufi, S.; Mutjé, P. Remarkable Increase of Paper Strength by Combining Enzymatic Cellulose Nanofibers in Bulk and TEMPO-Oxidized Nanofibers as Coating. *Cellulose* **23**, 3939–3950 (2016).

30. Delgado-Aguilar, M.; González, I.; Tarrés, Q.; Pèlach, M. À.; Alcalà, M.; Mutjé, P. The Key Role of Lignin in the Production of Low-Cost Lignocellulosic Nanofibres for Papermaking Applications. *Ind. Crops Prod.* **86**, 295–300 (2016).

31. González, I.; Oliver-Ortega, H.; Tarrés, Q.; Delgado-Aguilar, M.; Mutjé, P.; Andreu, D. Immobilization of Antimicrobial Peptides onto Cellulose Nanopaper. *Int. J. Biol. Macromol*. **105**, 741–748 (2017).

32. Turkevich, J.; Stevenson, P. C.; Hillier, J. A Study of the Nucleation and Growth Processes in the Synthesis of Colloidal Gold. *Discuss. Faraday Soc*. **11**, 55–75 (1951).

33. Shyu, R. H.; Shyu, H. F.; Liu, H. W.; Tang, S. S. Colloidal Gold-Based Immunochromatographic Assay for Detection of Ricin. *Toxicon* **40**, 255–258 (2001).

34. De La Escosura-Muñiz, A.; Parolo, C.; Merkoi, A. Immunosensing Using Nanoparticles. *Mater. Today* **13**, 24–34 (2010).

35. Parolo, C.; De La Escosura-Muñiz, A.; Polo, E.; Grazú, V.; De La Fuente, J. M.; Merkoçi, A. Design, Preparation, and Evaluation of a Fixed-Orientation Antibody/gold-Nanoparticle Conjugate as an Immunosensing Label. *ACS Appl. Mater. Interfaces* **5**, 10753–10759 (2013).

36. Fu, Q.; Wu, Z.; Xu, F.; Li, X.; Yao, C.; Xu, M.; Sheng, L.; Yu, S.; Tang, Y. A Portable Smart Phone-Based Plasmonic Nanosensor Readout Platform That Measures Transmitted Light Intensities of Nanosubstrates Using an Ambient Light Sensor. *Lab Chip* **16**, 1927–1933 (2016).

37. Quesada-González, D.; Merkoçi, A. Mobile Phone–based Biosensing: An Emerging "diagnostic and Communication" Technology. *Biosens. Bioelectron*. **92**, 549–562 (2016).

38. Coskun, A. F.; Wong, J.; Khodadadi, D.; Nagi, R.; Tey, A.; Ozcan, A. A Personalized Food Allergen Testing Platform on a Cellphone. *Lab Chip* **13**, 636–640 (2013).

39. Mudanyali, O.; Dimitrov, S.; Sikora, U.; Padmanabhan, S.; Navruz, I.; Ozcan, A. Integrated Rapid-Diagnostic-Test Reader Platform on a Cellphone. *Lab Chip* **12**, 2678–2686 (2012).

40. Coskun, A. F.; Nagi, R.; Sadeghi, K.; Phillips, S.; Ozcan, A. Albumin Testing in Urine Using a Smart-Phone. *Lab Chip* **13**, 4231–4238.

(41) Berg, B.; Cortazar, B.; Tseng, D.; Ozkan, H.; Feng, S.; Wei, Q.; Chan, R. Y. L.; Burbano, J.; Farooqui, Q.; Lewinski, M.; et al. Cellphone-Based Hand-Held Microplate Reader for Point-of-Care Testing of Enzyme-Linked Immunosorbent Assays. *ACS Nano*, **9**, 7857–7866 (2015).

42. Roda, A.; Michelini, E.; Cevenini, L.; Calabria, D.; Calabretta, M. M.; Simoni, P. Integrating Biochemiluminescence Detection on Smartphones: Mobile Chemistry Platform for Point-of-Need Analysis. *Anal. Chem*. **86**, 7299–7304 (2014).

43. Roda, A.; Michelini, E.; Zangheri, M.; Di Fusco, M.; Calabria, D.; Simoni, P. Smartphone-Based Biosensors: A Critical Review and Perspectives. *Trends Anal. Chem*. **79**, 317–325 (2016).

44. Álvarez-diduk, R.; Orozco, J.; Merkoçi, A. Paper Strip-Embedded Graphene Quantum Dots : A Screening Device with a Smartphone Readout. *Sci Rep.* **976**, 1–9 (2017).

45. Kühnemund, M.; Wei, Q.; Darai, E.; Wang, Y.; Iván, H. N.; Yang, Z.; Tseng, D.; Ahlford, A.; Mathot, L.; Sjöblom, T.; et al. Targeted DNA Sequencing and in Situ Mutation Analysis Using Mobile Phone Microscopy. *Nat. Commun*. **8**, 1–8 (2017).

46. You, M.; Lin, M.; Gong, Y.; Wang, S.; Li, A.; Ji, L.; Zhao, H.; Ling, K.; Wen, T.; Huang, Y.; et al. Household Fluorescent Lateral Flow Strip Platform for Sensitive and Quantitative Prognosis of Heart Failure Using Dual-Color Upconversion Nanoparticles. *ACS Nano* **11**, 6261–6270 (2017)

47. Brangel, P.; Sobarzo, A.; Parolo, C.; Miller, B. S.; Howes, P. D.; Gelkop, S.; Lutwama, J. J.; Dye, J. M.; McKendry, R. A.; Lobel, L.; et al. A Serological Point-of-Care Test for the Detection of IgG Antibodies against Ebola Virus in Human Survivors. *ACS Nano* **12**, 63–73 (2018).

48. Smart Micro Optics (Blips lenses) https://www.smartmicrooptics.com/blips/ (accessed Ago 09, 2018).

4.6. Contributions

This work has been performed in collaboration with LEPAMAP group, from the University of Girona, who synthetized and provided the CNFs. Christina Stefani and Dr. Neus Domingo, from ICN2, also collaborated in this work performing the AFM images and their study.

CHAPTER 5

Iridium oxide (IV) nanoparticle-based lateral flow immunoassay

Iridium oxide (IV) nanoparticles (IrO_2 NPs) were chosen as new labels for LFBs due their electrocatalytic properties (as will be explained later in the text). This chapter is composed by two different works in which these nanoparticles are applied, the electrochemical detection of a marine contaminant and a lateral flow assay for a model protein. The future perspectives are to combine both works to create LFs able to give both optical and electrochemical responses.

5.1. Iridium oxide (IV) nanoparticles synthesis

IrO_2 NPs were synthesized following the procedure reported by Harriman and Thomas[1] and also previously applied in our group[2-6]. A solution containing 1.24 mM K_2IrCl_6 and 3.80 mM sodium citrate sesquihydrate, in MilliQ water was taken to pH 7.5 by using 0.25 M NaOH. It was lead to ebullition in a reflux system for 30 min and the pH was checked after the solution was cooled down. If necessary, pH was readjusted to 7.5 and the 30 min ebullition step was repeated until pH was constant. Then, the solution was boiled during 2 h in presence of bubbling oxygen. The obtained final solution was dark blue. Color changes during the synthesis can be observed on Fig. 5.1.

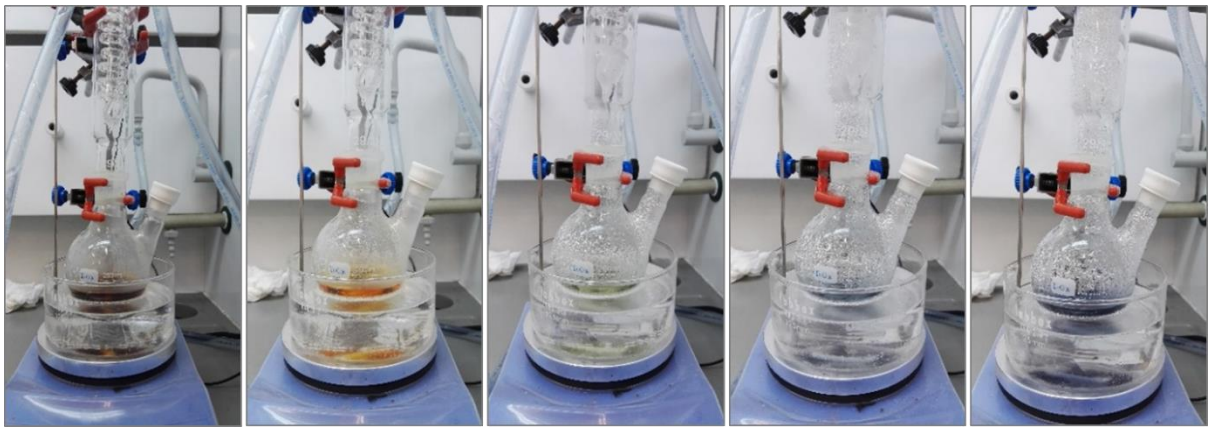

Figure 5.1. Color changes observed during IrO_2 NPs synthesis (from left to right: brown, orange, green, light blue, dark blue).

5.2. Capabilities of iridium oxide (IV) nanoparticles as electrocatalytical tags

5.2.1. Introduction

Polybrominated diphenyl ethers (PBDEs) have been used since 1970s as flame retardants in different products such as furniture, building materials or electronics[7,8]. However, it has been demonstrated that the exposure to these compounds causes severe health problems like neurodevelopmental deficits, thyroid homeostasis disruption, behavioural alteration, reproductive dysfunction and even cancer, reason why the use of PBDEs has been banned since 2004 in EU and USA[9-12]. Nevertheless, PBDE molecules are hard to degrade and can persist long time bioaccumulated in mammalian organisms (in fat tissues) and in the environment, especially in marine water[13-17]. Among the different PBDEs structures, 3,3',4,4'-tetrabromodiphenyl ether (BDE-47) is one of the most abundant and resistant to degradation[18,19].

Although commercial kits for the detection of BDE-47 are available (e.g. Abraxis PBDE ELISA Kit[20]), there is still a need of lower-cost, more portable, faster and more stable-in-time detection systems. The use of nanomaterials on sensing and biosensing is on the rise during last years[21-26] due to the sensitivity improvement and robustness, among other properties, that nanoparticles can offer. In this work we have chosen iridium oxide (IV) nanoparticles (IrO_2 NPs) owing to their electrocatalytical properties towards water oxidation reaction (WOR)[2], without requiring any other reagent. Screen printed carbon electrodes (SPCEs)[27-33] are a suitable platform to carry on the reaction since they are easy to be fabricated and modified (both the design and the composition) also avoiding the fouling effect that occurs on classical electrodes since they are single-use ones[34].

Herein we present a competitive electrochemical assay in which the measured current values (related to WOR, being catalysed by the presence of IrO_2 NPs) are inversely proportional to the concentration of BDE-47 in liquid sample. We take advantage of magnetic beads (MBs) coated with anti-PBDE antibodies to capture BDE-47 and horseradish peroxidase (HRP)-PBDE conjugate to link IrO_2 NPs to PBDE (HRP can be conjugated on IrO_2 NPs surface, as on other nanomaterials[35,36]. Then, in absence of BDE-47, the conjugate MBs/PBDE-IrO_2NPs will be formed, leading to a high electrocatalytic signal. In presence of free BDE-47 in the

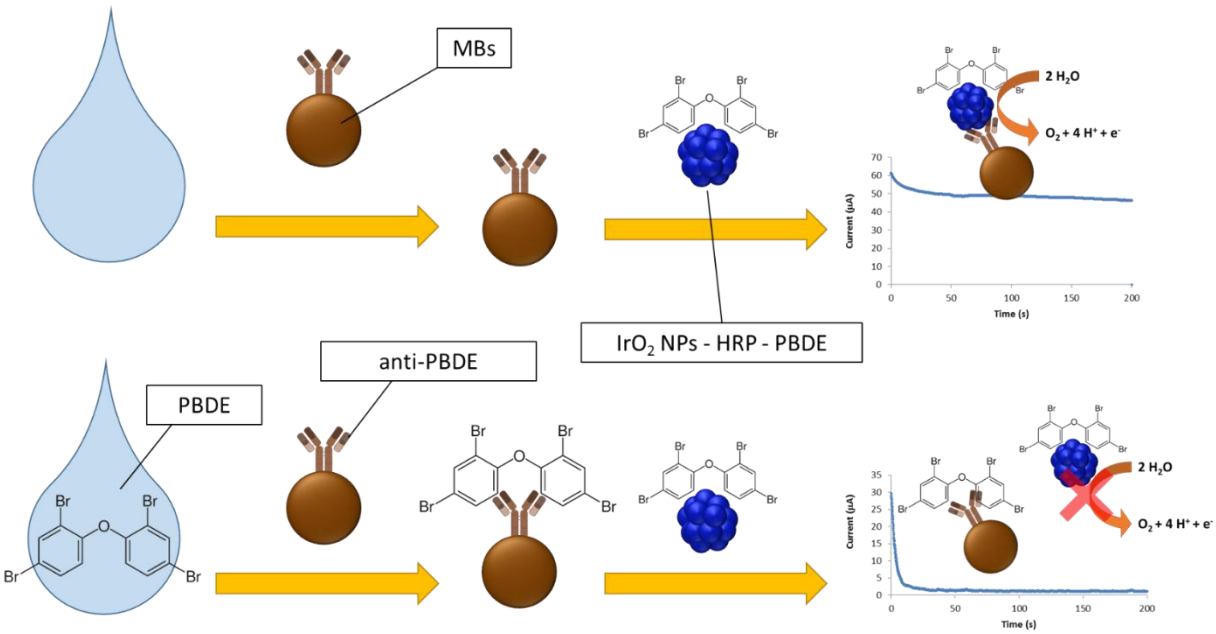

Fig. 5.2. Schematic representation of the competitive electrocatalytic assay. In absence of PBDE, PBDE-IrO_2 NPs conjugate is captured by MBs producing a current increase due the catalysis of WOR (up). In presence of PBDE, IrO_2 NPs are not captured and signal is inhibited (down).

sample, the conjugate PBDE-IrO_2 NPs will be displaced, thus giving a decrease in the signal that is related with the amount of analyte as illustrated at Fig. 5.2.

5.2.2. Materials and methods

5.2.2.1. Materials

BDE-47, bovine serum albumin (BSA), K_2IrCl_6, sodium citrate sesquihydrate, NaOH and phosphate buffer saline (PBS) tablets were purchased from Sigma-Aldrich. MBs coated with anti-PBDE antibody and PBDE-HRP conjugate were obtained from Abraxis PBDE ELISA Kit. The inks to fabricate the SPCEs (Electrodag 423SS carbon ink, Electrodag 6037SS Ag/AgCl ink, Minico 7000 blue insulating ink) were purchased from Acheson Industries and the substrate (Autostat HT5 polyester sheet) was purchased from McDermid Autotype.

5.2.2.2. Iridium oxide (IV) nanoparticles synthesis

IrO_2 NPs were synthetized as explained on point 5.1 and then suspension was cleansed and concentrated 9 times by centrifuging it at 35000 rcf and 4ºC during 2.5 h, reconstituting the solution in a third part of its original volume with MilliQ water. To achieve a 9-fold concentration, the process was repeated twice.

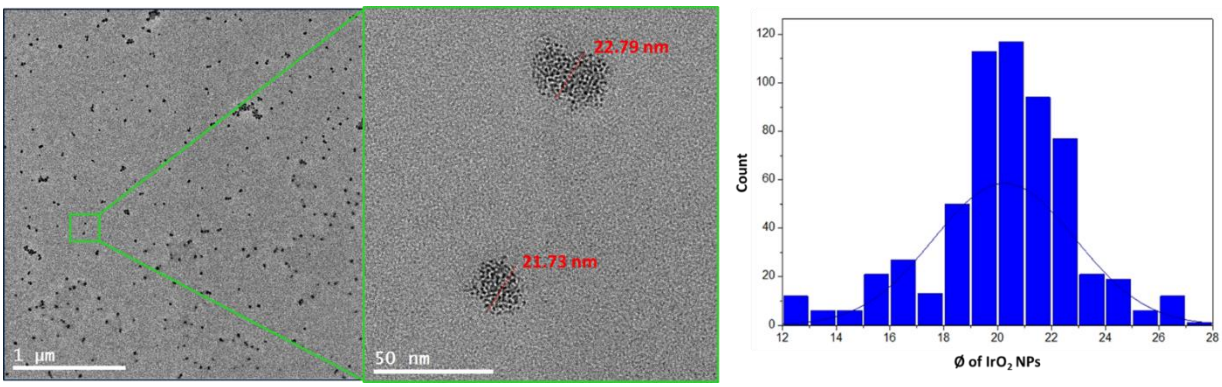

Fig. 5.3. TEM images of IrO_2 NPS and the corresponding histogram.

5.2.2.3. Iridium oxide (IV) nanoparticles-PBDE conjugation

100 µL of PBDE-HRP conjugate from Abraxis Kit (enzyme conjugate solution) were mixed with 1.75 mL of IrO_2 NPs during 2 h at 650 rpm and room temperature. The mixture was left in repose overnight at room temperature and then centrifuged at 35000 rcf and 4ºC during 2.5 h. The precipitate was reconstituted in 1.85 mL of MilliQ water which pH was previously adjusted to 7.0.

5.2.2.4. Iridium oxide (IV) nanoparticles characterization

IrO_2 NPs were characterized using transmission electron microscope (TEM) to evaluate their shape and homogeneity (Fig. 5.3). Z potential measurements at three different pH were carried out in order to verify the conjugation of IrO_2 NPs and PBDE-HRP conjugate (Table 5.1 and Fig. 5.4). The concentration of IrO_2 NPs, just synthetized and after centrifugation, was measured by inductively coupled plasma mass spectrometry (ICP-MS).

Table 5.1. Z Potential measurements of IrO_2 NPs and the IrO_2 NPs-PBDE conjugate at three different pH.

pH	IrO_2 NPs-PBDE	IrO_2 NPs
7	-42 ± 2	-54 ± 2
8	-45 ± 3	-55 ± 1
9	-49 ± 1	-55 ± 2

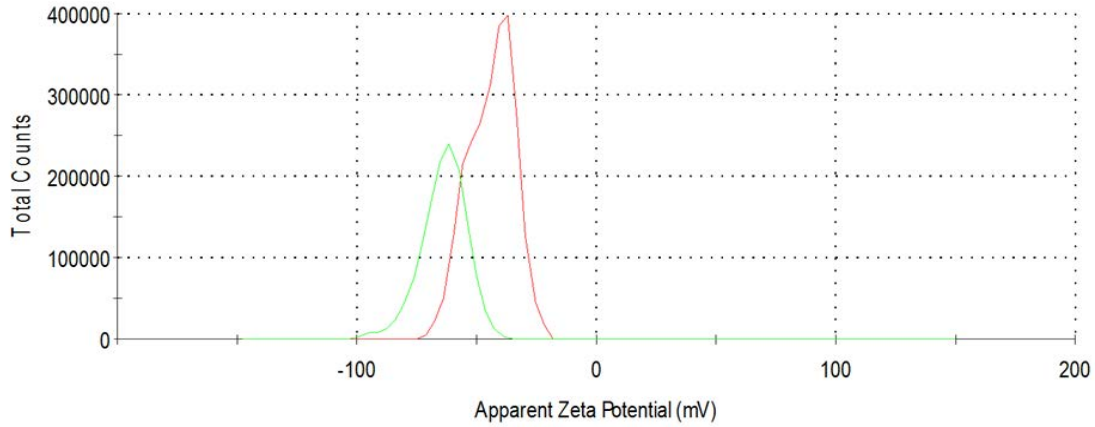

Fig. 5.4. Z Potential average measurements at pH 7 of IrO_2 NPs (green) and PBDE-IrO_2 NPs conjugate (red).

5.2.2.5. Screen printed carbon electrodes fabrication

A layer of carbon ink was printed onto a polyester sheet using a screen printer, forming the working and counter electrodes, later cured at 95ºC for 15 min. Then, a second layer composed by Ag/AgCl ink was printed for the reference electrode and was cured under the same conditions. Finally an insulating ink was printed and cured for 20 min at 95ºC. Fig. 5.5 shows the design of the SPCE.

To evaluate the correct performance of the SPCE four different solutions were measured (by chronoamperometry, as explained on section 5.2.2.7.): MBs, MBs incubated with PBDE-IrO_2 NPs conjugate, MBs with IrO_2 nanoparticles and MBs with PBDE.

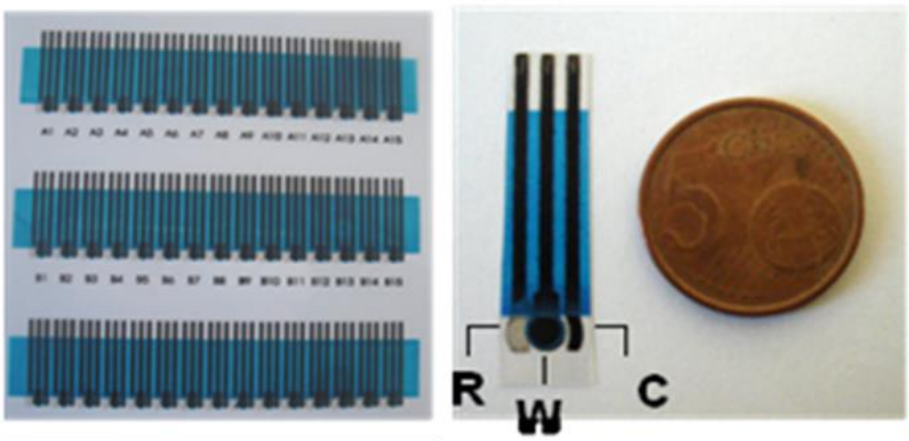

Figure 5.5. SPCEs sheet (left) and individual SPCE (right). The three electrodes integrated in a SPCE are reference (R), working (W) and counter (C).

5.2.2.6. Assay preparation

5.2.2.6.1. Magnetic beads blocking

500 µL of MBs with anti-PBDE antibody were incubated with 150 µL 5% BSA at 650 rpm and room temperature during 2h. The mixture was left in repose overnight at 4ºC and then washed twice with MilliQ water and twice with 0.1 M PBS solution at pH 7.4 using a magnetic rack. The solution was reconstituted in 500 µL of the PBS solution.

5.2.2.6.2. Samples preparation

500 µL of blocked MBs were mixed with 250 µL of sample solution (different concentrations of BDE-47 were evaluated, being MilliQ water used as blank) and incubated 20 min at room temperature and 650 rpm. Then, 250 µL of the PBDE-IrO_2 NPs conjugate were added and the incubation was repeated. The solution was washed in a magnetic rack and reconstituted in 250 µL of PBS 0.1 M.

5.2.2.7. Assay performance: PBDE detection

50 µL of the sample (incubated with MBs, PBDE-IrO_2 NPs conjugate and washed) were placed on the SPCE. The SPCE was placed over a magnet to ensure that the MBs are all deposited onto to the SPCE surface.

Following a previously reported procedure[2], a fixed oxidative potential of +1.3 V for 200 s was applied to achieve steady state current values. Hence, the current value at 200 s was considered as the analytical signal.

50 µL of concentrated IrO_2 NPs were measured on the SPCE under the same conditions. This value was used to normalize the analytical signal by dividing the values obtained by this one.

5.2.3. Results and discussion

5.2.3.1. Iridium oxide (IV) nanoparticles characterization

As seen on TEM image (Fig. 5.3), IrO_2 NPs have an average size of 20 ± 2 nm.

IrO_2 NPs and IrO_2 NPs-PBDE conjugate were stored 48h at three different pH (7, 8 and 9). Then, aliquots before and after forming the conjugate were measured on Z potential

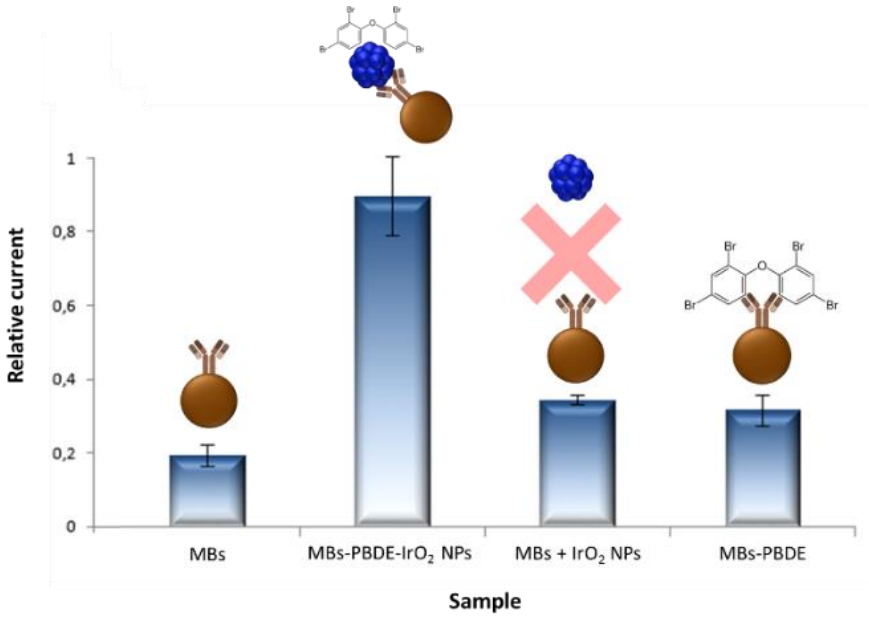

Figure 5.6. Relative current measurements on SPCE for MBs, MBs and PBDE-IrO_2 NPs conjugate, MBs and IrO_2 NPs, MBs and PBDE.

obtaining the values shown on Table 5.1. Due the absorption of PBDE on IrO_2 NPs surface a variation in the charge is expected[37] thus, since the highest variation was observed at pH 7 it was chosen as optimal pH for the conjugate formation.

The concentration of Ir on IrO_2 NPs should be around 1.24 mM regarding the concentration of the precursor, K_2IrCl_6. According to the results obtained from ICP-MS (measuring ^{193}Ir isotope) the concentration was 1.26 ± 0.08 mM in an aliquot of just synthetized nanoparticles and 0.60 ± 0.01 mM after centrifugation. It indicates that during centrifugation nearly half of Ir is lost (does not precipitate), thus further concentration of the IrO_2 NPs is necessary.

5.2.3.2. Sensing principle: specificity of the competitive assay

MBs, MBs incubated with PBDE-IrO_2 NPs conjugate, MBs with IrO_2 nanoparticles and MBs with PBDE solutions were washed on magnetic rack and measured on SPCE. At a potential of +1.3 V it is expected that neither MBs nor PBDE produce high current signals, while IrO_2 NPs should. On Fig. 5.6 it is observed how MBs and MBs with PBDE effectively barely produce analytical signal. In the case of MBs with IrO_2 NPs, since there is no presence of PBDE both particles cannot be linked and, after the washing step on magnetic rack, IrO_2 NPs are removed also not generating signal. Only in the case of MBs incubated with PBDE-

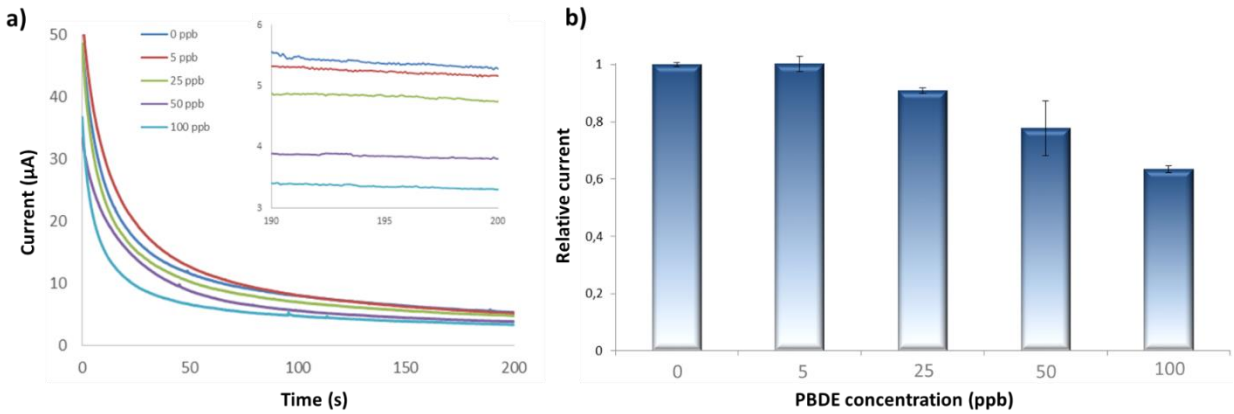

Figure 5.7. (a) Chronoamperograms recorded in PBS 0.1 M pH 7.4 at a fixed potential of +1.3 V, for a blank sample and for samples containing 5 , 25 , 50 and 100 ppb of PBDE (inset graph details the currents recorded at 200 seconds, which represent the analytical signal). (b) Corresponding relative current measurements PBDE concentrations. Samples correspond to the competitive assay detailed at the experimental section.

IrO_2 NPs conjugate, a signal increase is observed (IrO_2 NPs reach the electrode) demonstrating the good performance of the sensing system.

5.2.3.3. PBDE detection

Concentrations of 0 (blank; MilliQ water), 5, 25, 50 and 100 ppb of PBDE (BDE-47) were measured as explained at section 5.2.2.7. (and prepared as on section 5.2.2.6.2.). The results obtained are illustrated on Fig. 5.7, showing a good response of the current values related to the PBDE concentration in the sample since the current is decreased as higher is the concentration of PBDE, as expected from a competitive assay. The current response in a working range between 5 and 100 ppb of PBDE follows the equation:

relative current = -0.0351 [PBDE(ppb)] + 9.1413

With an r value of 0.989. The method shows a reproducibility (RSD) of 3 % (n=3) for a PBDE concentration of 5 ppb. A limit of detection (LOD) (calculated by dividing the average standard error of the measurements by the slope of the equation and then multiplying that value by 3.3)[38] of 21.5 ppb is estimated.

5.2.4. Conclusions

In this work we have demonstrated that IrO_2 NPs can work as electrocatalytic tags for the detection of PBDEs in a competitive assay. Chronoamperometric measurements were

performed obtaining higher current signal (related to water oxidation reaction) as higher was the amount of IrO_2 NPs, opposed to the concentration of BDE-47, an abundant and not degradable type of PBDE. The LOD obtained was of 21.5 ppb.

Our system is a promising tool for fast and cheap measurement of PBDEs, avoiding the use of enzymes and of additional reagents, since the catalytic reaction occurs in aqueous buffer. Furthermore, IrO_2 NPs are robust against temperature and stable in time. We believe that in the future it could easily become a miniaturized device, even coupled to a mobile phone[39].

5.3. Application of iridium oxide (IV) nanoparticles on lateral flow biosensors

5.3.1. Introduction

In this work we seek to improve the classical LF immunoassay with a new nanomaterial never applied before on this platform: iridium oxide (IV) nanoparticles (IrO_2 NPs). This nanomaterial exhibits a dark and intense blue color[1], demonstrated biocompatibility with antibodies[2] and a wide specific surface to conjugate those[40].

The assay herein we present is based on the detection of human immunoglobulin (H IgG) as model protein[41,42] using IrO_2 NPs as tags, as shown on Fig. 5.8A. The operation principle of this LF assay follows the "direct method" or "standard design"[24], obtaining one colored line for negative samples (Fig. 5.8B) and two lines for positives (Fig. 5.8C).

5.3.2. Materials and methods

5.3.2.1. Materials

Cellulose membrane (CFSP001700), nitrocellulose membrane (HF180), glass fibber (GFCP00080000) and adhesive laminated cards (HF000MC100) were purchased from Millipore. Bovine serum albumin (BSA), sucrose, polyclonal goat anti-human IgG (I1886), Human IgG (I2511), phosphate buffer saline (PBS) tablets, sodium dodecyl sulfate (SDS), sodium tetraborate, orthoboric acid, drying pearls "orange" and Tween 20 were purchased from Sigma-Aldrich. Chicken anti-goat IgG (ab86245) was purchased from Abcam.

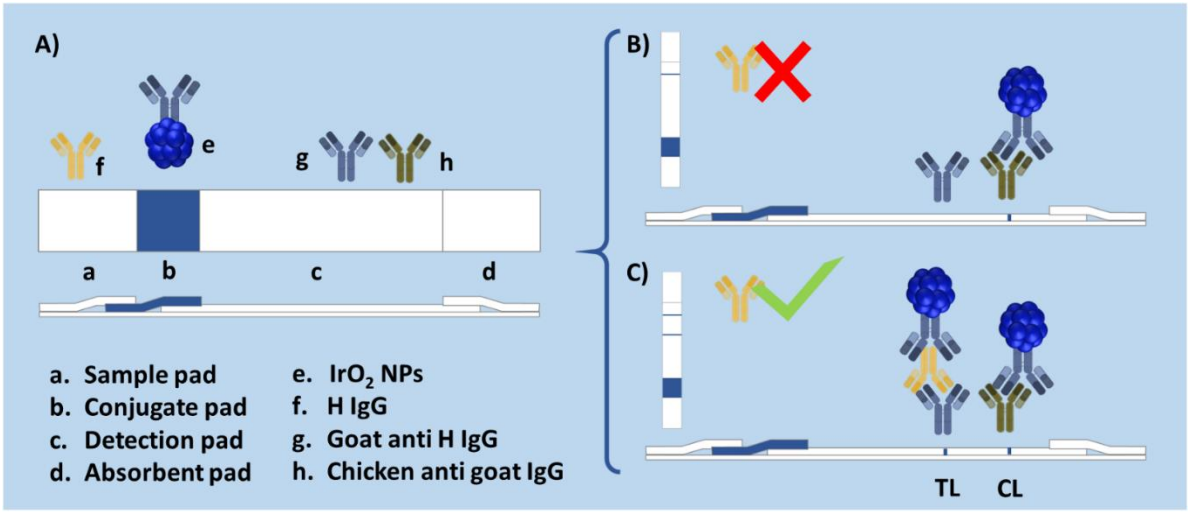

Figure 5.8. A) Schematic representation of a LF strip and its components a-h. B) Negative and C) positive performances.

5.3.2.2. Iridium oxide (IV) nanoparticles synthesis and characterization

IrO_2 NPs were synthetized and characterized as previously explained. Differently to the IrO_2 NPs used on electrochemical assays, these ones were not concentrated, during the conjugation step they were used directly as obtained from the synthesis.

5.3.2.3. Iridium oxide (IV) nanoparticles conjugation

100 µL of anti-human IgG antibody produced in chicken (250 µg/mL) were mixed with 1.5 mL of IrO_2 NPs solution during 2h at 650 rpm and room temperature. The solution was then centrifuged at 35000 rcf and 4ºC during 2.5h. The solid was reconstituted immediately in 0.5 mL of borate buffer (2 mM, pH 7.4; made by mixing 2 mM sodium tetraborate with 2 mM orthoboric acid until the desired pH was achieved) containing 10% sucrose and 25% BSA.

5.3.2.4. Lateral flow strips preparation

LFs are formed by 4 different pads assembled on a laminated card: sample, conjugate, detection and sample pads.

Both sample and absorbent pads consist of cellulose membrane. Sample pad was made by dipping the membrane on 10 mM PBS solution at pH 7.4 containing 5% BSA and 0.05% Tween 20, then leaving it to dry during 2h at 37ºC. In the case of the absorbent pad

treatments were not necessary. Sample and absorbent pad are placed on the bottom and the upper parts of the LFs respectively, as illustrated on Fig. 5.8A(a,d).

Conjugate pad consists of glass fiber storing IrO_2 NPs conjugated with antibody. The reconstituted solution of IrO_2 and antibody (section 5.3.2.3) was carefully dispensed by drop-casting over the glass fiber and it was vacuum dried during 3 h. After this time it was stored overnight at room temperature in a hermetic box containing dry pearls. Conjugate pad is placed between detection and sample pads (Fig. 5.8A(b)).

Detection pad consists of nitrocellulose membrane and contains test (TL) and control (CL) lines, anti-human IgG and anti-goat IgG antibodies respectively. Both antibodies were dispensed using a Biospot Workstation with a dispensing rate of 0.05 µL/mm. After drying the membrane during 2h at 37ºC it was blocked by dispersing on it, using a spray, a 10 mM PBS solution at pH 7.4 containing 5% BSA. After 5 min the membrane was introduced into washing solution (PBS 2 mM at pH 7.4 with 0.05 % SDS) and shaken vigorously twice during 15 min. Membrane was finally dried during 2h at 37ºC. Detection pad is placed between absorbent and detection pads (Fig. 5.8A(c)).

Once the strips were assembled, LFs were cut with a width of 6 mm.

5.3.2.5. Lateral flow immunoassay

Serial dilutions of H IgG were made in PBS (0.01 M, pH 7.4). The same buffer was used as blank. 200 µL of each solution, by triplicate, were dispensed on the sample pad of the LF strips and after 10 min the detection pads were photographed with a Moto Z mobile phone camera[39,43]. The images were later measured with ImageJ software[44-46]. TL were measured in grayscale obtaining a value from 0 to 255 (pure black and pure white, respectively); that value was normalized by applying the formula:

$$V_n = (1/V_o - 1/V_{low}) / (1/V_{high})$$

Where V_n is the normalized value (from 0 to 1; being 0 the signal corresponding to the less colored LFs and 1 the most colored one), V_o is the measured value from the LFs (from 0

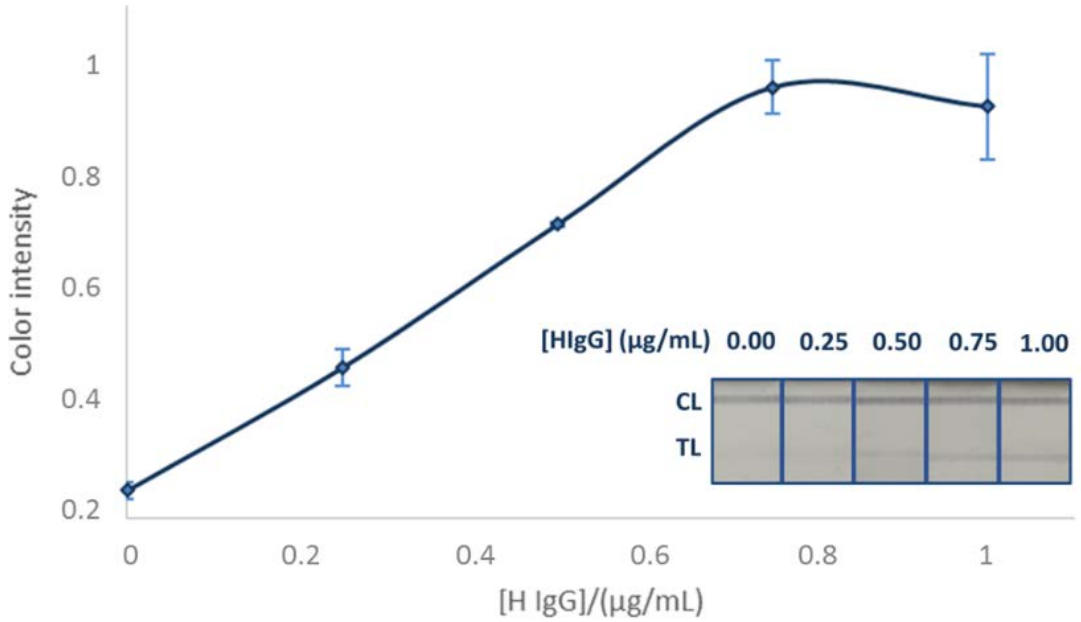

Fig. 5.9. Optical response of LFs to the concentration of HIgG. Inset of LFs detection pads.

to 255), V_{low} the whitest value (closest number to 255 among all the LF strips) and V_{high} the blackest (closest number to 0 among all LFs).

5.3.3. Results and discussion

H IgG was diluted to different concentrations: 0.25, 0.50, 0.75 and 1.00 µg/mL. The solutions and blank sample were applied on LFs. On Fig. 5.9 it is illustrated the measured intensities for each concentration and the images taken from different detection pads. At a concentration of H IgG over 0.75 µg/mL it is observed how the intensity is saturated; this effect is due an excess of analyte that is captured by all the antibodies linked to IrO_2 NPs and nitrocellulose TL, impeding the stopping of more IrO_2 NPs on that area. Thus, the working range was defined between 0 and 0.75 µg/mL and represented by the equation:

$$\textbf{color intensity} = 0.95\,[\text{H IgG}](\mu g/mL) + 0.24$$

The equation has an r value of 0.999. The method shows a reproducibility (RSD) of 3 % (n=3) for a H IgG concentration of 0.25 µg/mL. A limit of detection (LOD) (calculated from the calibration equation by substituting the “color intensity” value by the average signal of blank, 0.25 µg/mL, plus three times its standard deviation, 0.02 µg/mL) of 0.07 µg/mL is estimated.

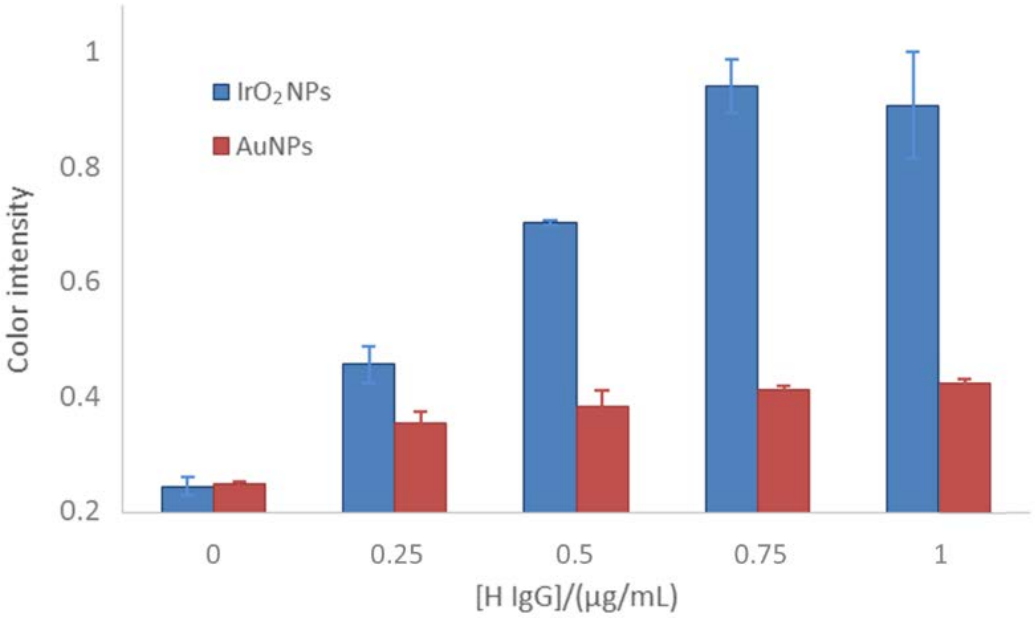

Fig. 5.10. Comparison of two LF tests, one using IrO_2 NPs as tags and the other Au NPs.

Gold nanoparticles (Au NPs) are commonly used on LF assays[41,47-49]. Comparing the results obtained from IrO_2 NPs LF test with a Au NPs LF test repeated under the same conditions and with the same reagents and antibodies (Fig. 5.10), IrO_2 NPs exhibit a higher intensity (2-fold at 1.00 µg/mL) when signal is captured by a smartphone. The dark blue color of IrO_2 NPs against the red color of AuNPs has a greater contrast in comparison with the white background of LF strips, which is an advantage for the adaptation to smartphone measurements, leaving aside tailor-made colorimetric readers (e.g. for AuNPs a colorimetric reader focused on 520 nm wavelength should be required).

5.3.4. Conclusions

We have demonstrated for the first time that IrO_2 NPs can be used on LF tests for the detection of a model protein, HIgG. Our test has exhibited good LOD (0.07 µg/mL) and sensitivity (twice the sensitivity of the classical Au NPs LF test) with a smartphone as recording tool, which makes our system an interesting tool in PoC diagnostics.

In future work, IrO_2 NPs could lead to the integration of other detection techniques on LF strips[24] as they are electrochemical measurements. It would be possible since IrO_2 NPs have demonstrated interesting electrocatalytical properties against water oxidation reaction even in buffer medium[2-6]; it would be an advantage in comparison to the currently reported

electrochemical LFBs in which the strips need to be treated with acid solutions in order to perform the measurements[50,51], thus adding extra steps to the system and damaging the strip.

5.4. Future perspectives

The objective of the two works reported in this section was to combine them obtaining LFs able to detect PBDE by both optical (semiquantitatively, with naked-eye) and electrochemical (fully quantitative) methods. However, it was an ambitious milestone not reached during this thesis due to the lack of time and probably tools and knowledge. The non-uniform surface of nitrocellulose hinders the integration of electrode inks on it (probably, this is one of the reasons why, as explained in chapter 1, many authors who reported the development of electrochemical LFs have to use acidic solutions dissolving the TL to make all the label particles or electrocatalytic reporters "drop" on the electrode).

We strongly believe that the integration of electrodes on nitrocellulose is possible and will continue this work in future projects. IrO_2 NPs do not need acidic solutions to catalyse the WOR, thus these nanoparticles may be used on a system in which the nitrocellulose does not need to be damaged (so, the strip can be read at the moment of the assay or later).

5.5. References

1. Harriman, A. & Thomas, J. M. Catalytic and structural properties of iridium-iridium dioxide colloids. *New J. Chem.* **11,** (1987).

2. Rivas, L.; de la Escosura-Muñiz, A.; Pons, J.; Merkoçi, A. Alzheimer Disease Biomarker Detection Through Electrocatalytic Water Oxidation Induced by Iridium Oxide Nanoparticles. *Electroanal.* **26**, 1287-1294 (2014).

3. Rivas, L., Mayorga-Martinez, C. C., Quesada-González, D., Zamora, A., de la Escosura-Muñiz, A., Merkoçi, A., Label-free Impedimetric Aptasensor for Ochratoxin-A Detection Using Iridium Oxide Nanoparticles. *Anal. Chem*. **87 (10)**, 5167–5172 (2015).

4. Mayorga-Martinez, C. C., Pino, F., Kurbanoglu, S., Rivas, L., Ozkan, S. A., Merkoçi, A. Iridium oxide nanoparticles induced dual catalytic/inhibition based detection of phenol and pesticide compounds. *J. Mater. Chem. B* **2**, 2233-2239 (2014).

5. Mayorga-Martinez, C. C., Chamorro-García, A., Serrano, L., Rivas, L., Quesada-González, D., Altet, L., Francino, O., Sánchez, A., Merkoçi, A. An iridium oxide nanoparticle and polythionine thin film based platform for sensitive Leishmania DNA detection. *J. Mater. Chem. B* **3**, 5166—5171 (2015).

6. Kurbanoglu, S., Rivas, L., Ozkan, S. A., Merkoçi, A. Electrochemically reduced graphene and iridium oxide nanoparticles for inhibition-based angiotensin-converting enzyme inhibitor detection. *Biosens. Bioelectron.* **88**, 122-129 (2017).

7. NOAA (National Oceanic and Atmospheric Administration), U.S. Department of Commerce, What are PBDEs? Webpage: https://oceanservice.noaa.gov/facts/pbde.html (last accessed: 24/02/2018).

8. *Chem. Eng. News* **49 (43)**, 16–19 (1971), DOI: 10.1021/cen-v049n043.p016

9. Guo, W., Holden, A., Smith, S. C., Gephart, R., Petreas, M., Park, J. S., PBDE levels in breast milk are decreasing in California . *Chemosphere* **150**, 505-513 (2016).

10. Linares, V., Bellés, M., Domingo, J. L., Human exposure to PBDE and critical evaluation of health hazards. *Arch. Toxicol*. **89**, 335–356 (2015).

11. The Stockholm Convention, 2009. Webpage: http://chm.pops.int/TheConvention/Overview/TextoftheConvention/tabid/2232/Default.aspx#LiveContent[convtext] (last accessed: 24/06/2018).

12. Ward, J., Mohapatra, S. P., Mitchell, A. An overview of policies for managing polybrominated diphenyl ethers (PBDEs) in the Great Lakes basin. *Environ. Int.* **34**, 1148–1156 (2008).

13. Hooper, K., McDonald, T. A., The PBDEs: an emerging environmental challenge and another reason for breast-milk monitoring programs. *Environ. Health Perspect*. **100 (5)**, 387-392 (2000).

14. Darnerud, P. O., Eriksen, G. S., Jóhannesson, T., Larsen, P. B., Viluksela, M., Polybrominated diphenyl ethers: occurrence, dietary exposure, and toxicology. *Environ. Health Perspect.* **109 (1)**, 49-68 (2001).

15. Stapleton, H. M., Sjödin, A., Jones, R. S., Niehüser, S., Zhang, Y., Patterson Jr., D. G., Serum Levels of Polybrominated Diphenyl Ethers (PBDEs) in Foam Recyclers and Carpet Installers Working in the United States. *Environ. Sci. Technol*. **42**, 3453–3458 (2008).

16. Butryn, D., Gross, M., Chi, L. H., Schecter, A., Olson, J., Aga, D., "One-shot" analysis of polybrominated diphenyl ethers and their hydroxylated and methoxylated analogs in human breast milk and serum using gas chromatography-tandem mass spectrometry. *Anal. Chim. Acta* **892**, 140–147 (2015).

17. Chałupniak, A., Merkoçi, A., Toward integrated detection and graphene-based removal of contaminants in a lab-on-a-chip platform. *Nano Res.* **10 (7)**, 2296–2310 (2017).

18. Ahn, K. C., Gee, S. J., Tsai, H. J., Bennett, D., Nishioka, M. G., Blum, A., Fishman E., Hammock, B. D., Immunoassay for Monitoring Environmental and Human Exposure to the Polybrominated Diphenyl Ether BDE-47. *Environ. Sci. Technol*. **43**, 7784–7790 (2009).

19. Li, W., Sheng, P., Cai, J., Feng, H., Cai, Q. Highly sensitive and selective photoelectrochemical biosensor platform for polybrominated diphenyl ether detection using the quantum dots sensitized three-dimensional, macroporous ZnO nanosheet photoelectrode. *Biosens. Bioelectron*. **61**, 209–214 (2014).

20. Abraxis PBDE ELISA Kit. Webpage:

http://www.abraxiskits.com/moreinfo/PN500090info.pdf (last accessed: 24/06/2018)

21. Riley, D. J. Electrochemistry in nanoparticle science. *Curr. Opin. Colloid Interface Sci.* **7**, 186-192 (2002).

22. De la Escosura-Muñiz, A., Merkoçi, A., Electrochemical detection of proteins using nanoparticles: applications to diagnostics. *Expert Opin. Med. Diagn*. **4,** 21-37 (2010).

23. De la Escosura-Muñiz, A., Merkoçi, A., Nanoparticles for Proteins and Cells Detection. Novel Tools for Clinical Diagnostics. *G.I.T. Laboratory Journal Europe* **16**, 21-23 (2012).

24. Quesada-González, D.; Merkoçi, A. Nanoparticle-Based Lateral Flow Biosensors. *Biosens. Bioelectron*. **73**, 47–63 (2015).

25. Quesada-González, D.; Merkoçi, A. Nanomaterial-Based Devices for Point-of-Care Diagnostic Applications. *Chem. Soc. Rev*. **47**, 4697–4709 (2018).

26. Robbs and Rees, Nanoparticle electrochemistry. *Phys. Chem. Chem. Phys*. **18**, 24812-24819 (2016).

27. Arduini, F., Zanardi, C., Cinti, S., Terzi, F., Moscone, D., Palleschi, G., Seeber, R. Effective electrochemical sensor based on screen-printed electrodes modified with a carbon black-Au nanoparticles composite. *Sens. Actuators B Chem.* **212**, 536-543 (2015).

28. De la Escosura-Muñiz, A., Parolo, C., Maran, F., Merkoçi, A. Size-dependent direct electrochemical detection of gold nanoparticles: application in magnetoimmunoassays. *Nanoscale* **3**, 3350-3356 (2011).

29. De la Escosura-Muñiz, A., Baptista-Pires, L., Serrano, L., Altet, L., Francino, O., Sánchez, A., Merkoçi, A. Magnetic Bead/Gold Nanoparticle Double-Labeled Primers for Electrochemical Detection of Isothermal Amplified Leishmania DNA. *Small* **12 (2)**, 205–213 (2016).

30. Parolo, C., Medina-Sánchez, M., Montón, H., de la Escosura-Muñiz, A., Merkoçi., A. Paper-Based Electrodes for Nanoparticle Detection. *Part. Part. Syst. Char.* **30(8)**, 662–666 (2013).

31. Talarico, D., Cinti, S., Arduini, F., Amine, A., Moscone, D., Palleschi, G. Phosphate Detection through a Cost-Effective Carbon Black Nanoparticle-Modified Screen-Printed Electrode Embedded in a Continuous Flow System. *Environ. Sci. Technol.* **49 (13)**, 7934–7939 (2015).

32. Talarico, D., Arduini, F., Amine, A., Moscone, D., Palleschi, G. Screen-printed electrode modified with carbon black nanoparticles for phosphate detection by measuring the electroactive phosphomolybdate complex. *Talanta* **15**, 267-272 (2015).

33. Wang, J., Tian, B., Nascimento, V. B., Angnes, L., Performance of screen-printed carbon electrodes fabricated from different carbon inks. *Electrochimica Acta* **43 (23)**, 3459-3465 (1998).

34. Dědík, J., Janovcová, M., Dejmková, H., Barek, J., Pecková, K., Utilization of unmodified screen-printed carbon electrodes in electroanalysis of organic compounds (an overview). *Sensing in Electroanal.* **6**, 129-138 (2011).

35. Cui, R., Huang, H., Yin, Z., Gao, D., Zhu, J. J. Horseradish peroxidase-functionalized gold nanoparticle label for amplified immunoanalysis based on gold nanoparticles/carbon nanotubes hybrids modified biosensor. *Biosens. Bioelectron*. **23 (11)**, 1666-1673 (2008).

36. Mohamed, S. A., Al-Harbi, M. H., Almulaiky. Y. Q., Ibrahim, H. I., El-Shishtawy, R. M. Immobilization of horseradish peroxidase on Fe3O4 magnetic nanoparticles. *Electron. J. Biotechnol*. **27**, 84-90 (2017).

37. Thielbeer, F., Donaldson, K., Bradley, M. Zeta Potential Mediated Reaction Monitoring on Nano and Microparticles. *Bioconjugate Chem*. **22**, 144–150 (2011).

38. Hayashi, Y., Matsuda, R., Maitani, T. Precision, Limit of Detection and Range of Quantitation in Competitive ELISA. *Anal. Chem*. **76**, 1295-1301 (2004).

39. Quesada-González, D. & Merkoçi, A. Mobile phone–based biosensing: an emerging 'diagnostic and communication' technology. *Biosens. Bioelectron.* **92,** 549–562 (2016).

40. Finkelstein-Shapiro, D., Fournier, M., Méndez-Hernández, D. D., Guo, C., Calatayud, M., Moore, T. A., Moore, A. L., Gust, D., Yarger, J. L. Understanding iridium oxide nanoparticle surface sites by their interaction with catechol. *Phys. Chem. Chem. Phys*. **19**, 16151-16158 (2017).

41. Parolo, C., Medina-Sánchez, M, de la Escosura-Muñiz, A., Merkoçi, A. Simple paper architecture modifications lead to enhanced sensitivity in nanoparticle based lateral flow immunoassays. *Lab Chip* **13**, 386-390 (2013).

42. Rivas, L., Medina-Sánchez, M., de la Escosura-Muñiz, A. & Merkoçi, A. Improving sensitivity of gold nanoparticle-based lateral flow assays by using wax-printed pillars as delay barriers of microfluidics. *Lab Chip* **14,** 4406–14 (2014).

43. Ozcan, A. Mobile phones democratize and cultivate next-generation imaging, diagnostics and measurement tools. *Lab Chip* **14**, 3187-3194 (2014).

44. Álvarez-Diduk, R., Orozco, J., Merkoçi, A. Paper strip-embedded graphene quantum dots: a screening device with a smartphone readout. *Sci. Rep*. **7**, 976 (2017).

45. Roda, A., Michelini, E., Cevenini, L., Calabria, D., Calabretta, M. M., Simoni, P. Integrating biochemiluminescence detection on smartphones: mobile chemistry platform for point-of-need analysis. *Anal. Chem*. **86**, 7299−7304 (2014).

46. Kühnemund, M., Wei, Q., Darai, E., Wang, Y., Hernández-Neuta, I., Yang, Z., Tseng, D., Ahlford, A., Mathot, L., Sjöblom, T., Ozcan, A., Nilsson, M., Targeted DNA sequencing and in situ mutation analysis using mobile phone microscopy. *Nat. Commun.* **8**, 13913 (2017).

47. Shyu, R. H., Shyu, H. F., Liu, H. W. & Tang, S. S. Colloidal gold-based immunochromatographic assay for detection of ricin. *Toxicon* **40,** 255–258 (2001).

48. Oh, J. S., Ha, G. W., Cho, Y. S., Kim, M. J., An, D. J., Hwang, K. K., Lim, Y. K., Park, B. K., Kang, B. K., Song, D. S. One-Step Immunochromatography Assay Kit for Detecting Antibodies to Canine Parvovirus One-Step Immunochromatography Assay Kit for Detecting Antibodies to Canine Parvovirus. *Clin. Vaccine Immunol.* **13**, 520–524 (2006).

49. Karakus, C. Development of A Lateral Flow Immunoassay Strip for Rapid Detection of CagA Antigen of Helicobacter pylori. *J. Immunoassay Immunochem*. **36**, 324–333 (2015).

50. Inoue, K., Ferrante, P., Hirano, Y., Yasukawa, T., Shiku, H., Matsue, T. A competitive immunochromatographic assay for testosterone based on electrochemical detection. Talanta 73, 886–892 (2007).

51. Wicaksono, W. P., Putri, A. P. Electrochemical Immunochromatographic Strip Test for Melamine Biosensor in Milk Products Using Silver Nanoparticles as Probe. *Applied Mech. Mater*. **490**, 1624-1628 (2014).

GENERAL CONCLUSIONS

Considering the exposed objectives in Chapter 2 and the specific conclusions given at the end of each chapter, the following conclusion remarks are given:

- LFs for the detection of U(VI) ions in groundwater were developed.
    - LFs exhibited a LOD of 6 nM in buffer medium and 36 nM in pre-treated environmental samples, both lower than 126 nM, the maximum concentration of U(VI) recommended for consume water in the US.
    - LFs were fabricated and tested in Spain and then sent to USA where, after one month, strips were tested again in buffer by a different user, obtaining a similar calibration plot as when the strips were just-made. It demonstrates the robustness and the reproducibility of the device.
    - The behaviour of LFs against real samples was acceptable. We strongly believe that the proposed system may be used as substitute of current methods after a larger statistical evaluation.
    - As future perspectives, it would be worth it the evaluation of the addition of an extra pad including the necessary reagents for real sample pre-treatment (e.g. Ca^{2+} ions capture, which can interfere in LFs response).
- The integration of cellulose nanofibers successfully allowed a signal increase on LFs of around 36.6%.
    - Although cellulose nanofibers are not clearly visible on SEM and AFM images, the AuNPs population increase demonstrates the presence and effect of them.
    - Combination of microscopic Blips Lenses on mobile phones eases and increases the reproducibility of TL imaging.
    - As future perspectives, we consider that this enhancement strategy is simple and facile to apply, so it could be integrated in future works and collaborations in which the sensitivity needs a boost.
- PBDE can be indirectly quantified by the electrocatalytic detection of IrO_2 NPs on SPCEs.

- A LOD of 21.5 ppb in buffer medium was achieved.
- Furthermore, IrO_2 NPs work on LFs with a similar performance to AuNP-based LFs. If the reader doesn't have a fixed wavelength detector, the contrast between the TL and the background is stronger with IrO_2 NPs (twice in comparison to AuNPs).
- As future work, strategies to integrate electrodes into LFs will be evaluated and the use of IrO_2 NPs will be further considered given their electrocatalytic properties able to be revealed even in saline medium.

- LFs have demonstrated to be a versatile type of biosensor. Currently mostly applied in development countries where resources are scarce, these tools may be of worldwide interest, to diagnose many types of disorders, check the potability of water, allergens detection, monitor chronic diseases, etc. Either in the hospital, in the field or at home.

ANNEXES

As annexes are attached the 3 following published review works:

Quesada-González, D. & Merkoçi, A. "Nanoparticle-based lateral flow biosensors". *Biosens. Bioelectron.* **73,** 47–63 (2015).

Quesada-González, D. & Merkoçi, A. "Mobile phone–based biosensing: an emerging 'diagnostic and communication' technology". *Biosens. Bioelectron.* **92,** 549–562 (2016).

Quesada-González, D. & Merkoçi, A. "Nanomaterial-Based Devices for Point-of-Care Diagnostic Applications". *Chem. Soc. Rev.* **47**, 4697–4709 (2018).

Also the following posters presented at different congresses:

Rivas, L., Mayorga-Martinez, C. C., Quesada-González, D., Zamora-Gálvez, A., de la Escosura-Muñiz, A. & Merkoçi, A. "Label-free impedimetric aptasensor for Ochratoxin‑A detection using Iridium Oxide nanoparticles" – Presented at: *Transfronterier Meeting on Sensors and Biosensors*, Perpignan (2015). And also at *International Congress of Biosensors,* Ankara (2016).

Quesada-González, D. & Merkoçi, A. "Nanotechnology-based lateral flow biosensors" – Presented at: *VII Jornades Doctorals de Química,* Bellaterra (2017).

Quesada-González, D., Baiocco, A., Martos, A. A., de la Escosura-Muñiz, A., Palleschi, A. & Merkoçi, A. "Nanoparticle-based electrocatalytic detection of PBDE in sea water" – Presented at: *Biosensors Congress*: Miami (2018).

Quesada-González, D., Sena-Torralba, A., Wicaksono, W. P., de la Escosura-Muñiz, A., Ivandini, T. A. & Merkoçi, A. "Iridium oxide nanoparticle-based lateral flow immunoassay" – Presented at: *Biosensors Congress*: Miami (2018).

Biosensors and Bioelectronics 73 (2015) 47–63

Contents lists available at ScienceDirect

Biosensors and Bioelectronics

journal homepage: www.elsevier.com/locate/bios

Nanoparticle-based lateral flow biosensors

Daniel Quesada-González [a], Arben Merkoçi [a,b,*]

[a] Nanobioelectronics & Biosensors Group, Institut Català de Nanociència i Nanotecnologia (ICN2), Campus UAB, 08193 Bellaterra, Barcelona, Spain
[b] ICREA, Institució Catalana de Recerca i Estudis Avançats, Barcelona 08010, Spain

ARTICLE INFO

Article history:
Received 23 April 2015
Received in revised form
15 May 2015
Accepted 22 May 2015
Available online 25 May 2015

Keywords:
Lateral flow
Nanoparticle
Optical detection
Electrochemical detection
Immunoassay

ABSTRACT

Lateral flow biosensors (LFBs) are paper-based devices which permit the performance of low-cost and fast diagnostics with good robustness, specificity, sensitivity and low limits of detection. The use of nanoparticles (NPs) as labels play an important role in the design and fabrication of a lateral flow strip (LFS). The choice of NPs and the corresponding detection method directly affect the performance of these devices. This review discusses aspects related to the application of different nanomaterials (e.g. gold nanoparticles, carbon nanotubes, quantum dots, up-converting phosphor technologies, and latex beads, between others) in LFBs. Moreover, different detection methods (colorimetric, fluorescent, electrochemical, magnetic, etc.) and signal enhancement strategies (affording secondary reactions or modifying the architecture of the LFS) as well as the use of devices such as smartphones to mediate the response of LFSs will be analyzed.

Contents

Abbreviations: AEC, 3-amino-9-ethylcarbazole; AuNPs, gold nanoparticles; CL, control line; CNPs, carbon nanoparticles; CNTs, carbon nanotubes; GMR, giant magnetoresistive sensor; HRP, horseradish peroxidase; IAs, immunochromatographic assays; LBs, latex beads; LFBs, lateral flow biosensors; LFS, lateral flow strip; MAR, magnetic assay readers; MNPs, magnetite nanoparticles; OVA, ovalbumin; TL, test line; TMB, 3,3′,5,5′-tetramethylbenzidine; QDs, quantum dots; QR, quick response code; SERS, surface-enhanced Raman scattering; UPTs, up-converting phosphor technologies

* Corresponding author at: Nanobioelectronics & Biosensors Group, Institut Català de Nanociència i Nanotecnologia (ICN2), Campus UAB, 08193 Bellaterra, Barcelona, Spain.
E-mail address: arben.merkoci@icn.cat (A. Merkoçi).

http://dx.doi.org/10.1016/j.bios.2015.05.050
0956-5663/

1. Introduction

Nowadays biosensors are very helpful tools in our everyday life, being used for the detection of allergens in food, toxicants in water, in chronic diseases control, pregnancy tests and other diagnostic applications. Certainly, it can be ensured that biosensors are going to enter even deeper in our life in the future, so it is a research field looking for new and improved easy-to-be-used device technologies.

Since the appearance of the first biosensor (Clark et al., 1953), the technology has evolved, but it is still not crowned with the expected devices that would work as easily as a glucose biosensor or a pregnancy test, present in any pharmacy all over the world. Low cost and efficient devices for the detection of other analytes such as DNA, proteins or even whole cells in real scenarios are still in the way.

One of the possible paths that the researchers could take to reach to this future is the development of paper-based biosensors, following the same principle as the immunochromatographic assays (IAs) (Lou et al., 1993; Cho and Paek, 2001; Lönnberg and Carlsson, 2001; Ho and Wauchope, 2002; Shyu et al., 2002): the separation of analytes which flow across a porous medium taking into account the specific interactions that occur between antigen and antibody, enzyme and substrate, or receptor and ligand. Paper is a simple, cheap, abundant and an easy-to-manufacture material that fulfils cost/efficient requirements in biosensing technology (Costa et al., 2014). It is noteworthy that it is in developing countries where this type of biosensors are more requested due to the lack of resources to use conventional laboratory tools which are more expensive and require trained operators, huge amount of equipment and installations, so the development of paper-based devices could be of vital importance in these regions.

Paper, this mere material made from cellulose (the most abundant polymer on Earth) or nitrocellulose, offers many others advantages in the development of biosensors. Various biochemical reactions with interest for biosensing applications can easily be carried out within this matrix. In addition, simple microfluidics including platform architectures tuning can be applied thanks to the controlled porosity and capillary forces of the nitrocellulose network in addition to simple modification or integration processes. Moreover paper-based platforms are compatible with either naked eye detection or simple optical or electrical readers.

1.1. Lateral flow biosensors (LFBs)

The aim of this review is to discuss and analyze the current advances concerning the class of paper-based biosensors, called lateral flow biosensors (LFBs), which are the modern version of paper IAs (Parolo and Merkoçi, 2013). These devices may fit all the requirements expected from a biosensor: low limit of detection, high sensitivity, good selectivity, low quantity of sample volume required, no washing steps are necessary, robustness, low cost, quick assay performance in just one step and a user-friendly format. Nevertheless LFBs also have some weaknesses, such as the fact that the response obtained with naked-eye is just qualitative, not quantitative, although with the help of certain reading devices it can be converted into semiquantitative. Another drawback is that the sample must be always in liquid state, with enough viscosity to flow across the porous of the nitrocellulose. These pores, in some cases, could be obstructed by different matrix compounds and provoke unspecific adsorptions in the membrane; it is in those cases when a sample pretreatment or predilution will be required. Because of the limitation of the detection area, the surface where receptors (e.g. antibodies, enzymes, proteins, etc.) are placed, at higher concentrations of analyte, can be oversaturated, giving false blank response; it is another factor to consider making the predilution of the sample before the analysis.

LFBs can be used to detect a large range of biomarkers that may include not only proteins but also nucleic acids and even whole cells, among other biocompounds. Furthermore, LFBs are not limited only to biomolecules detection; several publications have appeared in the last years about the detection of pollutants such as metallic ions, pesticides, etc. The range of LFBs applications is including detection of hazardous substances (Shyu et al., 2002), heavy metals in drinking waters (Mazumdar et al., 2010; Torabi and Lu, 2011; Kuang et al., 2013; López-Marzo et al., 2013a, 2013b), allergens and pathogens in food (Wang et al., 2007; Shukla et al., 2011; Preechakasedkit et al., 2012; Leem et al., 2014; Berlina et al., 2013; Anfossi et al., 2012, 2013), pesticides (Zhou et al., 2004; Kim et al., 2011; Wang et al., 2014a), drugs screening (Inoue et al., 2007), etc.

There exist different commercial LFBs (Cazacu et al., 2004; Held et al., 2013), being pregnancy and fertility tests the most known examples beside tests for HIV (Pesce et al., 2006), drugs of abuse, Malaria (Cordray and Richards-Kortum, 2012; He et al., 2014; Kersting et al., 2014), etc. Behind LFBs there is a well-known technology (Qian and Bau, 2003, 2004; Assadollahi et al., 2009; Lee et al., 2012; Linares et al., 2012) with several publications reporting different modifications of the standard designs/structure, either in terms of the materials used as transducers for the signal generation (Linares et al., 2012), in the methodology employed to translate the signal or in improving the device with different enhancement strategies.

With the recent development and explorations of nanomaterials in the field of sensors and biosensors LFBs have been taking advantages for their use as alternative materials to improve their performance requested in real sample applications. Application of nanomaterials in DNA, protein, cell and various inorganic/organic compounds in various biosensing technologies is now being extended to LFB field bringing interesting results to this technology (Walcarius et al., 2013; Merkoçi, 2010; De la Escosura-Muñiz et al., 2010, Parolo et al., 2013a; Perfezou et al., 2012; Aragay et al., 2011, 2012).

1.2. How lateral flow strips (LFS) work?

LFBs are manufactured in strip form, a convenient format for the user, normally with a width between 4 and 6 mm and a length no more than 6–7 cm. A standard lateral flow strip (LFS) consists of four main sections made of different materials, as shown in Fig. 1: sample pad, made of cellulose, where the sample is dropped; conjugate pad, made of glass fiber, impregnated with the bioconjugates solution (the label particle and a receptor for the analyte); detection pad, a nitrocellulose sheet (Lee et al., 2012; Ahmad et al., 2009) where test line (TL) and control line (CL) are printed; and absorption pad, also made of cellulose. Other

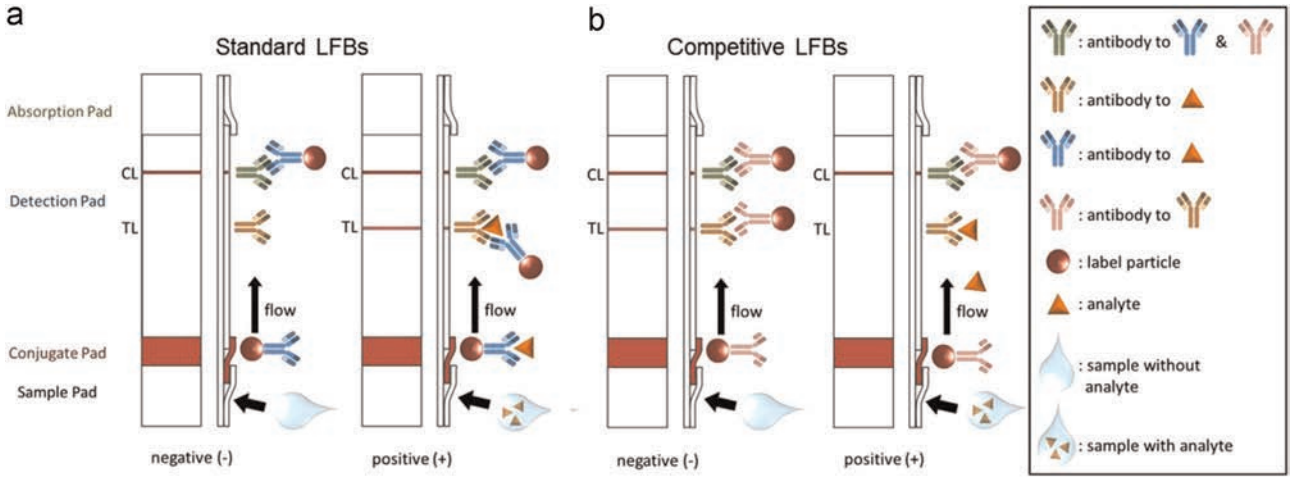

Fig. 1. Schematic representation of the different parts of a LFS (lateral flow strip) and movement of analytes and label particles across it with (a) standard and (b) competitive designs.

additional parts can be integrated on LFS as blood filters, substituting the sample pad, to retain big particles like red blood cells and avoiding their hemolysis. Another example of material which can be integrated on LFS is carbon nanotubes paper, with high conductive properties to connect LFS to electronic devices (Zhu et al., 2014).

The performance of an assay with a LFS is quite simple: the sample is added on the sample pad and then the liquid will start flowing to the conjugate pad where the analyte, if present on the sample, will be linked to the transducers (the label particles), previously conjugated with a bioreceptor specific to the analyte. The conjugate, rehydrated by the liquid, will flow by capillarity forces across the detection pad to the absorbent pad, passing through the TL, where it will be captured only if the conjugate has the analyte attached (positive response), and to the CL, being always captured, evidencing that the assay works. This design corresponds to a standard model of LFS (Fig. 1a), but there exists also the competitive model (Fig. 1b) in which the analyte and the transducers compete for being captured on TL, obtaining a response inversely proportional to the concentration of analyte.

2. Optical detection

Although a large variety of strategies to read the LFSs signal have been reported the optical methods remain the most explored because of their simplicity (even naked eye detection) and effectiveness (high sensitivity). Several types of nanomaterials can be used as colorimetric labels on LFBs conjugated with different kinds of bioreceptors (antibodies, aptamers, DNA, etc.). In the following sections we will revise the most relevant technological and analytical aspects related to the application of LFS labels such as gold nanoparticles (AuNPs), quantum dots (QDs), carbon nanotubes (CNTs), carbon nanoparticles (CNTs), liposomes, between others.

2.1. Gold nanoparticles (AuNPs)

AuNPs are easy to synthesize and manipulate, stable in time, size-tunable, biocompatible and have an intense red color easy to be detected even by naked eye or usually using color readers to achieve better detection limits. Because of these properties, AuNPs are the most reported nanomaterial used as optical label in LFSs.

2.1.1. Design and applications of LFSs with AuNPs

One of the first examples of the use of AuNPs as labels on LFSs was reported by Shyu et al. (2002) for the detection of ricin. On this LFS, without conjugate pad neither sample pad, anti-ricin antibody conjugated AuNPs were deposited over nitrocellulose membrane near the bottom of the strip.

A few years later, the number of reports about LFBs increased and the design evolved including a pad, made of glass fiber, for the AuNPs suspension (Oh et al., 2006). Also, besides antibodies, other biocompounds like aptamers (Liu et al., 2006; C. Liu et al., 2009; G. Liu et al., 2009; Xu et al., 2009) and DNA probes (Mao et al., 2009; He et al., 2012; Rohrman et al., 2012; Lie et al., 2012; Kolm et al., 2015) were conjugated with AuNPs. Xu et al. (2009) designed a LFS

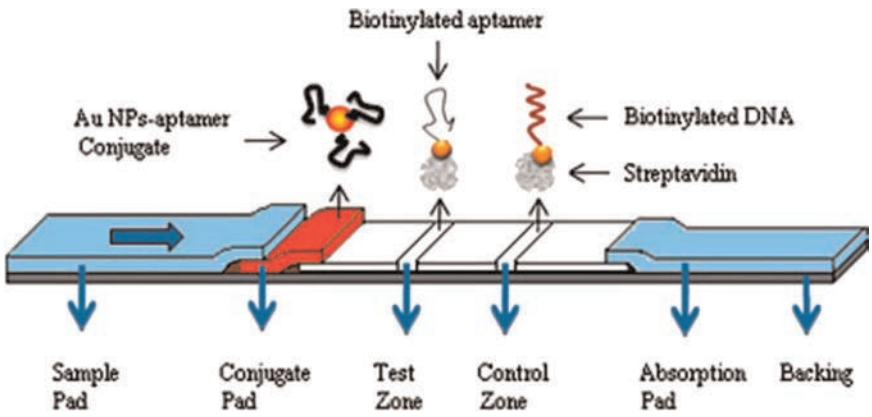

Fig. 2. LFS with aptamers conjugated AuNPs. Reprinted with permission from Xu et al. (2009), Copyright 2009 American Chemical Society.

with AuNP–aptamer conjugate as label (Fig. 2) for the detection of thrombin. The system demonstrates that the use of the thrombin aptamer exhibits a high sensitivity, comparable or even superior to the systems which use antibodies. The experiment shows that the color intensity of AuNPs can be detected up to a concentration of analyte of 0.6 pM in diluted plasma samples being this value lower than in antibody-based assays (Shyu et al., 2002; Oh et al., 2006; Karakus, 2015), without detecting any unspecific adsorption, that evidences the good selectivity of aptamers combined with AuNPs.

It was also demonstrated that AuNPs can be used not only for biocompounds detection (Karakus, 2015); toxins (Anfossi et al., 2012, 2013; B.H. Liu et al., 2014; C. Liu et al., 2014) and metallic cations (Mazumdar et al., 2010; Torabi and Lu, 2011; Kuang et al., 2013; López-Marzo et al., 2013a, 2013b; Fang et al., 2010) also can be detected using several strategies. In the case of the work of Fang et al. (2010), Cu^{2+} ions can be detected taking advantage of the cleavage that cooper causes, in presence of ascorbate, on Cu^{2+}-specific-DNAzymes (linked to AuNPs) which, if broken, will be captured on TL. This strategy grants a good selectivity against other metallic ions, but the limit of detection does not reach the levels achieved in the detection of antigens. An alternative high sensitive strategy to detect metallic ions consists on the use of antibodies specific to a metal–ligand complex but not to the free metal. The metal–ligand complex competes for being hooked on the test line with the same complex but already linked to AuNPs, thereby obtaining a competitive format of LFSs. This strategy is based on López-Marzo et al.'s (2013a) work to detect Cd^{2+} ions using EDTA as ligand. The system, nevertheless, is shown to have some problems of unspecificity to some metals; however it can be solved reducing the concentration of the ligand but also adding extra conjugation pad that ensures Cd^{2+} complexation with EDTA and interference masking through ovalbumin (OVA) (López-Marzo et al., 2013b; to be discussed in Section 2.1.2.2).

In some cases, multidetection of analytes could be required, so it would be necessary to use various nanoparticles easy to be concentrated so as to achieve an intense color. Hereby, AuNPs are a good choice to develop multidetection LFSs (Elenis et al., 2011; Y.K. Wang et al., 2013; Song et al., 2014; Kim et al., 2014). These LFSs could replace ELISA assays, which are time-consuming and expensive, as was demonstrated by the work of Song et al. (2014), developed to detect different mycotoxins at the same time (Fig. 3). Their work, additionally, demonstrates that LFSs, besides the qualitative response, permit the quantitative interpretation of the signal by means of a colorimetric reader. The quantitative response can be represented as relative optical density (the ratio in percentage between the signal of a positive sample and the blank). This data can be used to construct a calibration curve of the measuring system.

The work of Chen et al. (2012) and Huang et al. (2014) reveals another interesting application of AuNPs on LFSs, the development of logic gates systems. AuNPs can afford more than one biocompound conjugated on their surface, therefore a LFS could easily detect the presence of various analytes on the same line ("OR" logic gate: the LFS will mark positive signaling in the presence of any of the analytes). Also the signal can indicate only the presence of both analytes at the same time (Chen et al., 2012) ("AND" logic gate: the signal on TL will only appear if both analytes are present). Huang et al.'s (2014) system can also detect the presence of a single analyte in a system where the analytes are inhibited by each other ("INH" logic gate: the LFS will mark positive signaling in the presence of only one of the analytes, but not if both are present in the sample at the same time).

2.1.2. *Enhancement strategies*

Although LFBs with AuNPs have demonstrated to have good sensitivity and low limits of detection, there are cases when it is necessary to achieve better performance. Different enhancement strategies with potential to significantly improve LFSs devices have

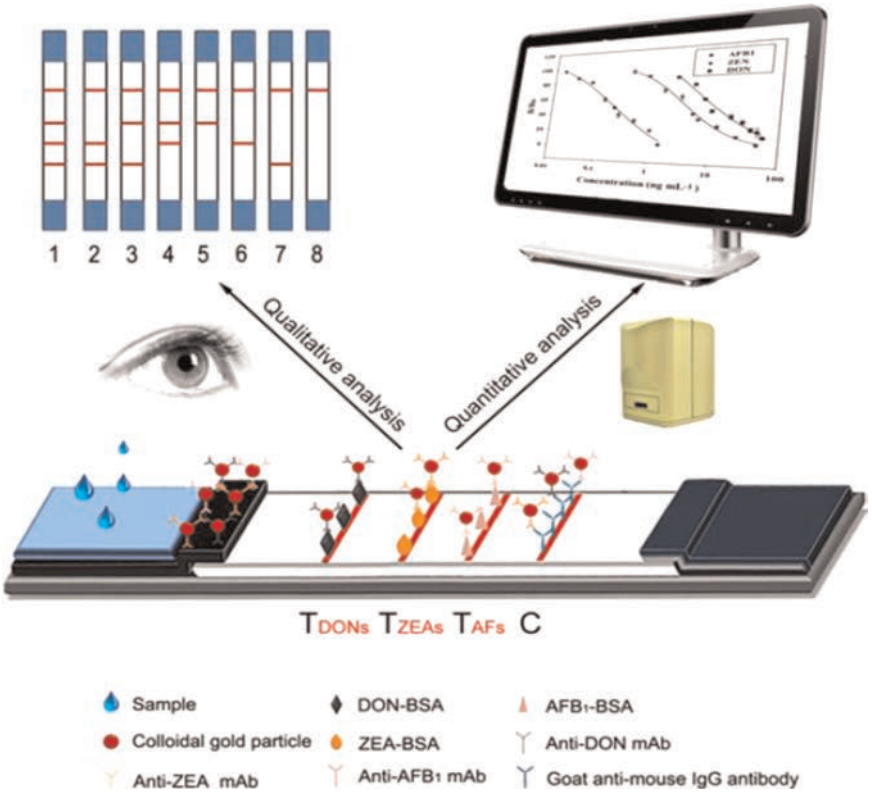

Fig. 3. LFS for the multidetection of different mycotoxins. Qualitative (left) and quantitative (right) response. Reprinted with permission from Song et al. (2014), Copyright 2014 American Chemical Society.

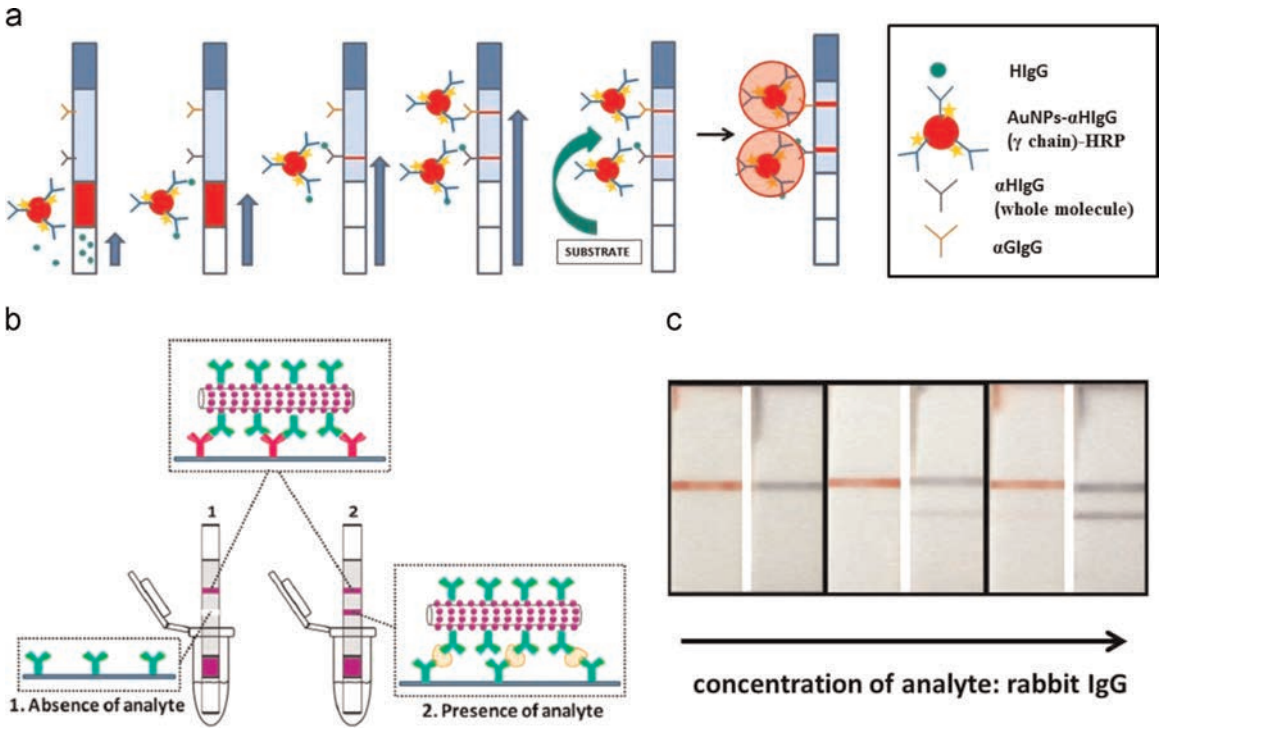

Fig. 4. (a) Signal enhancement strategy on LFS by means of enzymatic reactions. Adapted with permission from Parolo et al. (2013b), Copyright 2013 Elsevier. (b) AuNPs carried on silica nanorods: design and performance of the LFBs assay and (c) comparison of results with standard AuNPs labels (left strips) and silica nanorods decorated with AuNPs (right strips). Adapted with permission from Xu et al. (2014), Copyright 2014 American Chemical Society.

been reported. These strategies can be based on chemical methods, like the modifications of the label's surface (the AuNPs) to afford secondary reactions or attachments, or in altering the physical properties of the device (flow movement, speed, etc.) by modifying the design/architecture.

2.1.2.1. Modification of the labels. One of the strategies used to amplify the signal on TL and CL is to surround AuNPs with other compounds which enhance the color by means of enzymatic reactions (Fig. 4a), as the reaction occurring between HRP (horseradish peroxidase) and some chromogenic substrates (Mao et al., 2009; He et al., 2011; Parolo et al., 2013b), such as AEC (3-amino-9-ethylcarbazole) or TMB (3,3′,5,5′-tetramethylbenzidine). AEC mixed with H_2O_2 is used to provide color enhancement (and consequently, higher sensitivity) on HRP catalyzed reactions. Nevertheless it is when using TMB that the quantification limit is further decreased due to the fact that this substrate grants higher contrast between the lines and the background than the AEC. The reported detection limit of these enhancement strategies can reach up to 200 pg/mL (Parolo et al., 2013b).

Although enzymatic reactions exhibit low limit of detection and good sensitivity, the short stability of the reagents and the long conjugate development and testing times are drawbacks to consider. The amplification method proposed by Rastogi et al. (2012) by means of gold deposition over the strip after the assay solves the problem of reagents stability and seems to increase the signal effectively at low concentrations, but at higher concentrations, when detection lines are already saturated, the signal enhancement is slight. Fridley et al. (2012) studied the release of dry reagents stored in porous media (rehydrated afterwards) and demonstrated that this strategy could be used to enhance up to four times the intensity of AuNPs (previously deposited on the strip). This strategy, if developed on a real assay (with AuNPs and analyte flowing) could lessen the testing time in comparison with the methods in which amplification is performed after the assay. However, it is important to be taken into account the properties of the reagents to be stored on the membrane, their stability once dried and their potential as signal enhancers after rehydration.

Another interesting work was reported by Li et al. (2012). Taking advantage of the quenching effect of gold ions on QDs, they dissolved the AuNPs captured on TL using HCl–Br_2 mixed solution and, in a 96-well microplate, they measured the fluorescence of QDs. The method provides a good sensitivity, a wide working range and a fairly low limit of detection (90 pg/mL). Despite these advantages, the procedure is long and difficult to execute on field since it requires treating of the strips, fluorescence equipment to read the 96-well microplate and trained personnel. Instead of solving the AuNPs, Shi et al. (2015a) developed a system which allowed fluorescence quenching measurements without the need of dissolving the nanoparticles; they dispensed fluorescent polymer dots of 50 nm on the TL and CL and observed how the fluorescence decreased with the increase of concentration of AuNPs, which competed against the analyte. The detection limit of their method reached the 160 pg/mL. As an alternative to fluorescence detection, silver deposition onto AuNPs could be used to enhance the colorimetric response, turning into black the color of TL and CL (Anfossi et al., 2013). This strategy not necessary requires the use of colorimetric reader, if only qualitative assay is needed, but the detection limits achieved are not as low as when using QDs and fluorescence.

Recently, Xu et al. (2014) developed LFS in which, as labels, AuNPs were loaded over silica nanorods surface (Fig. 4b), raising quite a lot the sensitivity of the method due to the increase of AuNPs density over detection lines (Fig. 4c). The detection limit is also improved, in comparison to the previous mentioned strategies, being 10 pg/mL the estimated value. Another observable improvement of this method is that the amount of antibodies dispensed on TL and conjugated onto AuNPs could be reduced. Nevertheless, one should keep in mind that the silica nanorods preparation and their decoration with AuNPs could be a time-consuming step, besides that the size of the rods (tens of micrometers) slows the flow across the membrane thus increasing the

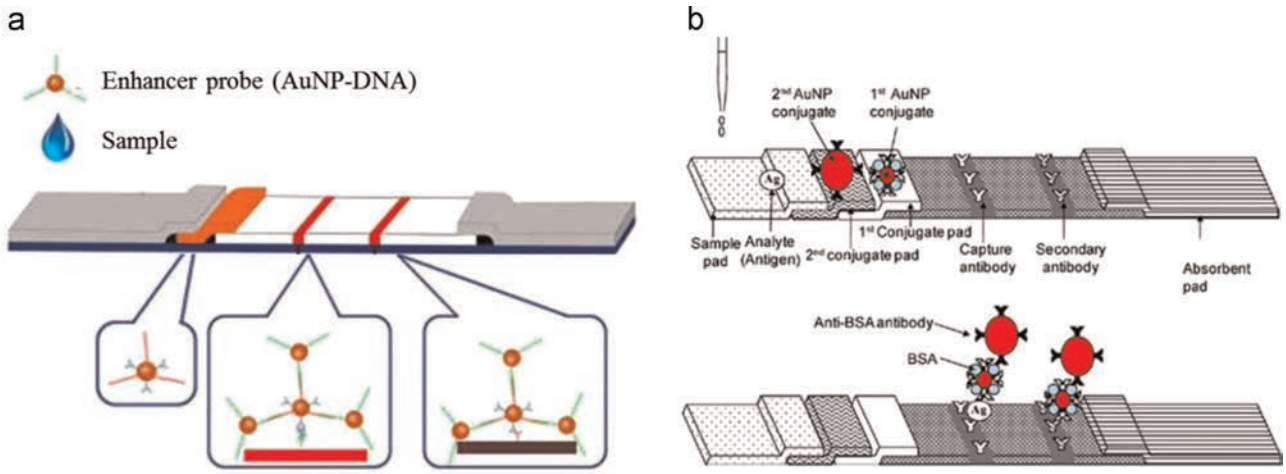

Fig. 5. Strategies to increase the density of AuNPs on TL and CL: (a) LFS with AuNPs–probes cocktail on the conjugate pad. Adapted with permission from Ge et al. (2013), Copyright 2013 American Chemical Society. (b) LFS with double conjugate pad. Reprinted with permission from Choi et al. (2010), Copyright 2010 Elsevier.

testing time. The size of the labels also precludes the use of small pore membranes, which are used to exhibit higher sensitivity than the membranes with bigger pores.

To increase the density of AuNPs on the detection lines, another strategy is to interconnect AuNPs by means of DNA probes (Hu et al., 2013; Ge et al., 2013) conjugated onto their surface. The binding between AuNPs can be performed previously to the assay, adding the AuNPs–probes cocktail to the conjugate pad (Hu et al., 2013), or during the assay, adding the enhancer nanoparticles mixed with the sample (Ge et al., 2013; Fig. 5a). As in the case of AuNPs decorated silica rods and the deposition of dry reagents on the membrane method, these designs are user-friendly, being able to be performed in one only step, without the need for post-treatments on the strip.

2.1.2.2. Architecture tuning. As mentioned, increasing the density of AuNPs on TL and CL is a good strategy to enhance the LFS signal. The LFS design modification can be easily achieved, for example, by adding an extra conjugate pad, as shown in the work of Choi et al. (2010). On this design, two different sized AuNPs conjugated with different types of antibodies on two pads are used. The smallest AuNPs are conjugated with the antibodies which are

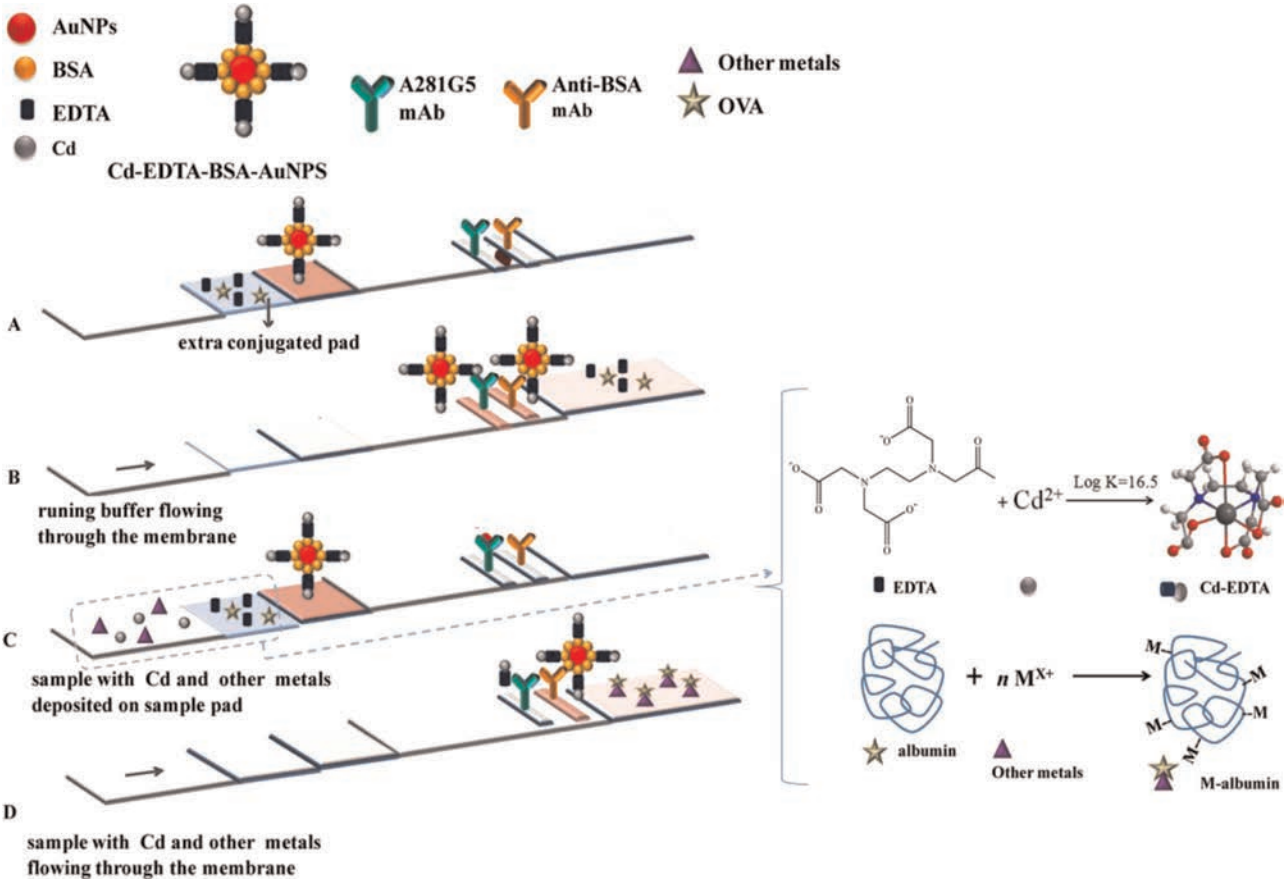

Fig. 6. LFS with additional conjugate pad for sample pre-treatment. Reprinted with permission from López-Marzo et al. (2013b), Copyright 2013 American Chemical Society.

selective to the antigen and will flow faster than the biggest AuNPs, which are conjugated with anti-BSA antibodies and will bind to the previous AuNPs, covered with BSA as blocking agent, obtaining an enhanced signal due to this new sandwich format (Fig. 5b). The detection limit of this LFS is 1 ng/mL, so the enhancement is not as good as in the previously discussed methods. Nevertheless this method is advantageous due to the fact that the assay is performed as a real one-step procedure, without pre-treatments on the sample neither post-treatments on the strip. It should also be noted that the preparation of both conjugates is simple and the biocompounds which are used are not very expensive. This technique was used again by Mei et al. (2013), demonstrating that it works as well for the detection of small molecules.

In cases where pre-treatment of the sample is required an extra pad can also be used to pre-treat the sample, simplifying the test procedure. In the work of López-Marzo et al. (2013b), an improvement of a previous design (López-Marzo et al., 2013a) by adding an extra pad with EDTA, which binds the metallic ions to allow their detection, and OVA, to help masking the interferences has been carried out (Fig. 6). More pads could be added, to enrich the flowing liquids with buffers or to improve the signal with enhancer solutions once the assay is finished, but it could require several steps, having to wait for the timely moment of each one, hindering the reproducibility of the device. That problem can be solved using the two-dimensional paper network format of Fu et al. (2011a). Buffer, sample and signal enhancer are added at the beginning of the assay, then the device is closed and, when the pads contact, the flowing across the paper network starts. In this manner the reproducibility of the liquid mixing is better controlled. In another work of Fu et al. (2012) they applied their knowledge about the behavior of the flow on paper-based materials (Fu et al., 2010, 2011b) to simplify their previous design. The possibilities are huge and of course this strategy can be adapted to many other designs (Kim et al., 2012) and transducers, not only to AuNPs (Cho et al., 2006; C. Liu et al., 2009; G. Liu et al., 2009; Jahanshahi-Anbuhi et al., 2012).

Multidetection of analytes is another interesting area in which architecture tuning can be helpful. Fu et al. (2010) and Fenton et al. (2009) experimented with the division of the flow on paper format, proving that multiplex design on lateral flow could work without the need of pumps or other auxiliary devices. Li et al. (2011) adapted LFS to the multiplex format in which three strips shared one sample pad (Fig. 7a).

At the beginning of this section it was discussed how increasing the quantity of gold nanoparticles in TL and CL boosts the sensitivity of the device. In the work of Parolo et al. (2013c) this purpose was reached modifying the architecture of paper. The authors tried different designs in which the flow was accelerated inside the detection pad due to a funnel effect, which at the same time was concentrating the amount of AuNPs and analytes inside (Fig.7b). The optimal results were obtained when the width of sample pad and conjugate pad was 3 times the width of the detection pad, enhancing the sensitivity and reducing about eight times the limit of detection in comparison to a standard LFS.

Another way to modify the flow is to disturb it, instead of provoking its acceleration the time that the transducers have to conjugate with analytes can be increased, ensuring that all AuNPs are conjugated and, consequently, captured on TL and CL. In the work of Hong et al. (2012) the antibodies were dispensed as patterns of parallel and zigzag dots on the detection pad, being the zigzag pattern the one which gave the highest intensities, presumably being flow slower on this design. Recently, it has been demonstrated that wax is a useful tool due its hydrophobicity to control flow on paper devices and create channels on it (Renault et al., 2014). In the work of Rivas et al. (2014), wax is used to create

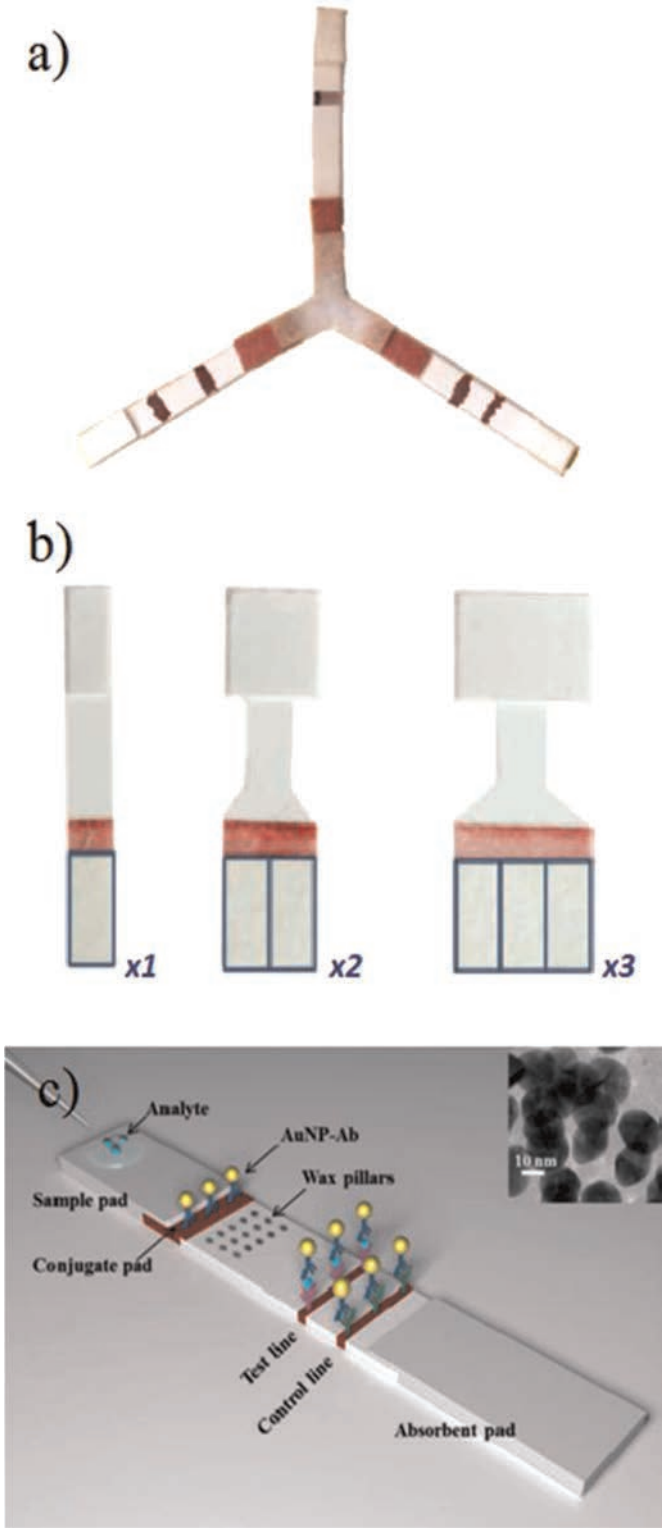

Fig. 7. Alternative LFS designs: (a) multidetection device composed by three LFS specific to different analytes. Reprinted with permission from Li et al. (2011), Copyright 2011 Elsevier. (b) Paper architecture modification to enhance the signaling. Reprinted with permission from Parolo et al. (2013c), Copyright 2013 Royal Society of Chemistry. (c) Design with wax pillars printed on LFS membrane, to modify the flow across the pores. Reprinted with permission from Rivas et al. (2014), Copyright 2014 Royal Society of Chemistry.

pillars inside the membrane (Fig.7c) slowing the movement of the fluids and amending their mixing. Furthermore, the pressure exercised when printing the wax patterns reduces the membrane's

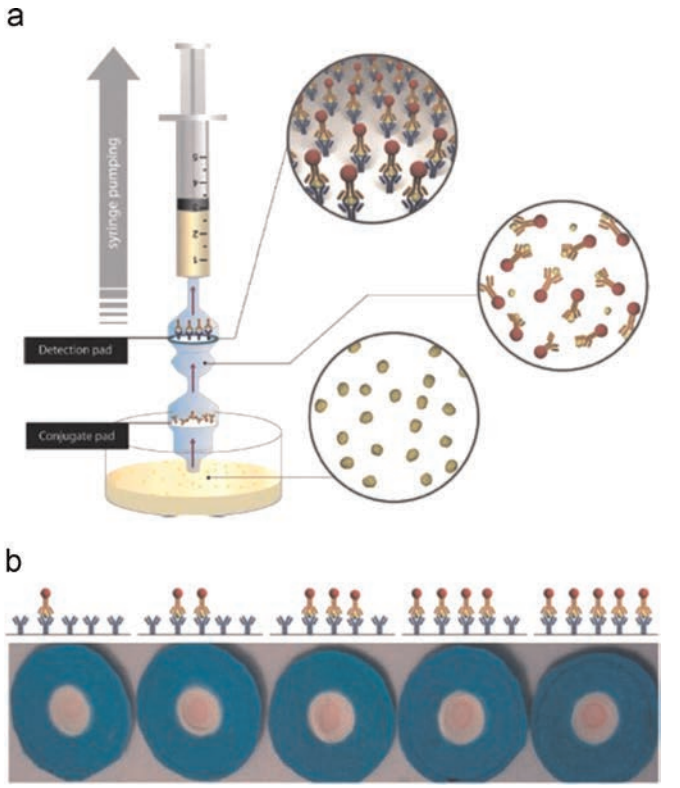

Fig. 8. Syringe design LFBs: (a) Working principle and (b) detection pads. Adapted with permission from Nunes Pauli et al. (2015), Copyright 2015 Royal Society of Chemistry.

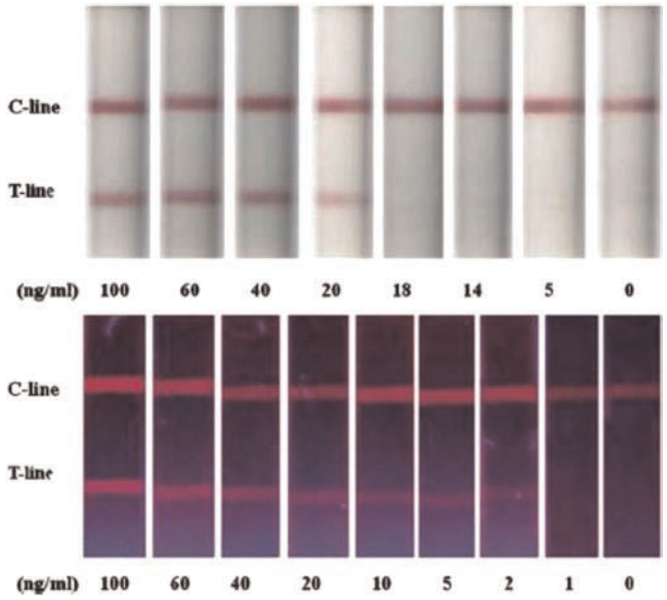

Fig. 9. Comparison of assay made with AuNPs (up) and silica nanoparticles loaded with QD (down). Reprinted with permission from Bai et al. (2012), Copyright 2012 Royal Society of Chemistry.

pore size, also contributing to the break of the flow. Again, as happened in Hong et al.'s (2012) work, the zigzag design exhibits the highest response. On Rivas et al.'s (2014) work the detection limit is improved three times regarding a non-modified strip, less than on Parolo et al.'s (2013c) method; however wax pillars compose a more inexpensive design, since it does not require higher quantities of AuNPs and antibodies, in addition that wax is a cheap material.

Probably, it is the recent design of Nunes Pauli et al. (2015) the most newfangled one. Instead the use of a LFS, the assay is carried out in a vertical flow mode inside a syringe (Fig. 8a); first, the sample is pumped to the conjugate pad and it interacts with it during a few minutes, allowing the conjugation of the analyte with AuNPs; then, it is aspirated to the upper part (detection pad that consists in a small cartridge with circular pieces of nitrocellulose with the detection antibodies retained inside a wax ring) where the signaling takes place (Fig. 8b). This technique requires high quantities of liquid in comparison to standard LFS to perform the assay; nevertheless, since the sample is being pre-concentrated in the syringe, the limit of detection is highly improved.

2.2. Fluorescent nanoparticles

It is well known that fluorescence methods use to exhibit higher sensitivity that those based on absorption colorimetry. The behavior of fluorescent nanomaterials with interest to be used in LFSs has been extensively explored and some reported examples discussed below.

2.2.1. Quantum dots (QDs)

In the already discussed work of Li et al. (2012) it was demonstrated that the use of quantum dots (QDs) exhibits a good sensitivity and a really low limit of detection; but on their work, quantum dots were used to indirectly detect the amount of AuNPs on TL by quenching effect. In other works QDs are used directly as labels on LFS, with both antibodies (Yang et al. 2010; Li et al., 2010; Berlina et al. 2013) and aptamers (Wang et al., 2011a; Bruno, 2014). The assays are as fast as with AuNPs, regardless the time that fluorimetric analysis could take, and the limits of detection achieved with QDs as tags are in the order of a few nanograms per milliliter. The differences between an AuNPs and a QDs LFS are heighten when QDs are carried (Bai et al., 2012) or encapsulated (Ren et al., 2014) in other materials. In the work of Bai et al. (2012), QDs were loaded over silica nanoparticles, which are between 10 and 20 times larger than QD, and these nanocomposites were used as labels obtaining a good sensitivity and a detection limit ten times lower than with AuNPs LFS (Fig. 9). These achievements were overwhelmed by Ren et al.'s (2014) work, who managed to encapsulate QDs on polymeric beads improving the limit of detection to only 0.42 pg/mL and fixing problems of flow and unspecific adsorptions of free QDs on nitrocellulose. In some cases, the conjugation of QDs with biocompounds can be a complex work due to their small size; also the number of antibodies per QDs is lower than in larger particles, so the probability of binding the label to the antigen is also a bit lower; therefore, the works of Bai et al. (2012) and Ren et al. (2014), besides enhancing the signal, are noteworthy easing the development and behavior of the LFS.

2.2.2. Other fluorescent materials

Besides QDs, other fluorescent materials, like the called up-converting phosphor technologies (UPTs) reporter particles. These type of nanoparticles are considered ceramic materials of large size, a few hundreds of nanometers, composed by the combination of rare earth elements, being europium one of the most used. UPT reporter particles transform low energies (infrared) into high energies (visible light, depending on their crystalline structure). Corstjens et al. (2001, 2003, 2008a, 2008b) worked with this materials to detect nucleic acids and antigens in complex matrixes with improved results in comparison to the ELISA tests. Paterson et al. (2014), B.H. Liu et al. (2014) and C. Liu et al. (2014) also worked with this type of materials on LFSs, obtaining similar results as Corstjens et al. (2001, 2003, 2008a, 2008b). UPTs seem more stable in front of photobleaching effect (decrease of

fluorescence) than QDs, making UPTs more suitable for direct assays and QDs for quenching related modes.

As seen with QDs, to carry the fluorescent tags on larger particles it helps enhancing the signal and avoids unspecific adsorptions onto the membrane. Europium, present on most of UPTs, emits fluorescence when reduced from Eu^{3+} to Eu^{2+}, so several researchers have exploited that property and combined europium with microparticles (Rundström et al., 2007) and silica beads (Xia et al., 2009; Tang et al., 2015; Zhang et al., 2014) to use them as transducers of LFS. Although the results are satisfying, QDs and UPTs exhibit better limits of detection and working ranges. Huang et al. (2013) covered silica microparticles with $Ru(phen)_3^{2+}$ complex, which also exhibits fluorescent properties, obtaining a good limit of detection, 20 pg/mL. Edwards and Baeumner (2006) and Khreich et al. (2008) used liposomes to encapsulate fluorescent dyes, getting higher sensitivity when using larger particles, with limits of detection close to 20 pg/mL. Commercial fluorescent microspheres which can be used on LFSs also are available (Xie et al., 2014; Wang et al., 2014b; Zhou et al., 2014). Interestingly, Xie et al. (2014) evaluated the optimal quantity of antibodies required to be conjugated with their microspheres and compared it with AuNPs, resulting that when using microspheres this quantity can be reduced four times; moreover, even using less quantity of antibodies in the labels, the sensitivity, the working range and the limit of detection are improved in comparison to AuNPs assays.

2.3. Other nanoparticles

2.3.1. Carbon based materials

AuNPs are the most known labels for LFSs; however other materials, without requiring enhancement strategies or designs, have been reported to improve limits of detection. This is for example the case of carbon nanoparticles (CNPs) which in the study of Linares et al. (2012) exhibit a limit of detection ten times lower than LFS in which AuNPs or LBs (latex beads) are used. CNPs, also known as carbon black, are strongly dark colored nanoparticles that exhibit a higher contrast against the background than AuNPs (Fig. 10), a factor which helps to obtain good parameters of sensitivity, working range and limit of detection. CNPs, as AuNPs, can be used for the detection of antigens (Lönnberg and Carlsson, 2001; Van Dam et al., 2004; Rayev and Shmagel, 2008), DNA chains (Kalogianni et al., 2011; Noguera et al., 2011) and molecules (Koets et al., 2006; Blažková et al., 2009, 2010), allowing also the development of multidetection LFS (Noguera et al., 2011).

Another allotropic form of carbon used on LFSs are carbon nanotubes (CNTs) (Abera and Choi, 2010; Qiu et al., 2015). CNTs are large materials, whereby using these materials on a LFSs will turn them in slow tests (around 20 min to see the response), on the other hand, Qiu et al.'s (2015) work demonstrated that the limit of detection is improved in comparison to related AuNPs systems. Furthermore, CNTs are stable in time and against aggregation, which increases the life time of the conjugates.

2.3.2. Colored nanoparticles

One of the first nanomaterials used to develop LFBs was colloidal selenium (Lou et al., 1993), with rust color. On this firstling design, the detection of analyte was semiquantitative by means of various TL on the membrane, instead of comparing the intensity of a single TL. The detection limit of this LFS was only of a few milligrams per milliliter, so rapidly selenium colloids were substituted by gold colloids which exhibit stronger color. However, several years later, Wang et al. (2014c) used again selenium nanoparticles, claiming the cost effectiveness of this material in comparison to AuNPs, to develop modern LFS. Wang et al. (2014c) could not obtain a low limit of detection, but their system with selenium nanoparticles proved to be quite specific to melamine in different matrixes.

Magnetite nanoparticles (MNPs) can be used as labels due to their strong brown color (also because of their magnetic properties, as will be discussed up ahead). Nevertheless, this strong color covers practically all the visible spectra obstructing its identification by means of colorimetric devices. The advantage of MNPs is that their optical properties do not change as much as AuNPs when aggregated. So Liu et al. (2011) took advantage of this property and created LFSs where MNPs were aggregated using poly-L-lysine on TL. The aggregated MNPs maintained a similar sensitivity to the non-aggregated MNPs, but the limit of detection was improved, reaching 1.7 ng/mL.

Silver can be used to enhance the intensity of AuNPs (Anfossi et al., 2013), but silver by himself is also an interesting nanomaterial. Silver nanoparticles present different colors depending on their size and shape, so Yen et al. (2015), exploiting this property, developed multiplexed LFS in which not only each antigen had their own line, but each of the lines had a different color, avoiding confusions to the final user (Fig. 11).

In the work done by Park et al. (2015) platinum nanoparticles are used as transducers due to their properties catalysing luminol oxidation provoking chemiluminiscence. In comparison with HRP, platinum nanoparticles are more stable-in-time and robust against environmental conditions. Park et al. (2015) compared the lighting response of platinum versus the conventional AuNPs LFS obtaining a higher working range and a limit of detection one thousand times lower.

2.3.3. Dyed beads and liposomes

Latex beads (LBs) or polystyrene nanoparticles are homogeneous-size particles which, after being dyed, can be used to develop LFSs. Several companies use LBs on their LFSs due to the fact it is a cheap material and has a similar behavior as AuNPs. Greenwald et al. (2003) compared AuNPs and LBs and observed that LFSs prepared with LBs on conjugate pad gave a higher

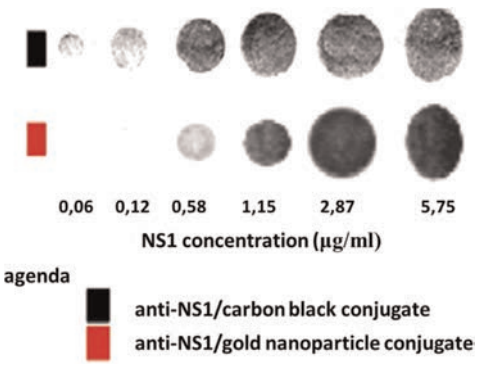

Fig. 10. Comparison of contrast obtained when using carbon nanoparticles (CNPs) and AuNPs. Reprinted with from Linares et al. (2012), Copyright 2012 Elsevier.

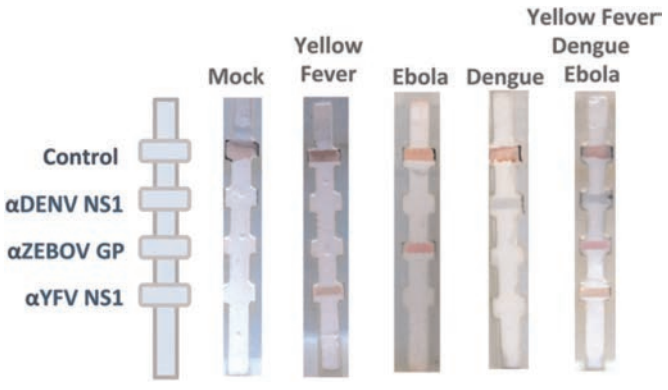

Fig. 11. Multiplex LFS developed with silver nanoparticles. Reprinted with permission from Yen et al. (2015), Copyright 2015 Royal Society of Chemistry.

sensitivity and specificity than the ones prepared with AuNPs. Comparing other studies with LBs (Waters et al., 2006; Campbell et al., 2007; Lyashchenko et al., 2007), the LFSs always show a good response in terms of selectivity and sensitivity; however the limits of detection are not as low as with other materials, which makes the strips suitable for qualitative assays, for clinic tests where it is only necessary to know if an antigen is over a determinate threshold. Instead of latex, cellulose can also be used (Choi et al., 2014) as dyed label on LFSs, which is an even cheaper material.

As discussed above in Edwards and Baeumner (2006) and Khreich et al. (2008) experiments, liposomes can be used to encapsulate dyes (whether fluorescent or not). There are some reports about the use of liposomes on LFBs (Ho and Wauchope, 2002; Baeumner et al., 2004a, 2004b; Wen et al., 2005; Edwards and Baeumner, 2006; Ho et al., 2008; Khreich et al., 2008; Shukla et al., 2011; Leem et al., 2014) with good levels of sensitivity due to the high quantities of dye that can be loaded inside the liposomes. Nevertheless, the synthesis of liposomes is often a long procedure, with difficult size-control, so the reproducibility of the test could be affected if the protocol is not well controlled.

3. Electrochemical detection

Despite the fact that LFB response can be quantitative, sometimes it can be hard to discriminate between the strips, especially by naked eye. The combination of LFBs with electrochemical detection is expected to provide a more sensitive response, higher reproducibility, wider working range and lower limits of detection than optical measurements. Nowadays electrodes can be easily miniaturized by different methods as screen printing, ink-jet printing or photolithography, allowing their easy incorporation into a LFS design. In the work of Inoue et al. (2007) the authors used photolithography to fabricate three gold electrodes, working, counter and reference (Fig. 12), over a glass slide and then coupled a small piece of nitrocellulose on a well into the device. They demonstrated that electrochemical reactions, cyclic voltammograms and amperometric measurements could be performed on nitrocellulose substrate so, then, they cut a small piece from a LFS, corresponding to the TL, and carried out the measurements. The amperometric responses, based on the reduction of ferrocenemethanol catalysed by HRP (which was previously linked to a known quantity of testosterone, used also as analyte), decreased when the concentration of the analyte was increased in the sample (competitive LFBs model), obtaining wider working range than by chemiluminiscence measurements and good values of sensitivity and limit of detection. The main drawback of Inoue et al.'s (2007) method is that the electrochemical assay is performed separately. As the reduction is carried out as an additional step, the electrodes are not truly integrated into the LFS and it has to be cut. Some later designs (Wang et al., 2011b; Du et al., 2011) tried to fuse the electrode and the strip inside a cassette, including a cutter to section/cut the TL once the immunoassay was completed.

Liu et al. (2007), Lin et al. (2008), Zhu et al. (2014) and Akanda et al. (2014) integrated the electrodes in the LFS on different ways. In the cases of Liu et al. (2007) and Lin et al. (2008), QDs containing cadmium were used; after the test was performed and QDs were captured on TL, chlorhydric acid was used to release cadmium ions from QDs, which were detected by the electrodes, located under the TL, when a detection solution (Hg/Bi) was added on it. The obtained limit of detection was really low, 30 and 20 pg/mL respectively in each report. Interestingly, Liu et al. (2007) observed that when the immunoassay time was extended, the detection limit was decreased to 10 pg/mL. In the work of Zhu et al. (2014) the colorimetric and electrochemical measurements were performed at the same time, without the addition of detection solution, thanks to the integration of commercial CNTs paper in the LFS as working electrode, placed on the CL, and printed silver/silver chloride ink as reference and counter electrode (Fig. 13a), being the electrodes laminated to ensure the contact between them and the nitrocellulose membrane (Fig. 13b). Following a competitive LFBs model and using AuNPs as labels, the colorimetric response was measured comparing the TL on photographs of the LFS and, at the same time, the chronoamperometric response was measured from the remaining AuNPs on the CL.

It must be highlighted the work of Akanda et al. (2014), where they report a really low limit of detection, of only 0.1 pg/mL. Their LFS includes an extra pad with different substrates to perform a redox reaction on the electrodes which allows detecting the analyte without being affected by electroactive interfering species present on the sample (Fig. 14). Thanks to this pad the need for

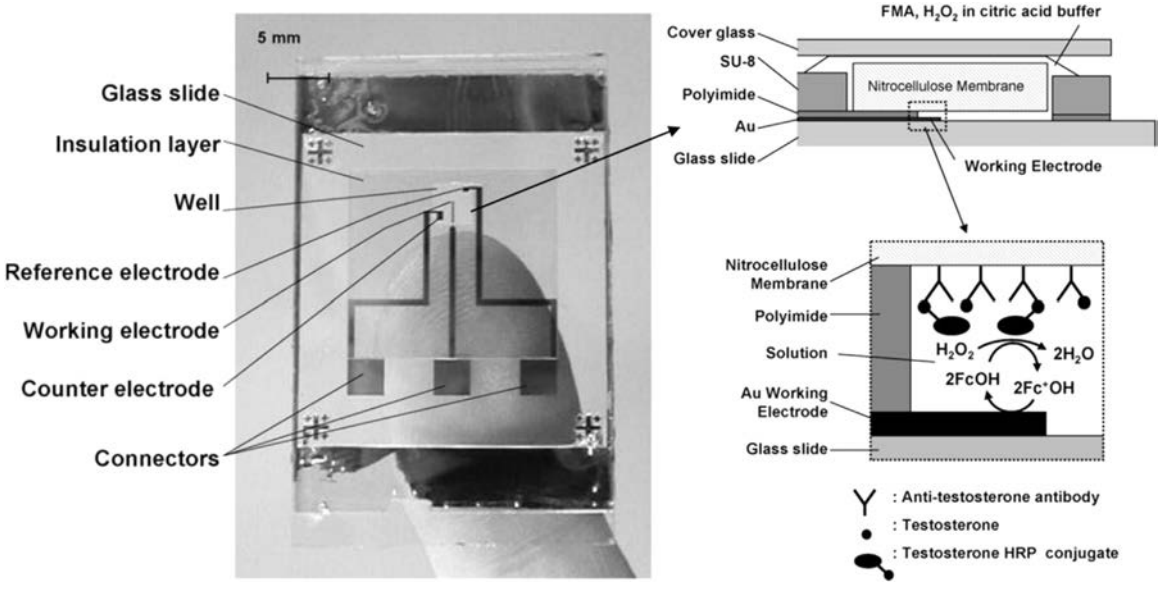

Fig. 12. Photograph of a standard electrode chip and the scheme of its well when LFS is coupled inside. Adapted with permission from Inoue et al. (2007), Copyright 2007 Elsevier.

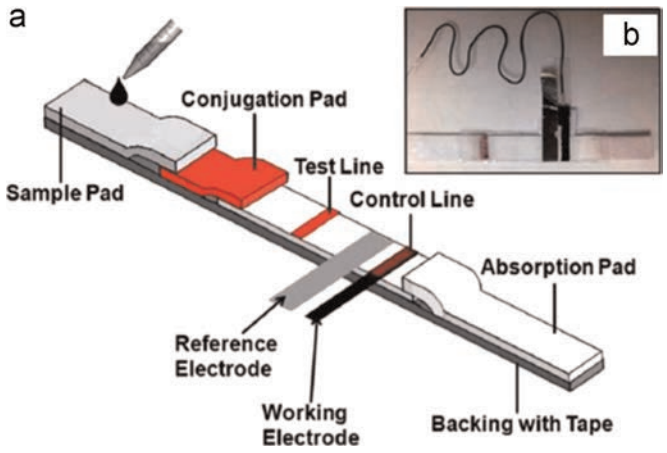

Fig. 13. (a) Schematic representation of a LFS with electrical chip coupled and (b) its corresponding photography. Reprinted with permission from Zhu et al. (2014), Copyright 2014 Royal Society of Chemistry.

sample pre-treating for both eliminating of interferences and to perform the electrochemical reaction is taken away, simplifying the test for the end user. On this design the electrodes, previously printed through photolithography on indium tin oxide substrate (ITO), were placed directly over the membrane, onto the detection antibodies. Hence, the detection on the LFS is only electrochemical and the strip does not provide optical checking.

4. Other detections

4.1. Magnetic methods

MNPs, as previously discussed, can be used as labels on lateral flow (Liu et al. 2011) due to the fact they are strongly colored and can be easily conjugated with biomarkers. Usually, MNPs are used to preconcentrate the analyte in a sample through an washing step (Fisher et al., 2009; Liu et al., 2015), or are conjugated with colored particles (e.g. AuNPs) to assemble them, to help in the purification of the conjugate by means of magnetic separation and to increase the intensity of the color in TL (Tang et al., 2009). Nevertheless, MNPs can be used to a more interesting purpose; the magnetic field that the nanoparticles generate can be measured through a proper magnetic reader and transformed into a useful analytical signal. The advantage of this technique is that all the nanoparticles in the detection line should produce signal, contrary to optical and electrochemical methods where only nanoparticles on the surface or in contact with the electrodes, respectively, contribute significantly on the signaling.

There exist several methods to produce and measure a signal using MNPs, being commercial magnetic assay readers (MARs) the most popular. MARs generate a magnetic field which excites the MNPs that simultaneously will produce their own magnetic field, detectable using the sensing coils of the apparatus. This effect can qualitatively measure groups of MNPs. Wang et al. (2009), Zheng et al. (2012), D.B. Wang et al. (2013), Shi et al. (2015b), Barnett et al. (2014) and Wang et al. (2015) reported the use of MAR on their works, obtaining wide working ranges, high selectivity, robust assays, good sensitivity and lower limits of detection than standard AuNPs LFs. However, the intensity of the signal was related to the size of the MNPs, being the larger ones which produced higher responses being this a drawback inasmuch as it slows significantly the assay time. Another manner to increase the signal, producing a higher magnetic field, is to increase the concentration of magnetite inside MNPs. It must not be forgotten that MNPs are strongly colored, so colorimetric response could also be measured from these LFs.

Even though nitrocellulose membranes contain pores with widths of some micrometers, the largest MNPs, combined with big analytes as spores, bacteria or cells, could clog the pores

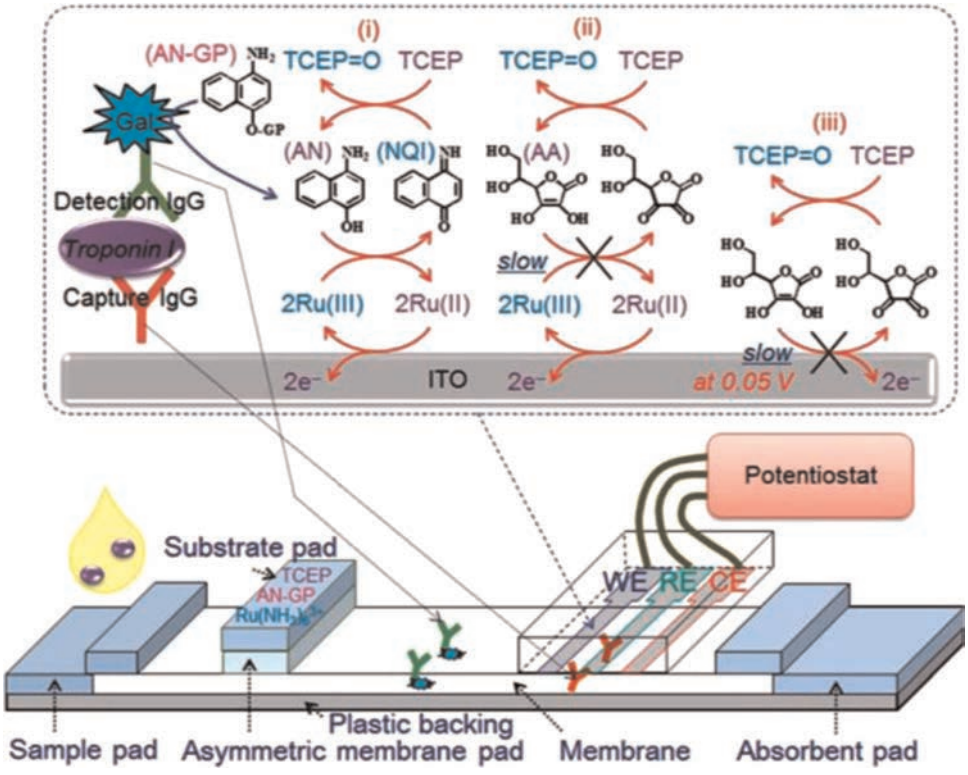

Fig. 14. Electrochemical immunoassay occurring on a LFS with an additional substrate pad. Reprinted with permission from Akanda et al. (2014), Copyright 2014 Royal Society of Chemistry.

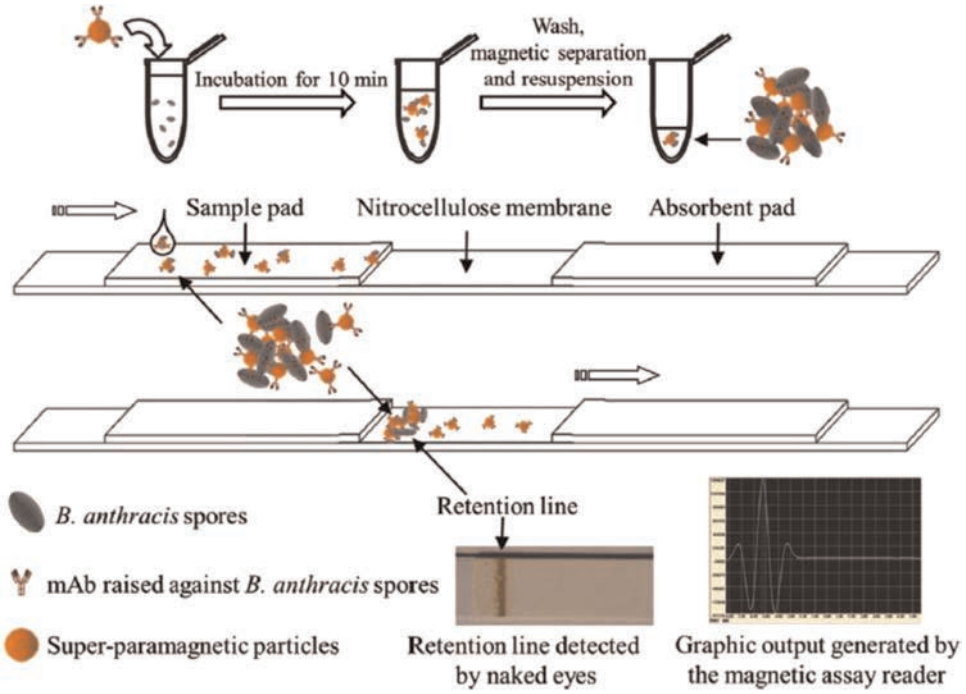

Fig. 15. LFS developed with MNPs as labels but without antibodies on the detection pad; "road closure effect". Reprinted with permission from Wang et al. (2015), Copyright 2015 Elsevier.

obstructing the flow of the conjugates across the membrane producing retention lines ("road closure effect"). Curiously, Wang et al. (2015) took advantage of this inconvenience to develop a novel LFs free of dispensed antibodies on the detection pad. Merely, in the presence of analyte, the MNPs–analyte conjugate formed the retention line at the beginning of the nitrocellulose membrane and it was measured with the MAR (Fig. 15). A clear advantage of this design is the cheapness of the LFSs, due to the fact that antibodies printed on it use to represent near the half of its costs; also the assay is faster than in the other magnetic LFs; nonetheless the absence of CL is a huge drawback because it impedes the detection of false positives.

In addition to MAR, other technologies like the use of giant magnetoresistive sensors (GMR) are emerging (Taton et al., 2009; Ryu et al., 2011; Marquina et al., 2012), GMR signaling is produced when the electrical resistance of the sensor is reduced by the effect of an external magnetic field derived from the MNPs. The technique can show a quite low limit of detection (12 pg/mL; Taton et al., 2009) but seems that its robustness and sensitivity still have to be improved.

4.2. Other methods

Thermal contrast is a technique that measures the radiation that the materials, over to absolute zero temperature, produce at infrared range. In LFS, thermal contrast can detect small variations

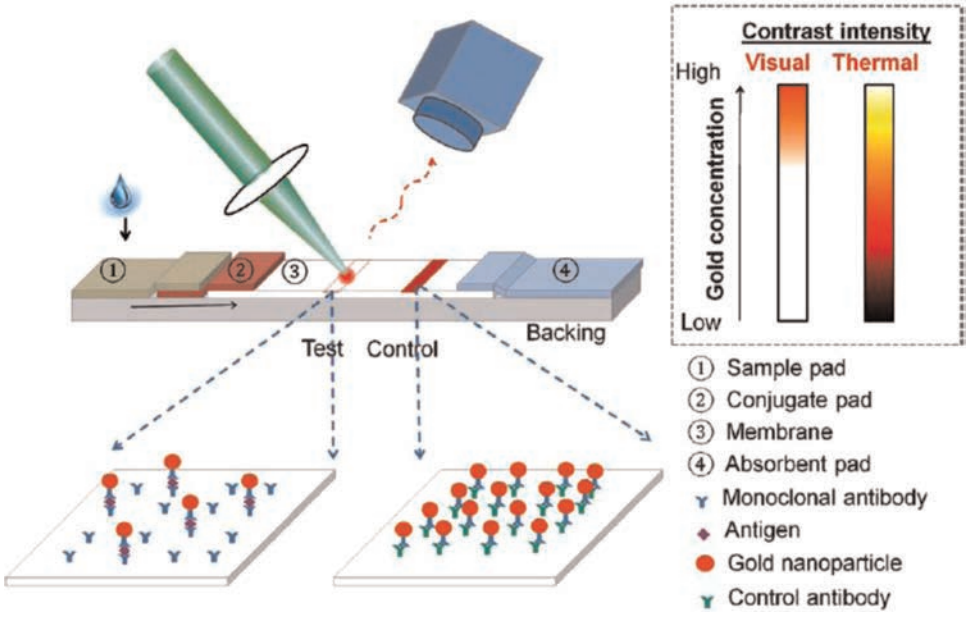

Fig. 16. (a) Thermal Contrast Sensor applied on LFS. Reprinted with permission from Qin et al. (2012), Copyright 2012 Wiley-VCH.

of concentration which are not detectable with visible light, providing lower limits of detection than in the optical methods, including fluorescence in comparison to which, furthermore, avoids photobleaching effect; for this reason thermal contrast is considered a really robust and reproducible technique. Qin et al. (2012) reported the use of thermal contrast sensor (Fig. 16) on AuNPs LFS and compared the registered data against visual detection, reaching a 32-fold improvement on the sensitivity. Besides spherical nanoparticles, other shapes were tested (nanorods and nanoshells), by becoming shell AuNPs the one which exhibited higher response on thermal contrast.

A technique which can be combined with LFBs to enhance its response is isotachophoresis, an electrophoretic technique used to displace and preconcentrate several kinds of compounds, from large biocompounds to small inorganic ions, forcing their displacement with other ions. Moghadam et al. (2014, 2015) used this technique on LFSs to concentrate the conjugate and to transport it to the TL. The time of the assay is reduced, as well as the limit of detection, however must be taken into account that this method requires calibration, membrane pretreatment and current application (in which is strongly dependent the sensitivity of the device).

Another detection method which can be applied on LFS is surface-enhanced Raman scattering (SERS), a technique that enhances the Raman scattering of molecules (Raman reporters: chromophores or fluorescent dyes with high photostability and that exhibit resonance at Raman frequencies) previously attached in the label nanoparticles, increasing significantly the sensitivity of the assay. Li et al. (2014) reported the use of LFSs on SERS, using AuNPs covered with 4-mercaptobenzoic acid (a Raman reporter).

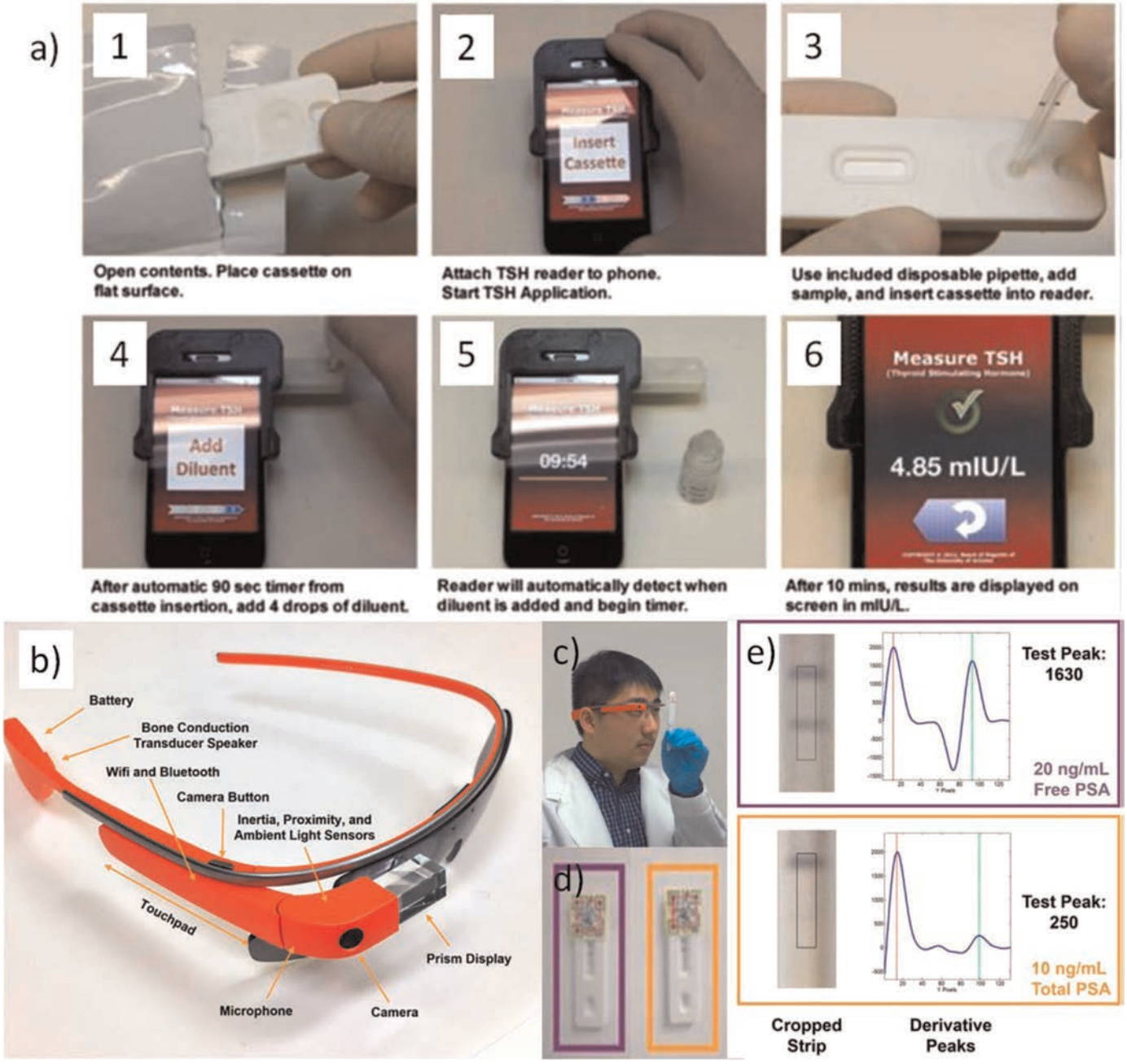

Fig. 17. (a) Performance of a lateral flow assay assisted with a smartphone. Smartphone is used as a LFS reader. Adapted with permission from You et al. (2013), Copyright 2013 Elsevier. (b) Google Glasses, used to read LFS (c), identified with QR codes (d) and the response obtained (e). Adapted with permission from Feng et al. (2014), Copyright 2014 American Chemical Society.

Their experiments demonstrated the great precision of the technology, the high selectivity against the reporters and a really low limit of detection, 0.32 pg/mL.

5. Integration and connection with real world applications

The use of LFBs is not restricted only to laboratory or hospital environments. LFBs are designed to be portable devices which can be used overall at home or in the field. Their use is expected to be increased in the future so, consequently, it is important to adapt LFBs to the end user. At that point, it is necessary to focus not only in the LFS design, but also to the reader that should be user-friendly and low-cost. For example, Gui et al. (2014) demonstrated that with a charge-coupled device-based reader, which works on a similar way as a bar-code reader (in addition to some algorithms) a LFS developed with QDs (fluorescent measurements) could be easily read with low noise and low detection limits (20 pg/mL).

Table 1
Comparison of most remarkable methods and materials used in lateral flow biosensors.

Detection method	Labels	Advantages	Disadvantages
Optical (colorimetry)		• Naked-eye detection • Fast qualitative response	• Normally, only qualitative or semiquantitative response
	AuNPs	• Easy to synthetize and modify • Highly biocompatible and versatile • Intense colored • Relatively inexpensive	• Without the application of enhancement techniques, poor sensitivity and limits of detection in comparison to other methods.
	Carbon based materials	• Strong contrast against background • Different shapes and behaviors • Inexpensive and stable-in-time	• Unspecific adsorptions • Some forms have big-size: slow response assay
	Nano-/micro-particles loaded/ modified with dyes	• Inexpensive and high variety of commercial products • Good sensitivity and limits of detection	Difficult to synthesize and modifyRequire to load high quantities of dye to have a good signaling
Optical (fluorescence)		• High sensitivity • Low limits of detection	• Naked- eye detection normally is not possible • Requires equipment with both excitation light and fluorescence measurement • Materials normally exhibit photobleaching effect, lose intensity in time
	QDs	• Small-sized: fast assay • Strong intensity	• Difficult to synthetize and conjugate
	Other fluorescent materials (ex. UPTs)	• Could require less energy to be excited than QDs	• Rare elements can be expensive • Big-sized: slow assay
Electrochemical	Electroactive nanoparticles	• Highly sensitive • Low limits of detection • Devices easily miniaturized and cheap	• Requires equipment to produce and translate the signal • Reproducibility problems related to electrodes
Magnetic	Nano-/micro-particles loaded/ modified with magnetite	• Relatively inexpensive	• Require magnetic detectors
		• Colorimetric response is also possible (multi signals)	• Sensitivity related to the size of the particles: slow assays
Thermal contrast	AuNPs	• High improvement of sensitivity and reproducibility • Any material can emit signal	• Expensive equipment
SERS	Raman reporter materials	• High improvement of sensitivity and detection limits	• Expensive equipment • Requires pretreatment of the nanomaterials

Nowadays, smartphones have become an almost indispensable tool for day to day life, with a countless number of applications and utilities; therefore, its connection with biosensing seems to be expectable. Mudanyali et al. (2012), You et al. (2013) and Zangheri et al. (2015) developed different user-friendly apps for smartphones which, with their respective adapter (containing LED-source of light, filtering lens and a space to introduce LFS), can be used to detect the TL and CL of LFSs and translate the signal meanwhile all the steps that the user should perform during the assay are explained on the smartphone's screen (Fig. 17a).

With the arrival of the new Google Glasses (Fig. 17b) and similar products in the market the integration of augmented reality apps in real life will start. Feng et al. (2014) developed a voice-controlled app for Google Glasses that allows, by looking with your own eyes a QR code (quick response code) (Fig. 17c and d) printed in the LFS, get a quantitative interpretation of what your naked-eyes are watching (Fig. 17e). When looking to the QR, the Google Glasses get access into a server where a LFS picture will be saved in a database, analyzed and translated, receiving a posteriori the data on Google Glasses display or checking them in internet browser.

6. Conclusions and future perspectives

LFSs have demonstrated to be affordable and portable tools to detect a huge variety of compounds (e.g. proteins, metallic ions, organic molecules, DNA, cells, etc.) in a really short period of time usually shorter than 30 min that may include pre- and post-treatments if necessary. As shown in Table 1, LFSs are compatible with different detection methods and nanomaterials in which strongly depend the costs, the robustness, the sensitivity and the detection limits of these devices. The variety of properties of nanoparticles allows the secondary reactions to be performed onto their surface or their assembly and other modifications enhancing the intensity of the analytical signals. However, the signal of a LFS can also be easily enhanced just by modifying its architecture allowing tuning of the microfluidics beside other changes.

The progress in the LFB field is strongly related with the development of new nanomaterials, strategies and methods to increase the sensitivity and decrease the limit of detection. To reach that goal various strategies may be followed: a) use of nanoparticle labels which are simple to detect, stable and ensure intense signals; b) development of strategies that increase the quantity of signaling labels per unit of analyte; c) application of detection methods that inherently provide strong signaling and a high level of quantification in the detection zone; d) combination of different detection techniques and enhancement strategies already reported could help to offset the drawbacks of each system. The increase recently of the research in the field of graphene may offer new opportunities also for LFB technology. The special properties of graphene oxide in various optical biosensing technologies (Morales-Narváez and Merkoçi, 2012) including its quenching properties on QDs (Morales-Narváez et al., 2012), if applied on LFSs, may bring interesting results in terms of sensitivity and limit of detection.

LFSs are expected to deepen more in fast diagnostics, enabling its use at home to identify diseases or allergens, or simply to watch over on biological parameters that affect our security and health; because of this, electronic devices of common use, like smartphones or augmented reality apparatus (like the new Google Glasses) or future technologies, may probably be able to work as readers of LFSs, providing comprehensible test instructions and results to the user.

Acknowledgments

The authors acknowledge support from the Severo Ochoa Program (MINECO, Grant SEV-2013-0295).

References

Abera, A., Choi, J.W., 2010. Anal. Methods 2, 1819–1822.
Ahmad, A.L., Low, S.C., Shukor, S.R.A., Ismail, A., 2009. Ind. Eng. Chem. Res. 48, 3417–3424.
Akanda, M.R., Joung, H.A., Tamilavan, V., Park, S., Kim, S., Hyun, M.H., Kim, M.G., Yang, H., 2014. Analyst 139, 1420.
Anfossi, L., Giovannoli, C., Giraudi, G., Biagioli, F., Passini, C., Baggiani, C., 2012. J. Agric. Food Chem. 60, 11491–11497.
Anfossi, L., Nardo, F.D., Giovannoti, C., Passini, C., Baggiani, C., 2013. Anal. Bioanal. Chem. 405, 9859–9867.
Aragay, G., Pons, J., Merkoçi, A., 2011. Chem. Rev. 111 (5), 3433–3458.
Aragay, G., Pino, F., Merkoçi, A., 2012. Chem. Rev. 112 (10), 5317–5338.
Assadollahi, S., Reininger, C., Palkovits, R., Pointl, P., Schalkhammer, T., 2009. Sensors 9, 6084–6100.
Baeumner, A.J., Jones, C., Wong, C.Y., Price, A., 2004a. Anal. Bioanal. Chem. 378, 1587–1593.
Baeumner, A.J., Pretz, J., Fang, S., 2004b. Anal. Chem. 76, 888–894.
Bai, Y., Tian, C., Wei, X., Wang, Y., Wang, D., Shi, X., 2012. RSC Adv. 2, 1778–1781.
Barnett, J.M., Wraith, P., Kiely, J., Persad, R., Hurley, K., Hawkins, P., Luxton, R., 2014. Biosensors 4, 204–220.
Berlina, A.N., Taranova, N.A., Zherdev, A.V., Vengerov, Y.Y., Dzantiev, B.B., 2013. Anal. Bioanal. Chem 405, 4997–5000.
Blažková, M., Mičková-Holubová, B., Rauch, P., Fukal, L., 2009. Biosens. Bioelectron. 25, 753–758.
Blažková, M., Rauch, P., Fukal, L., 2010. Biosens. Bioelectron. 25, 2122–2128.
Bruno, J.G., 2014. Pathogens 3, 341–355.
Campbell, K., Fodey, T., Flint, J., Danks, C., Danaher, M., O'Keeffe, M., Kennedy, D.G., Elliott, C., 2007. J. Agric. Food Chem. 55, 2497–2503.
Cazacu, A.C., Demmler, G.J., Neuman, M.A., Forbes, B.A., Chung, S., Greer, J., Alvarez, A.E., Williams, R., Bartholoma, N.Y., 2004. J. Clin. Microbiol. 42 (8), 3661–3664.
Chen, J., Fang, Z., Lie, P., Zeng, L., 2012. Anal. Chem. 84, 6321–6325.
Cho, J.H., Paek, S.H., 2001. Biotechnol. Bioeng. 75 (6), 725–732.
Cho, J.H., Han, S.M., Paek, E.H., Cho, I.H., Paek, S.H., 2006. Anal. Chem. 78, 793–800.
Choi, D.H., Lee, S.K., Oh, Y.K., Bae, W.B., Lee, S.D., Kim, S., Shin, Y.B., Kim, M.G., 2010. Biosens. Bioelectron. 25, 1999–2002.
Choi, E.S., Lee, S.G., Lee, S.J., Kim, E., 2014. Biotechnol. Lett. 37, 627–632.
Clark Jr., L.C., Wolf, R., Granger, D., Taylor, Z., 1953. J. Appl. Physiol. 6 (3), 189–193.
Cordray, M.S., Richards-Kortum, R.R., 2012. Am. J. Trop. Med. Hyg. 87 (2), 223–230.
Corstjens, P.L.A.M., van Lieshout, L., Zuiderwijk, M., Kornelis, D., Tanke, H., Deelder, A.M., van Dam, G.J., 2008a. J. Clin. Microbiol. 46 (1), 171–176.
Corstjens, P.L.A.M., Zuiderwijk, M., Brink, A., Li, S., Feindt, H., Niedbala, R.S., Tanke, H., 2001. Clin. Chem. 47 (10), 1885–1893.
Corstjens, P.L.A.M., Zuiderwijk, M., Nilsson, M., Feindt, H., Niedbala, R.S., Tanke, H., 2003. Anal. Biochem. 312, 191–200.
Corstjens, P.L.A.M., Zuiderwijk, M., Tanke, H., van der Ploeg-Schip, J., Ottenhoff, T.H. M., Geluk, A., 2008b. Clin Biochem. 41 (6), 440–444.
Costa, M.N., Veigas, B., Jacob, J.M., Santos, D.S., Gomes, J., Baptista, P.V., Martins, R., Inácio, J., Fortunato, E., 2014. Nanotechnology 25, 1–12.
De la Escosura-Muñiz, A., Parolo, C., Merloçi, A., 2010. Mater. Today 13, 24–34.
Du, D., Wang, J., Wang, L., Lu, D., Lin, Y., 2011. Anal. Chem. 84, 1380–1385.
Elenis, D.S., Ioannou, P.C., Christopoulos, T.K., 2011. Nanotechnology 22, 155501–155509.
Edwards, K.A., Baeumner, A.J., 2006. Anal. Bioanal. Chem. 386, 1335–1343.
Fang, Z., Huang, J., Lie, P., Xiao, Z., Ouyang, C., Wu, Q., Wu, Y., Liu, G., Zeng, L., 2010. Chem. Commun. 46, 9043–9045.
Feng, S., Caire, R., Cortazar, B., Turan, M., Wong, A., Ozcan, A., 2014. ACS Nano 8 (3), 3069–3079.
Fenton, E.M., Mascarenas, M.R., López, G.P., Sibbett, S.S., 2009. ACS Appl. Mater. Interfaces 1 (1), 124–129.
Fisher, M., Atiya-Nasagi, Y., Simon, I., Gordin, M., Mechaly, A., Yitzhaki, S., 2009. Lett. Appl. Microbiol. 48, 413–418.
Fridley, G.E., Le, H.Q., Fu, E., Yager, P., 2012. Lab Chip 12, 4321–4327.
Fu, E., Lutz, B., Kauffman, P., Yager, P., 2010. Lab Chip 10, 918–920.
Fu, E., Liang, T., Houghtaling, J., Ramachandran, S., Ramsey, S.A., Lutz, B., Yager, P., 2011a. Anal. Chem. 83, 7941–7946.
Fu, E., Liang, T., Spicar-Mihalic, P., Houghtaling, J., Ramachandran, S., Yager, P., 2012. Anal Chem. 84 (10), 4574–4579.
Fu, E., Ramsey, S.A., Kauffman, P., Lutz, B., Yager, P., 2011b. Microfluid. Nanofluid. 10, 29–35.
Ge, C., Yu, L., Fang, Z., Zeng, L., 2013. Anal. Chem. 85, 9343–9349.
Greenwald, R., Esfandiari, J., Lesellier, S., Houghton, R., Pollock, J., Aagaard, C., Andersene, P., Hewinson, R.G., Chambers, M., Lyashchenko, K., 2003. Diagn. Microbiol. Infect. Dis. 46, 197–203.
Gui, C., Wang, K., Li, C., Dai, X., Cui, D., 2014. Nanoscale Res. Lett. 9 (1), 57–64.
He, L., Nan, T., Cui, Y., Guo, S., Zhang, W., Zhang, R., Tan, G., Wang, B., Cui, L., 2014. Malar. J. 13, 127–136.

He, Y., Zhang, S., Zhang, X., Baloda, M., Gurung, A.S., Xu, H., Zhang, X., Liu, G., 2011. Biosens. Bioelectron. 26, 2018–2024.
He, Y., Zeng, K., Zhang, S., Gurung, A.S., Baloda, M., Liu, G., 2012. Biosens. Bioelectron. 31 (1), 310–315.
Held, J., Schmidt, T., Thornton, C.R., Kotter, E., Bertz, H., 2013. Infection 41 (1), 1163–1169.
Ho, J.A., Wauchope, R.D., 2002. Anal. Chem. 74, 1493–1496.
Ho, J.A., Zeng, S.C., Tseng, W.H., Lin, Y.J., Chen, C.H., 2008. Anal. Bioanal. Chem. 391, 479–485.
Hong, S.Y., Park, Y.M., Jang, Y.H., Min, B.H., Yoon, H.C., 2012. BioChip J. 6 (3), 213–220.
Hu, J., Wang, L., Li, F., Han, Y.L., Lin, M., Lu, T.J., Xu, F., 2013. Lab Chip 13, 4352–4357.
Huang, X., Aguilar, Z.P., Li, H., Lai, W., Wei, H., Xu, H., Xiong, Y., 2013. Anal. Chem. 85, 5120–5128.
Huang, Y., Wen, W., Du, D., Zhang, X., Wang, S., Lin, Y., 2014. Biosens. Bioelectron. 61, 598–604.
Inoue, K., Ferrante, P., Hirano, Y., Yasukawa, T., Shiku, H., Matsue, T., 2007. Talanta 73, 886–892.
Jahanshahi-Anbuhi, S., Chavan, P., Sicard, C., Leung, V., Hossain, S.M.Z., Pelton, R., Brennan, J.D., Filipe, C.D.M., 2012. Lab Chip 12, 5079–5085.
Kalogianni, D.P., Boutsika, L.M., Kouremenou, P.G., Christopoulos, T.K., Ioannou, P.C., 2011. Anal. Bioanal. Chem. 400, 1145–1152.
Karakus, C., 2015. J. Immunoassay Immunochem. 36, 324–333.
Kersting, S., Rausch, V., Bier, F.F., Nickisch-Rosenegk, V., 2014. Malar. J. 13, 99–107.
Khreich, N., Lamourette, P., Boutal, H., Devilliers, K., Créminon, C., Volland, H., 2008. Anal. Biochem. 377, 182–188.
Kim, K.Y., Shim, W.B., Kim, J.S., Chung, D.H., 2014. J. Food Sci. 79 (10), 2048–2055.
Kim, Y.A., Lee, E.H., Kim, K.O., Lee, Y.T., Hammock, B.D., Lee, H.S., 2011. Anal. Chim. Acta 693, 106–113.
Kim, Y.T., Chen, Y., Choi, J.Y., Kim, W.J., Dae, H.M., Jung, J., Seo, T.S., 2012. Biosens. Bioelectron. 33, 88–94.
Koets, M., Sander, I., Bogdanovic, J., Doekesc, G., van Amerongen, A., 2006. J. Environ. Monit. 8, 942–946.
Kolm, C., Mach, R.L., Krska, R., Brunner, K., 2015. Anal. Methods 7, 129–134.
Kuang, H., Xing, C., Hao, C., Liu, L., Wang, L., Xu, C., 2013. Sensors 13, 4214–4224.
Lee, J.Y., Kim, Y.A., Kim, M.Y., Lee, Y.T., Hammock, B.D., Lee, H.S., 2012. Anal. Chim. Acta 757, 69–74.
Leem, H., Shukla, S., Song, S., Heu, S., Kim, M., 2014. J. Food Saf. 34, 239–248.
Li, C., Vandenberg, K., Prabhulkar, S., Zhu, X., Schneper, L., Methee, K., Rosser, C.J., Almeide, E., 2011. Biosens. Bioelectron. 26, 4342–4348.
Li, M., Yang, H., Li, S., Zhao, K., Li, J., Jiang, D., Sun, L., Deng, A., 2014. J. Agric. Food Chem. 62, 10896–10902.
Li, X., Lu, D., Sheng, Z., Chen, K., Guo, X., Jin, M., Han, H., 2012. Talanta 100, 1–6.
Li, Z., Wang, Y., Wang, J., Tang, Z., Pounds, J.G., Lin, Y., 2010. Anal. Chem. 82, 7008–7014.
Lie, P., Liu, J., Fang, Z., Dun, B., Zeng, L., 2012. Chem. Commun. 48, 236–238.
Lin, Y.Y., Wang, J., Liu, G., Wu, H., Wai, C.M., Lin, Y., 2008. Biosens. Bioelectron. 23, 1659–1665.
Linares, E.M., Kubota, L.T., Michelis, J., Thalhammer, S., 2012. J. Immunol. Methods 375, 264–270.
Liu, B.H., Hung, C.T., Lu, C.C., Chou, H.N., Yu, F.Y., 2014a. J. Agric. Food Chem. 62, 1254–1260.
Liu, C., Jia, Q., Yang, C., Qiao, R., Jing, L., Wang, L., Xu, C., Gao, M., 2011. Anal. Chem. 83, 6778–6784.
Liu, C., Ma, W., Gao, Z., Huang, J., Hou, Y., Xu, C., Yang, W., Gao, M., 2014b. J. Mater. Chem. C 2, 9637–9642.
Liu, C., Qiu, X., Ongagna, S., Chen, D., Chen, Z., Abrams, W.R., Malamud, D., Corstjens, P.L.A.M., Bau, H.H., 2009a. Lab Chip 9, 768–776.
Liu, D., Huang, Y., Wang, S., Liu, K., Chen, M., Xiong, Y., Yang, W., Lai, W., 2015. Food Control 51, 218–224.
Liu, G., Lin, Y.Y., Wang, J., Wu, H., Wai, C.M., Lin, Y., 2007. Anal. Chem. 79, 7644–7653.
Liu, G., Mao, X., Phillips, J.A., Xu, H., Tan, W., Zeng, L., 2009b. Anal. Chem. 81, 10013–10018.
Liu, J., Mazumdar, D., Lu, Y., 2006. Angew. Chem. Int. Ed. 45, 7955–7959.
Lönnberg, M., Carlsson, J., 2001. Anal. Biochem. 293, 224–231.
López-Marzo, A.M., Pons, J., Blake, A.D., Merkoçi, A., 2013a. Biosens. Bioelectron. 47, 190–198.
López-Marzo, A.M., Pons, J., Blake, A.D., Merkoçi, A., 2013b. Anal. Chem. 85, 3532–3538.
Lou, S.C., Patel, C., Ching, S.F., Gordon, J., 1993. Clin. Chem. 39 (4), 619–624.
Lyashchenko, K.P., Greenwald, R., Esfandiari, J., Greenwald, D., Nacy, C.A., Gibson, S., Didier, P.J., Washington, M., Szczerba, P., Motzel, S., Handt, L., Pollock, J.M., McNair, J., Andersen, P., Langermans, J.A.M., Verreck, F., Ervin, S., Ervin, F., McCombs, C., 2007. Clin. Vaccine Immunol. 14 (9), 1158–1164.
Mao, X., Ma, Y., Zhang, A., Zhang, L., Zeng, L., Liu, G., 2009. Anal. Chem. 81, 1660–1668.
Marquina, C., de Teresa, J.M., Serrate, D., Marzo, J., Cardoso, F.A., Saurel, D., Cardoso, S., Freitas, P.P., Ibarra, M.R., 2012. J. Magn. Magn. Mater. 324, 3495–3498.
Mazumdar, D., Liu, J., Lu, G., Zhou, J., Lu, Y., 2010. Chem. Commun. 46, 1416–1418.
Mei, Z., Qu, W., Deng, Y., Chu, H., Cao, J., Xue, F., Zheng, L., El-Nezamic, H.S., Wu, Y., Chen, W., 2013. Biosens. Bioelectron. 49, 457–461.
Merkoçi, A., 2010. Biosens. Bioelectron. 26, 1164–1177.
Moghadam, B.Y., Connelly, K.T., Posner, J.D., 2014. Anal. Chem. 86, 5829–5837.
Moghadam, B.Y., Connelly, K.T., Posner, J.D., 2015. Anal. Chem. 87, 1009–1017.
Morales-Narváez, E., Merkoçi, A., 2012. Adv. Mater. 24, 3298–3308.
Morales-Narváez, E., Pérez-López, B., Baptista Pires, L., Merkoçi, A., 2012. Carbon 50, 2987–2993.
Mudanyali, O., Dimitrov, S., Sikora, U., Padmanabhan, S., Navruza, I., Ozcan, A., 2012. Lab Chip 12, 2678–2686.
Noguera, P., Posthuma-Trumpie, G.A., van Tuil, M., van der Wal, F.J., de Boer, A., Moers, A.P.H.A., van Amerongen, A., 2011. Anal. Bioanal. Chem. 399, 831–838.
Nunes Pauli, G.E., de la Escosura-Muñiz, A., Parolo, C., Bechtold, I.H., Merkoçi, A., 2015. Lab Chip 15, 399–405.
Oh, J.S., Ha, G.W., Cho, Y.S., Kim, M.J., An, D.J., Hwang, K.K., Lim, Y.K., Park, B.K., Kang, B.K., Song, D.S., 2006. Clin. Vaccine Immunol. 13 (4), 520–524.
Park, J.M., Jung, H.W., Chang, Y.W., Kim, H.S., Kang, M.J., Pyun, J.C., 2015. Anal. Chim. Acta 853, 360–367.
Parolo, C., Merkoçi, A., 2013. Chem. Soc. Rev. 42, 450–457.
Parolo, C., de la Escosura-Muñiz, A., Polo, E., Grazu, V., de la Fuente, J.M., Merkoçi, A., 2013a. ACS Appl. Mater. Interfaces 5, 10753–10759.
Parolo, C., de la Escosura-Muñiz, A., Merkoçi, A., 2013b. Biosens. Bioelectron. 40, 412–416.
Parolo, C., Medina-Sánchez, M., de la Escosura-Muñiz, A., Merkoçi, A., 2013c. Lab Chip 13, 386–390.
Paterson, A.S., Raja, B., Garvey, G., Kolhatkar, A., Hagström, A.E.V., Kourentzi, K., Lee, T.R., Willson, R.C., 2014. Anal. Chem. 86, 9481−−99488.
Perfezou, M., Turner, A., Merkoçi, A., 2012. Chem. Soc. Rev. 41, 2606–2622.
Pesce, M.A., Chow, K.F., Hod, E., Spitalnik, S.L., 2006. Am. J. Clin. Pathol. 126 (1), 61–70.
Preechakasedkit, P., Pinwattana, K., Dungchai, W., Siangproh, W., Chaicumpa, W., Tongtawe, P., Chailapakul, O., 2012. Biosens. Bioelectron. 31, 562–566.
Qian, S., Bau, H.H., 2003. Anal. Biochem. 322, 89–98.
Qian, S., Bau, H.H., 2004. Anal. Biochem. 326, 211–224.
Qin, Z., Chan, W.C.W., Boulware, D.R., Akkin, T., Butler, E.K., Bischof, J.C., 2012. Angew. Chem. Int. Ed. 51, 4358–4361.
Qiu, W., Xu, H., Takalkar, S., Gurung, A.S., Liu, B., Zheng, Y., Guo, Z., Baloda, M., Baryeh, K., Liu, G., 2015. Biosens. Bioelectron. 64, 367–372.
Rastogi, S.K., Gibson, C.M., Branen, J.R., Aston, D.E., Branen, A.E., Hrdlicka, P.J., 2012. Chem. Commun. 48, 7714–7716.
Rayev, M., Shmagel, K., 2008. J. Immunol. Methods 336, 9–15.
Ren, M., Xu, H., Huang, X., Kuang, M., Xiong, Y., Xu, H., Xu, Y., Chen, H., Wang, A., 2014. ACS Appl. Mater. Interfaces 6, 14215–14222.
Renault, C., Koehne, J., Ricco, A.J., Crooks, R.M., 2014. Langmuir 30, 7030–7036.
Rivas, L., Medina-Sánchez, M., de la Escosura-Muñiz, A., Merkoçi, A., 2014. Lab Chip 14, 4406–4414.
Rohrman, B.R., Leautaud, V., Molyneux, E., Richards-Kortum, R.R., 2012. PLoS One 7 (9), 45611–45618.
Rundström, G., Jonsson, A., Mårtensson, O., Mendel-Hartvig, I., Venge, P., 2007. Clin. Chem. 53 (2), 342–348.
Ryu, Y., Jin, Z., Kang, M.S., Kim, H.S., 2011. BioChip J. 5 (3), 193–198.
Shi, C.Y., Deng, N., Liang, J.J., Zhou, K.N., Fu, Q.Q., Tang, Y., 2015a. Anal. Chim. Acta 854, 202–208.
Shi, L., Wu, F., Wen, Y., Zhao, F., Xiang, J., Ma, L., 2015b. Anal. Bioanal. Chem. 407 (2), 529–535.
Shukla, S., Leem, H., Kim, M., 2011. Anal. Bioanal. Chem. 401, 2581–2590.
Shyu, R.H., Shyu, H.F., Liu, H.W., Tang, S.S., 2002. Toxicon 40, 255–258.
Song, S., Liu, N., Zhao, Z., Ediage, E.N., Wu, S., Sun, C., Saeger, S.D., Wu, A., 2014. Anal. Chem. 86, 4995–5001.
Tang, D., Sauceda, J.C., Lin, Z., Ott, S., Basova, E., Goryacheva, I., Biselli, S., Lin, J., Niessner, R., Knopp, D., 2009. Biosens. Bioelectron. 25, 514–518.
Tang, X., Zhang, Z., Li, P., Zhang, Q., Jiang, J., Wang, D., Lei, J., 2015. RSC Adv. 5, 558–564.
Taton, T., Johnson, D., Guire, P., Lange, E., Tondra, M., 2009. J. Magn. Magn. Mater. 321, 1679–1682.
Torabi, S.F., Lu, Y., 2011. Faraday Discuss. 149, 125–135.
Van Dam, G.J., Wichers, J.H., Falcao Ferreira, T.M., Ghati, D., van Amerongen, A., Deelder, A.M., 2004. J. Clin. Microbiol. 42 (12), 5458–5461.
Walcarius, A., Minteer, S.D., Wang, J., Lin, Y., Merkoçi, A., 2013. J. Mater. Chem. B 1, 4878–4908.
Wang, D.B., Tian, B., Zhang, Z.P., Deng, J.Y., Cui, Z.Q., Yang, R.F., Wang, X.Y., Wei, H.P., Zhang, X.E., 2013a. Biosens. Bioelectron. 42, 661–667.
Wang, D.B., Tian, B., Zhang, Z.P., Wang, X.Y., Fleming, J., Bi, L.J., Yang, R.F., Zhang, X.E., 2015. Biosens. Bioelectron 67, 608–614.
Wang, L., Cai, J., Wang, Y., Fang, Q., Wang, S., Cheng, Q., Du, D., Lin, Y., Liu, F., 2014a. Microchim. Acta 181, 1565–1572.
Wang, L., Chen, W., Ma, W., Liu, L., Ma, W., Zhao, Y., Zhu, Y., Xu, L., Kuang, H., Xu, C., 2011a. Chem. Commun. 47, 1574–1576.
Wang, L., Lu, D., Wang, J., Du, D., Zou, Z., Wang, H., Smith, J.N., Timchalk, C., Liu, F., Lin, Y., 2011b. Biosens. Bioelectron. 26, 2835–2840.
Wang, X., Li, K., Shi, D., Xiong, N., Jin, X., Yi, J., Bi, D., 2007. J. Agric. Food Chem. 55, 2072–2078.
Wang, Y., Xu, Y., Wei, M., Gu, H., Xu, Q., Zhu, W., 2009. Mater. Sci. Eng. C 29, 714–718.
Wang, Y.K., Yan, Y.X., Ji, W.H., Wang, H., Li, S.Q., Zou, Q., Sun, J.H., 2013b. J. Agric. Food Chem. 61, 5031–5036.
Wang, Z., Li, H., Li, C., Yu, Q., Shen, J., de Saeger, S., 2014b. J. Agric. Food Chem. 62, 6294–6298.
Wang, Z., Zhi, D., Zhao, Y., Zhang, H., Wang, X., Ru, Y., Li, H., 2014c. Int. J. Nanomed. 9, 1699–1707.
Waters, W.R., Palmer, M.V., Thacker, T.C., Bannantine, J.P., Vordermeier, H.M., Hewinson, R.G., Greenwald, R., Esfandiari, J., McNair, J., Pollock, J.M., Andersen, P., Lyashchenko, K.P., 2006. Clin. Vaccine Immunol. 13 (6), 648–654.

Wen, H.W., Borejsza-Wysocki, W., DeCory, T.R., Durst, R.A., 2005. Anal. Bioanal. Chem. 382, 1217–1226.
Xia, X., Xu, Y., Zhao, X., Li, Q., 2009. Clin. Chem. 55, 1179–1182.
Xie, Q.Y., Wu, Y.H., Xiong, Q.R., Xu, H.Y., Xiong, Y.H., Liu, K., Jin, Y., Lai, W.H., 2014. Biosens. Bioelectron. 54, 262–265.
Xu, H., Chen, J., Birrenkott, J., Zhao, J.X., Takalkar, S., Baryeh, K., Liu, G., 2014. Anal. Chem. 86, 7351–7359.
Xu, H., Mao, X., Zeng, Q., Wang, S., Kawde, A.N., Liu, G., 2009. Anal. Chem. 81, 669–675.
Yang, H., Li, D., He, R., Guo, Q., Wang, K., Zhang, X., Huang, P., Cui, D., 2010. Nanoscale Res. Lett. 5, 875–881.
Yen, C.W., de Puig, H., Tam, J.O., Gómez-Márquez, J., Bosch, I., Hamad-Schifferli, K., Gehrke, L., 2015. Lab Chip 15, 1638–1641.
You, D.J., Park, T.S., Yoon, J.Y., 2013. Biosens. Bioelectron. 40, 180–185.
Zangheri, M., Cevenini, L., Anfossi, L., Baggiani, C., Simoni, P., Di Nardo, F., Roda, A., 2015. Biosens. Bioelectron 64, 63–68.
Zhang, F., Zou, M., Chen, Y., Li, J., Wang, Y., Qi, X., Xue, Q., 2014. Biosens. Bioelectron. 51, 29–35.
Zheng, C., Wang, X., Lu, Y., Liu, Y., 2012. Food Control 26, 446–452.
Zhou, J., Zhu, K., Xu, F., Wang, W., Jiang, H., Wang, Z., Ding, S., 2014. J. Agric. Food Chem. 62, 12061–12066.
Zhou, P., Lu, Y., Zhu, J., Hong, J., Li, B., Zhou, J., Gong, D., Montoya, A., 2004. J. Agric. Food Chem. 52, 4355–4359.
Zhu, X., Shah, P., Stoff, S., Liu, H., Li, C.Z., 2014. Analyst 139, 2850–2857.

Biosensors and Bioelectronics 92 (2017) 549–562

Contents lists available at ScienceDirect

Biosensors and Bioelectronics

journal homepage: www.elsevier.com/locate/bios

Mobile phone-based biosensing: An emerging "diagnostic and communication" technology

Daniel Quesada-González[a], Arben Merkoçi[a,b,*]

[a] Nanobioelectronics & Biosensors Group, Institut Català de Nanociència i Nanotecnologia (ICN2), Campus UAB, 08193 Bellaterra, Barcelona, Spain
[b] ICREA, Institució Catalana de Recerca i Estudis Avançats, Pg. Lluís Companys 23, 08010 Barcelona, Spain

ARTICLE INFO

Keywords:
Biosensor
Mobile phone
m-Health
Point-of-care
Diagnostic and communicate
3D-printing

ABSTRACT

In this review we discuss recent developments on the use of mobile phones and similar devices for biosensing applications in which diagnostics and communications are coupled. Owing to the capabilities of mobile phones (their cameras, connectivity, portability, etc.) and to advances in biosensing, the coupling of these two technologies is enabling portable and user-friendly analytical devices. Any user can now perform quick, robust and easy (bio)assays anywhere and at any time. Among the most widely reported of such devices are paper-based platforms. Herein we provide an overview of a broad range of biosensing possibilities, from optical to electrochemical measurements; explore the various reported designs for adapters; and consider future opportunities for this technology in fields such as health diagnostics, safety & security, and environment monitoring.

1. Introduction

1.1. Capabilities of mobile phones

On April 3rd, 1973, Martin Cooper, who is considered the father of mobile phone technology, made the first public call using a cordless phone, which weighed nearly 1 kg (Kennedy, 2013). Since then, mobile phones have evolved continuously, becoming ever smaller and more powerful. The first mobile phone did not have internal memory, and its functionality was limited to making calls. In contrast, modern mobile phones boast up to several Gb of memory and their range of applications is quite wide, spanning high definition (HD) photography and video; internet browsing; sending and receiving emails and multi-media messages; electronic payment; videogames; music; health monitoring; etc. Moreover, these phones can regularly be upgraded by simply installing new applications.

In fact, the power of current mobile phones, also called *smart-phones*, is far beyond that of the computer that controlled Apollo 11, first rocket landing on the Moon (NASA). That computer had a processing unit of 1 MHz and an internal memory of roughly 4 kB. In comparison, the processing speed of an iPhone 6s is roughly 2 GHz and its storage capacity is 128 Gb. This means that today, anyone can carry in their pockets 32 million times more information, and access it 2000 times faster, than could the Apollo 11 crew.

Intriguingly, modern mobile phones may contain up to 70 different elements (Rohrig, 2015), including indium and rare-Earth metals. Indium, which, in its oxide form, is necessary for the fabrication of touch screens, is in fact a controversial element, due its abundance on Earth is not clear. Some scientists affirm that there is still more indium in the Earth's crust, whereas others believe that the indium mines will soon be fully depleted. A possible candidate to substitute indium on tactile screens is graphene, as it derives from carbon, which is cheap and abundant; its amenability to touch-sensitive devices has already been demonstrated (Baptista-Pires et al., 2016); and its physical properties enable flexible and more robust screens. Regarding mobile phone touch screens, there exist two main types: resistive and capacitive screens. Resistive screens are based on pressure: when the screen is pressed, the resistive layers enter into contact. In contrast, capacitive screens are based on electrical charge, which is modified when the screen is touched. Under the screen is located the display, also made of rare elements such as yttrium, lanthanum, europium or gadolinium. These elements are responsible for the color and brightness of the display. Other elements, such as tin, copper, silicon and iron, are also present in mobile phones: specifically, in the circuitry.

Abbreviations: AR, augmentedreality; AuNPs, gold nanoparticles; CV, cyclic voltammetry; DCT, "diagnostic and communicate" technology; ELISA, enzyme-linked immuno-sorbent assay; GPS, global positioning system; HD, high definition; LED, light-emitting diode; LF, lateral flow; LOD, limit of detection; NFC, near-field communication; RGB, red-green-blue; SERS, surface-enhanced Raman spectroscopy; PCR, polymerase chain reaction; POC, Point-of-care; QD, quantum dots; QR, code, quick response code; SPCE, screen printed carbon electrodes

* Corresponding author at: Nanobioelectronics & Biosensors Group, Institut Català de Nanociència i Nanotecnologia (ICN2), Campus UAB, 08193 Bellaterra, Barcelona, Spain.
E-mail address: arben.merkoci@icn2.cat (A. Merkoçi).

http://dx.doi.org/10.1016/j.bios.2016.10.062
Received 15 June 2016; Received in revised form 4 October 2016; Accepted 23 October 2016
Available online 27 October 2016
0956-5663/

Noble metals such as gold and silver can also be found in the circuitry, albeit in smaller amounts.

A crucial feature of mobile phones is their cameras. Modern mobile phones have at least two cameras: one on the front and one on the back, the latter normally of higher resolution. Some phones have two cameras on the back, to enable 3D imaging. However, a camera is much more than its lens: it includes ambient light sensors, stabilizers, optical zoom machinery, night-vision filters, and many other electronics for image enhancement. The quality of mobile phone camera images is on the order of megapixels, which means that each image is divided into millions of monochromatic portions. However, the number of megapixels are not the only parameter that defines the quality of a camera: a camera with fewer megapixels can obtain better quality photos and videos than a camera with a higher value, provided that the lens and sensors of the former are superior in terms of controlling ambient light, contrast, exposure time, etc.

As a last highlight, the several communication possibilities integrated into mobile phones, such as Bluetooth, WiWi-Fi, 3G/4G, near-field communication (NFC) and global positioning system (GPS), will help facilitate the future construction of Smart Cities. In the Smart City concept, sensors are located everywhere to report on urban parameters (e.g. traffic, weather and pollution) and are connected to mobile phones to form an expansive network. Thus, the combination of GPS and internet connections can yield accurate, real-time information on public transportation, parking spaces, air or water quality, etc. Lastly, but equally important, is NFC, a relatively young connection technology in which radio tags are used to label objects for close-range tracking and control. Such technology can be used in conjunction with mobile phones in a Smart House environment: for instance, as soon as someone enters their house, a central controller could detect their phone and automatically turn on the lights, turn off the alarm, adjust the heating/cooling, etc.

1.2. Mobile phone-based biosensing

Among the major concerns of mobile phone users is health, an area that can greatly benefit from biosensors (Nanhore and Bartere, 2013; Nasi et al., 2015). A mobile phone contains all the components required for a common analytical reader: the screen, which can act as display and controller; an input to capture a signal, which could work via the camera (Otten et al., 2013; Chen et al., 2014; Coskun et al., 2013a; Wei et al., 2014a; Oncescu et al., 2014); ambient light sensors (Fu et al., 2016) and headphone jacks (Wang et al., 2015); memory to store the data; and several wired and wireless (Wi-Fi, Bluetooth, NFC, etc.) connectivity modes. Therefore, considering the billions of mobile-phone users in the world, these phones are an invaluable resource for biosensing. This premise leads us to the emerging “diagnostic and communication” technology (DCT).

The data transmission capabilities of mobile phones are important for health applications: for example, through an internet connection, users can access data libraries (e.g. their medical records) or send biometric measurements to health specialists in real time. In addition, connectivity through GPS could enable studies on global health (e.g. tracking of pandemics) or even environmental monitoring. Along these lines, Wei et al. (2014a) used a Google Maps-based interface on a mobile phone to perform spatiotemporal mapping of mercury contamination in water.

Regarding the possibilities for signal measurement, most of the mobile phones currently on the market feature an HD camera that can detect visual stimuli at high resolution and sensitivity, either in solution (Otten et al., 2013; Chen et al., 2014; Coskun et al., 2013a; Wei et al., 2014a) or on a substrate such as paper (Shafiee et al., 2015; Guan et al., 2014; You et al., 2013). Paper is a cheap and abundant material on which several types of point-of-care biosensors, such as lateral flow (LF) strips, have been developed (Parolo and Merkoçi, 2013; Quesada-González and Merkoçi, 2015). Coupling of different gadgets has enabled optical measurement for colorimetric or fluorescent (Wei et al., 2013; Coskun et al., 2013b; Roda et al., 2014a), microscopic (Tseng et al., 2010; Navruz et al., 2013) or surface plasmon resonance (SPR) (Roche et al., 2011; Fu et al., 2016; Preechaburana et al., 2012) applications. Further possibilities to translate the signal include electrochemical measurements (Wang et al., 2015; Nemiroski et al., 2014; Sun et al., 2014), and even magnetoresistive (Choi et al., 2016) or NFC-based measurements (Azzarelli et al., 2014).

Sometimes adapters or other devices need to be connected to the mobile phone, in order to maintain the distance between the camera and the sample constant; to make a dark chamber for fluorescence; or simply to integrate the biosensing process without compromising the phone’s portability. However, creating a universal design is challenging, as each mobile phone has a different design and size. One possible solution for this problem is 3D-printing at home. Three-dimensional printers and related materials are becoming more affordable and offering increasingly higher resolution and material strength, thereby enabling ready fabrication—at home or in the laboratory—of personalized adapters for any mobile phone.

An interesting tool to connect mobile phones to biosensors or other devices, within the reach of any user, is the open-source platform Arduino. This combination of user-friendly software and tunable hardware can be configured to execute several tasks, including remote switching; facial recognition; motion detection; weather sensing; artificial intelligence; and even control of microfluidic systems (Chen et al., 2014). Furthermore, Arduino is remarkably affordable (the cheapest version costs roughly $50) and easy to use (it can be assembled by hand), embodies an open-source philosophy (the hardware and the software are both expandable), and offers wide compatibility with different operating systems (Windows, Linux or Macintosh).

In the future, other DC-based devices could coexist with mobile phones. A past example of such a device was Google Glass, a pair of spectacles designed to integrate augmented reality (AR) into daily life. This device had an integrated camera, such that it theoretically could have been linked directly to a biosensor (Feng et al., 2014). Unfortunately, the project to bring Google Glass to market has tentatively been stopped. Currently, Google is working on Google Lens (Google Official Blog), a smart contact lens that can perform biometric measurements (e.g. measuring glucose levels in the user’s tears) and then communicate the results directly to a mobile phone. Other notable devices that could be connected to mobile phones include electronic bandages (Kassal et al., 2015), drones (Priye et al., 2016) and videogame systems (Lee et al., 2011; Karim et al., 2012). Furthermore, new materials such as nanopaper (Morales-Narváez et al., 2015a) and graphene (Baptista-Pires et al., 2016) will soon be exploited for mobile phone-based biosensing.

Over the past few years, various reviews on wearable sensors (Patel et al., 2012) and on the use of mobile phones in biosensing (Vashist et al., 2014; Preechaburana et al., 2014; Xu et al., 2015; Zhang and Liu, 2016; Roda et al., 2016; Comina et al., 2016; Sun et al., 2016a) have been published. These focus mostly on different measurement methods. In contrast, in the present review, we provide a detailed discussion of the capabilities of mobile phones, the different adapters that can be designed for biosensing and how such measurements can be taken. Moreover, we discuss many of the companies currently working with this technology and consider how the marriage of biosensing to such smart devices will influence medicine in the future.

2. Optical-based biosensors

Optical-based biosensors are advantageous for their simplicity and low cost. Using these devices, a qualitative response (e.g. Yes/No) can often be gauged by the naked eye, although quantitative measurement requires an optical detector. In fact, the area of quantification is one in

which mobile phones are poised to play a decisive role.

2.1. Colorimetric detection

Mobile phone cameras can recognize small differences in color tone, as can be confirmed even in simple home experiments. This capability is based on the Beer-Lambert law, which relates the concentration of an analyte to the intensity of its color in solution (Kehoe and Penn, 2013; Otten et al., 2013; Knuston et al., 2015; Montangero, 2015; Koesdjojo et al., 2015; Kuntzleman and Jacobson, 2016). A mobile phone app that can assign quantifiable values to these tonality differences could be used to maximize the potential of mobile phones coupled to optical-based biosensors as DCTs.

The simplest apps for performing colorimetric detection are based on the detection of the primary colors: red, green and blue (RGB). The standard RGB scale assigns a whole-number value from 0 to 255 for each of these three colors in a given tone, such that [0, 0, 0] corresponds to absolute black and [255, 255, 255], to true white. A good HD camera should be able to distinguish until 16777216 colors. Yetisen et al. (2014) developed a smartphone application algorithm for commercial colorimetric tests based on RGB detection. However, accurate use of colorimetric measurements requires careful control over parameters such as ambient light, temperature, and the distance between the camera and the sample.

Otten et al. (2013) used a digital camera to capture images from an enzyme-linked immuno-sorbent assay (ELISA) in which they used gold nanoparticles (AuNPs) used as resolving agents, such that the intensity of the red in each cell corresponded to the quantity of protein immobilized onto it. The authors were able to count the number of pixels. They reported coupling of a mobile phone to this system to obtain a low-cost method for detection of different proteins. However, their system was neither portable nor user-friendly. An attempt to make ELISA tests more portable was made by Chen et al. (2014). They miniaturized the assay into a lab-on-a-chip microfluidic system controlled by an Arduino device that was able to automate the pumps and thus, drive the sample across the channels. The Arduino controller was connected to a mobile phone that served two purposes: it was an energy supply, and captured images from the incubation chamber for subsequent RGB analysis.

Berg et al. (2015) reported another interesting portable ELISA system, in which they 3D-printed a housing for the ELISA plates (Fig. 1). As shown in Fig. 1a, the device comprises a group of light-emitting diodes (LEDs) of blue wavelength that illuminate the 96 wells of an ELISA plate. The transmitted light is redirected via optical fibers to the camera of the mobile phone, for signal reading. Fig. 1b-d illustrates the device from different perspectives. Fig. 1e shows the camera reading the signal from the optical fibers, whereby each point corresponds to a single well on the ELISA plate (Fig. 1f). The device appears to be relatively portable and permits both qualitative and quantitative measurements with an acceptable error range and user-friendly interface. However, it has a few drawbacks: for example, it requires external batteries for the LEDs and it lacks an automation process, as the sampling and loading steps are not integrated into the device.

Coskun et al. (2013a) and Wei et al. (2014a) each reported obtaining a user-friendlier DCT device by integrating housings onto mobile phones (Fig. 2). The former group created a food-allergen detection platform with a very easy-to-use interface. The software gives step-by-step instructions to the user on the mobile phone screen: first the allergen is chosen on the app; then, the app explains to the user how to treat the sample (including which reagents they must add) and prepare the control solution; finally, the camera performs the analysis and displays the results. The system has two components: an LED, which serves as a light source that permeates both the sample and the control solutions; and the mobile phone camera, which works as a relative absorbance reader (Fig. 2a). Wei et al. (2014a) developed a similar device except that it had two separate light sources: green and red. These two sources simultaneously provided four data points: red-control, red-sample, green-control and green-sample (Fig. 2b). Combining these four values, the authors obtained a normalized response to quantify the amount of mercury in water. They achieved a limit of detection (LOD) of 3.5 ppb, a value close to the maximum mercury concentration allowed in consumer water in the USA. As we mentioned in the introduction, integration of GPS into mobile phones has also enabled spatial mapping of mercury-contaminated water areas through a Google Maps-based interface for environmental monitoring (Fig. 2c).

Comina et al. (2015) developed an adapter for glucose detection that was even smaller than the adapters mentioned above. Specifically, they miniaturized a microfluidic circuit that contained unidirectional valves and manual pumps, and then placed the circuit over the phone camera. By 3D-printing the lens, they were able to obtain enhanced images.

Performing a field test can be tedious, even with a portable device, because the user must still bring along numerous reagents, sampling materials, etc. Moreover, field assays often require pre-treatment of the sample and careful control of the incubation times. However, many of these problems can be circumvented by developing an assay that runs on a substrate, rather than in solution, as the former type occupies less space and normally does not require sample pre-treatment: the sample is simply added and allowed to flow through the substrate.

The most commonly used substrate is paper, which has been used in several types of biosensors (Parolo and Merkoçi, 2013) due to its simplicity, natural abundance (cellulose is the most abundant polymer on Earth), low-cost production and recyclability. Moreover, in paper-based biosensors microfluidics can be easily generated by simply printing out the desired features using a standard printer or ink-jet printer and hydrophobic materials such as wax (Wang et al., 2014; Chun et al., 2014), polystyrene (Zhang et al., 2015; Shafiee et al., 2015) or ink (Lopez-Ruiz et al., 2014). This approach can be used to fabricate channels, cells, wells and other types of chambers, which can subsequently be photographed using a mobile phone camera.

Guan et al., 2014 performed pioneering work by developing a paper-based assay for blood-typing, whereby they printed hydrophobic bar-channels, made of alkyl ketene dimer, onto Kleenex® paper. In their assay, drops of a blood sample are added to three different channels: one channel to determine the presence of antigen A; another one, for antigen B; and a third channel, to ascertain the Rh factor. Then, buffer is added to help the blood flow through the channels. Finally, the results are transferred to a mobile phone, which informs the user of the blood type (Fig. 3).

Lateral flow (LF) biosensors (Quesada-González and Merkoçi, 2015) and similarly-structured paper strips are easy to integrate into mobile phones, owing to their simple architecture and to the fact that they can usually just be dipped into the sample and subsequently read by a mobile phone camera. Examples of this approach have been reported by Mudanyali et al., 2012, Lee et al., 2013a, You et al., 2013, Oncescu et al., 2013, 2014 and Lee et al., 2014. Fig. 4 (taken from You et al., 2013) illustrates how LF strips are introduced onto an adapter (previously fabricated by stereolithographic 3D-printing) for reading via light-scattering. Mainly, these adapters exploit the mobile phone flash, as a light source and the camera, with collimating lenses, as the detector (You et al., 2013; Oncescu et al., 2013, 2014). Alternatively, in other designs (Mudanyali et al., 2012; Lee et al., 2013a, 2014) an LED is used as the light source. Using LEDs facilitates monitoring of the incipient light (e.g. wavelength, exposure time, light angle and intensity), but requires the use of an external battery. An example of test-strip reading and signal extraction is provided in Fig. 5 (from Mudanyali et al., 2012). The test-strip image is adapted to gray-scale, and then the signaling areas are compared against the background, so that the software can decide whether the signal corresponds to a negative or a positive sample. Importantly, the data recorded by their

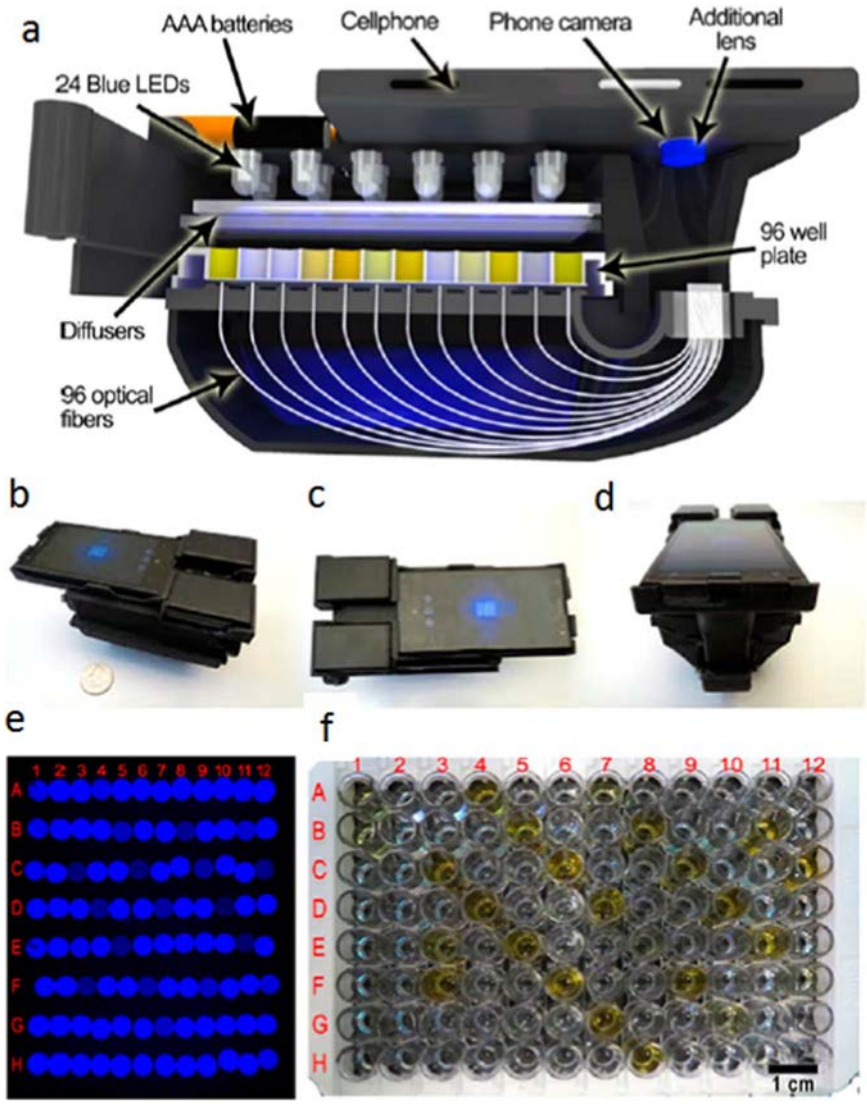

Fig. 1. Mobile phone adapter to perform ELISA tests. (a) Scheme of the device, (b) (c) (d) overview of the device and (e) image obtained from (f) ELISA plate. Adapted with permission from Berg et al. (2015). Copyright 2015 American Chemical Society.

app can be used to create a spatiotemporal map for tracking the possible spread of a disease. As in the previously mentioned work of Wei et al. (2014a), this was based on a Google Maps interface.

In addition to analysis of contaminants and pathogens, colorimetric detection on mobile phones can also be used to measure pH. For example, Lopez-Ruiz et al. (2014) developed a microfluidics-on-paper platform to simultaneously measure pH and nitrite levels in different cells (Fig. 6a). Their assay is based on colorimetric reactions and the results are read by the phone camera. In this case, the ambient light is controlled with the flash, such that no adapter is needed. Alternatively, Oncescu et al. (2013), used an adapter to read pH strips (Fig. 6b) as an indirect measurement of sodium ion levels in sweat or saliva samples. Sodium concentration is correlated with the probability of suffering muscle cramps while playing sports; with the risk of enamel decalcification in saliva; and with the risk of calcium removal from teeth, due to low pH. The strips can be stored in a compartment included in the adapter (Fig. 6b 1), thus making the system highly portable. The user can check the pH of their sweat by simply rubbing the strip onto their skin, or the pH of their saliva by spitting on the strip (Fig. 6b 2). Once the sample is added, the strip is placed onto the adapter (Fig. 6b 3), and then flash of the mobile phone is used as light source and the camera, as reader, as in the previously mentioned examples. Finally, the mobile phone screen displays the results (Fig. 6b 4), comprising the pH value (measured directly) and the sodium-ion concentration (as calculated based on the former, using special software).

Surprisingly, a mobile phone camera alone can be sufficient to detect harmful elements in a sample, without the need for paper, antibodies, colorimetric reagents or labeling particles. For instance, Liang et al. (2014) used a phone to detect the bacterium *Escherichia coli* on spoiled meat. Due to the refractive index of bacteria, which is generally quite high, their presence can be detected with the help of a light source, which could be a lamp or an LED. Liang et al. (2014) were able to detect *E. coli* on beef samples without any pre-treatment, by measuring the scattered light from a LED with the mobile phone camera. However, detection of bacteria by this method is only possible at high concentrations. They tested several angles between the colliding light and the detector, obtaining their best LOD, 10 colony-forming units per mL, at an angle of 45º.

Another application that can be performed with a mobile phone camera alone is measurement of heart rate (Jonathan and Leahy, 2010; Pal et al., 2014; Huang and Dung, 2016). In this case, the user simply places their finger on the camera and, with the help of a flash or LED light, the camera subsequently records small variations in the pixels. It then uses the values to calculate the user's heart rate.

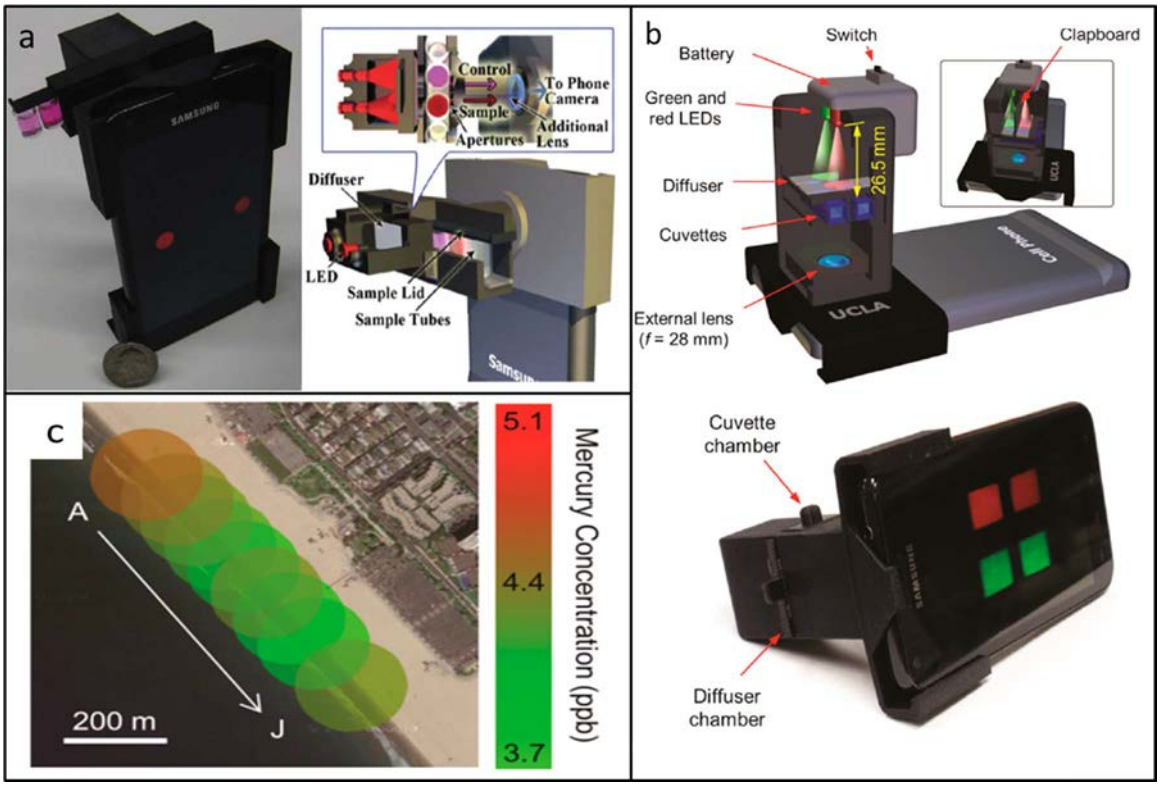

Fig. 2. Integration of different housings on mobile phones to perform colorimetric assays. (a) Colorimetric mobile phone reader for food allergens. Adapted with permission from Coskun et al. (2013a). Copyright 2013 Royal Society of Chemistry. (b) Colorimetric mobile phone reader for mercury detection and (c) spatial mapping of the contaminated areas registered with this device. Adapted with permission from Wei et al. (2014). Copyright 2014 American Chemical Society.

2.2. Luminescence and fluorescence detection

An advantage of luminescent DCT–based biosensors is that they typically exhibit higher sensitivity than devices based exclusively on colorimetric reading. Moreover, they do not require a source of light, excluding those devices based on fluorescent methods. This means that luminescent DCT–based biosensors can be created using only a mobile phone camera and an adapter, the latter of which often serves as a dark chamber.

Regarding fluorescence detectors, common choices for the source of the excitation light include lasers (Wei et al., 2013; Coskun et al., 2013b; Yu et al., 2014) and LEDs (Zhu et al., 2011, 2013; Awqatty et al., 2014). Lasers have the advantage that their light is monodirectional and powerful, and can penetrate the sample without losing too much signal on the way. However, the laser must remain motionless during the assay and the beam has to be placed perpendicular to the detector (the camera) to avoid reading errors or damaging the sensor. This in turn requires a wider and more complex adapter, one which is often equipped with mirrors to redirect the beam. A representative example of the resolution that lasers can provide for fluorescent techniques can be found in the work of Wei et al. (2013), who used a mobile phone camera to take images of isolated fluorescent nanoparticles 100 nm in diameter. Alternatively, LEDs, which are less powerful than lasers, can be used without the risk of damaging the camera or the user's eyes. Moreover, LED adapters are simpler, amenable to miniaturization and portable. This is another case in which the Arduino controller can be integrated into the system, as exemplified by Awqatty et al. (2014). They controlled the LED light emission using the mobile phone itself as energy source; as such, no external batteries were required.

Concerning adapters, they must completely isolate the system from ambient light to provide a dark chamber in which light emission can be measured without any background noise. Development of such chambers, which are important for both fluorescence (Coskun et al., 2013b; Lee et al., 2013b) and chemiluminescence (Roda et al., 2014a) work, should be easy through 3D-printing. Chemiluminescent assays exploit the fact that the sample can be excited without any light source: instead, it is excited using enzyme-coupled reactions, whereby the time elapsed between the addition of reagents and the integration of the samples in the device is not negligible. Roda et al. (2014a) 3D-printed a mobile phone dark chamber for a chemiluminescence assay to detect lactate in sweat or saliva. They achieved an LOD lower than that of commercially available colorimetric assays. Thus luminescence-based assays, which give a relatively strong response, should enable sample dilution to reduce matrix noise during analysis of complex samples.

Barbosa et al. (2015) integrated a magnifying lens into a mobile phone (Fig. 7a) to register the intensity of the fluorescence occurring on a microfluidic system (Fig. 7b) with good sensitivity and low error. The critical factor in the assay was the choice of the circuit material: fluorinated ethylene propylene co-polymer (FEP-Teflon), which provides a high index of transparency to avoid signal loss. Interestingly, the microfluidics portion is flexible, making the device relatively portable; however, the method is slower than other methods, such as test strips.

Over the past few years, quantum dots (QD) have risen to great importance for fluorescence biosensing (Noor and Krull, 2014; Morales-Narváez et al., 2015b) as well as for DCTs. For example, Petryayeva and Algar (2014) performed RGB measurements on images taken with a phone camera in a multiplex assay in which they used QD bioconjugates as labels. The QD emission is reduced by quencher molecules in the presence of an enzyme that can be linked to the QD and to the respective quencher. Using this method, the authors were able to measure the activity of the enzyme in a range of picomolar to nanomolar concentrations.

Regarding the materials mentioned in point 3.1 to fabricate microfluidic channels on paper substrates (Wang et al., 2014; Chun et al., 2014; Zhang et al., 2015; Shafiee et al., 2015; Lopez-Ruiz et al., 2014), another option is the use of photoresists. For instance, Park

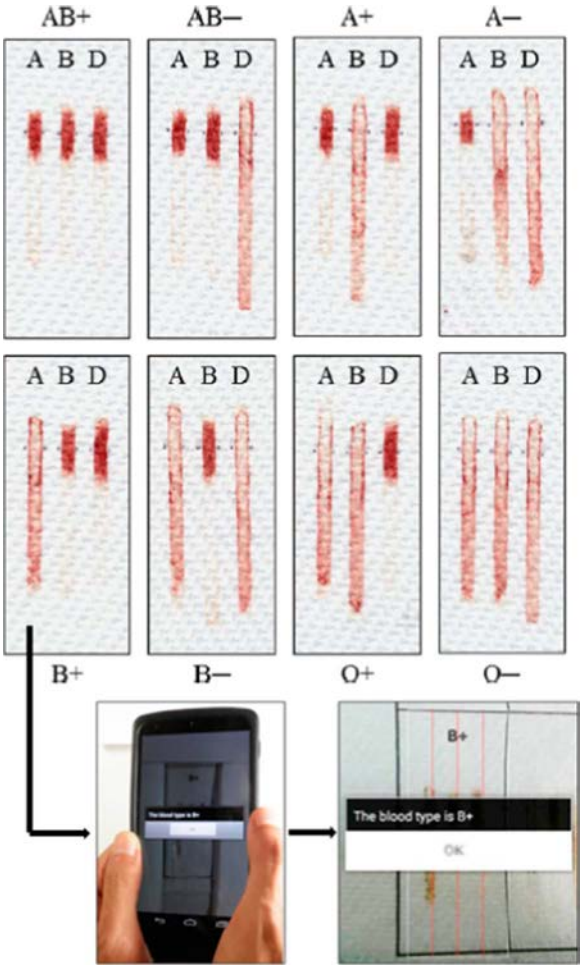

Fig. 3. Use of a mobile phone to interpret a paper-based biosensor for the determination of blood type. Adapted with permission from Guan et al. (2014). Copyright 2014 American Chemical Society.

et al. (2013) developed a paper-based system for the detection of *Salmonella* based on light scattering. This required a light source and calibration of the angle between the source of light, the paper and the detector. However, the authors were ultimately able to reduce the device down to three components: the paper component, a fluorescent lamp and a mobile phone (which automatically performed all the calibration in less than a minute, using special software).

Paper-based biosensors can perform luminescence assays and, as mentioned above, can be coupled to mobile phones. For example, Roda et al. (2014b), 3D-printed an adapter for mobile phones (Fig. 8a, b, c) and reported proof-of-principle luminescence assays done on paper membranes coupled to the device. The membranes were introduced onto a cassette with an interesting design (Fig. 8d). The reagents for the chemiluminescent reaction are pre-stored in the cassette, inside a reservoir that prevents them from mixing untimely; thus, field experiments can be performed using only the mobile phone and the cassettes. The sample is added onto the membrane, the cassette is introduced into the mobile phone (Fig. 8e) and, with a soft coup, the reagents should be liberated to react, and the measurement subsequently taken (Fig. 8f). There are also reports about the coupling of fluorescent (Lee et al., 2013b; Rajendran et al., 2014) or chemiluminescent (Zangheri et al., 2015) LF biosensors to mobile phones. Adapters for the former are wider and less portable than those for the latter, as they require insertion of LEDs, batteries and mirrors.

2.3. Surface Plasmon Resonance (SPR)

Surface Plasmon Resonance (SPR) is a physical phenomenon that occurs when the electrons of a conductive material oscillate due to the excitation provoked by a source of energy, which could be incident light, reemitting part of this energy. SPR has important implications for biosensing, as small changes on the surface of the material (e.g. a crystal or a nanoparticle with antibodies conjugated on its surface) will provoke detectable changes in the reemitted energy. In optics, this phenomenon is often identified by a shift in the maximum absorbance peak of the reflected light. SPR is advantageous in that it is a label-free technique that has high sensitivity yet requires only small volumes of analyte.

Nanoparticle surfaces are surrounded by strong electromagnetic fields that make the SPR effect stronger, especially for noble metals such as gold (Roche et al., 2011) or silver (Fu et al., 2016). This in turn facilitates measurement by mobile phone. Fu et al. (2016) developed a very small adapter for SPR measurements using AgNPs and AuNPs. The most interesting point of their device is that, instead of using the mobile phone camera as detector, they use the ambient light sensor (Fig. 9), a component that is integrated in most current mobile phones, where it regulates the intensity of the display according to the ambient light. They claim that using this sensor for their adapter obviates the need for a large dark room and for a lens to refocus the emitted light, thus providing a cheap sensor (less than $1). Gallegos et al. (2013) fabricated a mobile phone adapter with a photonic crystal fabricated on a plastic substrate attached to a lens system. To demonstrate the feasibility of SPR detection on mobile phones using crystals, they incubated a monolayer of proteins on the crystal and recorded the spectra variations.

Liu et al. (2015) created a quite interesting device that they fabricated with optical fibers to redirect light from a mobile phone flash (an LED light source) to its camera (Fig. 10a, b, c, d). The device has a flow cell (Fig. 10a) into which samples and reagents are placed. The image obtained from glass fibers on the mobile phone can be observed on Fig. 10d (measurement, control and reference channels) and its respective data processing. Another interesting device was reported by Preechaburana et al. (2012), who used the mobile phone screen itself as the light source (Fig. 10e, f, g). An advantage of this method is that the emission wavelength can be easily controlled by simply changing the color on the display (in this case, between green and red).

When plasmons are excited by a stronger source of energy (e.g. a laser), the electric fields surrounding the metallic material are increased, resulting in Raman scattering, a spectroscopic technique named after the physicist Sir Chandrasekhara Venkata Raman. Ayas et al. (2014) applied Surface-enhanced Raman spectroscopy (SERS) to a mobile phone to count molecules in a sample. Although the experiment was performed with a non-portable Raman microscope, they proved that a phone camera could detect single sparkles related to individual molecule vibrations.

2.4. Microscopy

Optical mobile phone-based biosensing has yet another major application: microscopy. Even before the arrival of smart phones, there had already been a few reports of microscopes coupled to mobile phones (Breslauer et al., 2009; Tseng et al., 2010). Breslauer et al., 2009 designed a prototype of a portable fluorescence microscope (Fig. 11a) with the images obtained from 6-μm fluorescent beads. An LED was used as light source, and the condensing lens from a real microscope provided the imaging amplification. Tseng et al. (2010) developed a lens-free microscopy technique based on hologram production and interpretation. In this method, the light emitted by an LED is scattered by the sample, thus providing a hologram that is captured and translated by the mobile phone. Fig. 11b illustrates the

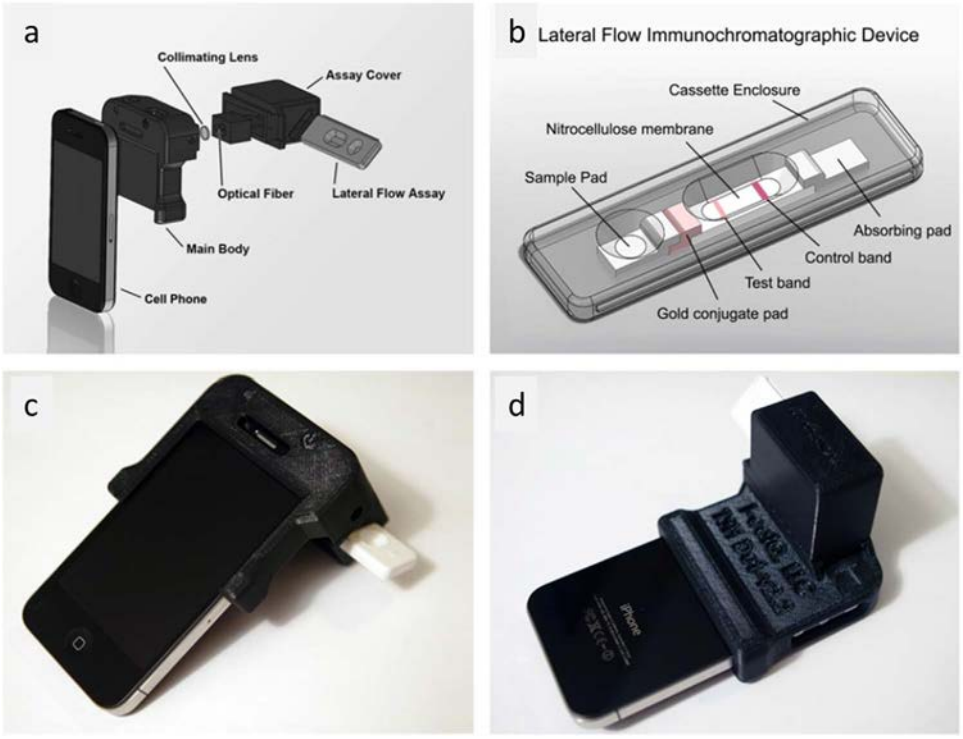

Fig. 4. (a) Schematic representation of LF adapter for mobile phones, (b) LF cassette composition and (c) and (d) images of the real adapter. Adapted with permission from You et al. (2013). Copyright 2013 ElSevier.

design of the microscope as well as the comparison between a 10-μm bead observed on a real microscope and the corresponding hologram from the new technique (alongside its reconstruction, which closely resembles the original bead).

More reports about these optical devices have recently appeared, with several interesting applications in biosensing such as microbial detection (Kadlec et al., 2014), DNA imaging (Khatua and Orrit, 2013; Wei et al., 2014b), blood-cell characterization (Navruz et al., 2013), etc. Regarding the latter, Navruz et al. (2013) designed a device in which the sample was placed into contact with a glass tape that crossed two collimating lenses up to a mobile phone camera. If the glass tape manually rotated, but the sample is held fixed, the device can obtain images from different angles, which, when combined with a customized app, give high-resolution images such as that shown in Fig. 12a.

Digital diffraction is an interesting tool for performing microscopy measurements with a mobile phone (Im et al., 2015, 2016). This technique compares two light beams (one of which passes through the sample), and then constructs a diffraction scheme (Fig. 12b). The diffraction is normally applied on beads or nanoparticles, where the analyte is captured by bioreceptors. Comparison of the results to those from blank samples enables biosensing. Another interesting strategy for microscopy was implemented by Lee and Yang (2014), who described a device that can work with only ambient solar light. In this device, the sample is placed just over the phone camera lens, which

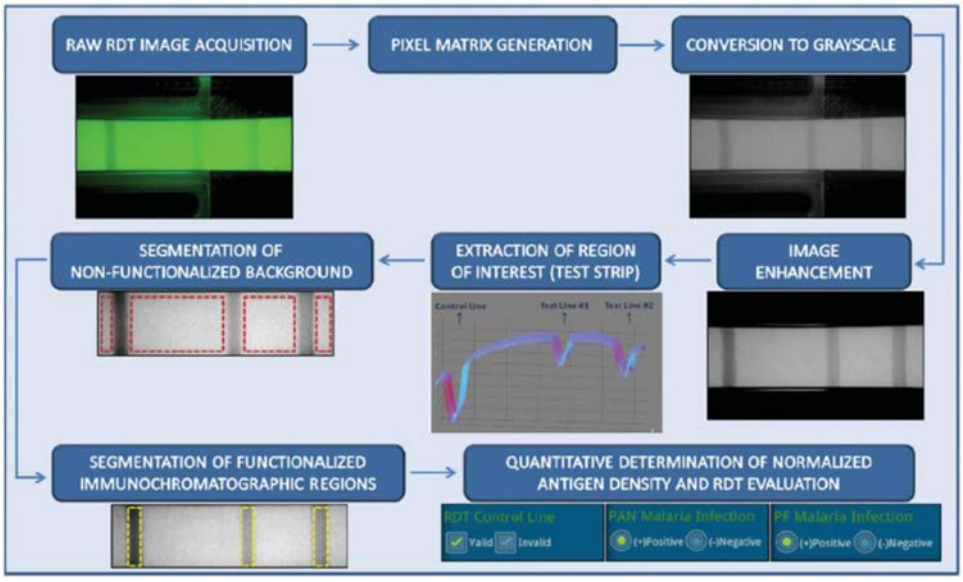

Fig. 5. Different steps during the image processing of a LF strip with mobile phone software. Adapted with permission from Mudanyali et al. (2012). Copyright 2012 Royal Society of Chemistry.

Fig. 6. pH detection by using mobile phones as colorimetric readers. (a) Detection on paper microfluidic system. Adapted with permission from Lopez-Ruiz et al. (2014). Copyright 2014 American Chemical Society. (b) Detection by using test strips: (b1) Strip is removed from storage compartment, (b2) sample, sweat or saliva, is applied, (b3) the strip is placed on the adapter, in front of the camera and (b4) response is obtained. Adapted with permission from Oncescu et al. (2013). Copyright 2013 Royal Society of Chemistry.

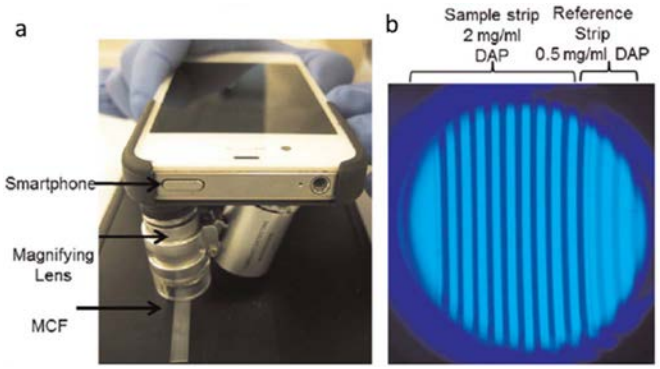

Fig. 7. (a)Magnifying lens used to read the fluorescence on a microfluidic system (b). Adapted with permission from Barbosa et al. (2015). Copyright 2015 ElSevier.

detects the shadows under the object from the sunlight. The user has to move the mobile phone in order to obtain several pictures that are then combined (in specially designed software) to produce the imaging, similarly to in the previously described holographic technique of Tseng et al. (2010). Recently, Zhang et al. (2016) published a study on holographic microscopy, in which they measured tissue samples with a free-lens microscope and combined the images then with colored images taken with a mobile phone microscope. The combination provided high-resolution images with high color fidelity.

3. Electrochemical biosensors

Electrical measurements often permit sample quantification with higher sensitivity and reproducibility than do optical methods. Nevertheless, it is impossible to interpret electrical response without a device, and the assemblage of electrodes is complicated and is sensitive to environmental conditions. Fortunately, electrodes can now easily be miniaturized and produced at much lower cost than before, thus eliminating the assembly procedure and making them adaptable to mobile phones and other common portable devices (e.g. glucose detectors, wearable hear-rate monitors, etc.) In fact, electrodes can perform many functions. For example, Chen et al. (2014), in their previously mentioned ELISA assay using the Arduino controller, employed copper electrodes to control the flow rate in the microfluidics. The electrodes were powered by the mobile phone through the Arduino connection.

Among the different electrochemical detection techniques, cyclic voltammetry (CV) and chronoamperograms stand out for the simplicity of interpreting the results. Nemiroski et al. (2014) applied both techniques via a portable device compatible with several types of electrodes such as glucose tests (Fig. 13a) or SPCE (screen printed carbon electrodes). Their device takes advantage of mobile-phone connectivity to send the analytical data to a global network and subsequently relay a message with the results back to the user. Wang et al. (2015) developed a CV-based device for nitrate sensing in water that, curiously, is connected to the mobile phone via the audio jack (Fig. 13b). There are two main advantages of using the audio jack connection (Wang et al., 2015; Sun et al., 2014, 2016b): it can simultaneously send and receive information, and nearly all mobile phones have one (however, it has been omitted from some of the latest smartphone models, such as the iPhone 8 and Moto Z). Another connection option is the USB port. However, not all USB ports can simultaneously send and receive information (only the newest ones), and their design often differs with each mobile phone, meaning that a universal device would be difficult to create. Devices can also be powered by a USB connection. Lillehoj et al. (2013) reported a microfluidic system with integrated electrodes (Fig. 13c) connected to a mobile phone (Fig. 13d). Their system was able to perform the assay, run the fluidics and acquire the amperometric measurements in 15 min. The flow is moved by capillarity, so no pumps are required.

Impedance is an electrical technique that permits the detection of miniscule changes in a system, even if it is not conductive. However, this type of measurement is usually slower than other electrical measurements, as it requires a wide scan of different frequencies, whereby the system must be stabilized for each one. Jiang et al. (2014) reported a device for bacteria pre-concentration and detection using

Fig. 8. Adapter for chemiluminescent strips reading. (a), (b), (c) images of the devices, (d) scheme of the cassette for the strips, (e) coupling of the cassette on the mobile phone and (f) signal procurement. Adapted with permission from Roda et al. (2014b). Copyright 2014 American Society of Chemistry.

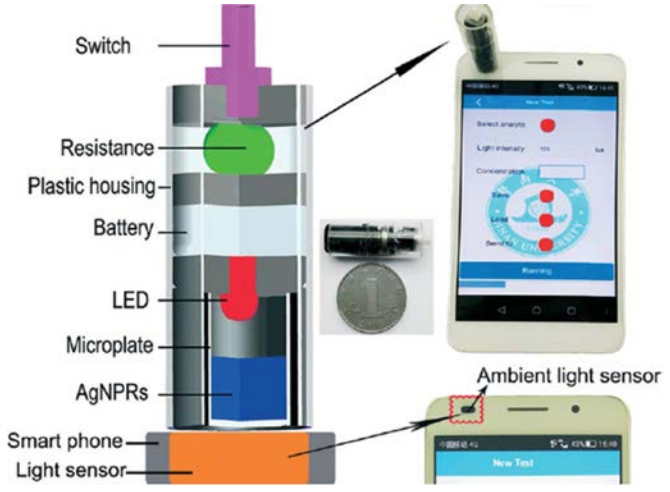

Fig. 9. Tiny SPR adapter using the ambient light sensor present in the mobile phone as reader. Adapted with permission from Fu et al. (2016). Copyright 2016 Royal Society of Chemistry.

microfluidics and impedance measurements, respectively. Their device incorporates a Bluetooth generator for wireless connection with the mobile phone, enabling transmission of the results in real time.

Kim et al. (2015) have created a wireless oral device for detection of uric acid in saliva (Fig. 14), which is placed directly inside the mouth. It uses amperometric measurements to perform real-time monitoring of the uric acid concentration, and can send the data via Bluetooth to a mobile phone or other device. Nevertheless, their device is only a prototype, and it must be subjected to further studies on toxicity and biocompatibility.

4. Other biosensing methods and DCT-based devices

4.1. Other mobile phone-based biosensing strategies

Optical and electrochemical methods are well-known and highly applied biosensing techniques, but mobile phones offer new sensing possibilities such as sound-recording. A phone's microphone can be used to perform spirometry (i.e. measurement of lung capacity) by measuring the sound of a patient blowing into it (Larson et al., 2012; Goel et al., 2016). To optimize performance of this assay, Goel et al., (2016) 3D-printed a spirometry whistle that enabled enhanced recording.

Mobile phones can be coupled to several biosensing techniques, mainly as reader devices; however, they can execute even simpler tasks, serving, for example, as a simple display or network connector. Stedtfeld et al. (2012) fabricated a device for genetic testing based on fluorescence, using photodiodes for collecting the signal. They coupled their device to a mobile phone, which serves as a wireless interface to collect and send the data. Similarly, Choi et al. (2016) developed a giant-magnetoresistance biosensing platform in which a mobile phone serves both as display (to control the machine) and for sending data to the network.

As we previously mentioned, mobile phones, besides working as detectors, displays or network connectors, can also serve as signal producers. This occurs either via the current generated by the phone's battery, or via the light emitted from the phone's flash or screen.

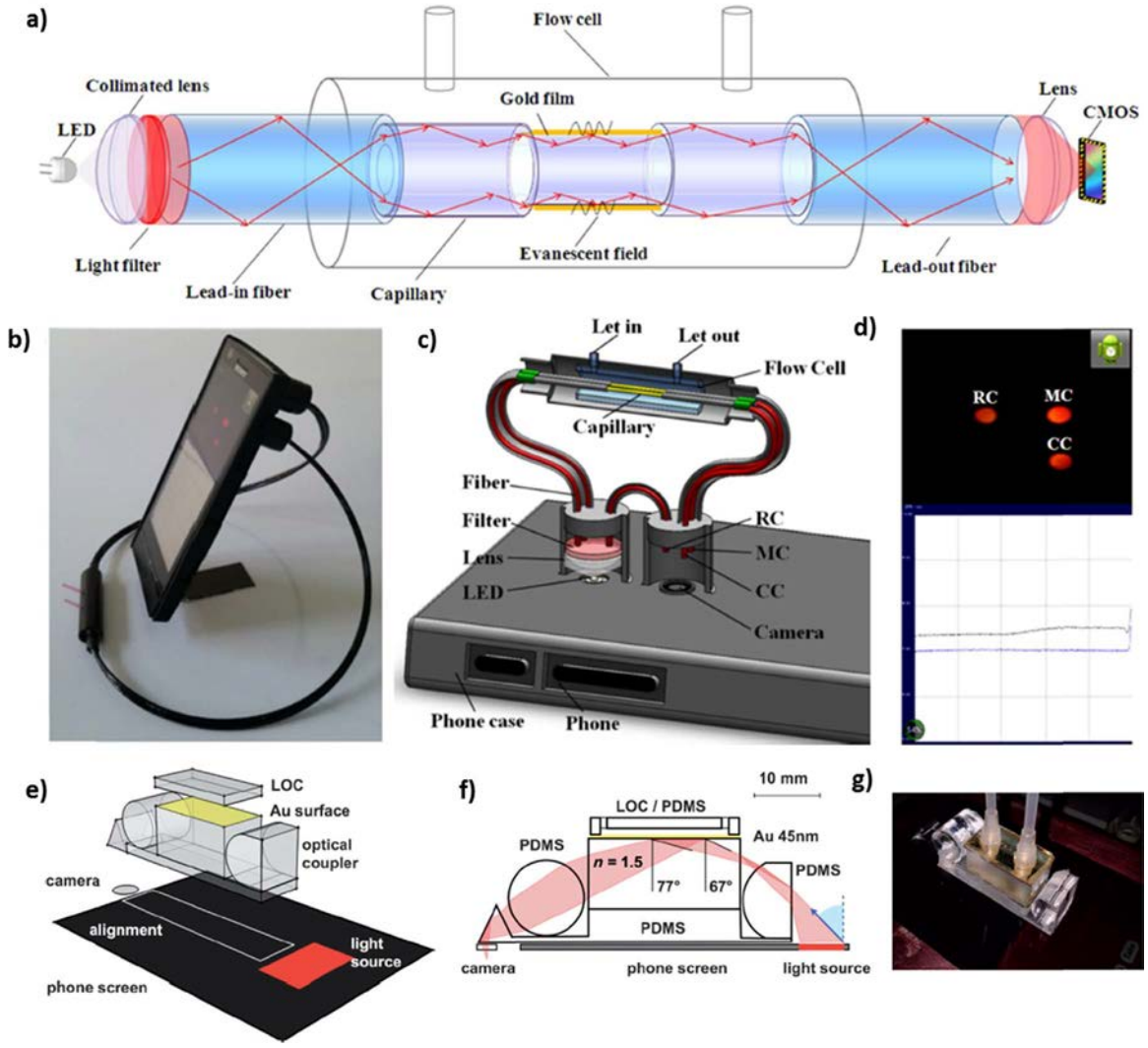

Fig. 10. SPR-based mobile phone biosensor: (a) scheme of the device, which is integrated (b) on the mobile phone (c) connecting the flash camera and the camera with optical fibbers; (d) response registered. Adapted with permission from Liu et al. (2015). Copyright 2015 Nature. (e) Scheme of SPR biosensor that uses the screen as source of light: (f) explanation mechanism, (g) image of the device. Adapted with permission from Preechaburana et al. (2012). Copyright 2012 Wiley-VCH.

Surprisingly, mobile phones offer yet another integrated tool that can both produce and read signals: NFC. This technology is based on a device that can send energy to a nearby NFC tag (which does not require batteries) and read the signal that is bounced back. Azzarelli et al. (2014) reported the first NFC-based detector for chemical gas sensing. They modified an NFC tag by replacing part of the circuit with carbon nanotubes, whose interaction with ammonia and hydrogen peroxide is well known. In this case, this interaction gives a chemo-resistive response that works similarly to an on/off logic gate in the NFC tag circuit (Fig. 15a). Therefore, in relation to the presence of analyte, the energy transfer from the NFC to the mobile phone is decreased. Another interesting application of NFC technology has been reported by Kassal et al. (2015), who fabricated a smart bandage for monitoring skin wounds (Fig. 15b) and reporting, by wireless connection, on their status. As in their previous work (oral salivary device, Kim et al., 2015) they detected uric acid via electrochemical methods but in this case, instead of Bluetooth, they opted for NFC technology.

4.2. Other DCT-based devices

Indisputably, mobile phones have become the ideal tools for development of DCT devices. However, in the near future, will they remain the best option? Other devices could appear that supersede mobile phones. A recent example that ultimately did not arrive to market is Google Glass, an eyeglasses-like device that was supposed to integrate AR in our life by displaying images (messages, maps, video chats, text, etc.) directly in front of our eyes. In terms of the potential of Google Glass, Feng et al. (2014) showed that LF strips could be read by simply looking at a quick response (QR) code stamped on the cassette (Fig. 16a), and then having Google Glass check the data base to determine the analyte that is being measured and its concentration relative to the intensity of the lines. Currently, Google is working on another wearable device, Google Lens (Google Official Blog), which can continuously monitor glucose levels in the user's tears via integrated electrodes (Fig. 16b).

Drones, which have become a trending topic over the past few years, offer great potential as remote biosensing platforms: specifically, for transporting sensors to places that humans cannot easily reach. Priye et al. (2016) fabricated a lab-on-a-drone system able to perform several lab functions, including centrifugation (using the drone motors and 3D-printed structures), a polymerase chain reaction (PCR) in a portable heater, and sample-sensing (using a mobile phone). Thus drones, which offer impressively low weight (less than half a kilogram), could be used as portable labs.

Oxford Nanopore Technologies has reported a portable device for nanopore-based DNA sequencing that is small enough to be carried

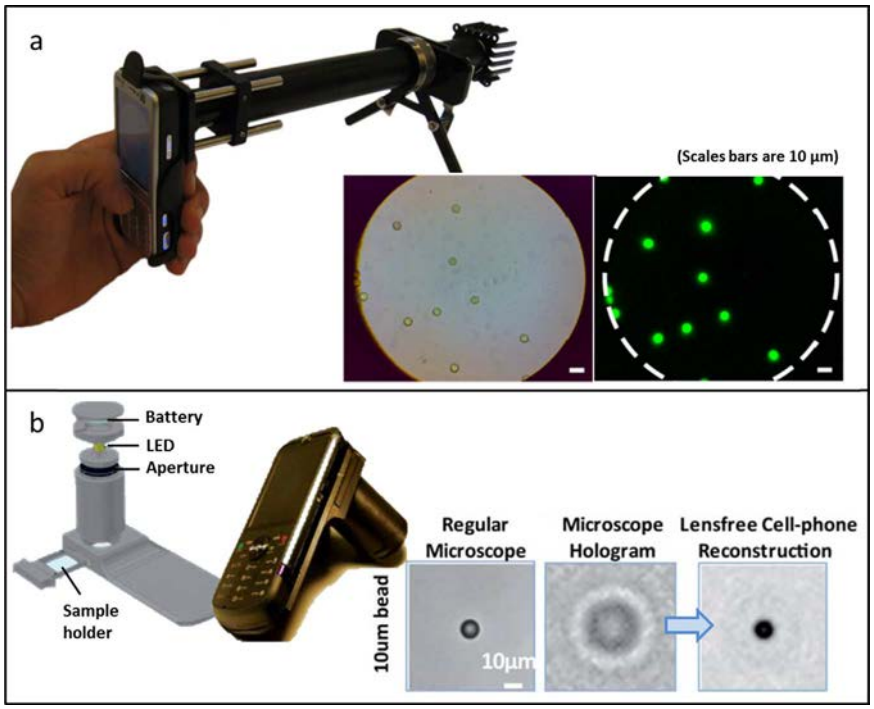

Fig. 11. (a) Fluorescent microscope adapted for its use on mobile phones. Brightfield (on the left) and fluorescent (on the right) captures of fluorescent beads are shown. Adapted with permission from Breslauer et al. (2009). Copyright 2009 Public Library of Science. (b) Free-lens microscope based on hologram imaging. Adapted with permission from Tseng et al. (2010). Copyright 2010 Royal Society of Chemistry.

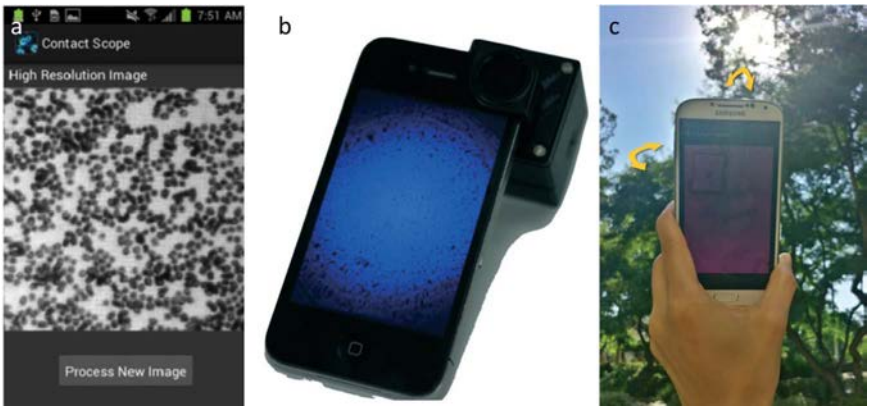

Fig. 12. (a) Image of blood cells obtained with a mobile phone microscope. Adapted with permission from Navruz et al. (2013). Copyright 2013 Royal Society of Chemistry (b) Digital diffraction scheme obtained from a sample of beads. Adapted with permission from Im et al. (2016). Copyright 2016 National Academy of Sciences. (c) Microscopic imaging with just ambient light. Adapted with permission from Lee and Yang (2014). Copyright 2014, Royal Society of Chemistry.

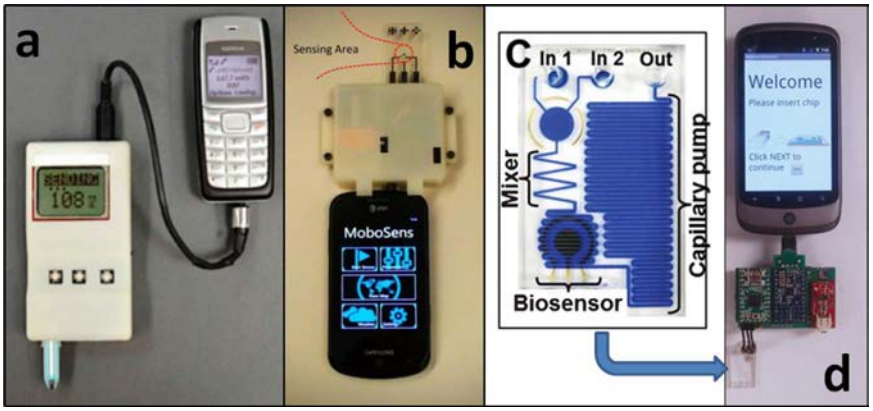

Fig. 13. (a) Portable device to read different types of electrodes with a mobile phone. Adapted with permission from Nemiroski et al. (2014). Copyright 2014 National Academy of Sciences. (b) Device for CV measurement coupled on the headphone jack of a mobile phone. Adapted with permission from Wang et al. (2015). Copyright 2015 ElSevier. (c) Microfluidic system with electrodes that can be connected to (d) a mobile phone. Adapted with permission from Lillehoj et al. (2013). Copyright 2013 Royal Society of Chemistry.

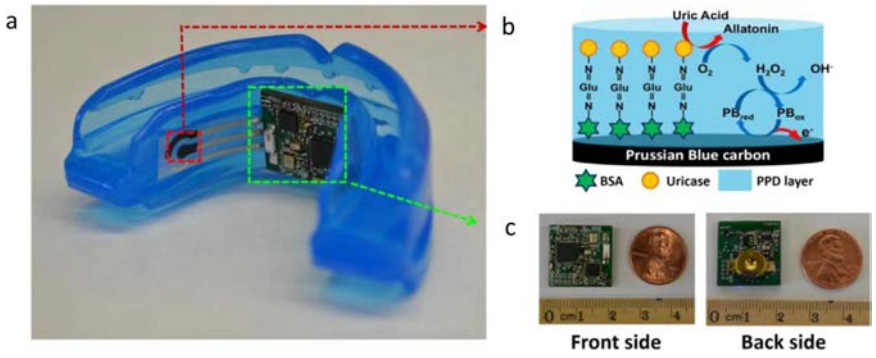

Fig. 14. Wearable salivary device for uric acid control. (a) The device. (b) Electrodes reaction. (c) Wireless amperometric chip. Adapted with permission from Kim et al. (2015). Copyright 2015 ElSevier.

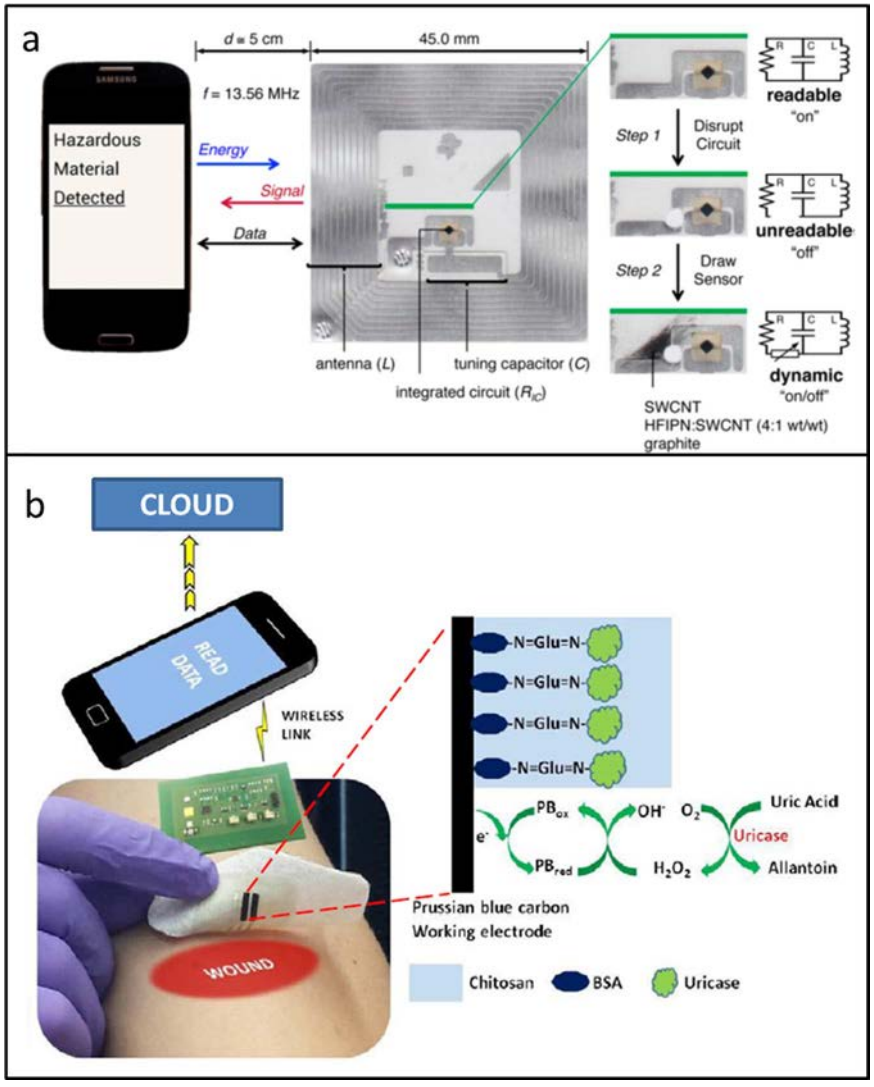

Fig. 15. (a) NFC-based sensor for gases. Adapted with permission from Azzarelli et al. (2014). Copyright 2014 National Academy of Sciences. (b) Sensor on a bandage. Adapted with permission from Kassal et al. (2015). Copyright 2015 ElSevier.

and used everywhere. Sample DNA sequences are passed through the nanopore, which has its own current that varies according to the DNA base passing through, which enables characterization of the DNA chain. In the future, these types of devices will surely be within reach of the common consumer, enabling anyone to readily detect the presence of bacteria in the environment—for example, to establish the freshness of food or in other areas concerning the user's health.

5. Commercially available mobile phone-based biosensing systems

Although mobile-phone biosensing is still under development, several companies are already offering software and hardware to adapt phones for biosensing applications. One such company is Mobili, a company that develops sensors and software related to health, sports, safety, transport, education and research. They develop sensors for

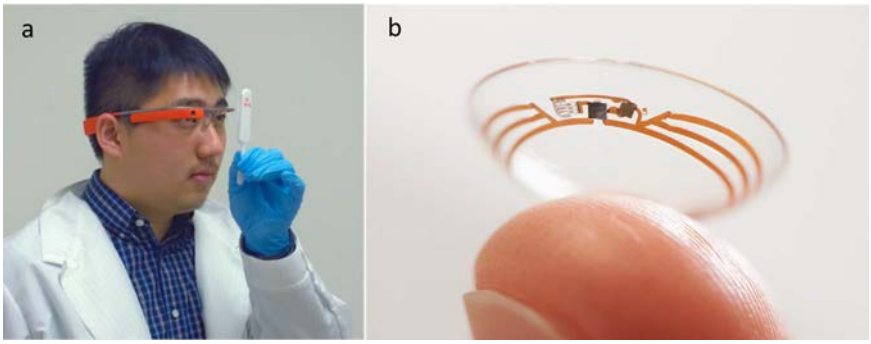

Fig. 16. (a) Using Google Glass to translate the response of LF strip. Adapted with permission from Feng et al. (2014). Copyright 2014 American Chemical Society. (b) Google Lens, for glucose sensing. Adapted with permission from Google Official Blog. Copyright 2014 Google.

Table 1
Comparison of different detection methods applicable on mobile phones.

Detection method	Signal generation	Transducers	Comments
Optical			Assay performed on:
• Colorimetric • Luminescent • Fluorescent • SPR • Microscopy	• Ambient light • LEDs • Laser • Mobile phone screen • Chemical reaction	• Camera • Additional lens • Ambient light sensor • External devices	• Paper • Cuvettes • ELISA • Microfluidics • Skin
Electrochemical	Current from:		Connection:
• Cyclic voltammetries • Chronoamperograms • Impedance	• External batteries • Mobile phone battery	• Earphone jack • USB port • External devices	• Direct • Bluetooth • Wi-fi • NFC
Other			Interaction with:
• Sound recording • Magnetoresistance • NFC interference • Other devices connection (e.g. ultrasound scanner)	• Mobile phone features • External devices	• Mobile phone • External devices	• AR devices • Drones • Portable laboratory systems

mobile phones that can measure parameters such as heart rate, skin temperature, acceleration, distance traveled, etc. There are emerging companies dedicated to developing software for reading and processing the data from LF strips using mobile phones, through personalized software in each case. For example, Novarum has created mobile phone apps that read a QR code integrated onto LF cassettes. The system knows how to scan and interpret the response by simply comparing pixel colors. The phone does not require any adapter. Continuing with optical sensors, there are also companies that are developing mobile phone camera lenses that offer enhanced zoom or image quality, or even enable true microscopy. For example, BLIPS Lenses is a crowd-funded project that offers cheap lenses compatible with any mobile phone. They work by simply being attaching onto the camera. The company Cellscope has developed another type of lens, Oto, for transforming mobile phones into otoscopes that are specially designed to examine children's ears. Through special software, the images can be sent directly to a doctor.

iHealth is a company specialized in wearable devices (e.g. blood-pressure monitors) and analytical devices (e.g. glucometers) that employ mobile phones as displays via wireless connections. Another interesting device that can be coupled to mobile phones is the MobiUS System (sold by MobiSante), a portable ultrasound machine with a resolution comparable to hospital equipment (Wojtczak and Bonadonna, 2013).

Regarding electrochemical measurements, PalmSens sells the EmStat, a portable potentiostat with a wide working range (1 nA to 100 mA) and a resolution of 1 pA. This device is compatible with computers, tablets and mobile phones, and can perform several techniques, including CV and amperometry.

6. Conclusions and future perspectives

Mobile phone devices have been shown to offer great utility for biosensing applications and as DCT, whether in solution, on a substrate or even in gas. As summarized in Table 1, this has been made possible in part by a broad array of analytical techniques, including colorimetry, fluorescence, SPR, microscopy and electrochemistry. Also invaluable are the latest advances in mobile phone technology, including increases in memory and in processing power, the resolution of cameras powered by ambient light sensors, GPS, wireless connectivity (internet, Bluetooth and NFC technology), portability, apps, etc. Nevertheless, the success of mobile phone-based biosensing will strongly depend on biosensing technology, which still is the bottleneck of such impressive coupling.

Among various biosensing technologies, paper-based biosensing is very promising for coupling to smart phones. This is due to the advantages of paper, including its natural abundance, recyclability, low-cost and simplicity, both in its development and in its use. Furthermore, paper-based biosensors have proven to be truly portable: in most cases, they do not require additional reagents or devices, or any additional energy source beyond the mobile phone itself.

We strongly believe that mobile-phone biosensing is going to decentralize current healthcare systems and environmental, safety and security labs. We predict the rapid spread of POC (point-of-care) devices and other user-friendly monitoring devices for use at home or elsewhere. These developments will fall in line with the future development of Smart Cities, in which mobile phones will be crucial for network connections. In addition, other devices (e.g. smart glasses or dermal wearables) may soon appear that could co-exist with mobile phones for health monitoring.

Acknowledgments

The authors acknowledge MINECO (Spain) for the Severo Ochoa Program (Grant SEV-2013-0295) and project MAT2014-52485-P and support from the *Secretaria d'Universitats i Recerca del Departament d'Economia i Coneixement de la Generalitat de Catalunya* (2014 SGR 260).

References

Arduino: ⟨https://store.arduino.cc/⟩
Awqatty, B., Samaddar, S., Cash, K.J., Clark, H.A., Dubach, J.M., 2014. Analyst 139, 5230–5238.

Ayas, S., Cupallari, A., Ekiz, O.O., Kaya, Y., Dana, A., 2014. ACS Photonics 1, 17–26.
Azzarelli, J.M., Mirica, K.A., Ravnsbæk, J.B., Swager, T.M., 2014. PNAS 111 (51), 18162–18166.
Baptista-Pires, L., Mayorga-Martínez, C.C., Medina-Sánchez, M., Montón, H., Merkoçi, A., 2016. ACS Nano 10, 853–860.
Barbosa, A.I., Gehlot, P., Sidapra, K., Edwards, A.D., Reis, N.M., 2015. Biosens. Bioelectron. 70, 5–14.
Berg, B., Cortazar, B., Tseng, D., Ozkan, H., Feng, S., Wei, Q., Chan, R.Y.L., Burbano, J., Farooqui, Q., Lewinski, M., Di Carlo, D., Garner, O.B., Ozcan, A., 2015. ACS Nano 9, 7857–7866.
BLIPS: ⟨http://www.smartmicrooptics.com/⟩
Breslauer, D.N., Maamari, R.N., Switz, N.A., Lam, W.A., Fletcher, D.A., 2009. PLoS One 4 (7), 6320–6326.
Cellscope: ⟨https://www.cellscope.com/⟩
Chen, A., Wang, R., Bever, C.R.S., Xing, S., Hammock, B.D., Pan, T., 2014. Biomicrofluidics 8, 064101.
Choi, J., Gani, A.W., Bechstein, D.J.B., Lee, J.R., Utz, P.J., Wang, S.X., 2016. Biosens. Bioelectron. 85, 1–7.
Chun, H.J., Park, Y.M., Han, Y.D., Jang, H.J., Yoon, H.C., 2014. Bio Chip J. 8 (3), 218–226.
Comina, G., Suska, A., Filippini, D., 2015. Angew. Chem. Int. Ed. 54, 8708–8712.
Comina, G., Suska, A., Filippini, D., 2016. Biosens. Bioelectron. 77, 1153–1167.
Coskun, A.F., Wong, J., Khodadadi, D., Nagi, R., Tey, A., Ozcan, A., 2013a. Lab Chip 13, 636–640.
Coskun, A.F., Nagi, R., Sadeghi, K., Phillips, S., Ozcan, A., 2013b. Lab Chip 13, 4231–4238.
Feng, S., Caire, R., Cortazar, B., Turan, M., Wong, A., Ozcan, A., 2014. ACS Nano 8, 3069–3079.
Fu, Q., Wu, Z., Xu, F., Li, X., Yao, C., Xu, M., Sheng, L., Yu, S., Tang, Y., 2016. Lab Chip 16, 1927–1933.
Gallegos, D., Long, K.D., Yu, H., Clark, P.P., Lin, Y., George, S., Natha, P., Cunningham, B.T., 2013. Lab Chip 13, 2124–2132.
Goel, M., Saba, E., Stiber, M., Whitmire, E., Fromm, J., Larson, E.C., Borriello, G., Shwetak, N.P., 2016. CHI. Spiro Call device.
Google Official Blog, 2014. 16th January: ⟨https://googleblog.blogspot.com.es/2014/01/introducing-our-smart-contact-lens.html⟩
Guan, L., Tian, J., Cao, R., Li, M., Cai, Z., Shen, W., 2014. Anal. Chem. 86, 11362–11367.
Huang, R.Y., Dung, L.R., 2016. Biomed. Eng. Online 15 (11).
iHealth: ⟨https://ihealthlabs.com/⟩
Im, H., Castro, C. M., Shao, H., Liong, M., Song, J., Pathania, D., Fexon, L., Min, C., Avila-Wallace, M., Zurkiya, O., Rho, J., Magaoay, B., Tambouret, R. H., Pivovarov, M., Weissleder, R., Lee, H., 2015. Proc. Natl. Acad. Sci. USA. 112, pp. 5613–5618.
Im, H., Park, Y.I., Pathania, D., Castro, C.M., Weissleder, R., Lee, H., 2016. Lab Chip 16, 1340–1345.
Jianga, J., Wanga, X., Chao, R., Rena, Y., Hu, C., Xu, Z., Liu, G.L., 2014. Sens. Actuator B-Chem. 193, 653–659.
Jonathan, E., Leahy, M., 2010. Physiol. Meas. 31 (11), 79–83.
Kadlec, M.W., You, D., Liao, J.C., Wong, P.K., 2014. J. Lab. Autom. 19 (3), 258–266.
Karim, H., Schmidt, B., Dart, D., Beluk, N., Huppert, T., 2012. Gait Posture 35, 367–372.
Kassal, P., Kim, J., Kumar, R., de Araujo, W.R., Steinberg, I.M., Steinberg, M.D., Wang, J., 2015. Electrochem. Commun. 56, 6–10.
Kehoe, E., Penn, R.L., 2013. J. Chem. Educ. 90, 1191–1195.
Khatua, S., Orrit, M., 2013. ACS Nano 7 (10), 8340–8343.
Kennedy, P., 2013. march 15, The New York Times, Who Made That Cellphone?
Kim, J., Imani, S., Araujo, W.R., Warchall, J., Valdés-Ramírez, G., Paixão, T.R.L.C., Mercier, P.P., Wang, J., 2015. Biosens. Bioelectron. 74, 1061–1068.
Knuston, T.R., Knuston, C.M., Mozzetti, A.R., Campos, A.R., Haynes, C.L., Penn, R.L., 2015. J. Chem. Educ. 92, 1692–1695.
Koesdjojo, M.T., Pengpumkiat, S., Wu, Y., Boonloed, A., Huynh, D., Remcho, T.P., Remcho, V.T., 2015. J. Chem. Educ. 92, 737–741.
Kuntzleman, T., Jacobson, E.C., 2016. J. Chem. Educ. ASAP. http://dx.doi.org/10.1021/acs.jchemed.5b00844.
Larson, E.C., Goel, M., Boriello, G., Heltshe, S., Rosenfeld, M., Patel, S.N., 2012. Ubi. Comp. Conf., 280–289.
Lee, S.J., Kim, J., Lee, M., 2011. Telemed. J. E. Health 17 (2), 124–130.
Lee, S., Kim, G., Moon, J., 2013a. Sensors 13, 5109–5116.
Lee, L.G., Nordman, E.S., Johnson, M.D., Oldham, M.F., 2013b. Biosensors 3, 360–373.
Lee, S., Oncescu, V., Mancuso, M., Mehta, S., Erickson, D., 2014. Lab Chip 14, 1437–1442.
Lee, S.A., Yang, C., 2014. Lab Chip 14, 3056–3063.
Liang, P.S., Park, T.S., Yoon, J.Y., 2014. Sci. Rep. 4, 5953.
Lillehoj, P.B., Huang, M.C., Truong, N., Ho, C.H., 2013. Lab Chip 13, 2950–2955.
Liu, Y., Liu, Q., Chen, S., Cheng, F., Wang, H., Peng, W., 2015. Sci. Rep. 5, 12864.
Lopez-Ruiz, N., Curto, V.F., Erenas, M.M., Benito-Lopez, F., Diamond, D., Palma, A.J., Capitan-Vallvey, L.F., 2014. Anal. Chem. 86, 9554–9562.
Mobili: ⟨http://www.mobili.si/products/sensor-smartphone⟩
MobiSante: ⟨http://www.mobisante.com/products/⟩
Montangero, M., 2015. J. Chem. Educ. 92, 1759–1762.
Morales-Narváez, E., Golmohammadi, H., Naghdi, T., Yousefi, H., Kostiv, U., Horak, D., Pourreza, N., Merkoçi, A., 2015a. ACS Nano 9, 7296–7305.
Morales-Narváez, E., Naghdi, T., Zor, E., Merkoçi, A., 2015b. Anal. Chem. 87 (16), 8573–8577.
Mudanyali, O., Dimitrov, S., Sikora, U., Padmanabhan, S., Navruza, I., Ozcan, A., 2012. Lab Chip 12, 2678–2686.
Nanhore, S.D., Bartere, M.M., 2013. IJSR 2 (4), 252–255.
NASA: ⟨http://history.nasa.gov/computers/Part1.html⟩
Nasi, G., Cucciniello, M., Guerrazzi, C., 2015. J. Med. Internet Res. 17 (2), e26.
Navruz, I., Coskun, A.F., Wong, J., Mohammad, S., Tseng, D., Nagi, R., Phillips, S., Ozcan, A., 2013. Lab Chip 13, 4015–4023.
Nemiroski, A., Christodouleas, D.C., Henneka, J.W., Kumar, A.A., Maxwell, E.J., Fernández-Abedul, M.T., Whitesides, G.M., 2014. PNAS 111 (33), 11984–11989.
Noor, M.O., Krull, U.J., 2014. Anal. Chem. 86, 10331–10339.
Novarum: ⟨http://www.novarumreader.com/⟩
Oncescu, V., O'Dell, D., Erickson, D., 2013. Lab Chip 13, 3232–3238.
Oncescu, V., Mancuso, M., Erickson, D., 2014. Lab Chip 14, 759–763.
Otten, L., Richards, S.J., Fullam, E., Besra, G.R., Gibson, M.I., 2013. J. Mater. Chem. B 1, 2665–2672.
Oxford Nanopore Technologies: ⟨https://www.nanoporetech.com/products-services/minion-mki⟩
Pal, A., Visvanathan, A., Choudhury, A.D., Sinha, A., 2014. SAC, 8–13.
PalmSens: ⟨http://www.palmsens.com/en/instruments/emstat/⟩
Patel, S., Park, H., Bonato, P., Chan, L., Rodgers, M., 2012. J. Neuroeng. Rehabil. 9 (21).
Park, T.S., Li, W., McCracken, K.E., Yoon, J.Y., 2013. Lab Chip 13, 4832–4840.
Parolo, C., Merkoçi, A., 2013. Chem. Soc. Rev. 42, 450–457.
Petryayeva, E., Algar, W.R., 2014. Anal. Chem. 86, 3195–3202.
Preechaburana, P., Collado Gonzalez, M., Suska, A., Filippini, D., 2012. Angew. Chem. 124, 11753–11756.
Preechaburana, P., Suska, A., Filippini, D., 2014. Trends Biotechnol. 32 (7), 351–355.
Priye, A., Wong, S.S.S., Bi, Y., Carpio, M., Chang, J., Coen, M., Cope, D., Harris, J., Johnson, J., Keller, A., Lim, R., Lu, S., Millard, A., Pangelinan, A., Patel, N., Smith, L., Chan, K., Ugaz, V.M., 2016. Anal. Chem. 88 (9), 4651–4660.
Quesada-González, D., Merkoçi, A., 2015. Biosens. Bioelectron. 73, 47–63.
Rajendran, V.K., Bakthavathsalam, P., Ali, B.M.J., 2014. Microchim. Acta 181, 1815–1821.
Roche, P.J.R., Filion-Côté, S., Cheung, M.C.K., Chodavarapu, V.P., Kirk, A.G., 2011. J. Sens.. http://dx.doi.org/10.1155/2011/406425.
Roda, A., Guardigli, M., Calabria, D., Calabretta, M.M., Cevenini, L., Michelini, E., 2014a. Analyst 139, 6494–6501.
Roda, A., Michelini, A., Cevenini, L., Calabria, D., Calabretta, M.M., Simoni, P., 2014b. Anal. Chem. 86, 7299–7304.
Roda, A., Michelini, A., Zangheri, M., Di Fusco, M., Calabria, D., Simoni, P., 2016. Trends Anal. Chem. 79, 317–325.
Rohrig, B., 2015. april/may. Chem Matters, 10–12
Shafiee, H., Asghar, W., Inci, F., Yuksekkaya, M., Jahangir, M., Zhang, M.H., Durmus, N.G., Gurkan, U.A., Kuritzkes, D.R., Demirci, U., 2015. Sci. Rep. 5, 8719.
Stedtfeld, R.D., Tourlousse, D.M., Seyrig, G., Stedtfeld, T.M., Kronlein, M., Price, S., Ahmad, F., Gulari, E., Tiedje, J.M., Hashsham, S.A., 2012. Lab Chip 12, 1454–1462.
Sun, A., Wambach, T., Venkatesh, A.G., Hall, D.A., 2014. IEEE Biomed. Circuits Syst. Conf., 312–315.
Sun, R., Chang, Y.C., Wang, L.J., Li, L., 2016a. IJNST 5 (2), 102–109.
Sun, A.C., Yao, C., Venkatesh, A.G., Hall, D.A., 2016b. Sens. Actuator B-Chem. 235, 126–135.
Tseng, D., Mudanyali, O., Oztoprak, C., Isikman, S.O., Sencan, I., Yaglidere, O., Ozcan, A., 2010. Lab Chip 10, 1787–1792.
Vashist, S.K., Schneider, E.M., Luong, J.H.T., 2014. Diagnostics 4, 104–128.
Wang, H., Li, Y., Wei, J., Xu, J., Wang, Y., Zheng, G., 2014. Anal. Bioanal. Chem. 406, 2799–2807.
Wang, X., Gartia, M.R., Jiang, J., Chang, T.W., Qian, J., Liu, Y., Liu, X., Liu, G.L., 2015. Sens. Actuator B-Chem. 209, 677–685.
Wei, Q., Qi, H., Luo, W., Tseng, D., Ki, S.J., Wan, Z., Göröcs, Z., Bentolila, L.A., Wu, T.T., Sun, R., Ozcan, A., 2013. ACS Nano 7, 9147–9155.
Wei, Q., Nagi, R., Sadeghi, K., Feng, S., Yan, E., Ki, S.J., Caire, R., Tseng, D., Ozcan, A., 2014a. ACS Nano 8, 1121–1129.
Wei, Q., Luo, W., Chiang, S., Kappel, T., Mejia, C., Tseng, D., Chan, R.Y.L., Yan, E., Qi, H., Shabbir, F., Ozkan, H., Feng, S., Ozcan, A., 2014b. ACS Nano 8, 12725–12733.
Wojtczak, J., Bonadonna, P., 2013. Am. J. Emerg. Med. 31, 573–577.
Xu, X., Akay, A., Wei, H., Wang, S., Pingguan-Murphy, B., Erlandsson, B.E., Li, X., Lee, W., Hu, J., Wang, L., Xu, F., 2015. Proc. IEEE, 103(2), pp. 236–247.
Yetisen, A.K., Martinez-Hurtado, J.L., Garcia-Melendrez, A., da Cruz Vasconcellos, F., Lowe, C.F., 2014. Sens. Actuator B-Chem. 196, 156–160.
You, D.J., Park, T.S., Yoon, J.Y., 2013. Biosens. Bioelectron. 40, 180–185.
Yu, H., Tan, Y., Cunningham, B.T., 2014. Anal. Chem. 86, 8805–8813.
Zangheri, M., Cevenini, L., Anfossi, L., Baggiani, C., Simoni, P., Di Nardo, F., Roda, A., 2015. Biosens. Bioelectron. 64, 63–68.
Zhang, L., Cao, X., Wang, L., Zhao, X., Zhang, S., Wang, P., 2015. Analyst 140, 4105–4113.
Zhang, D., Liu, Q., 2016. Biosens. Bioelectron. 75, 273–278.
Zhang, Y., Wu, Y., Zhang, Y., Ozcan, A., 2016. Sci. Rep. 6, 27811.
Zhu, H., Mavandadi, S., Coskun, A.F., Yaglidere, O., Ozcan, A., 2011. Anal. Chem. 83, 6641–6647.
Zhu, H., Sencan, I., Wong, J., Dimitrov, S., Tseng, D., Nagashima, K., Ozcan, A., 2013. Lab Chip 13 (7), 1282–1288.

Chem Soc Rev

TUTORIAL REVIEW

Cite this: *Chem. Soc. Rev.*, 2018, **47**, 4697

Received 7th December 2017

DOI: 10.1039/c7cs00837f

rsc.li/chem-soc-rev

Nanomaterial-based devices for point-of-care diagnostic applications

Daniel Quesada-González [a] and Arben Merkoçi *[ab]

In this review, we have discussed the capabilities of nanomaterials for point-of-care (PoC) diagnostics and explained how these materials can help to strengthen, miniaturize and improve the quality of diagnostic devices. Since the optical, electrochemical and other physical properties of nanomaterials are dictated by their composition, size and shape, these factors are critical in the design and function of nanomaterial-based PoC diagnostics.

Key learning points
(1) Needs and challenges of point-of-care diagnostics.
(2) Nanomaterials as interesting building blocks for biosensing.
(3) Overview of the different detection methods offered by using nanomaterials.
(4) Advantages and drawbacks of nanomaterial-based sensing strategies.
(5) Opportunities offered by paper as a cost-efficient biosensing platform.

1. Introduction

The advancements made in medicine in the last few years are impressive. However, diseases not detected on time or not properly monitored are still currently the main causes of death. Ischemic heart diseases, respiratory infections, diabetes and bacterial infections, such as tuberculosis or diarrheal diseases, are some of the leading causes of deaths worldwide, but if detected on time, they can be prevented. Nowadays, we have potential technologies and tools to detect all of them; therefore, why so many people are still dying due to these diseases? There are two main possible reasons. First, the lack of equipment, especially in the developing countries, where the costs are not affordable for the whole population or even for medical centers. Second, the time frame between the moment when the symptoms are appreciable by the patient and when diagnostics is accomplished by a specialist. Then, how can these problems be solved? Should a doctor be present for a single patient, ready at any time with accurate and fast diagnostics or is this a utopia? Now, instead of having a real doctor, imagine having a small device that is portable, easy-to-use, and able to monitor several parameters and variables similar to a portable laboratory.[1] When all the data is collected this tiny device, it can decide in a few minutes either by itself or by immediate communication with a specialist/medical doctor what action is required by the patient, with everything done at home or even in the field without requiring any kind of medical knowledge by the user. This futuristic idea is exemplified in Fig. 1, where a mother is using a portable device to diagnose what virus has her daughter, send the data to the pharmacy and conclude that some chicken soup may make the child feel better (no need for any medication at all).

Nowadays, some portable devices that can monitor and diagnose the condition of the user are already available. A well-known example is the glucose meter, which with a few microliters of blood, can determine the glucose concentration in the sample and notify the diabetes patient if there is any action required, such as the injection of insulin or the intake of food.

It is noteworthy that mobile phones have the capability to carry out this type of tasks,[2] especially since most of the population has at least one mobile phone. The tools that these devices contain include a camera, light sensor, power source, movement detector and wireless connection, among others (and more will appear in the future). In this review we show how some parts of a mobile phone such as the camera,[3] light

[a] *Nanobioelectronics & Biosensors Group, Catalan Institute of Nanoscience and Nanotechnology (ICN2), CSIC and BIST, Campus UAB, Bellaterra, 08193 Barcelona, Spain. E-mail: arben.merkoci@icn2.cat*
[b] *ICREA, Institució Catalana de Recerca i Estudis Avançats, Pg. Lluís Companys 23, 08010 Barcelona, Spain*

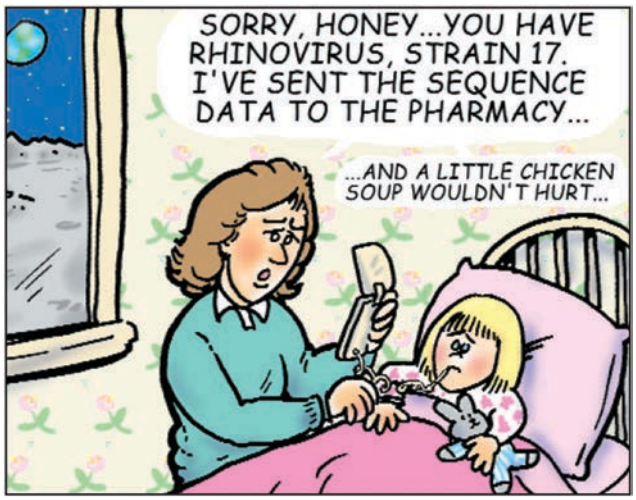

Fig. 1 Caricature illustrating the simplicity expected from a PoC device. Reprinted with permission from ref. 1, Copyright 2002 American Association for the Advancement of Science.

sensor[4] and even the NFC (near-field communication) antenna[5] are used to monitor different variables in nanomaterial-based platforms with interest for future diagnostics.

1.1. Point-of-care tests

Devices that can perform fast analysis and accurate diagnostics near the patient are known as bedside or point-of-care (PoC) tests. The ideal PoC test should be user-friendly and as simple as possible so that any user, even those without any type of medical or laboratory knowledge, will be able to use it and understand its response (as shown in the example in Fig. 1). Also, low cost is an important and desirable quality of PoC to ensure that the device is easily acquired by everyone and anywhere. Thus, one of the most popular materials employed as a substrate for PoC devices is paper,[6–8] which is cheap, abundant, recyclable and biosustainable. Other qualities that PoC tests should possess are robustness (the capacity to withstand changes in environmental conditions), selectivity (the ability to respond to a unique analyte or parameter and not affected by interferences) and sensitivity (the quality to discriminate between similar values).

Different methodologies exist to produce a signal in PoC devices (or in any other type of sensor and biosensor), and in most of the cases the chosen methodology will depend on the transducer employed. Optical and electrochemical-based PoC devices are probably the most popular, examples of which are pregnancy tests and glucose meter, respectively. With the development of nanotechnology, both types of devices utilize the advantages of nanomaterials by integrating them in different parts of existing sensing platforms or offering quite innovative detection systems.

1.2. Nanomaterials for point-of-care

Regarding the transducer, synthetic nanomaterials (with a diameter ranging between 1 and 100 nm) offer a wide range of possibilities due to their size, shape and properties such as biocompatibility, fluorescence, electrical and thermal conductivity, and magnetism. Nanomaterials can be classified according to their shape as: 0D (spherical nanomaterials), 1D (*e.g.* nanotubes and nanowires),

Daniel Quesada-González

Daniel Quesada-González obtained his BSc in Chemistry at the Autonomous University of Barcelona in 2013 and an MSc degree in Nanotechnology and Materials Science in 2014 at the same University. In 2012 he started working at the Nanobioelectronics & Biosensors group in the Catalan Institute of Nanoscience and Nanotechnology under the supervision of Prof. Dr Arben Merkoçi. In 2014 he started his PhD, which is currently in progress, in this group. His work is focused on the development of nanoparticle-based biosensors on paper substrate for the detection of biomarkers and heavy metals.

Arben Merkoçi

Arben Merkoçi is an ICREA Professor and Head of the Nanobioelectronics and Biosensors Group at the Catalan Institute of Nanoscience and Nanotechnology. He obtained a PhD in Chemistry at the University of Tirana and afterwards, followed various postdoctoral research positions at various international centers. His research is focused on the integration of biological molecules and other receptors with micro- and nanostructures of interest for the design of novel sensors and biosensors. He is the author of over 270 manuscripts, special journal issues and books, and collaborates as an Editor of Biosensors and Bioelectronics, the principal international journal devoted to the research, design development and application of biosensors and bioelectronics. Prof. Merkoçi has supervised around 25 PhD students and has been invited to give Plenary Lectures and Keynote Speeches on around 100 occasions in various countries. He is the co-founder of two spin-off companies, PaperDrop and GraphenicaLab, which are dedicated to nanodiagnostics and electronic printing, respectively.

2D (*e.g.* graphene), and 3D (*e.g.* nanoprisms and nanoflowers).[9] In the following sections POC systems based on different types of nanomaterials and the advantages and drawbacks of their application in diagnostics will be reviewed.

2. Spherical nanomaterials (0D)

The most widely used nanomaterials are spherical nanomaterials owing to their simple preparation and manipulation. When a spherical nanoparticle is attached to a biomarker, a molecule that reacts only under specific pathological conditions is formed, and the resulting functionalized nanosphere can serve as a biological label for instance, to signal the presence of a given analyte or pathogen. The detection mechanisms for such nanoparticles can be quite diverse[10] including measuring the light absorption of the nanoparticles attached to the analyte (after a cleaning step), measuring the shift in the peak wavelength due to the agglomeration of the nanoparticles, enhancement by secondary enzymatic reactions onto the nanoparticle surface *via* a quenching effect (an intensity decrease in the fluorescence signal), surface plasmon resonance (optical changes and radiative enhancements in a nanomaterial due to disturbance of the dielectric constant induced by the adsorption of a molecule), electrical or electrochemical changes (when the nanomaterial is conductive or can catalyze a reaction that is electrochemically detectable), and electrical impedance spectroscopy (changes in the electrical resistance of a medium).

Among all the 0D nanomaterials, gold nanoparticles (AuNPs) have been widely reported and discussed.[11] This nanomaterial stands out due to its high bioaffinity, strong colour (its wavelength varies with small changes in its diameter or its surface) and even catalytic properties. Thus, it is commonly used for both optical and electrochemical PoC devices.

2.1. 0D optical-based PoC devices

Lateral flow biosensors (LFBs)[7] are optical-based PoC devices fabricated on paper substrates, one of the best-known examples of which is the common pregnancy test. LFBs evolved from thin-layer immunoaffinity chromatography,[12] a method based on the formation of a ''sandwich'' comprising a primary biomarker (often an antibody) attached to a paper substrate (cellulose or to favor the attachment of biomarkers, nitrocellulose), an analyte (proteins, cells, bacteria, molecules and even heavy metals) and a secondary biomarker, which is conjugated to the tag nanoparticle. The formation of this sandwich triggers the appearance of colour in the ''test zone'' (where the first biomarker has been deposited) for the positive sample, and if the sandwich is not assembled (lack of analyte in the sample), the test zone remains colourless (a negative sample). Latex beads were commonly used on LFBs and still are used for most commercial pregnancy tests. However, the inclusion of AuNPs on LFBs,[13] among other nanomaterials, improves the sensitivity of the method due to the strong colour of the nanomaterial, which is ascribed to the surface plasmon resonance effect present in metallic nanoparticles but not on latex beads. Furthermore, the shrinking of the label size down to the nanoscale eases the flow and boosts the label/analyte ratio. These improvements enable semi-quantitative assays, relating the color intensity with the analyte concentration, similarly to pH paper. By using a colorimetric reader or even a mobile phone,[2] the quantification level can be improved.

Besides AuNPs, other nanomaterials such as silver nanoparticles (AgNPs) have been used in LFBs; however, the wavelength variations triggered by size and shape modifications are bigger with AgNPs than with AuNPs, leading to color tonalities quite different between nanoparticles with less than 10 nm difference in size. Thus, AgNPs permit multiplexed tests to be performed[14] (*i.e.* for the simultaneous detection of different analytes on the same device), in which a different colour is obtained in each test zone. Also, fluorescent nanoparticles such as quantum dots[15] (QDs) or up-converting phosphor reporters[16] (UCPs are expensive because they are made using rare elements such as europium and yttrium), are being used in LFBs. Fluorescent nanoparticles lead to greater sensitivity and specificity than non-fluorescent nanomaterials since in fluorescence methods only the signal originating from the nanomaterial is read. However, the response cannot be observed by the naked eye. Equipment is necessary to excite and read the resulting fluorescence signal.

Various signal enhancement strategies exist for nanoparticles on paper substrates;[7] however, they often require the user to apply several additional steps, making the PoC system less user-friendly and increasing the human error factor. A way to simplify these steps was reported by Fu *et al.*[17] They presented a two-dimensional paper network combining LFBs with other paper pads, which were used for storing enhancement reagents (as shown in Fig. 2A). In this PoC system, the user must add the sample to the conjugate pad, on which the analyte is captured by AuNPs, and water to the other pads and then close the system. Initially, it works like a conventional LFB strip, where AuNPs stop in the detection zone, but once the enhancement reagents reach the detection zone the colour of the AuNPs changes to dark purple as their size increases. Against the white background, the dark purple grants a higher contrast compared to the original red. The limit of detection (LOD) achieved with this enhancement strategy was four times lower than that with standard LFBs. Rodriguez *et al.*[18] also proposed an interesting LFB to isolate, amplify and detect nucleic acids, all-in-one, equipment-free and much faster than conventional methods. Their system was comprised of an LFB strip equipped with some additional removable parts (Fig. 2B), a pad for washing the sample but retaining the purified DNA (Fig. 2b.1), a tab to prevent the evaporation of the isothermal amplification reagents (Fig. 2b.2), and some hydrophobic tape barriers to prevent DNA and other solvents from flowing prematurely to the LFB strip (Fig. 2b.3). Besides the LFB strips format, other possibilities to store nanomaterials on paper have been reported, but with the same signaling mechanism in the previously mentioned immunoassays. One example is the prototype proposed by Pauli *et al.*,[19] a lab-on-a-syringe used to collect urine and pump it to paper pads stored in serially connected cartridges. The first cartridge contained AuNPs for the capture of the analyte, a

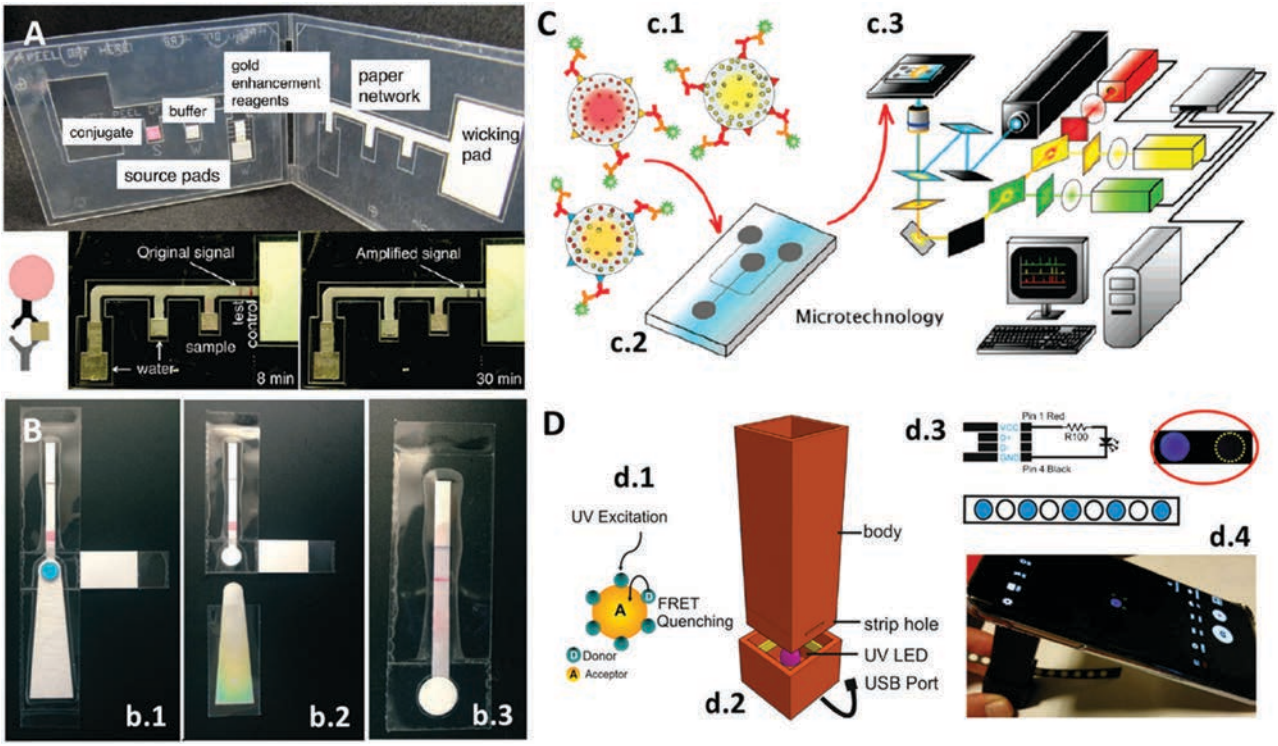

Fig. 2 (A) PoC colorimetric device in which the signal of the LFB system is increased *via* a paper network consisting of paper pads storing the colour enhancement reagent. Adapted with permission from ref. 17, Copyright 2012 American Chemical Society. (B) LFB system to extract, amplify and detect nucleic acids: (b.1) sample is added on the sample port, (b.2) absorbent pad is removed after washing steps, and (b.3) after the addition of the amplification reagents, the purified analytes flow across the LFBs. Adapted with permission from ref. 18, Copyright 2016 Royal Society of Chemistry. (C) Multiplexed barcode system containing QDs: (c.1) QDs of different colours encapsulated into microbeads with specific biomarkers for different targets, (c.2) microfluidics system, and (c.3) detection platform. Adapted with permission from ref. 22, Copyright 2007 American Chemical Society. (D) Mobile phone integrated PoC system: (d.1) graphene QDs are quenched in the presence of acceptor compounds, (d.2) 3D-printed device with UV LED, (d.3) LED mechanism and paper substrate containing dried graphene QDs, and (d.4) mobile phone measuring the quenching of QDs. Adapted with permission from ref. 3, Copyright 2017 Nature Publishing Group.

cancer biomarker, and the second cartridge contained the detection pad. The detection pad consisted of nitrocellulose paper with detection antibodies inside a wax ring to focus the flow to pass through the antibodies. Similar to AuNPs-based LFBs, the inner part of the ring will turn redder with a higher amount of analyte. In contrast to LFBs, the lab-on-a-syringe requires the user to control the flow, thus it less user-friendly than a paper strip. However, it permits the modification of the incubation times for the AuNPs with analyte, which can lead to improved sensitivities. Also, a filter can be coupled to the syringe to reduce matrix effects.

The application of nanopaper, also known as bacteria cellulose paper, is remarkable because it is produced by bacteria. As reported by Morales-Narváez *et al.*,[20] 0D nanoparticles can be stored and even produced on this colorless substrate resulting in plasmonic or fluorescent paper with great potential as an alternative to enzyme-linked immunosorbent assay (ELISA) plates. Their work demonstrated that PoC devices fabricated with nanopaper can take other forms besides ELISA plates such as cuvettes or simple spots on a piece of paper. Plasmonic resonance, fluorescence and quenching effects are some of the measurements that can be performed with these systems by using nanomaterials such as AgNPs, AuNPs and QDs. Similar to nanopaper, hydrogels can be used to store nanomaterials for use in PoC applications, which Yetisen *et al.*[21] demonstrated with AgNPs and a phenylboronic acid-functionalized hydrogel. Their system could filter urine samples and retain glucose. Then, within five minutes a laser could measure the diffraction provoked by the interaction of the AgNPs and glucose. Surprisingly the system is reusable, unlike paper-based systems.

As previously mentioned, QDs are small 0D nanomaterials with fluorescent properties. Klostranec *et al.*[22] utilized the intense signal of QDs to construct a multiplex system for the detection of different blood infectious disease-related targets using a "barcode" system (Fig. 2C). Different colored QDs were encapsulated into microbeads (Fig. 2c.1), and each bead was conjugated with antibodies specific to a different target, and the particles then were mixed inside a microfluidic system (Fig. 2c.2) with the sample. The incubation inside the microfluidics was controlled electrokinetically. Data collection was performed with software and a detection platform (Fig. 2c.3), which the authors claimed could be miniaturized for PoC diagnosis in the future. Their platform can identify independently the wavelength of each QD type, normalize it and, similarly to a barcode reading, estimate the amount of each target.

Another interesting work involving QDs was reported by Álvarez-Diduk *et al.*[3] As shown in Fig. 2D, they took advantage of the fluorescence quenching effect occurring on graphene QDs in the presence of some polyphenolic compounds (Fig. 2d.1). They fabricated a 3D-printed dark chamber (Fig. 2d.2) with a UV LED powered by a mobile phone to excite the QDs (Fig. 2d.4). Using wax-printed traced spots on a paper strip, the QDs were physisorbed inside the spots to give an ELISA plate-like system (Fig. 2d.3). When polyphenolic compounds are dropped onto the spots, the fluorescence is quenched and captured by a mobile phone camera (Fig. 2d.4). The images can be analyzed directly on the mobile phone with an app or later with computer software.

2.2. 0D electrochemical-based PoC devices

Electrochemical measurements allow the identification of electrical phenomena related to a chemical change. The function of nanomaterials in this type of measurement is not limited to analyte labelling. Nowadays, nanoparticles are commonly used in commercial inks for the fabrication of electrodes. 0D nanomaterials as AuNPs or AgNPs and 1D nanomaterials such as carbon nanotubes (CNTs) are the most commonly used nanoparticles. As an example, da Silva *et al.*[23] used commercial AgNPs to fabricate a miniaturized and portable Ag/AgCl reference electrode with a known and stable potential. They printed the electrode on two different flexible substrates, paper and polyethylene terephthalate (PET), using a high resolution piezoelectric inkjet material printer (Fig. 3A). After printing, the AgNPs ink was cured at 120 °C and treated with bleach (sodium hypochlorite, NaClO) to produce an Ag/AgCl mixture, which served as a pseudo reference electrode.

The reduction of silver is catalyzed by AuNPs, which in turn are extensively reported as transducers in electrochemical assays due to their high affinity to biological molecules.[24] Another reaction that is often applied in electrochemistry and catalyzed by AuNPs is the hydrogen evolution reaction, which is the formation of H_2 gas by the reduction of H^+ ions. This reaction

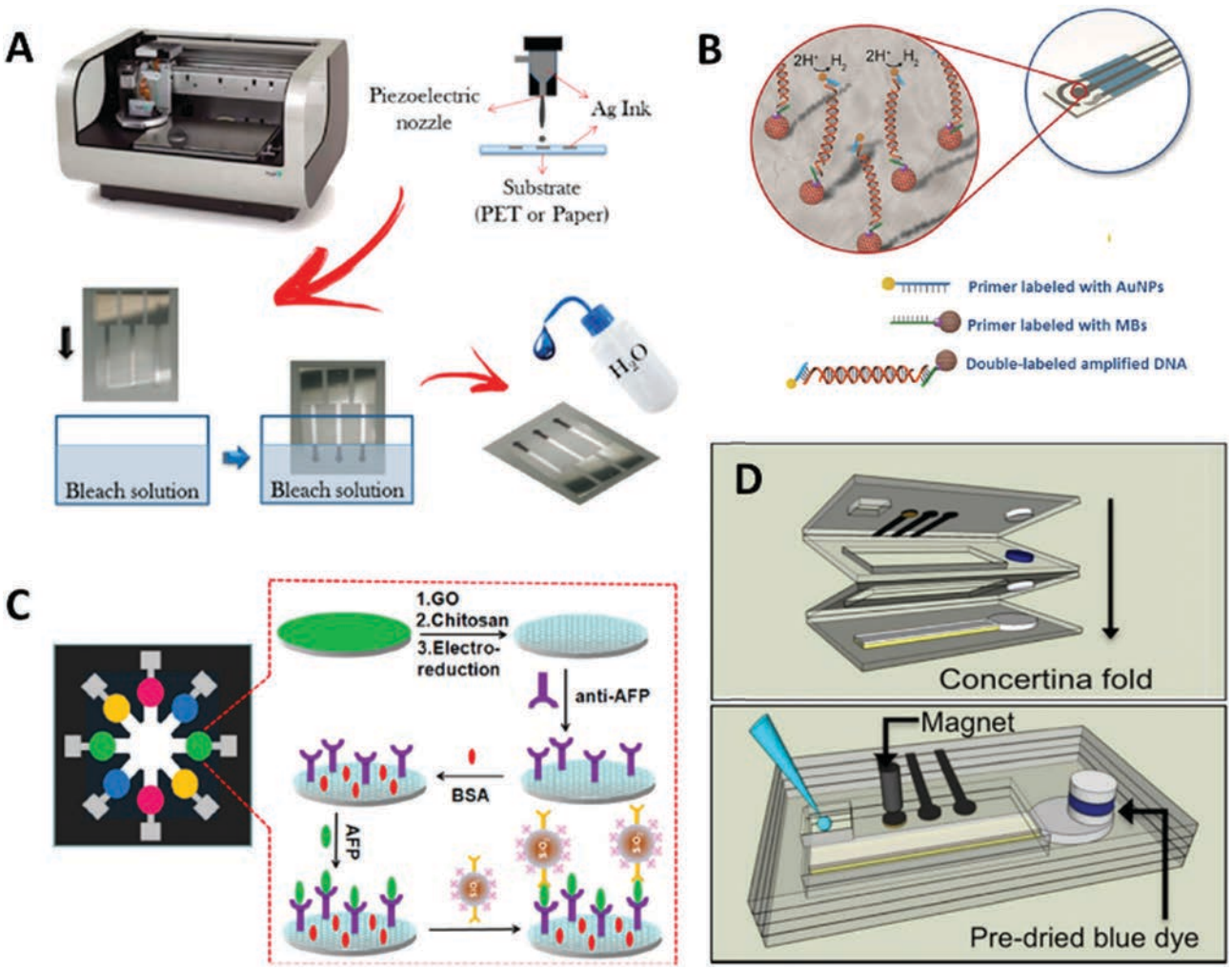

Fig. 3 (A) Ag/AgCl reference electrodes fabricated from AgNPs using inkjet technology and bleach treatment. Adapted with permission from ref. 23, Copyright 2014 American Chemical Society. (B) Combination of AuNPs and MBs for the detection of DNA on an SPCE. Adapted with permission from ref. 25, Copyright 2015 John Wiley and Sons. (C) Paper PoC device for the electrochemical measurement of eight samples. Adapted with permission from ref. 30, Copyright 2013 American Chemical Society. (D) Paper origami PoC for the electrochemical detection of AgNPs. Unfolded (up) and folded (down). Adapted with permission from ref. 31, Copyright 2016 American Chemical Society.

was measured by de la Escosura-Muñiz *et al.*[25] who, combining DNA amplification strategies, magnetic beads (MBs) and AuNPs, developed a system on screen printed carbon electrodes (SPCE) that discriminates dog DNA from Leishmania parasite DNA hosted inside the cells. MBs and AuNPs are linked to the amplified DNA and, using a magnet, the conjugate is placed onto the working electrode of the SPCE for the signal to be measured efficiently (Fig. 3B). Iridium oxide nanoparticles (IrO_2NPs) are another 0D nanomaterial used due to their catalytic properties towards the water oxidation reaction,[26] which is the production of oxygen from water, and their application in impedimetric sensors.[27,28] Impedance is a technique used to measure the frequency changes in the dielectric medium close to the nanoparticles. Thus, by binding biomarkers on IrO_2 NPs, it is possible to detect variations in the conductivity of the medium depending on the capture of the biomarker by the target analyte.

Regarding AuNP-based LFBs, which are analogous to optical detection, some researchers are trying to integrate electrochemical sensing strategies into paper strips to achieve lower detection limits and higher sensitivity than colorimetric techniques.[29] However, this requires the detection zone of the strips to be cut and dissolved in acid, thus the detection is performed with external electrodes on the dissolved nanoparticles. The addition of this extra step enhances the quantification on LFBs, but the methodology still needs to be improved either by including the step in an automated PoC device or by finding an alternative to dissolving part of the strip. A more user-friendly paper-based PoC tool was designed by Wu *et al.*,[30] which permits the electrochemical analysis of eight samples sequentially (Fig. 3C). This device is comprised of eight electrodes pre-treated with antibodies specific to the target analyte. The samples are added to the electrodes and then SiO_2 nanoparticles are dispensed on the electrodes (note that SiO_2 nanoparticles are inexpensive and easy to load with various compounds such as dyes, proteins and enzymes). In this case, the SiO_2 nanoparticles are loaded with antibodies specific to the analyte to perform a sandwich assay with horseradish peroxidase, the enzyme that triggers the electrochemical reaction. The electrodes are washed and then a reactive solution is added to the core of the device, which then flows to the electrodes, thereby activating an electrochemical reaction. Another interesting paper PoC device was fabricated by Cunningham *et al.*,[31] an origami-styled system that as proof-of-concept was used for the detection of AgNPs by oxidizing them using a gold working electrode. The device consists of four folded paper layers (Fig. 3D), where the first layer contains the electrodes, inlet and outlet; the second and third layers contain a paper circuit delimited by wax and a blue dye that works as an indicator for the stoppage of the flow; and the forth layer contains a "sink" to redirect all the flow there.

2.3. 0D magnetic PoC devices

MBs and magnetic nanoparticles (MNPs) are often used as supports in PoC devices, usually in the washing and pre-concentration/amplification steps or in the precipitation of the analyte and other nanoparticles for example onto an electrode.[25] Some researchers are also taking advantage of the magnetic properties of MNPs and use these as transducers[32,33] by means of nuclear magnetic resonance (NMR). This technique is highly sensitive due to the low back-ground signal since non-magnetic substances exhibit no interference. In addition, NMR can detect all the tags present in the detection zone; whereas in optical and electrochemical sensors this is not always possible (in optical sensors, generally only the tags on the substrate surface are visible; and in electrochemical sensors, it is often required that the tags are in contact with the electrode to be able to generate a signal). In addition, the detection time is faster than electrochemical assays. However, NMR systems are expensive and may not be affordable to all possible users.

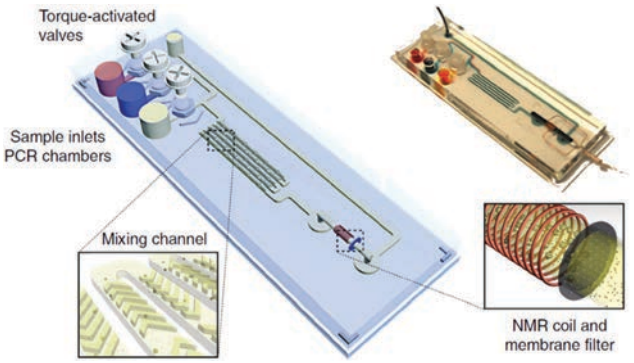

Fig. 4 NMR-based microfluidic PoC device. Reprinted with permission from ref. 32, Copyright 2013 Nature Publishing Group.

Liong *et al.*[32] proposed a microfluidics PoC device (Fig. 4) to detect amplified nucleic acids from a bacterium related to tuberculosis. The device can perform DNA amplification, MNPs-DNA incubation, washing and NMR detection. The device has three inlets for DNA, MNPs and washing buffer; some mixing channels for the incubation steps and an NMR coil that counts the amount of MNPs, which is proportional to the initial value of DNA concentration. As the main drawback in this device, although the NMR detection is fast, the amplification and incubation steps can prolong the duration of the assay by more than two hours. Anyhow, it is faster than other tuberculosis detection methods based on cell culture and microscopy. Chung *et al.*[33] developed another NMR-based microfluidics PoC device, which they used for the detection of a biomarker in urine. Although its matrix is complex, the noise signal is low because non-magnetic substances do not interfere with the readout, as previously mentioned. Their device exhibited a LOD 8 times lower than a comparable reported colorimetric dipstick method.

3. One-dimensional nanomaterials (1D)

1D nanomaterials are materials in which growth is oriented in one dimension, in a linear way. Their thickness can be as small as just one nanometer such as single-walled carbon nanotubes (SWCNTs), but their length could be a million times larger, such as hundreds of micrometers. The shape of these nanomaterials has an important effect on their application, where their length and diameter define their absorption wavelengths. Moreover, their length and thickness also grant mechanical

strength, which is useful in the creation of larger nanostructured materials. Nonetheless, the growth of 1D nanomaterials is not simple and often requires meticulous synthetic routes that in turn determine their homogeneity.

Nanowires are the simplest 1D nanomaterial, which can be created from other 0D nanomaterials or directly, and copper, nickel, silver, gold, platinum and silicone the most used elements. In the work of Mostafalu and Sonkusale,[34] they introduced nanowires (made from platinum, nickel and copper) into paper substrates to create electrodes for electrocardiogram monitoring by means of tissue-electrode impedance, which work in dry conditions. This approach does not require the addition of an electrolytic gel between the electrodes and the skin, which is advantageous since gels dry quickly and are degraded with movement. The high surface area of the nanowires provides a good quality response in the electrodes, which ranged from 100 to 1 KΩ in the impedimetric measurements. Besides medical application, Mostafalu and Sonkusale demonstrated that the same paper electrodes worked properly as cathodes in an acidic battery.

In recent years, CNTs and SWCNTs have been widely used in electrochemical applications[35–37] since these nanomaterials are highly conductive, both electrically and thermally. Additionally, CNTs are easily functionalized not only with biological compounds, but also with other nanomaterials (especially with metallic oxide nanoparticles), provoking an enhancement in their electrical properties, among others.[35] CNTs have also been utilized in several commercial inks for the fabrication of screen printed electrodes (also, AgNPs are commonly used for the fabrication of reference electrodes and CNTs are used for the fabrication of counter and working electrodes[36]). In comparison to metallic nanowires, CNTs contribute to the fabrication of larger nanostructured materials with new properties such as high flexibility, elasticity and low weight since they are hollow inside. Also, CNTs are more robust than nanowires against temperature variations because the thermal expansion coefficient of carbon bonds is much lower than that in metals. However, it is important to consider that many reactions that can be applied on their surface will not be reversible, making the lifetime of CNTs shorter than other materials applied in sensing. As an example of the use of these materials, the work of Nemiroski *et al.*[37] should be mentioned, where they integrated electrodes made with CNTs into a mobile phone system *via* the audio jack of the device (the audio jack has the advantage that it can send and receive information at the same time).

In a very smart way and for the first time, Azzarelli *et al.*[5] used SWCNT to apply NFC technology for sensing. NFC technology can detect an antenna without requiring it to have an electrical power supply. This technology nowadays is present in most smartphone models, hotel door lock systems, metro stations, toys and even in mail stamps. Thus, NFC tags are becoming cheaper daily and easier to fabricate and modify. They tuned an NFC tag by replacing part of the circuit with SWCNTs, which by means of a chemiresistive reaction, alter the conductivity in the circuit depending on the presence of different compounds in the air, consequently making it act as an on/off logic gate inside the NFC tag (Fig. 5a). This technique was applied for the detection of compounds in the air, but for future PoC applications it can be used to detect analytes in the breath or probably even in bodily fluids such as blood and sweat.

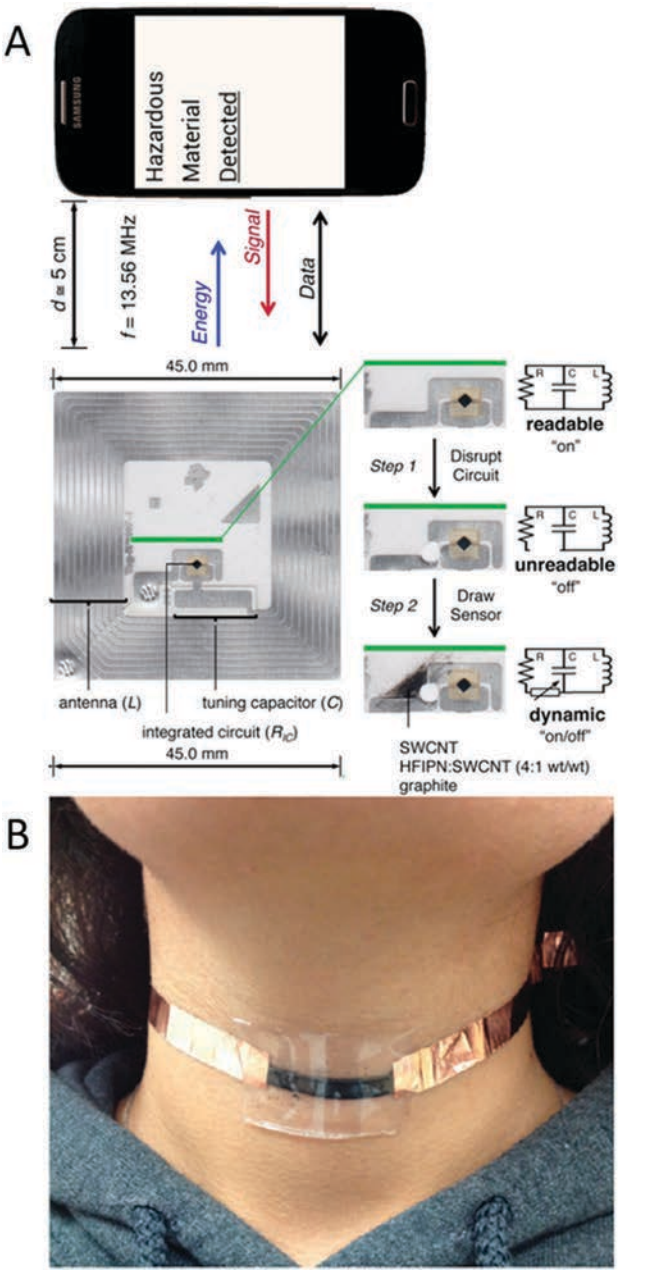

Fig. 5 (A) NFC tag circuit modified with SWCNTs to work as an on/off logic gate in the presence of different analytes. Adapted with permission from ref. 5, Copyright 2014 National Academy of Sciences. (B) Chewing gum containing CNTs adapted for motion monitoring. Reprinted with permission from ref. 38, Copyright 2015 American Chemical Society.

One more surprising use of CNTs was by Darabi *et al.* in chewing gum.[38] They washed a chewing gum with water and ethanol and mixed it with a solution containing CNTs. Then, the mixture was stretched and folded several times in one direction to favor the orientation of the CNTs. This sensor worked properly for the detection of humidity in the medium

(dryness of the mouth can be caused by certain medications or illnesses, by damage to the salivary glands or by hormonal changes) by measuring the electrical resistance in the gum. Also, as a motion sensor, as shown in Fig. 5b, it can detect not only body (neck in the figure) movements, but also the breath of the user. This device can be very interesting for PoC diagnostics (biting problems, dry mouth, and pulsations, and even take advantage of chemical reactions to detect different targets). However, there are two important drawbacks that preclude the introduction of the device into the mouth: its response is measured using electrical circuits and CNTs are currently classified as cytotoxic nanomaterials.

4. Single-layer nanomaterials (2D)

The compounds classified as 2D-nanomaterials can expand themselves in two directions and are composed of a monolayer of atoms or an ultrathin layer of a few atom. Albeit there exist several inorganic 2D nanomaterials, graphene has been by far the most used 2D material in the last years. Although graphene is considered a material composed of a single layer of atoms, it is quite difficult to find it in that state because it is usually found in groups of graphene layers. Depending on the number of layers, the electrical, optical and mechanical properties of graphene may differ. Other important parameters that affect the behavior of graphene are its oxidation level, the number of structural defects, purity degree, *etc.*,[39] which can be controlled *via* its synthetic route.

Graphene can be combined with QDs to work as a quencher (silencing the fluorescence signal of QDs when both are in contact). This property was harnessed for the fabrication of LFBs by Morales-Narváez *et al.*[15] In their system, they dispensed two lines of QDs on a paper substrate, as the test and control, where the first line was capable of capturing some bacteria (by means of antibodies attached on QDs). After adding the sample on the LFBs, a solution of graphene oxide (GO) is added, which is the oxidized form of graphene containing epoxy bridges, carboxyl and hydroxyl groups. GO will turn off the fluorescence of the QDs in the control line and the test line if there are no bacteria in the sample. However, in presence of bacteria captured on the test line it will produce a gap between the GO and QDs, resulting in the emission of fluorescence. In comparison to traditional LFBs, this method prevents the formation of false positives during the assay since a negative sample will always turn off both lines (in the case where something external causes the test line not to be quenched, the control line will be also affected, obtaining an invalid strip but not a false positive). However, the assay time (more than 1 h) is longer than that for standard LFBs (usually of 5–10 min) due to the extra step of GO addition and drying, including the waiting time for the bacteria to flow across the strip.

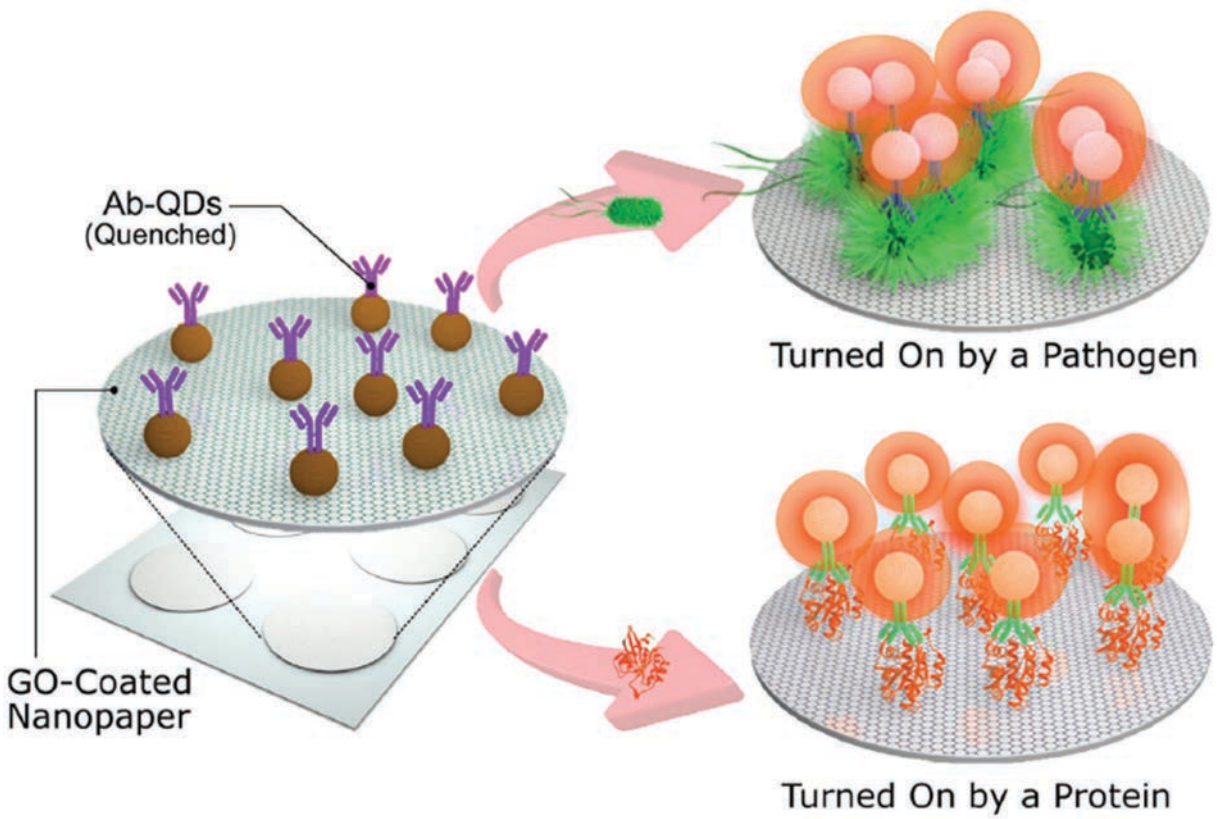

Fig. 6 Nanopaper coated with GO. QDs can be stored inside remaining quenched but when the analyte, *e.g.* bacteria or proteins, is added fluorescence is observed. Adapted with permission from ref. 40, Copyright 2017 John Wiley and Sons.

Cheeveewattanagul *et al.*[40] coated nanopaper with GO and introduced on this composite a suspension of antibodies attached to QDs. Again, the quenching effect keeps the fluorescence of the QDs silenced. Then, when an analyte (*e.g.* bacteria or proteins for which the antibodies are selective) is added, a gap is produced between the QDs and GO, negating the quenching effect and allowing fluorescence (Fig. 6). This technique is quite advantageous since it does not require washing steps, is portable and fast. Thus, it is a promising alternative to ELISA tests.

Owing to its electrical properties, graphene can be used for the fabrication of working electrodes.[41,42] Antibodies can be conjugated onto the surface of graphene by coating pure graphene with polymers or by exploiting the chemistry of the carboxylic or hydroxyl groups in GO. Moreover, since graphene is planar, the antibodies can all be oriented perpendicularly to the graphene layer to increase the probability of capturing the analyte.[41] Furthermore, graphene electrodes are sufficiently sensitive to allow label-free sensing, and small changes (*i.e.* electrochemical[41,42] or impedimetric[39,43] alterations) on the electrode surface are easy to detect. On the other hand, as a drawback, graphene demands highly meticulous control of its synthesis for reproducibility, especially regarding the number of layers and structural defects.

Baptista-Pires *et al.*[43] designed a new solvent-free method for printing GO on different substrates using wax-printed patterns *via* printing on nitrocellulose membranes and vacuum filtration. GO remains on the non-wax-printed areas and is transferred to the target substrate by pressure. To demonstrate the possibilities of this technique, a touch sensor was printed, which was based on the resistance changes provoked by a finger in contact with the GO-printed circuit. This GO touch sensor is shown in Fig. 7A, which was connected to an LED and a power source (Fig. 7a.1), where the sensor works as a simple switch, turning on/off the LED (Fig. 7a.2 and a.3, respectively). This technology can be used to replace current touchscreens, which use controversial elements such as indium and rare-Earth metals,[2] and in wearable PoC applications that require flexible devices (*e.g.* skin tattoo sensors[34]) or those based on contact-sensing (*e.g.* pressure or motion sensors[38]).

Besides its mentioned characteristics, graphene is also an electrochromic material, and it can be tuned to change its colour in a reversible way depending on the current supplied. Polat *et al.*[44] developed different electrochromic flexible devices using this property. In one of their devices they attached two plastic substrates coated on one side with graphene electrodes and a liquid electrolyte in between. When a voltage is applied across the electrodes, graphene turns translucent because the

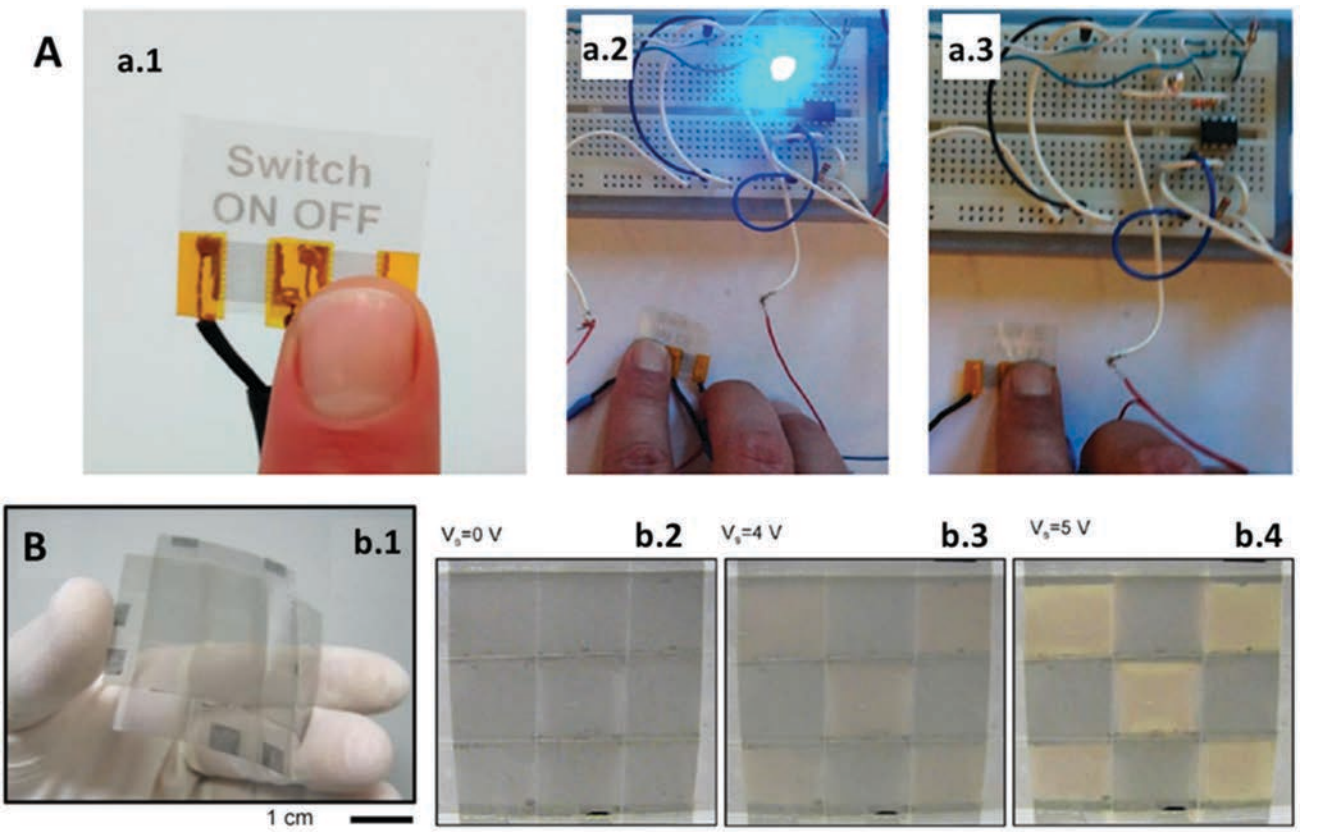

Fig. 7 (A) GO tactile device: (a.1) GO switch works by skin contact turning a LED from (a.2) ON to (a.3) OFF status. Adapted with permission from ref. 43, Copyright 2016 American Chemical Society. (B) Electrochromic device composed of (b.1) flexible graphene electrodes whose transmittance increases when a current is applied: (b.2) 0 V and (b.3 and b.4) chess pattern visible at a higher voltage. Adapted with permission from ref. 44, Copyright 2014 Nature Publishing Group.

voltage is enough to penetrate the graphene layers creating structural defects, which fade its characteristic black colour. Their final device is shown in Fig. 7B, which was fabricated using various graphene electrodes. The device is flexible (Fig. 7b.1) and graphene can resist curvature with a 1 cm radius without being damaged. By applying different voltages on some of the electrodes, they create a chess pattern since transmittance is increased on the layers where the current is increased, including 0 V (Fig. 7b.2), 4 V (Fig. 7b.3), and 5 V (Fig. 7b.4). Thanks to this technology, electrochemical signaling can be converted into optical responses *in situ*, resulting in more user-friendly wearable PoC devices.

5. Other nanomaterials (3D)

There are an extensive variety of 3D materials varying both in shape and size, which lead to different possibilities in the final sensing application. Non-spherical nanoparticles exhibit properties quite similar to 0D nanomaterials; however, changes in shape often lead to absorbance changes (*i.e.* the colour of a solution of gold nanospheres may be different from a solution of nanocubes or nanotriangles, even when their chemical composition and size are the same). Taking advantage of this fact, plasmonic-based PoC sensors can be fabricated, such as that reported by Fu *et al.*[4] Their device is portable and can be coupled into a mobile phone, using its light sensor, which is included on most modern mobile phones to improve their photograph quality or control the screen brightness. The device consists of a plate, where the sample is added, and an LED, which illuminates the sample in the plate and reaches the light sensor. To demonstrate the capabilities of their device they used it to measure the plasmonic changes occurring on triangular silver nanoprisms in the absence of a cancer biomarker. This is an indirect detection method, which triggers a shape transformation in the nanoparticles with hydrogen peroxide. Li *et al.*[45] also used a 3D silver nanomaterial, nanoporous silver, which can be used as signal enhancer, label and metallic ion carrier. Their system consists of a multiplex electrochemical origami paper device (Fig. 8) that uses nanoporous silver loaded with different metallic ions as labels for tumor sensing. A silver electrode is used as the reference electrode (Fig. 8A) and screen-printed carbon electrodes as the counter and working electrodes (Fig. 8B). This paper device can be folded (Fig. 8C) and integrated into an electrical circuit (Fig. 8D).

Some non-spherical nanoparticles exhibit electrochromic properties such as the WO_3 nanoparticles used by Marques *et al.*[46] on a paper substrate. The nanoparticles change from yellow to blue in the presence of electrochemically active bacteria. Thus, this is a simple sensor that functions similarly to ELISA assays but without time-consuming steps or the use of delicate reagents (*i.e.* biological reagents have short expiration dates; whereas,

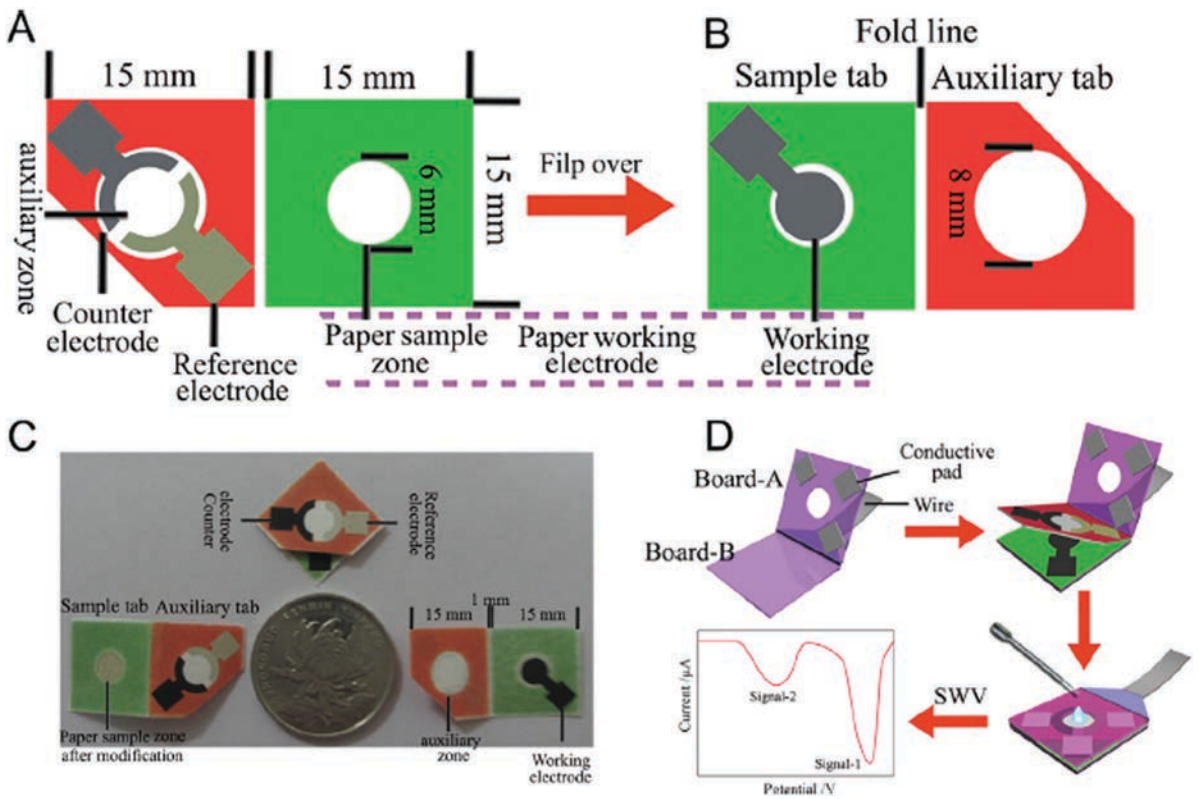

Fig. 8 Multiplex electrochemical origami paper device: (A) front part: silver reference electrode and carbon counter electrode; (B) back part: carbon working electrode; (C) size comparison of the device and (D) its application for electrochemical measurements. Adapted with permission from ref. 45, Copyright 2014 Elsevier.

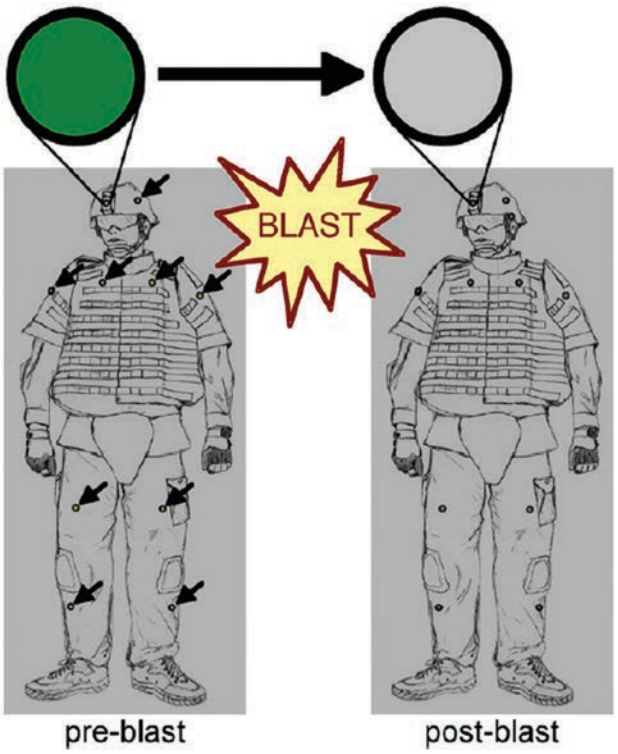

Fig. 9 PC-based wearable that changes colour in response to the shock wave of a blast. Reprinted with permission from ref. 50, Copyright 2011 Elsevier.

nanomaterials can last long periods of time, even when stored at room temperature). Photonic crystals (PC) are other example of electrochromic materials often composed of other nanoparticles, which are assembled following a crystalline pattern. These nanomaterials demonstrate good adaptability in different types of sensors due to their resistance to being bent,[47] and are used in microfluidic systems both in polymeric channels[48] and paper,[49] which permit label-free sensing (a colour change occurs when the analyte attaches or passes near the PC). Cullen *et al.*[50] converted PC into simple PoC wearable stickers that can be settled on clothes to warn its user in a war zone about possible aftermaths related to the expansive wave of a blast (Fig. 9). PC are broken when subjected to high pressure as consequence of an explosion thus changing their colour, which notifies the user that the blast may have induced non-visible injuries such as internal trauma or brain damage.

6. Conclusions

Daily, PoC devices are becoming indispensable tools for diagnostics, which are required not only by medical specialists at hospitals or the doctor's office but anyone, even at home or outdoors. Although most of the discussed devices are only demonstrated as proof-of-concept, it is clearly shown that nanomaterials exhibit several advantages when integrated in PoC systems.

Table 1 summarizes the different nanomaterial types, with the most common examples of each classification, the possible detection methods that the final PoC can employ and some of the strengths and weaknesses in each case. Depending on the properties of the nanomaterials and the way they are integrated within PoC devices, various detection technologies can be used, where optical and electrochemical detection are the most reported.

Although electrical techniques employing nanomaterials as electrodes or electrocatalysts are well-known to exhibit higher sensitivity and lower detection limits, optical techniques are emerging given their simplicity and easy integration in paper/plastic platforms, including easy and efficient coupling with smartphones.

The synergy of nanomaterials with a variety of biosensing systems and communication technologies is excepted to yield innovative PoC systems that may develop from research labs to fulfil the ASSURED (Affordable, Sensitive, Specific, User-friendly, Rapid & Robust, Equipment-free and Deliverable to end-users) criteria by the WHO[6] for applications in diagnostics.

Table 1 Summary of the nanomaterial types: examples, corresponding PoC detection principles, advantages and disadvantages

Nanomaterial type	Examples of nanomaterials	PoC detection principle	Advantages	Disadvantages
0D	• AuNPs • AgNPs • QDs • UPCs • Magnetic nanoparticles	• Optical • Fluorescent • Electrochemical • Magnetic	• Simple synthetic procedures • Small size • Easy to bioconjugate • Adaptable into other nanomaterials	• No special structural properties • Some 0D nanomaterials can easily agglomerate
1D	• Nanowires • CNTs	• Electrochemical • Motion	• Highly conductive • Orientable • Structurally resistant	• Complex synthesis • Difficult to control their shape
2D	• Graphene	• Electrochemical • Fluorescence • Tactile	• Easy to modify • Flexible • Fluorescence quencher	• Difficult to separate a single graphene sheet • Structural defects are common
3D	• Non-spherical nanoparticles • PCs	• Optical • Electrochemical	• Can combine the properties of other nanomaterials • Tunable optical properties	• Like 0D nanomaterials, 3D nanomaterials can easily agglomerate • Usually, not as small as 0D nanomaterials

Conflicts of interest

There are no conflicts of interest to declare.

Acknowledgements

The ICN2 is funded by the CERCA Programme/Generalitat de Catalunya. The ICN2 is supported by the Severo Ochoa program of the Spanish Ministry of Economy, Industry and Competitiveness (MINECO, grant no. SEV-2013-0295). We acknowledge support from the Spanish MINECO under project PCIN-2016-066 (program Euronanomed 2). This work has been done in the framework of PhD Programme in Chemistry of Universitat Autònoma de Barcelona.

References

1 M. A. Burns, *Science*, 2002, **296**, 1818–1819.
2 D. Quesada-González and A. Merkoçi, *Biosens. Bioelectron.*, 2017, **92**, 549–562.
3 R. Álvarez-Diduk, J. Orozco and A. Merkoçi, *Sci. Rep.*, 2017, **7**, 976.
4 Q. Fu, Z. Wu, F. Xu, X. Li, C. Yao, M. Xu, L. Sheng, S. Yu and Y. Tang, *Lab Chip*, 2016, **16**, 1927–1933.
5 J. M. Azzarelli, K. A. Mirica, J. B. Ravnsbæk and T. M. Swager, *PNAS*, 2014, **111**(51), 18162–18166.
6 A. K. Yetisen, M. S. Akram and C. R. Lowe, *Lab Chip*, 2013, **13**, 2210–2251.
7 D. Quesada-González and A. Merkoçi, *Biosens. Bioelectron.*, 2015, **73**, 47–63.
8 M. Sher, R. Zhuang, U. Demirci and W. Asghar, *Expert Rev. Mol. Diagn.*, 2017, **17**(4), 351–366.
9 J. N. Tiwari, R. N. Tiwari and K. S. Kim, *Prog. Mater. Sci.*, 2012, **57**, 724–803.
10 M. Perfézou, A. Turner and A. Merkoçi, *Chem. Soc. Rev.*, 2012, **41**, 2606–2622.
11 M. Wuithschick, A. Birnbaum, S. Witte, M. Sztucki, U. Vainio, N. Pinna, K. Rademann, F. Emmerling, R. Kraehnert and J. Polte, *ACS Nano*, 2015, **9**(7), 7052–7071.
12 S. Birnbaum, C. Udén, C. G. M. Magnusson and S. Nilsson, *Anal. Biochem.*, 1992, **206**, 168–171.
13 R. H. Shyu, H. F. Shyu, H. W. Liu and S. S. Tang, *Toxicon*, 2002, **40**, 255–258.
14 C. W. Yen, H. de Puig, J. Tam, J. Gómez-Márquez, I. Bosch, K. Hamad-Schifferli and L. Gehrke, *Lab Chip*, 2015, **15**(7), 1638–1641.
15 E. Morales-Narváez, T. Naghdi, E. Zor and A. Merkoçi, *Anal. Chem.*, 2015, **87**, 8573–8577.
16 P. L. A. M. Corstjens, C. J. de Dood, D. Kornelis, E. M. T. K. Fat, R. A. Wilson, T. M. Kariuki, R. K. Nyakundi, P. T. Loverde, W. R. Abrams, H. J. Tanke, L. V. Lieshout, A. M. Deelder and G. J. Van Dam, *Parasitology*, 2014, **141**, 1841–1855.
17 E. Fu, T. Liang, P. Spicar-Mihalic, J. Houghtaling, S. Ramachandran and P. Yager, *Anal. Chem.*, 2012, **84**, 4574–4579.
18 N. M. Rodriguez, W. S. Wong, L. Liu, R. Dewar and C. M. Klapperich, *Lab Chip*, 2016, **16**, 753–763.
19 G. E. N. Pauli, A. de la Escosura-Muñiz, C. Parolo, I. H. Bechtold and A. Merkoçi, *Lab Chip*, 2015, **15**, 399.
20 E. Morales-Narváez, H. Golmohammadi, T. Naghdi, H. Yousefi, U. Kostiv, D. Horák, N. Pourreza and A. Merkoçi, *ACS Nano*, 2015, **9**(7), 7296–7305.
21 A. K. Yetisen, Y. Montelongo, F. da Cruz Vasconcellos, J. L. Martinez-Hurtado, S. Neupane, H. Butt, M. M. Qasim, J. Blyth, K. Burling, J. B. Carmody, M. Evans, T. D. Wilkinson, L. T. Kubota, M. J. Monteiro and C. R. Lowe, *Nano Lett.*, 2014, **14**, 3587–3593.
22 J. M. Klostranec, Q. Xiang, G. A. Farcas, J. A. Lee, A. Rhee, E. I. Lafferty, S. D. Perrault, K. C. Kain and W. C. W. Chan, *Nano Lett.*, 2007, **7**(9), 2812–2818.
23 E. T. S. G. da Silva, S. Miserere, L. T. Kubota and A. Merkoçi, *Anal. Chem.*, 2014, **86**, 10531–10534.
24 S. J. Park, T. A. Taton and C. A. Mirkin, *Science*, 2002, **295**, 1503–1506.
25 A. de la Escosura-Muñiz, L. Baptista-Pires, L. Serrano, L. Altet, O. Francino, A. Sánchez and A. Merkoçi, *Small*, 2016, **12**(2), 205–213.
26 L. Rivas, A. de la Escosura-Muñiz, J. Pons and A. Merkoçi, *Electroanalysis*, 2014, **26**(6), 1287–1294.
27 L. Rivas, C. C. Mayorga-Martínez, D. Quesada-González, A. Zamora, A. de la Escosura-Muñiz and A. Merkoçi, *Anal. Chem.*, 2015, **87**(10), 5167–5172.
28 C. C. Mayorga-Martinez, A. Chamorro-García, L. Serrano, L. Rivas, D. Quesada-González, L. Altet, O. Francino, A. Sánchez and A. Merkoçi, *J. Mater. Chem. B*, 2015, **3**, 5166–5171.
29 X. Mao, M. Baloda, A. S. Gurung, Y. Lin and G. Liu, *Electrochem. Commun.*, 2008, **10**, 1636–1640.
30 Y. Wu, P. Xue, Y. Kang and K. M. Hui, *Anal. Chem.*, 2013, **85**, 8661–8668.
31 J. C. Cunningham, M. R. Kogan, Y. J. Tsai, L. Luo, I. Richards and R. M. Crooks, *ACS Sens.*, 2016, **1**, 40–47.
32 M. Liong, A. N. Hoang, J. Chung, N. Gural, C. B. Ford, C. Min, R. R. Shah, R. Ahmad, M. Fernandez-Suarez, S. M. Fortune, M. Toner, H. Lee and R. Weissleder, *Nat. Commun.*, 2013, **4**, 1752.
33 H. J. Chung, K. L. Pellegrini, J. Chung, K. Wanigasuriya, I. Jayawardene, K. Lee, H. Lee, V. S. Vaidya and R. Weissleder, *PLoS One*, 2015, **10**(7), e0133417.
34 P. Mostafalu and S. Sonkusale, *RSC Adv.*, 2015, **5**, 8680–8687.
35 A. Ali, P. R. Solanki, S. Srivastava, S. Singh, V. V. Agrawal, R. John and B. D. Malhotra, *ACS Appl. Mater. Interfaces*, 2015, **7**, 5837–5846.
36 S. Teixeira, R. S. Conlan, O. J. Guy and M. G. F. Sales, *Electrochim. Acta*, 2014, **136**, 323–329.
37 A. Nemiroski, D. C. Christodouleas, J. W. Hennek, A. A. Kumar, E. J. Maxwell, M. T. Fernández-Abedul and G. M. Whitesides, *PNAS*, 2014, **111**(33), 11984–11989.
38 M. A. Darabi, A. Khosrozadeh, Q. Wang and M. Xing, *ACS Appl. Mater. Interfaces*, 2015, **7**, 26195–26205.
39 E. Morales-Narváez, L. Baptista-Pires, A. Zamora-Gálvez and A. Merkoçi, *Adv. Mater.*, 2017, **29**, 1604905.

40 N. Cheeveewattanagul, E. Morales-Narváez, A. R. H. A. Hassan, J. F. Bergua, W. Surareungchai, M. Somasundrum and A. Merkoçi, *Adv. Funct. Mater.*, 2017, **27**, 1702741.
41 S. Teixeira, R. S. Conlan, O. J. Guy and M. G. F. Sales, *J. Mater. Chem. B*, 2014, **2**, 1852–1865.
42 S. K. Tuteja, Priyanka, V. Bhalla, A. Deep, A. K. Paul and C. R. Suri, *Anal. Chim. Acta*, 2014, **809**, 148–154.
43 L. Baptista-Pires, C. C. Mayorga-Martínez, M. Medina-Sánchez, H. Montón and A. Merkoçi, *ACS Nano*, 2016, **10**, 853–860.
44 E. O. Polat, O. Balcı and C. Kocabas, *Sci. Rep.*, 2014, **4**, 6484.
45 W. Li, L. Li, S. Ge, X. Song, L. Ge, M. Yan and J. Yu, *Biosens. Bioelectron.*, 2014, **56**, 167–173.
46 A. C. Marques, L. Santos, M. N. Costa, J. M. Dantas, P. Duarte, A. Gonçalves, R. Martins, C. A. Salgueiro and E. Fortunato, *Sci. Rep.*, 2015, **5**, 9910.
47 X. Xu, H. Subbaraman, S. Chakravarty, A. Hosseini, J. Covey, Y. Yu, D. Kwong, Y. Zhang, W. C. Lai, Y. Zou, N. Lu and R. T. Chen, *ACS Nano*, 2014, **8**(12), 12265–12271.
48 C. J. Choi and B. T. Cunningham, *Lab Chip*, 2007, **7**, 550–556.
49 B. R. Schudel, C. J. Choi, B. T. Cunningham and P. J. A. Kenis, *Lab Chip*, 2009, **9**, 1676–1680.
50 D. K. Cullen, Y. Xu, D. V. Reneer, K. D. Browne, J. W. Geddes, S. Yang and D. H. Smith, *NeuroImage*, 2011, **54**, S37–S44.

Label-free impedimetric aptasensor for Ochratoxin-A detection using Iridium Oxide nanoparticles

Lourdes Rivas[a,b], Carmen C. Mayorga-Martinez[a], Daniel Quesada-González[a]
Alejandro Zamora-Gálvez[a], Alfredo de la Escosura-Muñiz[a] and Arben Merkoçi[*,a,c]*

[a] ICN2 – Nanobioelectronics & Biosensors Group, Institut Català de Nanociència i Nanotecnologia, Campus UAB, 08193 Bellaterra (Barcelona), Spain
[b] Departament de Química, Universitat Autònoma de Barcelona, 08193, Bellaterra (Barcelona), Spain
[c] ICREA – Institució Catalana de Recerca i Estudis Avançats, 08010 Barcelona, Spain.

*arben.merkoci@icn.cat

Introduction

Ochratoxin A (OTA) is a mycotoxin generated by different fungi species such as Aspergillus and Penicillium during their growth. This toxin is an hazardous contaminant present in a great number of agricultural products such as cereals, coffee beans, dried fruits, cocoa, nuts, beer and wine, causing economic losses to agricultural trade [1]. Different methods are routinely used for analysis of mycotoxins, such as chromatography, enzyme-linked immunosorbent assay (ELISA), and lateral flow assays (LFA), but label-free and highly sensitive methods are still strongly required. In this context, we present here [2] a novel aptasensor for ochratoxin A (OTA) detection based on a screen-printed carbon electrode (SPCE) modified with polythionine (PTH) and iridium oxide nanoparticles (IrO_2 NPs) [3, 4], which exhibit good stability, biocompatibility and catalytic properties. The electrotransducer surface is modified with an electropolymerized film of PTH followed by the assembly of IrO_2 NPs on which the aminated aptamer selective to OTA is exchanged with the citrate ions surrounding IrO_2 NPs via electrostatic interactions with the same surface. Electrochemical impedance spectroscopy (EIS) in the presence of the $[Fe(CN)_6]^{-3/-4}$ redox probe is employed to characterize each step in the aptasensor assay and also for label-free detection of OTA in a range between 0.01 and 100 nM, obtaining one of the lowest limits of detection reported so far for label-free impedimetric detection of OTA (14 pM; 5.65 ng/kg). The reported system also exhibits a high reproducibility, a good performance with a white wine sample, and an excellent specificity against another toxin present in such sample.

Electrodes preparation and system performance

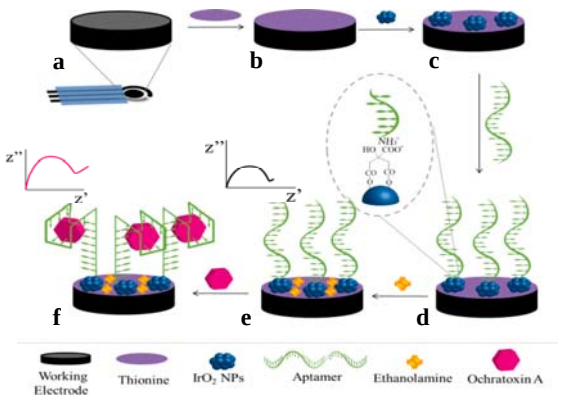

Figure 1. Schematic illustration of the fabrication steps and working principle of the developed impedimetric aptasensor for OTA detection.

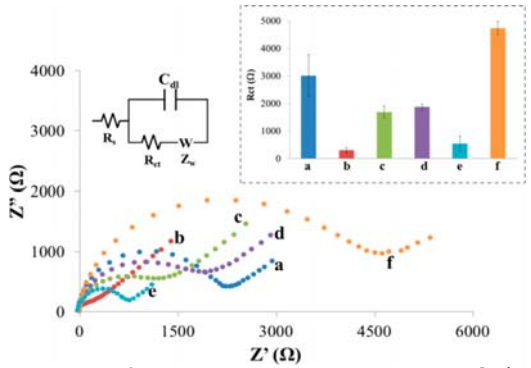

Figure 2. Nyquist plots for the aptasensor recorded in 1.0 mM $[Fe(CN)_6]^{-3/-4}$ in 0.1 M KCl solution by applying bias potential of 0.24 V vs pseudo Ag/AgCl reference electrode and an AC amplitude of 10 mV in a frequency range of 100 kHz to 0.1 Hz. Rct values correspond to each fabrication step.

Ochratoxin-A detection

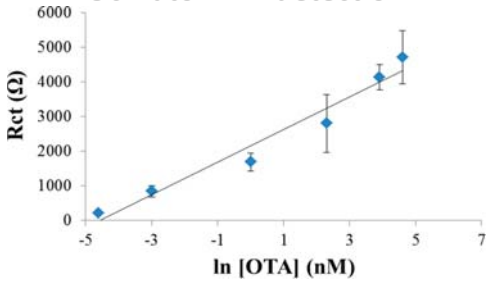

Figure 3. Calibration curve obtained by plotting the Rct values vs ln of OTA concentration in the range of 0.01 to 100 nM.

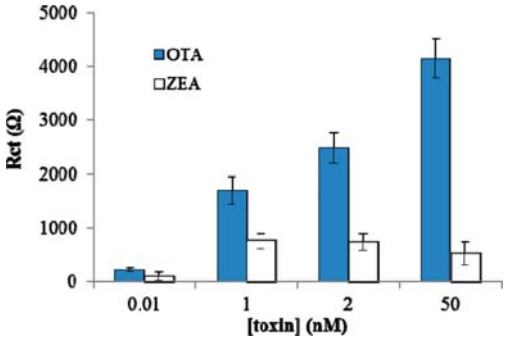

Figure 4. R_{ct} values for the selectivity of the impedimetric OTA aptasensor against ZEA (an interfering toxin) for different toxin concentrations.

spiked OTA (nM)	R_{ct} in buffer (Ω)	R_{ct} in wine (Ω)	recovery (%)
0.01	221 ± 37	295 ± 47	133
1	1160 ± 174	1370 ± 219	118
50	4140 ± 662	5200 ± 780	125

Table 1. Spike and recovery assay data. The study was done by spiking 0.01, 1 and 50 nM of OTA in white wine sample (n = 3 for each sample) and the percentage recovery was obtained as comparing with buffer.

Conclusions

- A novel nanostructured platform based on SPCE/PTH/IrO_2/aptamers is presented as an alternative to improve the performance of carbon-based electrodes used in impedimetric biosensors.
- The developed aptasensor shows the widest linear range of response, from 0.01 to 100 nM, and one of the lowest limit of detection (14 pM; 5.65 ng/kg) found in the literature for label-free impedimetric detection of OTA.
- The system demonstrated to be robust against interfering toxins (i.e. ZEA) and real matrixes (i.e. white wine), which would allow the usage of this biosensor on real scenarios.

References

1. Food and Agricultural Organization (FAO). Manual on the application of the HACCP system in mycotoxin prevention and control; FAO: Rome, 2001; p 124

2. Rivas, L.; Mayorga-Martinez, C.; Quesada-González, D.; Zamora-Gálvez, A.; de la Escosura-Muñiz, A.; Merkoçi, A. Anal. Chem. 2015, 87, 5167−5172.

3. Mayorga Martinez, C.; Pino, F.; Kurbanoglu, S.; Rivas, L.; Ozkan, S.; Merkoçi, A. J. Mater. Chem. B 2014, 2, 2233−2239.

4. Rivas, L.; de la Escosura-Muñiz, A.; Pons, J.; Merkoçi, A. Electroanalysis 2014, 26, 1287−1294.

Acknowledgements: The authors acknowledge support of the Spanish MINECO under Project MAT2011−25870 and through the Severo Ochoa Centers of Excellence Program under Grant SEV-2013-0295. ICN2 also acknowledges the E.U.'s support under FP7-OCEAN 2013.1 contract number 613844 "SMS". L.R. also acknowledges Universitat Autònoma de Barcelona for her predoctoral grant.

Nanotechnology-based lateral flow biosensors

Daniel Quesada-González[a] and Arben Merkoçi*[,a,b]

[a] ICN2 – Nanobioelectronics & Biosensors Group, Institut Català de Nanociència i Nanotecnologia, Campus UAB, 08193 Bellaterra (Barcelona), Spain

[b] ICREA – Institució Catalana de Recerca i Estudis Avançats, 08010 Barcelona, Spain.

*arben.merkoci@icn2.cat

Introduction

Nowadays, biosensors have become tools of great importance in our daily life, being the control of chronic diseases, the detection of pollutants in water or pregnancy tests some of the most popular examples. Paper-based biosensors[1,2] permit the performance of low-cost and fast diagnostics, making them portable and removing the need of expensive equipment. Among the different types of paper-based biosensors, lateral flow devices stand out due their easy-to-use design and their demonstrated robustness and specificity. The inclusion of nanoparticles[3] on these devices has lead into an enhancement of their sensibility, allowing quantitative detection and the possibility of reaching lower limits of detection, as well as the application of different detection methods and signal enhancement strategies on paper assays. It is also worth noting that lateral flow biosensors can be easily coupled into mobile phones[4] giving place to strong and portable analytical devices full of possibilities due their connectivity (i.e. wireless communication) and capabilities (e.g. cameras, light sensors, etc.).

How do lateral flow biosensors work?

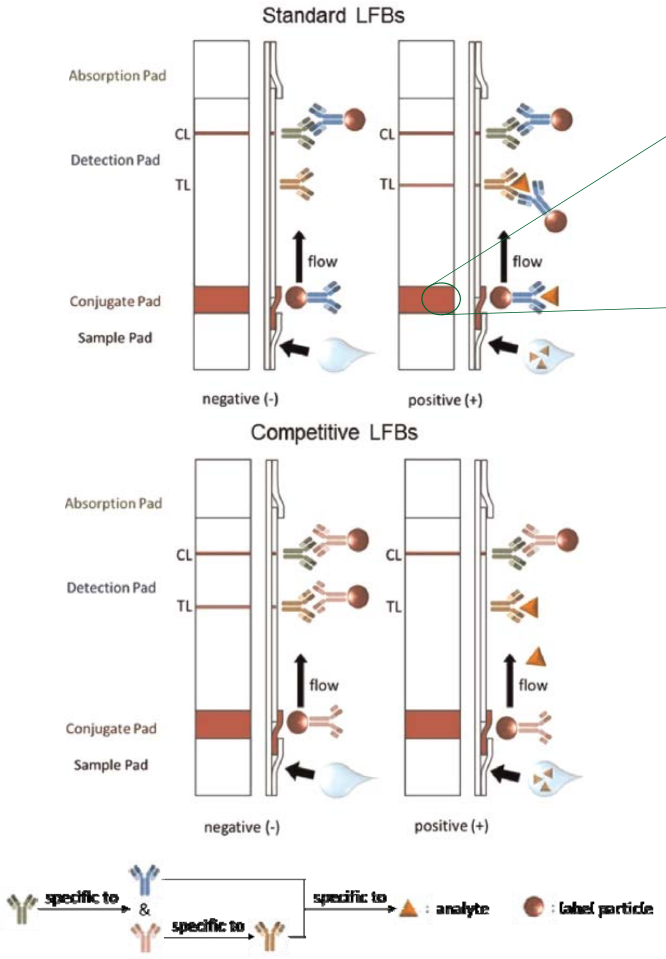

Figure 1. Schematic representation of the different parts of a lateral flow strip and movement of analytes across it with (a) standard and (b) competitive designs. Adapted with permission from ref. 3. Copyright 2015, Elsevier.

The possibilities of nanotechnology

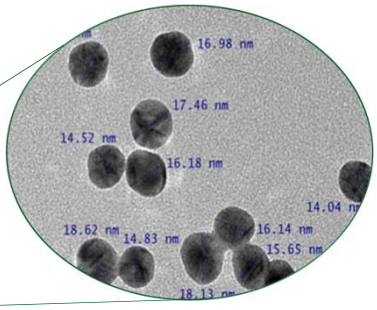

Figure 2.
Au nanoparticles are a common nanomaterial used on lateral flow biosensors. Image was obtained using transmission electron microscope.

Average nanoparticle diameter: 18 ± 1 nm

Table 1. Comparison of most remarkable methods and materials used in lateral flow biosensors. Adapted with permission from ref. 3. Copyright 2015, Elsevier.

Detection method	Labels	Advantages	Disadvantages
Optical (colorimetry)		• Naked-eye detection • Fast qualitative response	• Normally, only qualitative or semiquantitative response
	AuNPs	• Easy to synthetize and modify • Highly biocompatible and versatile • Intense colored • Relatively inexpensive	• Without the application of enhancement techniques, poor sensitivity and limits of detection in comparison to other methods.
	Carbon based materials	• Strong contrast against background • Different shapes and behaviors • Inexpensive and stable-in-time	• Unspecific adsorptions • Some forms have big-size; slow response assay
	Nano-/micro-particles loaded/ modified with dyes	• Inexpensive and high variety of commercial products • Good sensitivity and limits of detection	Difficult to synthesize and modifyRequire to load high quantities of dye to have a good signaling
Optical (fluorescence)		• High sensitivity • Low limits of detection	• Naked- eye detection normally is not possible • Requires equipment with both excitation light and fluorescence measurement • Materials normally exhibit photobleaching effect, lose intensity in time
	QDs	• Small-sized: fast assay • Strong intensity	• Difficult to synthetize and conjugate
	Other fluorescent materials (ex. UPTs)	• Could require less energy to be excited than QDs	• Rare elements can be expensive • Big-sized: slow assay
Electrochemical	Electroactive nanoparticles	• Highly sensitive • Low limits of detection • Devices easily miniaturized and cheap	• Requires equipment to produce and translate the signal • Reproducibility problems related to electrodes
Magnetic	Nano-/micro-particles loaded/ modified with magnetite	• Relatively inexpensive • Colorimetric response is also possible (multi signals)	• Require magnetic detectors • Sensitivity related to the size of the particles: slow assays
Thermal contrast	AuNPs	• High improvement of sensitivity and reproducibility • Any material can emit signal	• Expensive equipment
SERS	Raman reporter materials	• High improvement of sensitivity and detection limits	• Expensive equipment • Requires pretreatment of the nanomaterials

Conclusions

- Lateral flow biosensors are easy-to-use, fast, robust, selective and affordable types of paper-based biosensors able to detect a huge amount of analytes as proteins, whole cells and even heavy metals.
- By merging nanotechnology into lateral flow devices it is possible to apply different detection methods, as shown in **Table 1**.
- The inclusion of nanoparticles on this devices has also increased the sensitivity of the assays, allowing quantitative detection of the analytes by coupling external devices as it could be just a mobile phone.

References

1. Parolo, C.; Merkoçi, A. Chem. Soc. Rev. 2013, 42, 450-457
2. López-Marzo, A. M.; Merkoçi, A. Lab Chip 2016, 17, 3150-3176
3. Quesada-González, D.; Merkoçi, A. Biosens. Bioelectron. 2015, 73, 47-63
4. Quesada-González, D.; Merkoçi, A. Biosens. Bioelectron. 2017, 92, 47-63

Acknowledgements: The authors acknowledge MINECO (Spain) for the Severo Ochoa Program (Grant SEV-2013-0295) and project MAT2014-52485-P and support from the Secretaria d'Universitats i Recerca del Departament d'Economia i Coneixement de la Generalitat de Catalunya (2014 SGR 260).

Nanoparticle-based electrocatalytic detection of PBDE in sea water

Daniel Quesada-González[1], Alessandra Baiocco[1,2], Andrea A. Martos[1], Alfredo de la Escosura-Muñiz[1], Giuseppe Palleschi[2], Arben Merkoçi[1,3]*

[1]Institut Català de Nanociència i Nanotecnologia (ICN2), CSIC and The Barcelona Institute of Science and Technology (BIST), Campus UAB, 08193, Bellaterra, Barcelona, Spain.
[2]Dipartamento di Scienze e Technologie Chimiche, Università di Roma, Tor Vergata, Rome, Italy.
[3]Institució Catalana de Recerca i Estudis Avançats (ICREA), P. Lluis Companys 23, 08010 Barcelona, Spain.

*arben.merkoci@icn2.cat

Introduction

Polybrominated diphenyl ethers (PBDEs) have been used since 1970s as flame retardants in different products such as furniture, building materials or electronics. However, it has been demonstrated that the exposure to these compounds causes severe health problems like neurodevelopmental deficits, thyroid homeostasis disruption, behavioural alteration, reproductive dysfunction and even cancer, reason why the use of PBDEs has been banned since 2004 in EU and USA[1]. Nevertheless, PBDE molecules are hard to degrade and can persist long time bioaccumulated in mammalian organisms (in fat tissues) and in the environment, especially in marine water[2].
Herein we present a biosensor for the detection of PBDEs using screen printed carbon electrodes (SPCEs) based on the electrochemical detection of water oxidation reaction catalysed by iridium oxide nanoparticles (IrO_2 NPs)[3]. Our assay shows a limit of detection of around 30 ppb PBDE in distilled water. We believe that such an IrO_2 NPs-based electrocatalytic sensing system can lead to a rapid, sensitive, low cost and miniaturizable device for the selective detection of PBDEs.

Principle

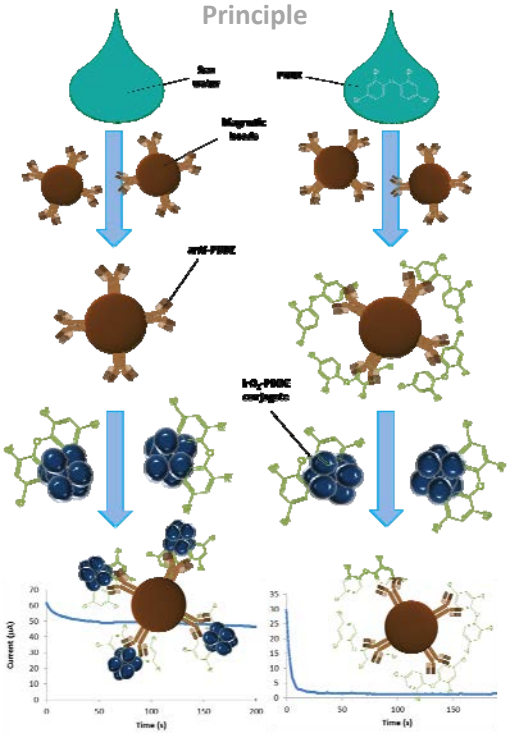

Figure 1. Principle of the electrochemical assay. PBDE is captured by an antibody conjugated onto magnetic beads. IrO_2 NPs and PBDE conjugate is mixed with the magnetic beads. At a fixed potential, current is measured, being higher as greater is the amount of IrO_2 NPs linked to magnetic beads, which in turn is inversely proportional to the concentration of PBDE.

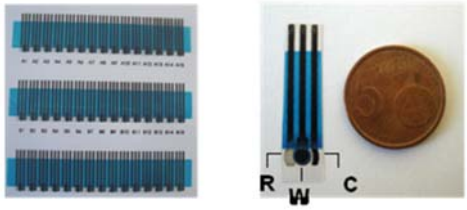

Figure 2. Screen Printed Carbon Electrodes (SPCEs) used in the last step of the assay.

IrO_2 characterization

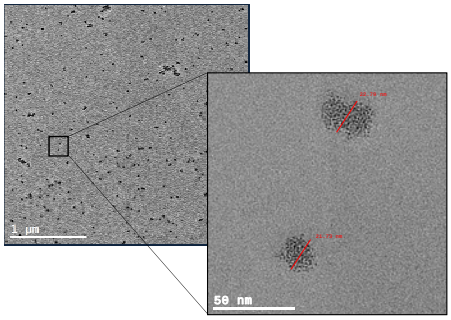

Figure 3. TEM characterization of IrO_2 NPs.

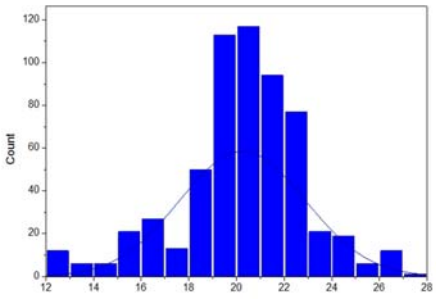

Figure 4. IrO_2 NPs histogram (20 ± 2 nm).

Table 1. Evaluation of IrO_2 NPs-PBDE conjugate at different pH. Z potential measurements are shown in the table.

	IrO_2 NPs –PBDE	IrO_2 NPs
pH 7	-42±2	-54±4
pH 8	-43±3	-55±1
pH 9	-49±1	-55±2

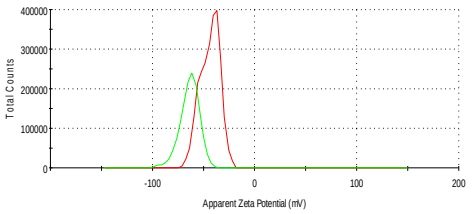

Figure 5. Z potential peaks related to Table 1.

Electrodes evaluation

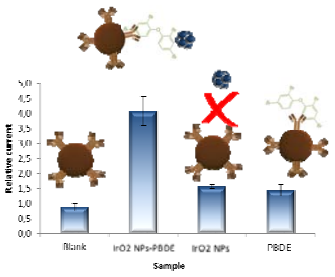

Figure 6. SPCE were evaluated against different assay situations.

PBDE detection

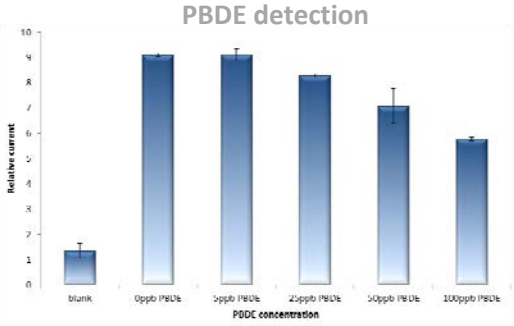

Figure 7. Relative current signal obtained from IrO_2 NPs. The signal decreases as higher is the amount of PBDE in the sample.

Conclusions

- The electrocatalytic properties of IrO_2 NPs towards water oxidation reaction make them a good candidate to take into account on electrochemical biosensors.
- There is no unspecific adsorption of IrO_2 NPs on magnetic beads during the assay (Fig. 6).
- By means of our assay, PBDE (BDE 47) can be detected with a detection limit of 30 ppb (Fig. 7).

References

1. Guo, W., Holden, A., Smith, S. C., Gephart, R., Petreas, M., Park, J. S., 2016. Chemosphere 150, 505-513.
2. Chałupniak, A., Merkoçi, A., 2017. Nano Res. 10 (7), 2296–2310.
3. Rivas, L., de la Escosura-Muñiz, A., Pons, J., Merkoçi, A., 2014. Electroanalysis, 2014, 26 (6), 1287–1294.

Acknowledgements: We acknowledge support from EU (FP7, SMS project) and MINECO (Spain) MAT2017-87202-P. This work is also funded by the CERCA Programme / Generalitat de Catalunya. ICN2 is supported by the Severo Ochoa program from Spanish MINECO (Grant No. SEV-2013-0295).

Iridium oxide nanoparticle-based lateral flow immunoassay

Daniel Quesada-González[1], Amadeo Sena-Torralba[1], Wiyogo Prio Wicaksono[1,2], Alfredo de la Escosura-Muñiz[1], Tribidasari A. Ivandini [2], Arben Merkoçi[1,3]*

[1]Institut Català de Nanociència i Nanotecnologia (ICN2), CSIC and The Barcelona Institute of Science and Technology (BIST), Campus UAB, 08193, Bellaterra, Barcelona, Spain.
[2] Department of Chemistry, Faculty of Mathematics and Science, University of Indonesia, Kampus UI Depok, Jakarta 116424, Indonesia
[3]Institució Catalana de Recerca i Estudis Avançats (ICREA), P. Lluís Companys 23, 08010 Barcelona, Spain.

*arben.merkoci@icn2.cat

Introduction

Lateral flow biosensors (LFBs) are paper-based devices that allow the detection of different types of analytes (from small proteins to whole cells, including even heavy metals and single molecules) with quickness, robustness and selectivity, without leaving behind paper sensors benefits as low-cost, recyclability and sustainability[1,2]. Nanomaterials have been widely reported in LFBs[3], offering new sensing strategies based on optical, electrical or magnetic detection techniques. Looking for other advantageous nanomaterials, we propose for the first time the use of iridium oxide nanoparticles (IrO_2 NPs) in LFB for the detection of Human Immunoglobulin (HIgG) as a model protein. These nanoparticles can be easily prepared and conjugated with biomarkers. Their dark blue colour gives a high contrast against the white background of the strips being in this way excellent labels. In addition, electrocatalytic properties of IrO_2 nanoparticles[4], can in the future facilitate their electrochemical detection being this integrated within the strips and even combined with optical detection.

IrO_2 NPs synthesis

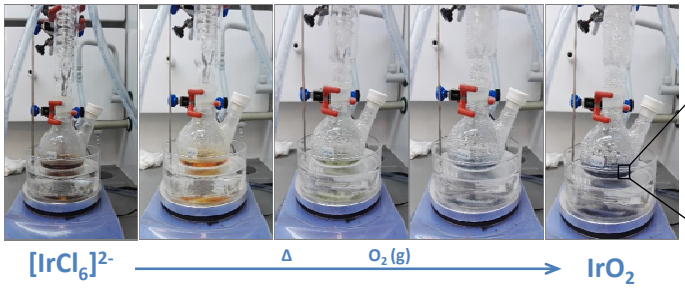

Figure 1. Color changes during IrO_2 synthesis.

IrO_2 NPs characterization

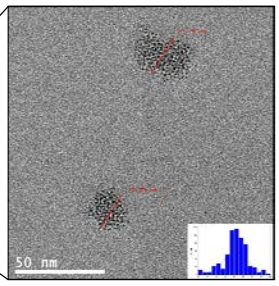

Figure 3. IrO_2 NPS characterized on TEM.
Diameter 20 ± 2 nm.

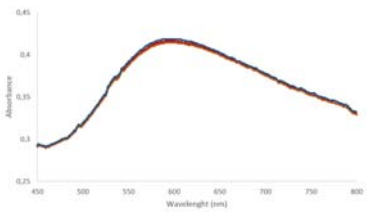

Figure 4. IrO_2 NPS exhibit a maximum absorbance peak at wavelength 588 nm.

Lateral flow immunoassay

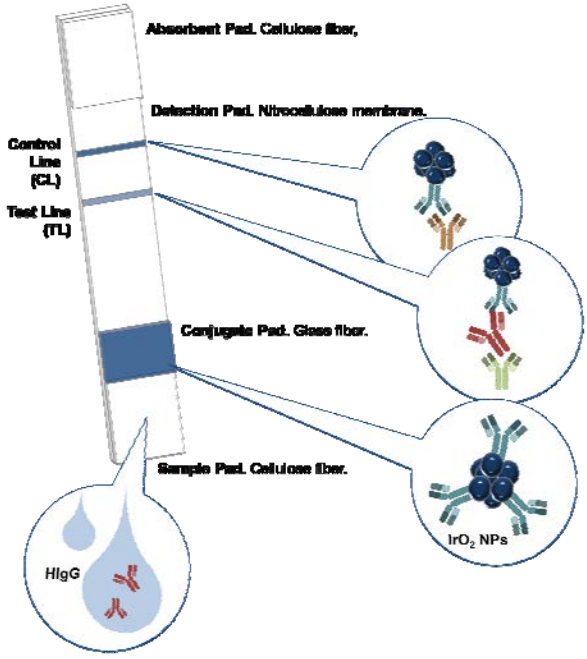

Figure 2. Schematic representation of a IrO_2 NPS-LFBs, its different pads and composition.

Strips evaluation

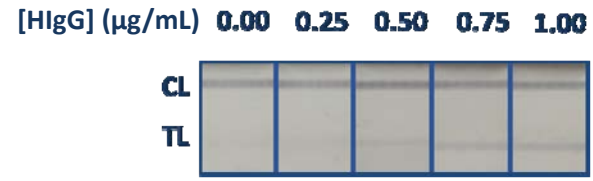

Figure 5. IrO_2 NPS-LFBs, the intensity of TL increases with the concentration of HIgG.

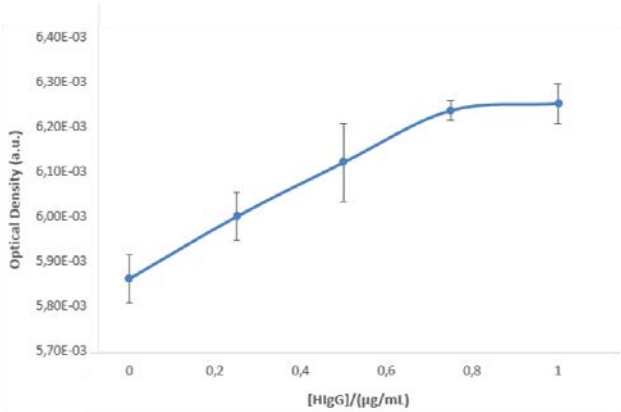

Figure 6. Optical density measured from IrO_2 NPS-LFBs strips by using a mobile phone[5] (Moto Z) and Image J software.

Conclusions

- IrO_2 NPs can be conjugated with antibodies for their application in the development of biosensors.
- IrO_2 NPS-LFBs exhibit a working range between 0.25 - 1.00 µg/mL of HIgG (used as model protein).
- The contrast between blue IrO_2 NPS and the white background of nitrocellulose membrane can be easily measured and quantified by using a mobile phone[5].

References

1. Parolo, C., Merkoçi, A., 2013. Chem. Soc. Rev. 42, 450-457.
2. López-Marzo, A. M., Merkoçi, A., 2016. Lab chip 16, 3150–3176.
3. Quesada-González, D., Merkoçi, A., 2015. Biosens. Bioelectron. 73, 47–63.
4. Rivas, L., de la Escosura-Muñiz, A., Pons, J., Merkoçi, A., 2014. Electroanalysis, 2014, 26 (6), 1287–1294.
5. Quesada-González, D., Merkoçi, A., 2017. Biosens. Bioelectron. 92, 549–562.

Acknowledgements: We acknowledge support from MINECO (Spain) MAT2017-87202-P. This work is also funded by the CERCA Programme / Generalitat de Catalunya. ICN2 is supported by the Severo Ochoa program from Spanish MINECO (Grant No. SEV-2013-0295).